Reversible Addition-Fragmentation Chain Transfer-Hetero Diels-Alder (RAFT-HDA) Chemistry as an Efficient Conjugation Technique for Macromolecular Surface Engineering

Zur Erlangung des akademischen Grades eines

DOKTORS DER NATURWISSENSCHAFTEN

(Dr. rer. nat.)

Fakultät für Chemie und Biowissenschaften

Karlsruher Institut für Technologie (KIT) – Universitätsbereich

Genehmigte

DISSERTATION

von

Leena Nebhani

aus

Jaipur, Indien

Dekan: Prof. Dr. Stefan Bräse

Referent: Prof. Dr. Christopher Barner-Kowollik

Korreferent: Prof. Dr. Manfred Wilhelm

Tag der mündlichen Prüfung: 12. Juli 2010

Die vorliegende Arbeit wurde von September 2007 bis Juni 2010 unter Anleitung von Prof. Dr. Christopher Barner-Kowollik an der Universität von New South Wales, Sydney, Australien (September 2007-Juni 2008) und am Karlsruher Institut für Technologie (KIT) (Juli 2008-Juni 2010)– Universitätsbereich angefertigt.

One should perform karma with nonchalance without expecting the benefits because sooner or later one shall definitely get the fruits.

-Bhagavad-Gita

Abstract

Molecular design to control the properties of polymeric materials is gaining increasing attention and applications in materials science in recent years. One of the major scientific challenges is to attain well-defined properties and structural order on the surface of variable materials. With respect to the modification of surfaces, *click* chemistry in general and specifically cycloaddition reactions (which include 1,3-dipolar cycloadditions as well as Diels-Alder reactions) are preferentially employed and are generating significant interest for the alteration of surfaces. These transformations represent a convenient strategy for the highly efficient coupling of chemical species to solid substrates.

In an attempt to address the existing short comings of the classical *click* and Diels-Alder conjugations, a combination of *reversible addition-fragmentation chain transfer (RAFT)* polymerization and *hetero Diels-Alder (HDA)* chemistry was recently developed. In the RAFT-HDA approach, the polymers synthesized *via* RAFT polymerization in the presence of electron-deficient dithioesters are conjugated to materials bearing a suitable diene through a hetero Diels-Alder (HDA) cycloaddition. Thus, RAFT-HDA chemistry provides a convenient methodology employing RAFT generated polymers directly and without any further modification as a reactive heterodienophile. In the current study – to achieve the modification of solid substrates in an efficient fashion – the next generation of RAFT agents capable of rapidly undergoing HDA reactions under ambient conditions and in the absence catalyst were synthesized. In addition, a range of highly innovative protocols for the orthogonal modification of solid substrates were established. The surfaces which have been successfully modified using RAFT-HDA chemistry include divinylbenzene based microspheres and Si surfaces. The microspheres were also studied in-depth to obtain information about the amount of accessible active sites (*e.g.* vinyl groups) on the surface of the particles as well as functionalization or grafting densities achieved on those substrates. Furthermore, an extremely rapid functionalization of the surface of fullerenes has also been achieved utilizing Diels-Alder chemistry.

Finally, the application of the above discussed RAFT-HDA chemistry to achieve rapid bonding-debonding on demand was explored in an industrial collaboration.

Table of Contents

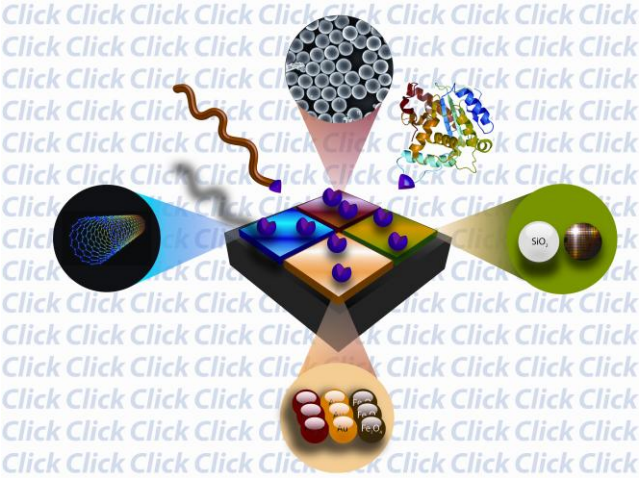

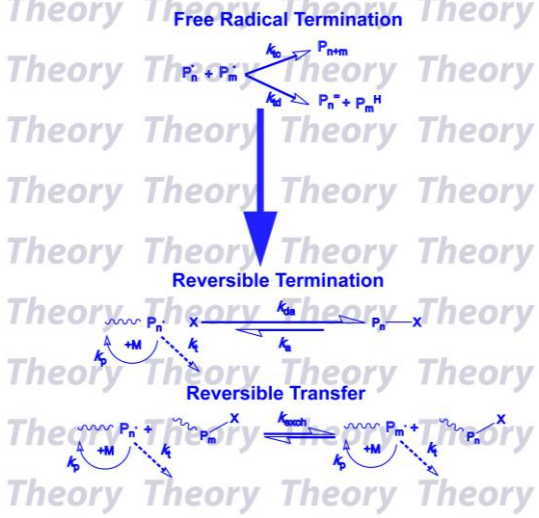

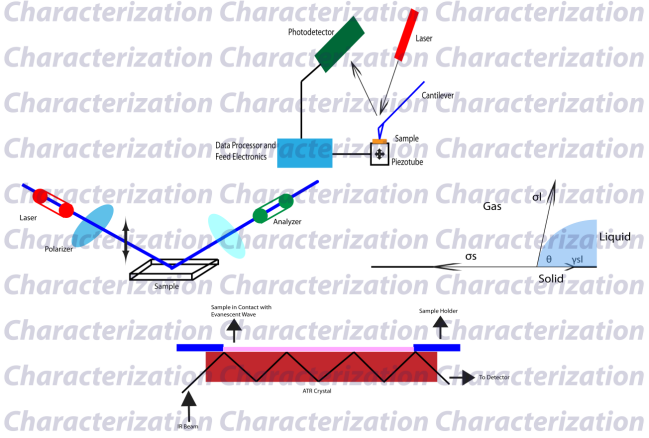

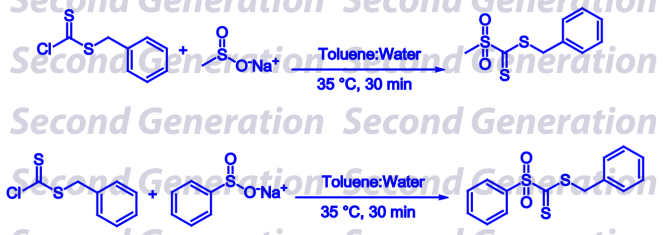

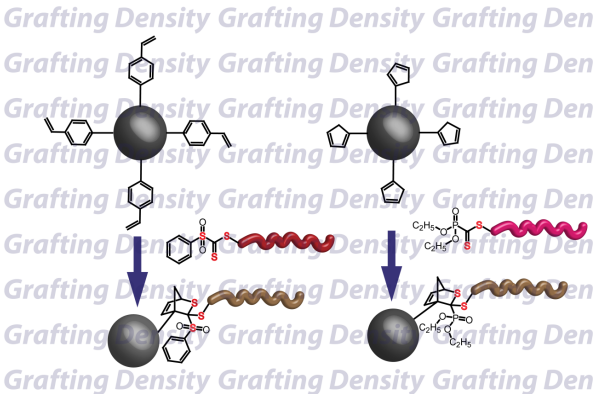

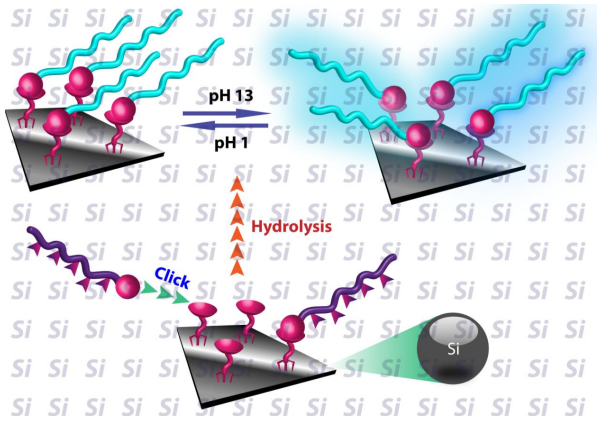

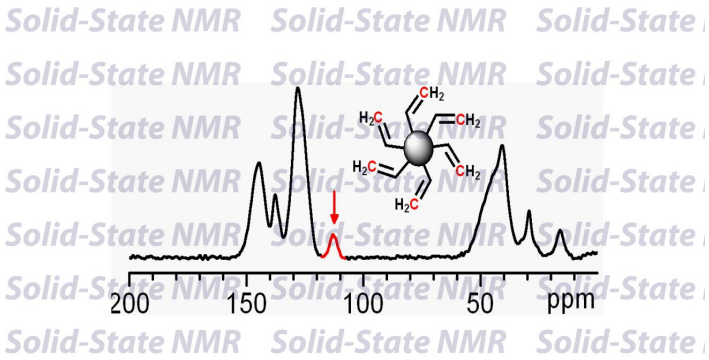

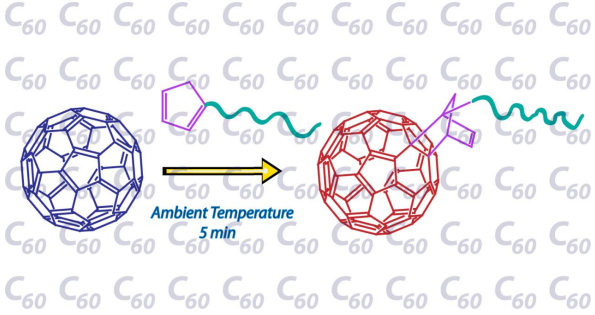

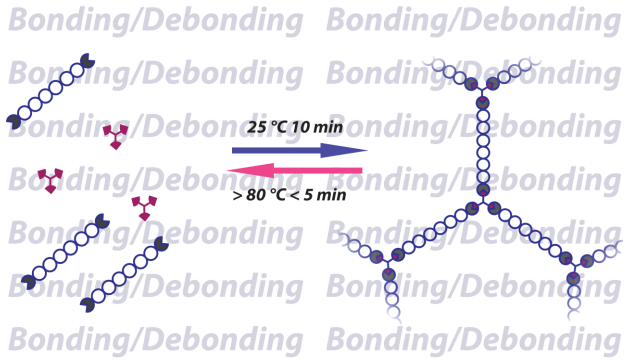

Chapter 1 Introduction

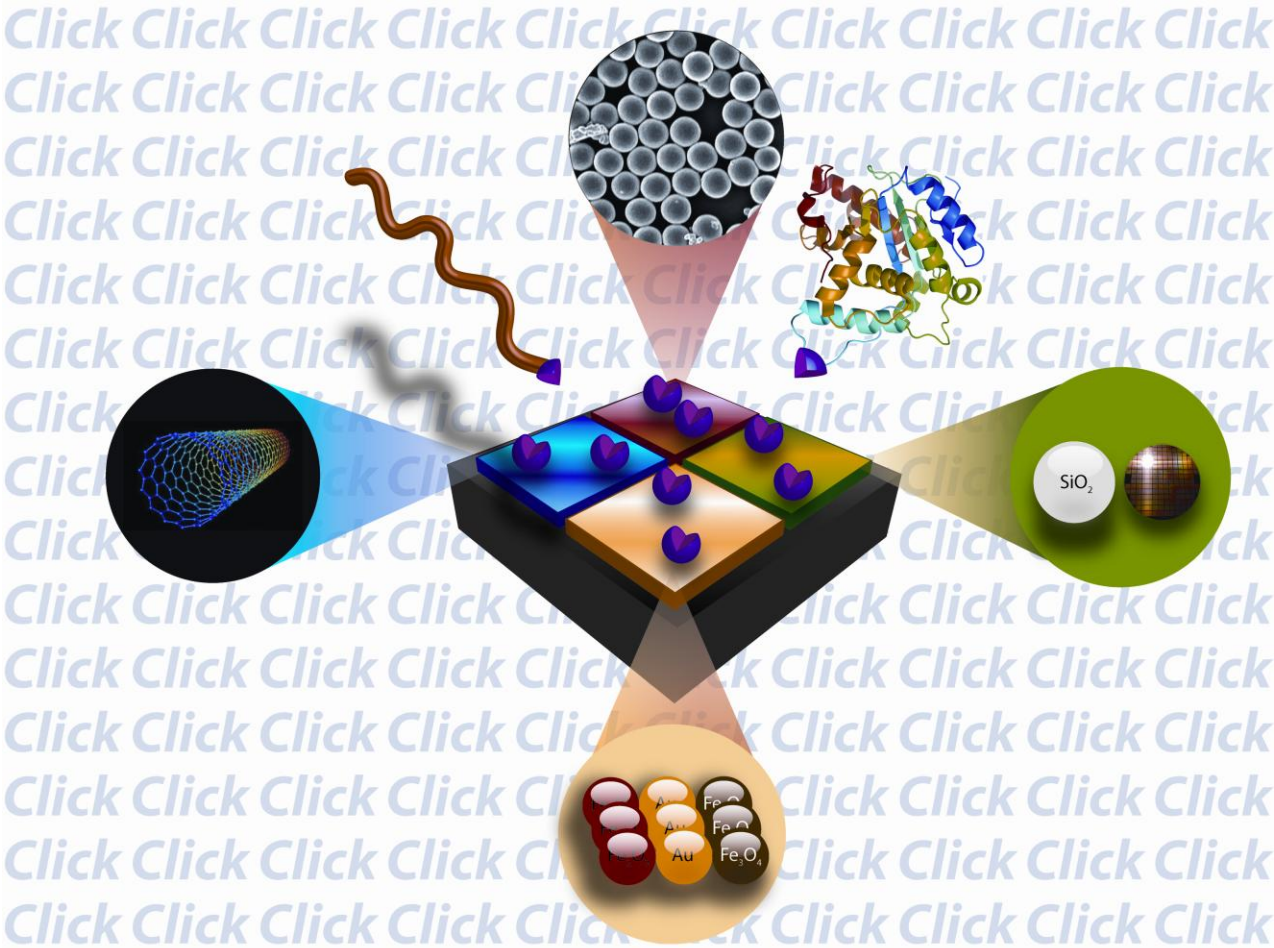

1.1 Introduction

Molecular design for controlling the properties of polymeric materials is gaining increasing attention and applications in materials science in recent years. One of the major scientific challenges is to attain well-defined properties and structural order in the bulk as well as on the surface of variable materials.[1]

The modification of materials/surfaces is central to numerous applications ranging from biomedical implants and drug delivery systems to opto-electronic devices. Thus, there exists a high motivation for improving the methodologies which can be employed in order to modify surfaces in a selective and efficient fashion. One of the major goals of surface engineering is to control the chemical composition at the material interface. The fine control of the surface properties is a field of intense research as the performance of functional materials is strongly related to the processes and interactions that are occurring at the materials' interface. In a minimalist sense, surface properties are dependent on the nature of the chemical functions as well as on their spatial arrangement on the surface.

In general, the modification or transformation of surfaces can be achieved *via* various chemical and physical methods. However, many of the chemical modification methods often fall short of providing efficient transformations because the reagents used do not yield specific functionalities or the highly oxidative reactions involved in some treatments are difficult to control.[2] Physical methods on the other hand, such as polymer adsorption[3-8] or the formation of self assembled monolayers (SAMs)[9-11] have shown great promise for the quantitative control of the surface composition and functionality of material substrates. Yet, these modifications may not be as robust due to physisorption instead of chemisorption. However, if a surface contains reactive groups, chemical reactions can be performed employing these reactive entities as chemical anchors. The exact nature of the surface can also be quantitatively controlled through methods that provide a well-defined surface functionality.

Although there is a general need for simple and convenient methods to covalently conjugate a molecule of interest to a surface, no single coupling strategy has been broadly adopted. Instead, numerous coupling strategies have been reported in the literature. Clearly, the reason underpinning this observation is that most of the coupling

methods suffer from one or more problems, including: incomplete surface functionality transformation, requirement of harsh conditions, the need for highly reactive coupling partners, side reactions or extensive organic synthesis. In addition, carrying out chemistry on surfaces is very challenging due to several problems which are not encountered during conventional solution chemistry. These may include the inability to perform standard separation procedures to remove unreacted molecules or undesired side-products and difficulty in quantitatively characterizing heterogeneous substances to determine reaction yields.

With respect to the modification of surfaces, *click* chemistry represents a strategy for the efficient coupling of chemical species to surfaces, thus allowing complex molecular architectures to be generated on solid materials. Examples of *click* reactions on polymers and solid surfaces have been thoroughly reviewed.[1,12,13] Numerous strategies are available to exploit these reactions enabling surface scientists to benefit from its high selectivity, high yields and remarkable tolerances to varying reaction conditions.[14-17]

Out of the various reactions which fall under the *click* criteria, it can be observed that cycloaddition reactions are mostly and preferentially used for surface modifications. The reason for the synthetic preference of pericyclic reactions over alternative *click* concepts may lie in the fact that alternative reactions do not reach the level of yield, simplicity and ease of product isolation that are often desired. The most frequently employed *click* conjugation is the Cu(I) catalyzed 1,3-dipolar cycloaddition between azides and alkynes.[18,19] Alternatives to azide-alkyne *click* conjugations include Diels-Alder cycloadditions which have been successfully employed for the generation of a variety of polymeric architectures.[20-21] Both of the above approaches have their specific strengths and weaknesses. For example, most azide-alkyne coupling reactions require a copper catalyst to function at ambient temperatures. The use of a copper catalyst can limit the application of azide-alkyne conjugations in systems which are sensitive to heavy metal ions *e.g.* in biological applications.[22]

Copper has an adverse interaction with several biomolecules, such as proteins and DNA, which can introduce undesirable structural and biological modifications.[22] For *click* reactions to be used in contact with living systems the copper catalyst must be

removed or alternatives, such as Staudinger ligation[23] or strain-promoted [3+2] heterocycloaddtions,[24] must be employed. Azides,[25] among the prime reactants for the Huisgen's 1,3-dipolar cycloaddition reactions, are also often associated with potential toxic side effects and certain azides may bear a very real explosive potential.

The most significant limitation in many Diels-Alder-type conjugations is the requirement of higher temperatures to drive the reaction to completion.

1.2 Research Goals

In an attempt to address the existing short comings of the classical *click* conjugation and the Diels-Alder conjugation, a combination of reversible addition-fragmentation chain transfer (RAFT) polymerization and hetero Diels-Alder (HDA) chemistry was recently described. RAFT-HDA chemistry provides a convenient methodology employing RAFT generated polymers directly and without any further modification as a reactive heterodienophile. The combination of RAFT-HDA chemistry is a versatile method for the construction of macromolecular architectures as well as for the modification of surfaces. In addition to being one of the most recent forms of efficient conjugation chemistries, the RAFT-HDA concept is an atom-economical approach. The entire concept is based upon an electron-withdrawing dithioester end-group that is inherent in polymers prepared with specially chosen controlling agents used within RAFT polymerizations. Unlike the copper catalyzed azide-alkyne coupling (CuAAC) or the carbo Diels-Alder approach, the used RAFT agent does not require additional functionalities to be further employed in the post-polymerization conjugation step. In the RAFT-HDA approach, the polymers synthesized *via* RAFT polymerization in the presence of electron-deficient dithioesters are conjugated to materials bearing a suitable diene through a hetero Diels-Alder (HDA) cycloaddition.

The aim of current research work can be summarized as follows:

1) To synthesize the next generation of RAFT agents capable of undergoing HDA reactions to further enhance their applicability for polymer-polymer conjugation. The synthetic strategy entails the use of extremely electron withdrawing moieties in the Z-

position,[26] so that even less reactive dienes (*e.g.* based on butadiene) can be conjugated at ambient temperatures and in the absence of catalysts.

2) To functionalize a variety of surfaces (*e.g.* polymeric microspheres[14] and Si surfaces[27]) *via* highly orthogonal RAFT-HDA chemistry.

3) To quantify the degree of functionalization achieved[28] on the surface of microspheres using RAFT-HDA chemistry.

4) To study in-depth polymeric microspheres *via* solid-state NMR spectroscopy to obtain information about the amount of accessible active sites (*e.g.* vinyl groups) on the surface of the particles.[29]

5) To efficiently and rapidly functionalize fullerenes[30] with polymeric building blocks using the Diels-Alder reaction.

6) To synthesize reversibly cross-linked functional polymeric networks *via* hetero Diels-Alder chemistry.[31]

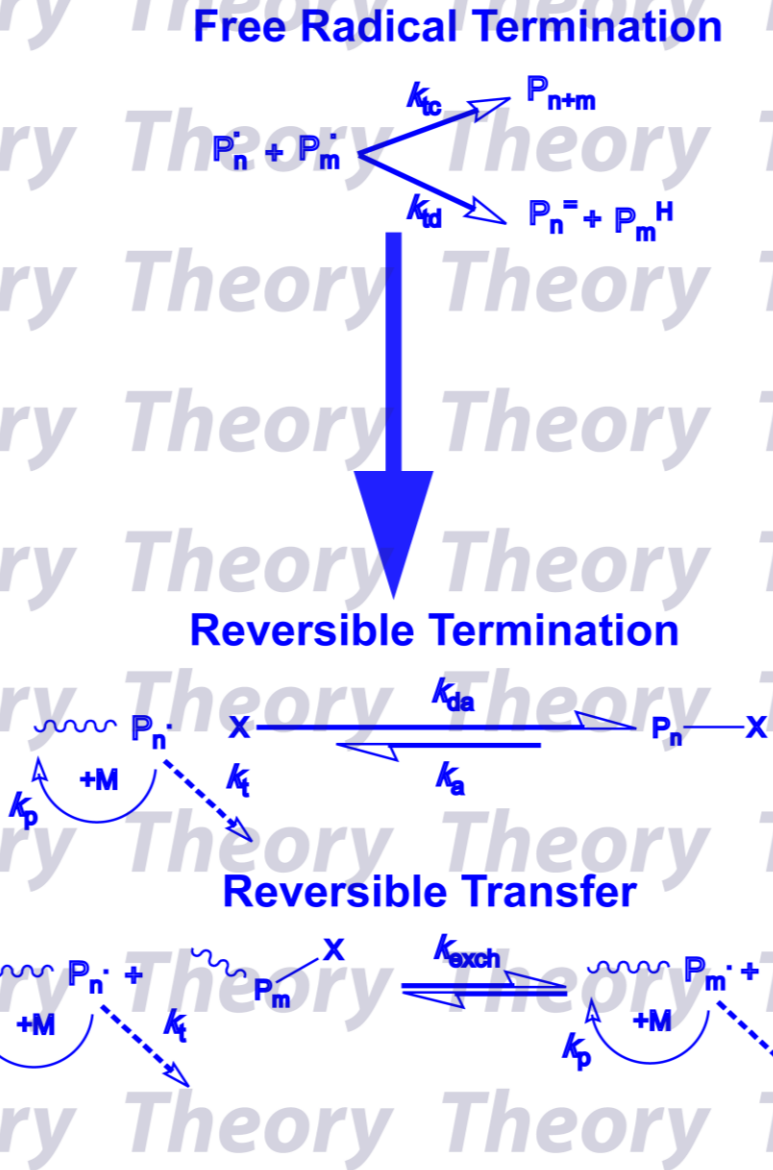

2.1 Radical Polymerization

Free radical polymerization is one of the most widely used processes in the field of industrial polymer synthesis and is the preferred route for the production of commercial polymers[32,33] There are number of factors responsible for the pre-eminent position of radical polymerization. One is the large variety of monomers which can be polymerized and copolymerized under relatively simple experimental conditions. While the absence of oxygen is required, it is possible to conduct such reactions in the presence of water, *e.g.* in suspension or emulsion polymerization where reaction takes place within a convenient temperature range, typically between 0 and 100 °C. Other advantages of radical polymerization are that in most cases monomer purification is not required to a high extent and initiator residues need not be removed from polymer products for several applications because they have little or no effect on the polymer properties.

2.1.1 Kinetics of Radical Polymerization

The four processes of importance in polymerization by free radical mechanisms are:

1) *Initiation:* The initiation process is usually composed of two processes: the generation of primary initiating radicals ($I^{\cdot}$) and the reaction of these radicals with monomers (M) as shown in equation (2.1) and (2.2). Typically, the generation of radicals is much slower than the addition of radicals to monomers and therefore the rate determining step with typical values of $k_d \approx 10^{-5}$ s^{-1} and $k_i \approx 10^4$ $M^{-1} \cdot s^{-1}$, depending on the reaction temperature.

$$I\text{-}I \xrightarrow{k_d} 2\,I^{\cdot} \qquad (2.1)$$

$$I^{\cdot} + M \xrightarrow{k_i} P_1^{\cdot} \qquad (2.2)$$

2) *Propagation:* Propagation occurs by successive additions of the growing radical to the double bond. The typical value for the rate coefficients of propagation is $k_p \approx 10^{3\pm1}$ $M^{-1}\cdot s^{-1}$.[34,35]

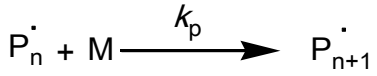

$$P_n^{\cdot} + M \xrightarrow{k_p} P_{n+1}^{\cdot} \quad (2.3)$$

3) *Termination*: Termination is the reaction between two growing radicals which can occur either *via* combination (k_{tc}) (as shown in equation (2.4)) or *via* disproportionation (k_{td}) (as shown in equation (2.5)), with rate coefficients approaching diffusion controlled limits, k_t (10^8 $M^{-1}\cdot s^{-1}$. The bimolecular termination reaction is diffusion controlled at any stage of the polymerization process. The Trommsdorff-Norrish or gel effect[36,37] is a consequence of termination being diffusion controlled. The diffusive motion of molecules depends on numerous factors. The important factors to mention are solvent viscosity, monomer-to-polymer conversion, the characteristics of the polymer from preceding reaction (the so-called polymer matrix) and the size of the individual macroradicals.

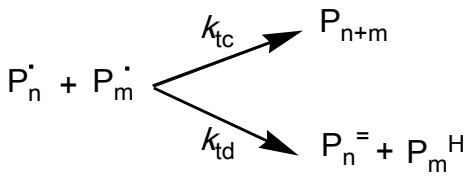

$$P_n^{\cdot} + P_m^{\cdot} \xrightarrow{k_{tc}} P_{n+m} \quad (2.4)$$

$$P_n^{\cdot} + P_m^{\cdot} \xrightarrow{k_{td}} P_n^{=} + P_m^{H} \quad (2.5)$$

4) *Transfer:* The transfer reaction can occur *via* various pathways, for example, *via* transfer to monomer (as shown in equation (2.6)), to polymer (as shown in equation (2.7)) or to other transfer agents (as shown in equation (2.8)). Chain-transfer is a chain breaking reaction; it limits the size of the final polymer chain. The effect of chain transfer on the polymerization rate is dependent on whether the rate of reinitiation is comparable to that of the original propagating radical.

(2.6)

(2.7)

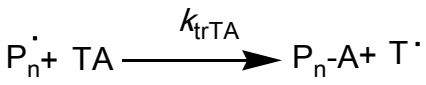

(2.8)

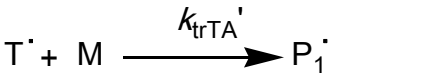

(2.9)

In the case of transfer to chain transfer agents, TA represents the species to which the radical functionality is transferred. A combined parameter, the transfer constant C_{tr} which is the ratio of the rate coefficients of transfer to propagation, is usually used to describe transfer reaction. The equation 2.10 shows the transfer constant for transfer reaction.

$$C_{tr} = \frac{k_{tr}}{k_p} \tag{2.10}$$

In radical polymerization, the polymerization rate is first order with respect to the monomer and 0.5 order with respect to initiator as shown in equation (2.11). First-order kinetics with respect to monomer is due to the steady concentration of radicals resulting from equal rates of initiation and termination. The rate of polymerization (R_p) is a function of the efficiency of initiation (f) and the rate constants for initiation (k_d), propagation (k_p) and termination (k_t) as shown in equation (2.11).

$$R_p = k_p[M]\left(\frac{fk_d[I_0]}{k_t}\right)^{1/2} \tag{2.11}$$

Note that this is a simplified version, using chain length independent rate coefficient giving instantaneous rate of polymerization. However, the conventional radical process has some notable limitations. Using the current technology available for conventional free radical processes, the preparation of well-defined polymers from unsaturated monomers has been limited. In particular, such processes do not allow for

precise control over molar masses and tend to give products with broad polydispersity because not all the chains are initiated at the same time and terminate randomly. Due to lack of control over chain breaking reactions, that is both the termination and transfer step, the ability to control polymer architectures is very limited in conventional free radical polymerization process. Thus, such polymers tend to contain significant amounts of high and very low molar mass chains, which can give unattractive properties as well as a very variable polymer composition. Moreover, the synthesis of block copolymers is practically impossible *via* the sequential addition of monomers in a conventional free radical polymerization. Such a procedure leads to a mixture of homopolymers since there are often no living radicals at the end of each monomer addition step and new radicals need to be produced to re-start the polymerization process.

Therefore, the development of techniques to overcome the largest negative feature of the free radical process, *i.e.* to introduce controlled synthesis and livingness into radical polymerization, has become the focus of recent free radical polymerization research.

2.2 Controlled/Living Radical Polymerization

To achieve controlled synthesis of polymeric materials, it is required that the chain breaking reactions be minimized and the apparent simultaneous growth of all chains is attained. However, the conventional radical polymerization proceeds *via* slow initiation and fast termination in which all chains are essentially dead at any given instant. The concept of controlled/living polymerization was originally applied to cationic ring-opening polymerization,[38] which was successfully extended to carbo-cationic systems[39] and later to anionic polymerization,[40] in which growing centers are in equilibrium with various dormant species.

The dynamic equilibrium between propagating radicals and various dormant species is key to all controlled radical polymerization systems.[41,42] The two main types of equilibria are shown in **Scheme 2.1**. Radicals may be ‘reversibly terminated’ in a deactivation/activation process or they can be involved in ‘reversible transfer’, *i.e.* a degenerative exchange process.

In the case of the reversible termination approach, a persistent radical effect (PRE) is observed.[43] In a PRE, the newly generated radicals are rapidly trapped in a deactivation process (with the rate constant of deactivation k_{da}) by species X (which is typically a stable radical such as a nitroxide[44,45] or an organometallic species such as a cobalt porphyrin.[46] When the dormant species are reactivated (k_a) and reform growing centers, they can propagate (k_p) but can also terminate (k_t).

In systems based on a PRE, a steady state of growing radicals is established through the activation-deactivation mechanism and not initiation-termination. As the rate of initiation is much faster than termination, this essentially leads to the instantaneous growth of all the chains. However, such capping reactions lower the free-radical concentration and hence significantly decrease termination events. Concomitantly, the rate of polymerization is strongly decreased.

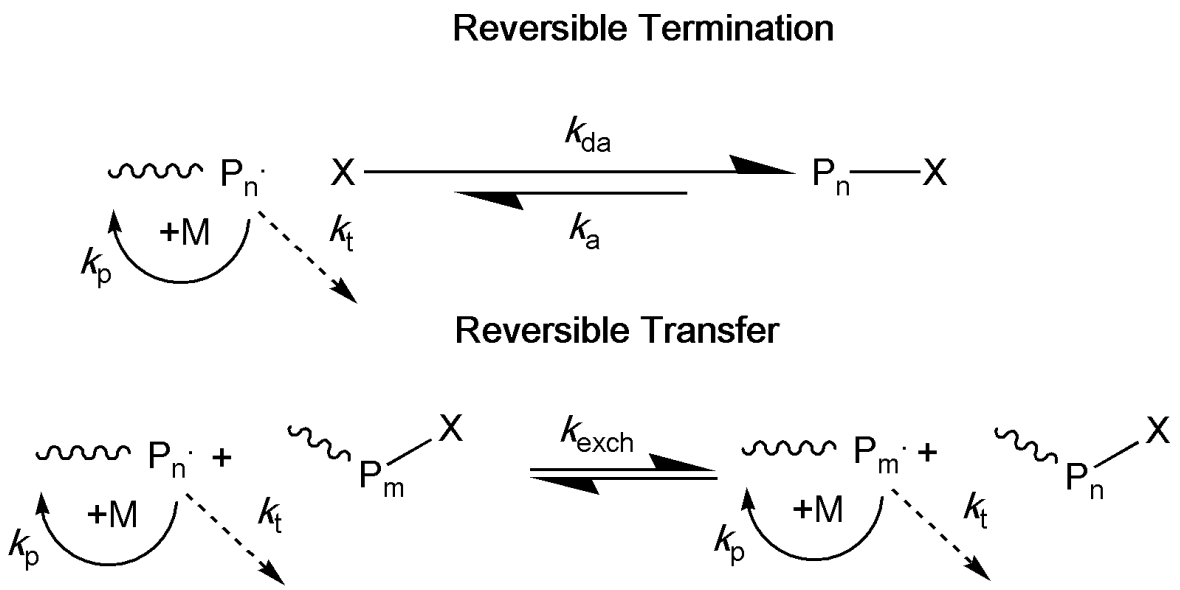

Scheme 2.1 Dynamic equilibrium between propagating radicals and various dormant species in controlled radical polymerization process

The systems which are based on degenerative chain transfer are not based on a PRE.[47] They follow repeated reversible transfer events during the polymerization without changing the free radical concentration inducing equilibrium of dormant and living chains. In such an ideal system based on degenerative chain transfer, no rate

retardation effects and other kinetic phenomena occur that may alter the radical concentration and therefore, the overall rate of polymerization, R_p, and the rate of the individual reaction steps remain unaltered from the free radical process.

2.2.1 Similarities and Differences between Radical Polymerization (RP) and Controlled Radical Polymerization (CRP)

CRP and RP proceed *via* the same radical mechanism, can exhibit chemo-, regio and stereo-selectivity and can polymerize a similar range of monomers. However, several important differences between CRP and RP exist which are summarized below:

1) The lifetime of growing chains is extended from ~1 s in RP to more than 1 h in CRP through the participation of dormant species and intermittent reversible activation.

2) Initiation is slow and free radical initiator is often left unconsumed at the end of a conventional RP. In most CRP systems, initiation is very fast and near instantaneous growth of all chains can be achieved, which ultimately enables control over the chain architecture.

3) Nearly all chains are dead in RP whereas in CRP the proportion of dead chains is usually <10 %.

4) Polymerization in CRP is often slower than in RP. However, the rates may be comparable in certain cases (*e.g.* when the targeted molecular weight in CRP is relatively low) or even identical as in the case of degenerative chain transfer process.

5) A steady state radical concentration is established in RP with similar rates of initiation and termination whereas in CRP systems a steady radical concentration is achieved by balancing the rates of activation and deactivation.

6) Termination usually occurs between long chains and constantly generated new chains in RP. In CRP, all chains are short at the early stages of reaction and become

progressively longer; thus, the termination rate significantly decreases with time (as termination rate coefficient is chain-length-dependent[48] due to diffusion control).

2.2.2 Examples of Variable Controlled/Living Radical Polymerization Processes

2.2.2.1 Stable Free Radical Polymerization (SFRP) / Nitroxide Mediated Polymerization (NMP)

Nitroxide mediated polymerization relies on the reversible homolytic cleavage of a relatively weak bond in a covalent species to generate a growing radical and a less reactive radical (this less reactive radical is a persistent radical or stable free radical). The stable free radicals do not react with themselves or with monomers to initiate the growth of new chains; they only react reversibly with growing radicals. In addition, the stable free radicals should not participate in side reactions such as the abstraction of β-H atoms. The best known and most investigated stable radicals have been nitroxides, especially 2,2,6,6-tetramethylpiperidinyoxy (TEMPO). The equilibrium reaction between dissociation (activation) and coupling (deactivation) for the polymerization of styrene using TEMPO[49] is shown in **Scheme 2.2**.

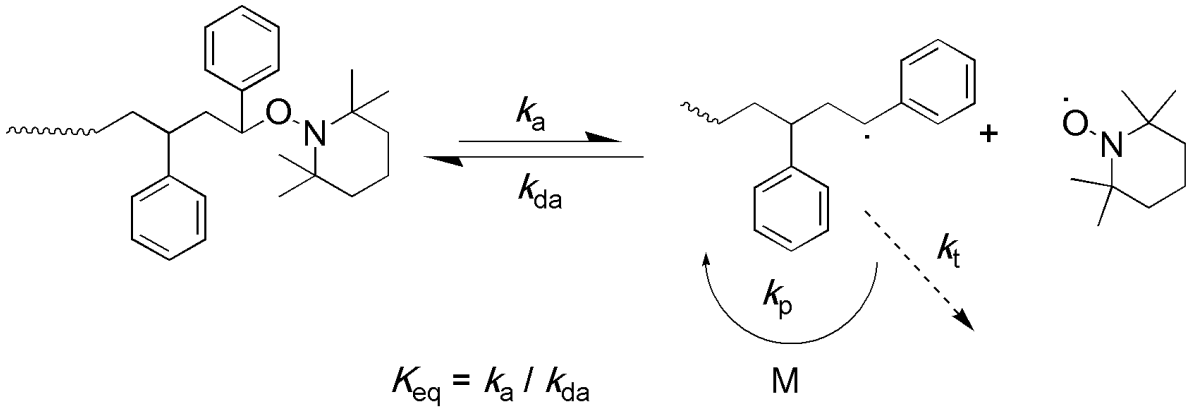

Scheme 2.2 Deactivation and activation step for the polymerization of styrene using TEMPO. The ratio of rate constants of dissociation (activation) and coupling (deactivation) $k_a/k_{da} = K_{eq}$ for styrene[49] at 120 °C is $2.0 \cdot 10^{-11}$ M

Although NMP is one of the simplest methods of controlled/living free radical polymerization, it has some disadvantages. Many monomers do not undergo polymerization because of the stability of the dormant alkoxyamines. In addition, the NMP reaction is kinetically slow; therefore high temperatures and bulk solutions are required. In literature, several types of nitroxides have been reported,[50] although the vast majority could only control the polymerization of styrenic monomers and copolymerization involving styrene. The applicability of NMP to a wider range of monomers as well as reasonable low temperatures (≤110 °C) was made possible by the introduction of asymmetric open-chain nitroxides containing α-hydrogen,[51,52] including *N*-*tert*-butyl-*N*-[1-diethylphosphono-(2,2-dimethylpropyl)] nitroxide (DEPN) (more commonly known as SG1) and *N*-*tert*-butyl-*N*-[1-phenyl-2-(methylpropyl)]nitroxide TIPNO (chemical structures are shown in **Scheme 2.3**). The range of monomers that can now undergo controlled/living NMP using these nitroxides includes styrenes, acrylate, acrylic acid, acrylamide and acrylonitrile.

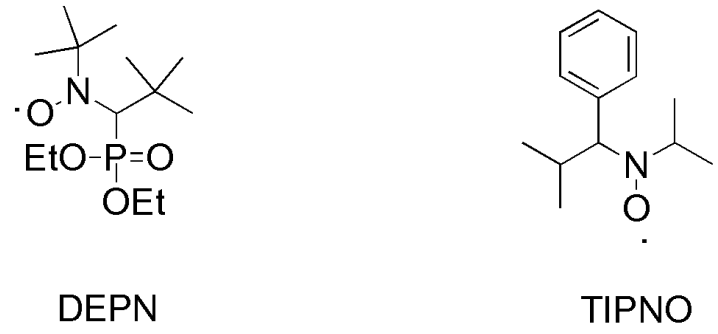

DEPN TIPNO

Figure 2.1 Structures of the nitroxides DEPN (SG1) and TIPNO

2.2.2.2 Atom Transfer Radical Polymerization (ATRP)

The basic working mechanism of ATRP involves homolytic cleavage of an alkyl halide bond, R-X, by a transition metal complex Mt^n-Ligand (*e.g.* CuBr-bipyridyl) to generate (with the activation rate constant k_a) the corresponding higher oxidation state metal halide complex X-Mt^{n+1}-Ligand (such as $CuBr_2$-bipyridyl) and an alkyl radical $R^{\cdot}$ (as shown in **Scheme 2.3**). $R^{\cdot}$ can then propagate with a vinyl monomer (k_p), terminate by coupling and/or disproportionation (k_t) or be reversibly deactivated in this equilibrium by X-Mt^{n+1}-Ligand (k_{da}). The radical termination is diminished as a result of a PRE that

ultimately shifts the equilibrium towards the dormant species (activation rate constant « deactivation rate constant).

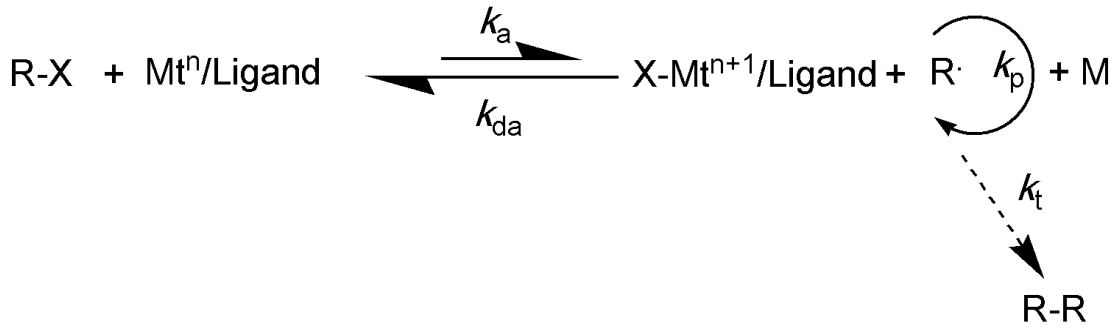

Scheme 2.3 Basic mechanism of the ATRP process

The important difference between SFRP and ATRP is that the kinetics and control in ATRP depend not only on the persistent radical (X-Mt^{n+1}-Ligand) but also on the activator (R-X). Molecular weights are defined by the $\Delta[M]/[RX]_0$ ratio and are not affected by the concentration of the transition metal. The polymerization rate increases with initiator concentration (R-X) and is proportional to the ratio of concentrations of activator and deactivator according to equation (2.12).

$$R_p = \frac{-d[M]}{dt} = k_p[M][R^\bullet] = \frac{k_p[M](k_a[RX][Mt^nL])}{k_{da}[XMt^{n+1}L]} \qquad (2.12)$$

An ideal ATRP process proceeds *via* an inner sphere electron-transfer process, *i.e.* atom transfer. However, under certain conditions the oxidation or reduction of radicals to carbocations or carbanions by transition metal complexes can occur as a side reaction.[53,54] Other side reactions include the formation of organometallic species, monomer[55,56] or solvent coordination to the transition metal catalyst, dissociation of the halide from the deactivator[57] and HBr elimination[58-60] Therefore, the appropriate selection of an initiator and catalyst not only depends on the monomer or targeted molecular architecture but also on the occurrence of potential side reactions.

2.2.2.3 Reversible Addition-Fragmentation Chain Transfer (RAFT) Polymerization

RAFT is an acronym for reversible addition-fragmentation chain transfer. The term RAFT polymerization was first coined in 1998 when the use of thiocarbonyl thio RAFT agents was first reported in open literature[61] by the Commonwealth Scientific and Industrial Research Organization (CSIRO) in Australia. Almost at the same time, macromolecular design *via* the interchange of xanthates (MADIX)[62] was patented by group of researchers in France. The MADIX process employed xanthates as controlling agents but proceeds by an identical mechanism as the RAFT process. However, both processes are based on earlier developed chemistries, such as the small radical reactions reported by Zard and coworkers.[63]

RAFT is the most versatile controlled radical polymerization process with respect to the types of monomers and the reaction conditions that enables the formation of polymer with controlled molecular weight, low polydispersity and complex architecture. The RAFT process relies upon a kinetic strategy for controlling molecular weight and architecture of the resulting polymer. It utilizes different mechanism as compared to SFRP/NMP and ATRP process. The RAFT process makes use of repeated reversible transfer events during the polymerization without changing the free radical concentration to induce the equilibrium of dormant and living chains. In such an ideal RAFT system, where no rate retardation effects and other kinetic phenomenon occurs that may alter the radical concentration, the overall rate of polymerization, R_p and rate of individual reaction steps remain unaltered.

The mediating compounds employed in RAFT polymerizations are thiocarbonyl thio compounds, Z-C(=S)S-R, which have been developed in wide structural variety with respect to their leaving R-groups and to their stabilizing Z-moieties.[64,65] The main features of ideal RAFT polymerization can be summarized as follows. With the appropriate selection of RAFT agent for monomers and reaction conditions used, all or most of the below can be routinely achieved.

1) RAFT polymerization can be performed by simply adding a chosen quantity of an appropriate RAFT agent to a conventional free radical polymerization. The same monomers, initiators, solvents and temperature can be used.

2) RAFT polymerization possesses characteristics usually associated with living polymerization. All chains begin growth at the commencement of polymerization and continue to grow until the monomer is consumed. Molecular weights increases linearly with conversion. Active chain ends are retained during the RAFT process.

3) RAFT polymerization process results in narrow molecular weight distributions.

4) It is possible to generate complex macromolecular architectures, for example, Block, star etc. using RAFT process.

The key feature of the mechanism of RAFT polymerization with thiocarbonyl thio compounds is generally divided into two sets of reactions, that is, pre-equilibrium, which involves the initial RAFT agent and includes the initialization of the living process and the main equilibrium between growing and dormant polymer chains (as depicted in **Scheme 2.4**). The pre-equilibrium step takes place in the early stages of the RAFT polymerization, the propagating macroradical ($P_m^{\cdot}$), which is mainly oligomeric at this stage, adds to the sulfur-carbon double bond of the initial RAFT agent (**1**), resulting in the generation of carbon-centered intermediate radical (**2**). The addition of primary initiator derived radicals to the initial RAFT agent has been generally neglected but it may become important in case of high initiating radical concentrations. Such reactions induce the transformation of the leaving group of the initial RAFT agent and may have an impact on the kinetics in the early phase of the RAFT polymerization.

The adduct radical (**2**) formed in the pre-equilibrium undergoes β-scission, either yielding back the reactants or releasing an initiating leaving group radical $R^{\cdot}$ with concomitant formation of polymeric dithioester compound (**3**), which constitutes the dormant species. A similar set of reactions are operating in the main equilibrium, in which propagating macroradical $P_n^{\cdot}$ reacts with polymeric RAFT agent (**3**). The recurring RAFT events establish the equilibrium between dormant and living chains, by which living/controlled characteristics are induced in the polymerization. The individual reactions of these pre and main equilibrium are described kinetically *via* so-called addition rate coefficient, k_{ad} and fragmentation rate coefficient k_{β} (as shown in **Scheme**

2.4). The reactions associated with RAFT equilibria shown in **Scheme 2.4** are in addition to those (*i.e.* initiation, propagation, and termination) that occur during conventional radical polymerization.

I. Initiation

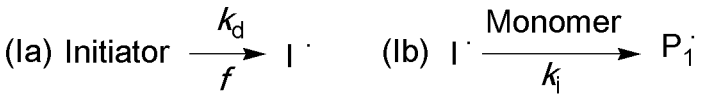

II. Pre-equilibrium

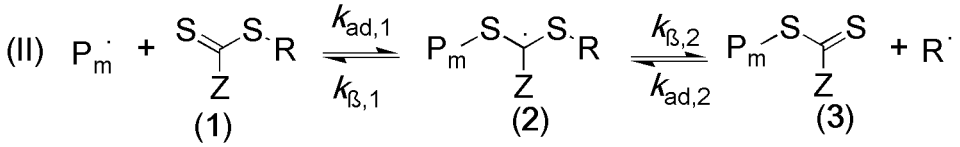

III. Propagation

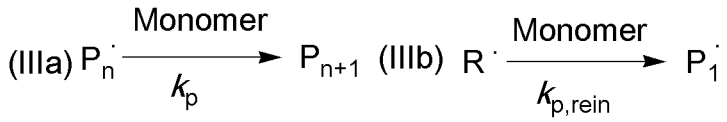

IV. Main Equilibrium

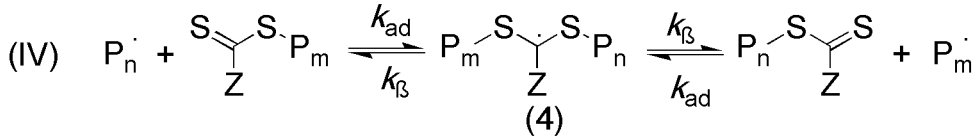

V. Termination

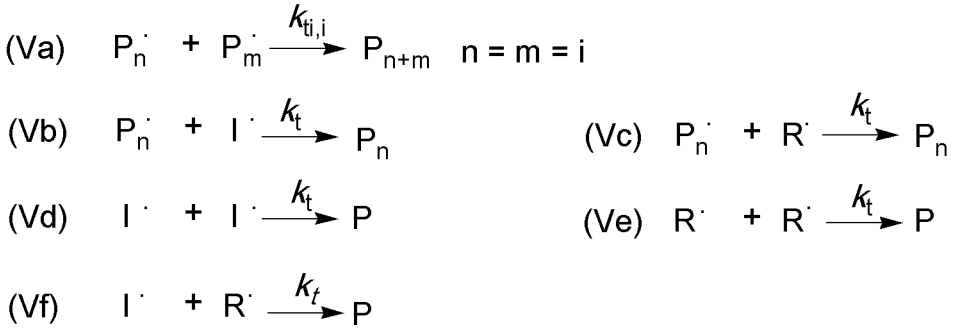

Scheme 2.4 Currently accepted fundamental mechanism of reversible addition-fragmentation chain transfer (RAFT) process

In an ideal RAFT process, the RAFT agent should behave as a perfect transfer agent. Therefore, as with radical polymerization with conventional chain transfer, the kinetics of polymerization should not be directly affected beyond those effects attributable to the differing molecular weights of the reacting species *i.e.* chain length dependent effects.[47] However, RAFT polymerizations can also stray from the ideal situation.[66]

2.2.2.3.1 Deviation from Ideal RAFT Processes

Although the basic mechanism shown in **Scheme 2.4** is generally not disputed, much debate continues on the kinetics of the RAFT process, the rapidity with which the various equilibria are established and what side reactions might occur to complicate the process, the kinetics and polymer synthesis.[66]

In an ideal RAFT process, addition and fragmentation are fast reactions compared to chain growth and the equilibrium constant, K_{eq}, should be low. Usually, the lifetimes of the intermediate radical species (**2**) or (**4**) are highly dependent on the structure of the leaving groups and especially the stabilizing Z group. Depending on the chemical structure of these R-, P or Z-groups and on the monomer to be polymerized, the rate of fragmentation can be significantly lower than the rate of addition reaction thus yielding a larger K_{eq}.[66,67] In this case, K_{eq} is extremely large; radicals are stored in the intermediate radical species to significant amount thus reducing the average concentration of free radicals until a steady state is reached. Due to this, the whole polymerization rate is reduced. In addition high K_{eq} values favor cross-termination reaction of the intermediate radicals either with propagating radicals or possibly themselves.

While the rate retardation in RAFT polymerization can be adequately described by high values of K_{eq}, termination of the intermediate radical species (**2**) or (**4**) can lead to deceleration of polymerization rate as well.[68] Potentially, the intermediate radical can terminate with a free radical or with a radical of its own species. Whether the rate retardation is caused *via* slow fragmentation of intermediate radicals or cross termination of these species is not yet completely clear. The solution to this question is system dependent, however, Perrier *et al.* has proposed a compromising solution to this problem.[69]

2.3 Macromolecular Architectures *via* Controlled Radical Polymerization (CRP)

The high concentration of dormant radical species in controlled/living free radical polymerizations opens up a number of possibilities for the synthesis of complex macromolecular architectures as shown in **Figure 2.2**. One of the prime advantage of these controlled/living systems as compared to traditional free radical procedures are very low occurrence of side reactions such as radical-radical chain coupling.

Controlled/living free radical polymerization[70,71] and their combinations serve as a very important method for the synthesis of well-defined polymeric materials with pre-determined properties. Examples of the variety of applications are shown in **Figure 2.2**. In the following section various architectures achieved *via* CRP techniques are briefly discussed.

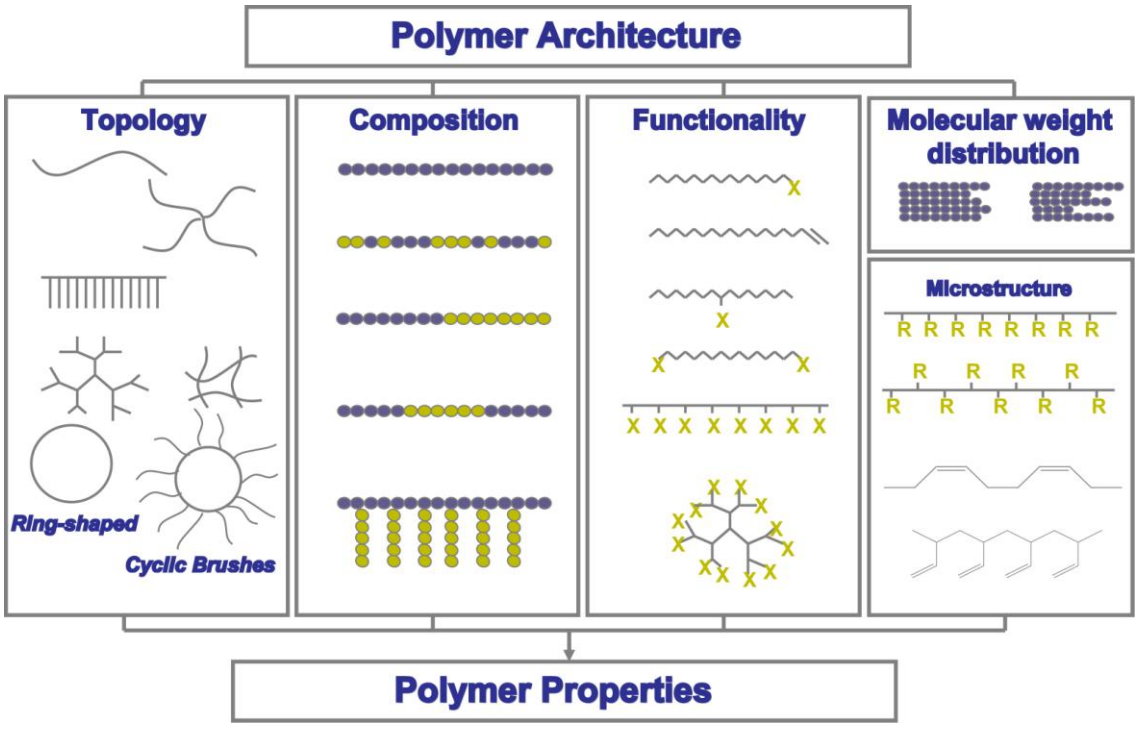

Figure 2.2 Representative examples of complex architectures achieved *via* controlled/living free radical polymerization [Figure adapted from the lecture script of Prof. Dr. Christopher Barner-Kowollik "Synthetic Polymer Chemistry" (the original source was adapted from Prof. Dr. A. H. E. Müller, Bayreuth, with kind permission)]

2.3.1 Star Polymers

Star polymers have linear branches of controlled molecular weight linked to a common core. Star polymers can be synthesized *via* various controlled radical polymerization methods, some of which are discussed below:

1) *Using Multi-Functional Initiators:* Multi-functional initiators (**5**) are compounds capable of simultaneously initiating several polymer chains to form the arms of the star polymer, while the remaining moiety composes the core of the star. ATRP polymerization (as shown in **Scheme 2.5,** core first approach) initiated by tetra- and hexa-functional initiators have been used for the polymerization of variety of monomers (**6**).[72,73]

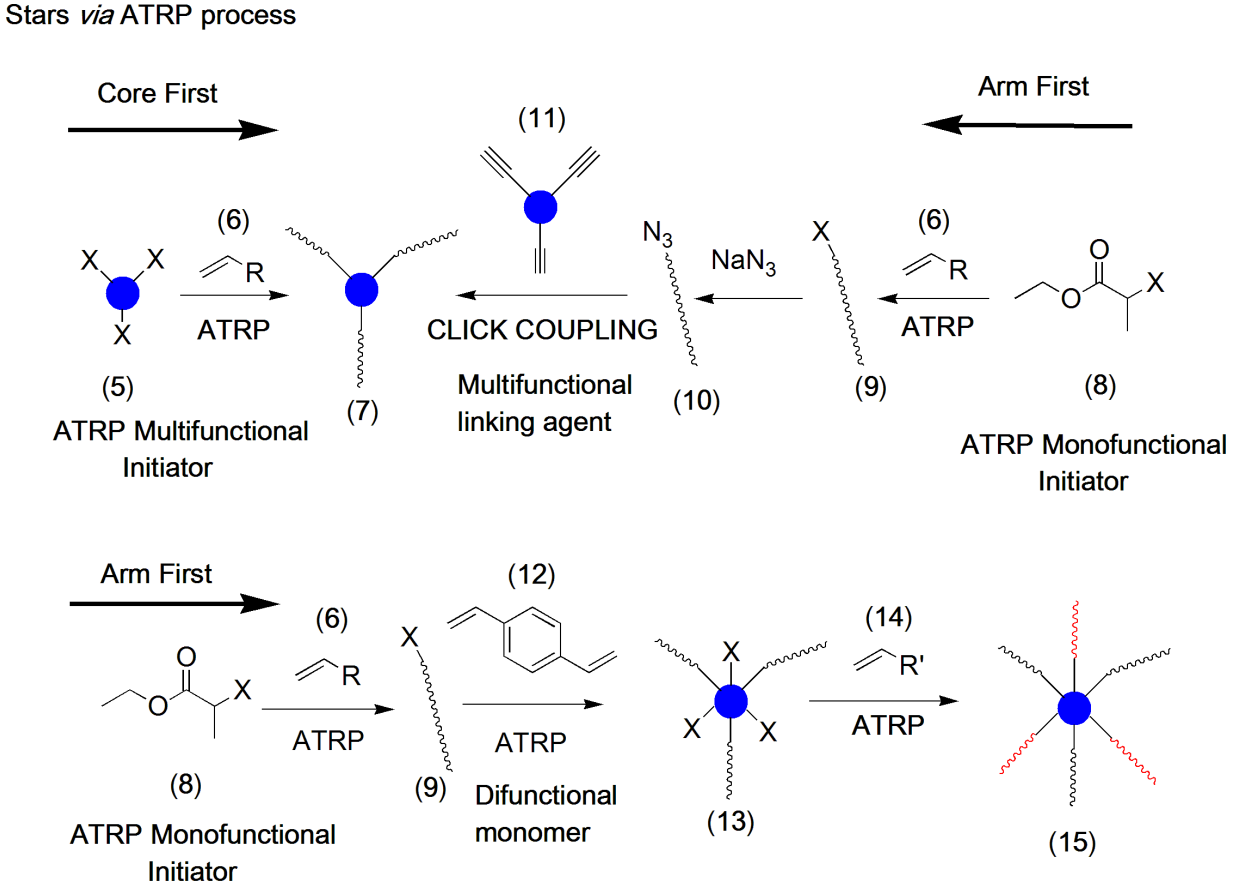

Scheme 2.5 Variable approaches to star polymers (core first and arms first) *via* the ATRP technique. The Figure is adapted from reference 70

The core first approach employs multifunctional initiators. The number of arms achieved is directly related to the number of initiating sites on the core. The RAFT technique (as shown in **Scheme 2.6**) is also being utilized for the construction of star-shaped structures. This has been achieved either *via* the synthesis of dendritic multifunctional RAFT initiators[74] carrying 6 and 12 external 3-benzylsulfanylthiocarbonylsulfanylpropionic acid groups or *via* a series of multi-thiocarbonyl compounds with 2, 4, 6 or 8 functional groups[75] which are subsequently used as chain transfer agents for the synthesis of star polymers. This is similar to core first process used for generation of stars polymers using ATRP approach. However, unique to the RAFT process is division of this core first approach into R-group and Z-group approach which is shown in **Scheme 2.6**. In the synthesis of stars *via* R group approach, the RAFT agent is attached to the core *via* R-group while in the Z-group approach, the RAFT agent is attached to the core *via* Z-group. As shown in **Scheme 2.6**, in the Z-group approach, the RAFT agent stays permanently attached to the core and the core will not carry any propagating radical functions. In this case, propagation occurs exclusively in the solution surrounding the core. In contrast, in the R-group approach, the dithioester moiety leaves the core structure and mediates the polymerization detached from the core, while the core itself becomes a radical. Because of the generation of the radical centre on the core, the core can undergo coupling reactions and this may in turn prevent the formation of well-defined macromolecular material. It thus seems apt that Z-group architecture is always preferred over R-group approach as it avoids the formation of higher order coupling products. The Z-group approach generally leads to generation of extremely pure star polymer products up to high monomer-to-polymer conversions without the added complexity of cross coupling reactions.

2) *Using Multifunctional Linking Agents:* Multifunctional linking agents (**11**) are compounds with several reactive sites (as shown in **Scheme 2.5,** arm first approach) which can react with living chains. They represent the most efficient way to synthesize well-defined stars polymers due to the absolute control afforded by all the synthetic steps. The combination of ATRP and copper catalyzed azide-alkyne cycloaddition

(CuAAC) chemistry has been used for the synthesis of three- and four-arm polystyrene stars.[76]

Stars *via* RAFT process

Via a Z-group approach

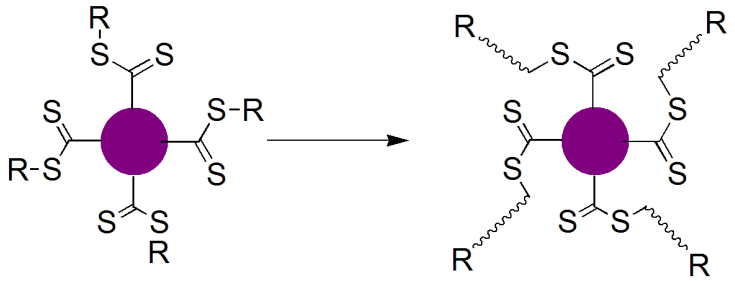

Via a R-group approach

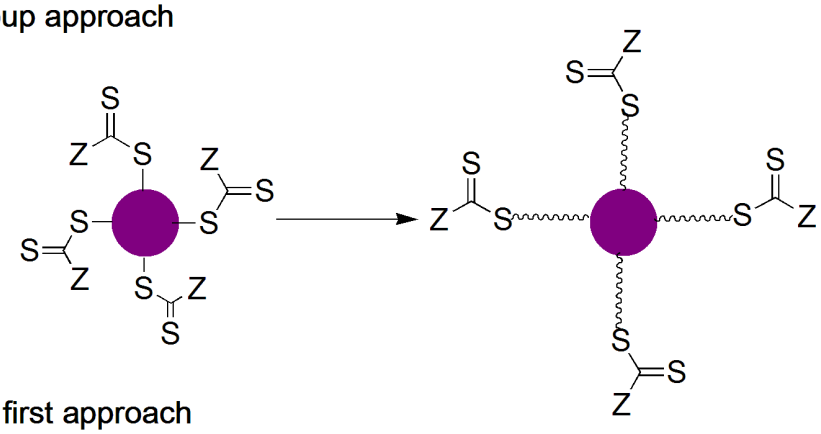

Via an arm first approach

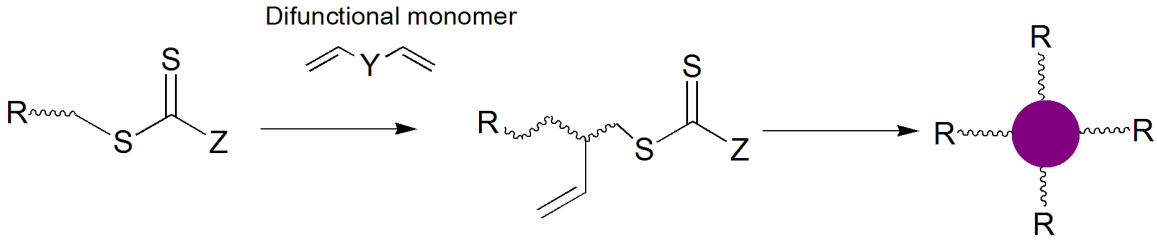

Scheme 2.6 Synthesis of star polymers *via* RAFT process utilizing R-group and Z-groups approach. The Figure is adapted from reference 76

3) *Using Difunctional Monomers:* In this method, an end-reactive polymer precursor (synthesized *via* controlled polymerization technique (**9**)) is used as initiator for the polymerization of a small amount of a suitable difunctional monomer (**12**). This leads to

the formation of star shaped structure or microgels with controlled branch lengths and cross-linked cores as shown in **Scheme 2.5**. The RAFT process also makes use of difunctional monomer when star polymers are synthesized using an arm first approach as shown in **Scheme 2.6**. The RAFT process is applied for the synthesis of polystyrene-microgels, using polystyrene macro-RAFT and divinyl benzene as cross-linker.[77] A variety of star-block copolymers have been synthesized using this difunctional monomer methodology, for example, using TEMPO star-block copolymers with a great variety of chemically different chains, in terms of molecular weight and composition, were synthesized.[78] The difunctional monomer methodology and ATRP were employed for the synthesis of polystyrene (PS) and poly(*t*-butyl acrylate) (P*t*-BA) star copolymers.[79]

2.3.2 Comb Polymers and Graft Polymers

Comb polymers and graft copolymers are composed of a main polymer chain, the backbone, to which one or more side chains, branches, are chemically connected through covalent bonds. Three general methods have been developed for the synthesis of graft polymers: (1) *grafting-from*, (2) *grafting-to* and (3) *grafting-through*, all of which are shown in **Figure 2.3**.

1) *Grafting-from*: In the *grafting-from* method, the backbone contains active sites which are capable of initiating polymerization of a second monomer. It is often used to synthesize graft copolymers with different composition of the backbone to the side chains. The *grafting-from* approach is the most common method and is similar to the core first approach for the synthesis of stars. A combination of metallocene and NMP[80] has been utilized for the synthesis of polypropylene-*g*-polystyrene copolymers. In this case, the backbone is synthesized *via* metallocene copolymerization of propylene and TEMPO functionalized derivative. The TEMPO was subsequently used for the polymerization of styrene by NMP.

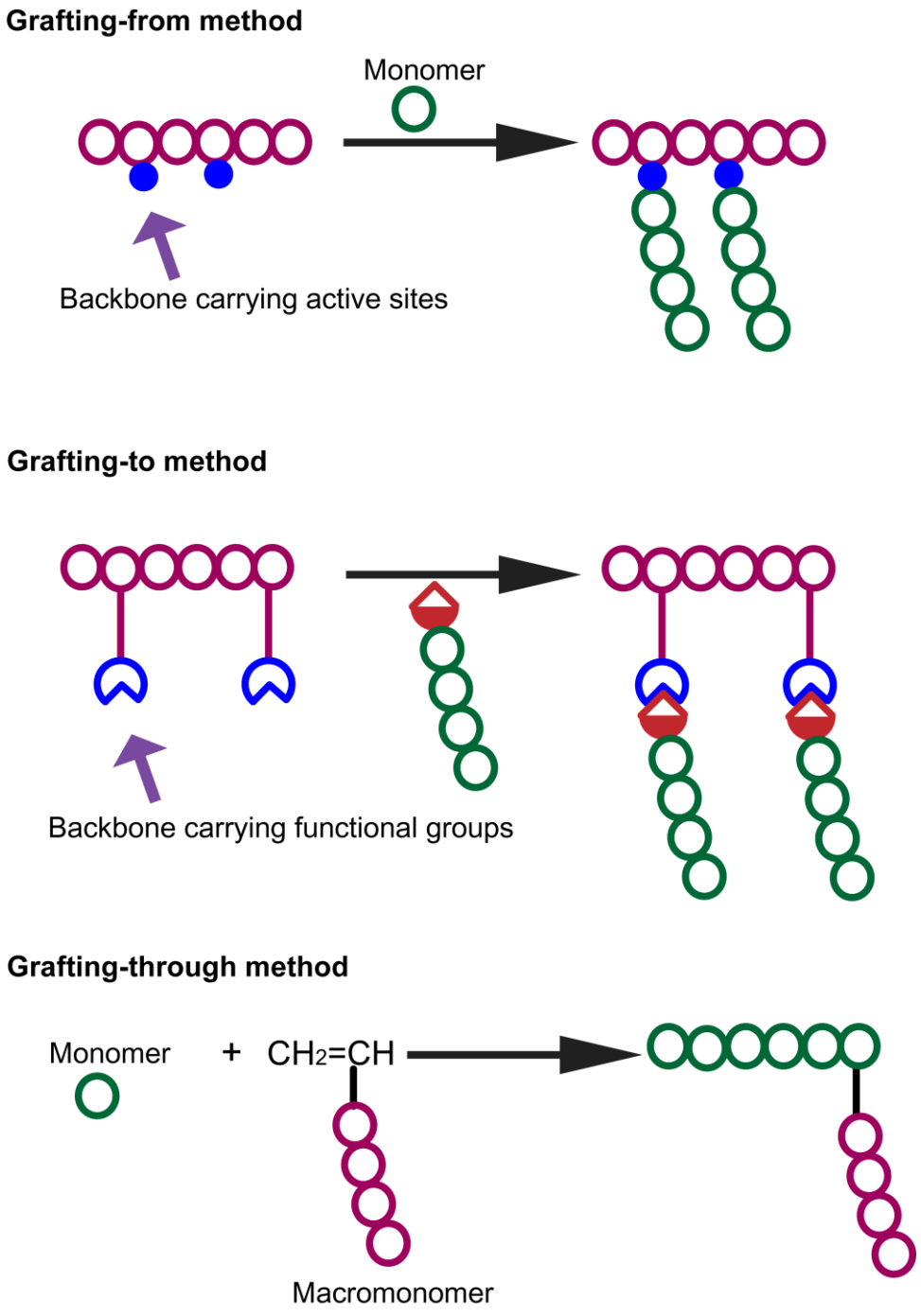

Figure 2.3 *Grafting-from*, *grafting-to* and *grafting-through* methods for the synthesis of comb and graft polymers

Using ATRP an elaborate range of macromolecular brushes has been synthesized, for example, in the synthesis of poly(2-hydroxyethyl methacrylate)-*g*-polystyrene (PHEMA-*g*-PS) and PHEMA-*g*-poly(*n*-butyl acrylate),[81] block-brush

copolymers of type poly(octadecyl methacrylate)-*b*-poly(2-bromopropionyloxy)ethyl methacrylate-*g*-*n*-butyl acrylate)[82] and copolymers of poly(vinyl chloride) with various grafted chains, *e.g.* poly(*n*-butyl acrylate), poly(methyl methacrylate)and polystyrene.[83] The RAFT process is also used extensively for the synthesis of comb polymers *via* attachment of RAFT agent *via* R- or Z-group and its mechanism is similar to the synthesis of star polymers using RAFT approach.[84]

2) *Grafting-to approach:* The *grafting-to* method involves reaction of preformed polymeric chains carrying active chain ends. It is very similar to arm first approach used for the synthesis of star polymers as shown in **Scheme 2.5**. CuAAC is widely used for *grafting-to* methods.[85]

3) *Grafting-through* approach: In *grafting-through* method,[86] monofunctional macromonomers are utilized as comonomer together with a low-molecular weight monomer, which permits the incorporation of macromonomer prepared by other controlled polymerization processes into the backbone of polymer synthesized *via* CRP technique.[87,88]

2.3.3 Other Macromolecular Architectures

A variety of complex architectures can be achieved *via* combination of various CRP techniques with other polymerization techniques like polycondensation and ring-opening polymerization to facilitate the synthesis of hyperbranched polymers,[89-91] dendritic structures,[92] microgels[93] and cyclic polymers.[94]

Other than achieving complex macromolecular architectures, CRP is advantageous for the preparation of copolymers with precisely controlled composition. CRP combines facile cross-propagation with controlled/living character that can be applied to many monomers. Using CRP it is possible to incorporate functionalities into specific parts of polymer chains.[95] This is not possible using radical polymerization as it is not as tolerant to many polar groups as is CRP.

2.4 Macromolecular Surface Engineering

Polymer grafting techniques provide a versatile tool to modify the surface of materials. These techniques can be categorized into *grafting-to* and *grafting-from* approaches. These grafting approaches are similar to the one used for the synthesis of comb polymeric structures but the principle difference is that instead of the polymeric backbone the grafting is carried out on surfaces. In the *grafting-to* technique, the polymer (bearing an appropriate functional group) reacts with the material surface to form covalently attached chains, whilst in the *grafting-from* approach, polymerization initiators are initially anchored to the surface and subsequently used to initiate the polymerization of monomers from the surface (as illustrated in **Figure 2.3**).

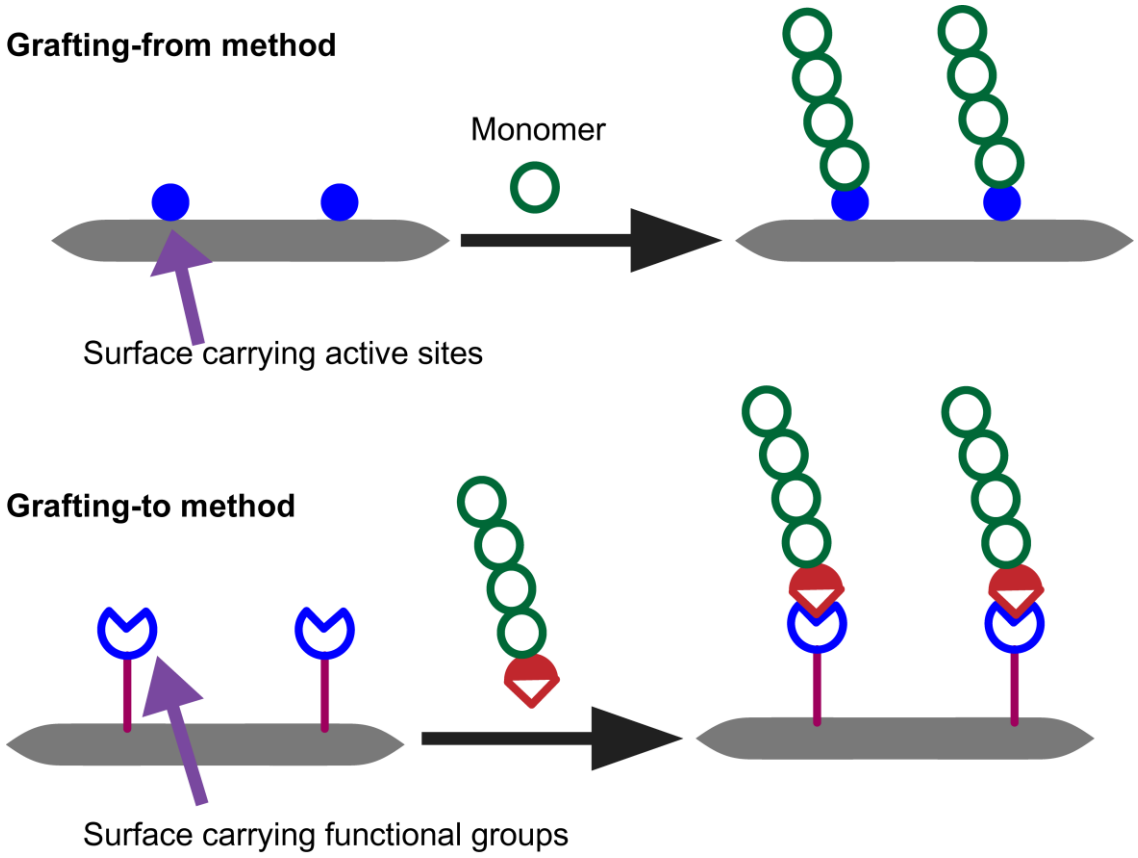

Figure 2.4 Modification of surfaces using *grafting-from* and *grafting-to* approach

The *grafting-from* approach can be coupled with various living/controlled free radical polymerization techniques, *e.g.* NMP,[96-98] ATRP[99-101] and RAFT.[102,103] RAFT

polymerization has already been widely used to generate complex macromolecular architectures with well-defined end groups and narrow polydispersity,[104-107] whereas Barner and co-workers employed RAFT polymerization to exert additional control over the design of core-shell divinylbenzene (DVB) microspheres and functional particles.[108-111] Polymerization techniques including cationic, anionic and ring-opening metathesis in combination with controlled radical polymerizations makes it possible to provide considerable control over both the structure of the polymer to be grafted onto the material surface and the surface grafting densities. The combination of these polymerization methods with polymer grafting techniques has been successfully used as an approach to modify a number of surfaces with a variety of functional polymers.

With respect to the modification of surfaces using the *grafting-to* approach, *click* chemistry[112-114] is preferentially employed and is generating significant interest for the alteration of surfaces as it represents a convenient strategy for the highly efficient coupling of chemical species onto solid substrates.

2.4.1 *Click* Chemistry

The *click* concept (or philosophy) was first reported in 2001 by Sharpless[112] with the objective to establish an ideal set of efficient and highly selective reactions in synthetic chemistry. However, directed by efforts to make *click* reactions more regiospecific, the turning point came with the discovery that Cu(I) not only promotes the rate of the Huisgen 1,3-dipolar cycloaddition[115,116] but also the regiospecificity with the exclusive generation of the 1,4-triazole isomer. Meldal *et al.*[113] outlined the use of Cu(I) in the cycloaddition reaction for a triazole synthesis on a solid phase. The reaction was an organic solvent based procedure that used copper (I) iodide with *N,N*-diisopropylethylamine (DIPEA) in various solvents with the terminal alkyne immobilized on a swollen solid support. These initial reports were closely followed by the study of Fokin and Sharpless *et al.*[117] which demonstrated that the azide-alkyne coupling reaction is highly regiospecific when carried out in an aqueous phase employing copper sulfate and sodium ascorbate. Since then these reactions have found numerous applications in fields as diverse as drug discovery and material sciences.[118-123]

The required process characteristics for a *click* reaction in general include mild and non-demanding reaction conditions (ideally, the process should be insensitive to oxygen and water), readily available starting materials and reagents, the use of no solvent or a solvent that is benign (such as water) or easily removable, as well as simple product isolation. Purification – if required – must be by non-chromatographic methods, such as crystallization or distillation and the product should be stable under physiological conditions. In chemical terms, a *click* reaction must be orthogonal (*i.e.* highly specific and regioselective).

Some of the required characteristics of *click* reactions are achieved by chemical transformations having a high thermodynamic driving force, usually close to 80 $kJ \cdot mol^{-1}$. Such processes proceed rapidly to completion and also tend to be highly selective towards a single product. Common examples of *click* reactions (as shown in **Scheme 2.7**) are:

1) Cycloaddition reactions of unsaturated species, especially 1,3-dipolar cycloaddition reactions and Diels-Alder type cycloadditions.[124,125]

2) Nucleophilic substitution chemistry, particularly ring-opening reactions[126-128] of strained heterocycles such as epoxides, aziridines, aziridinium ions and episulfonium ions.

3) Carbonyl chemistry of 'non-aldol' type reactions, such as the formation of ureas, thioureas, aromatic heterocycles, oxime ethers, hydrazones as well as amides.[129]

4) Additions to carbon-carbon multiple bonds, especially oxidative cases such as epoxidation,[130-132] dihydroxylation,[133] aziridination[134,135] and sulfenyl halide addition, also Michael additions of Nu-H reactants.

Cycloadditions of unsaturated species

1,3-dipolar cycloaddition

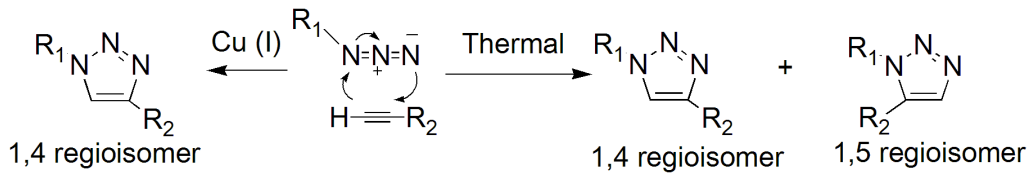

Diels-Alder cycloaddition

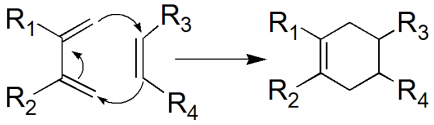

Ring opening reactions of strained heterocycles

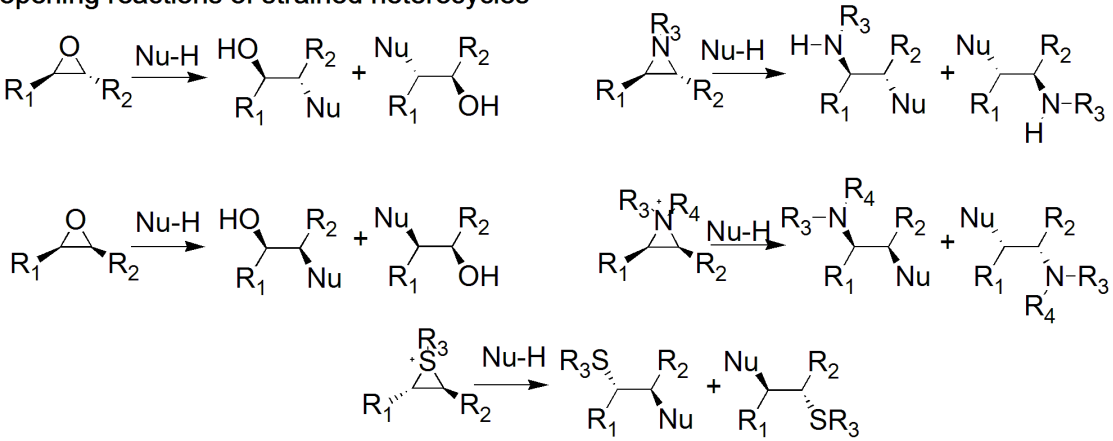

Carbonyl chemistry of non-aldol type

Synthesis of oxime ethers

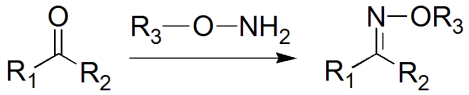

Synthesis of amides

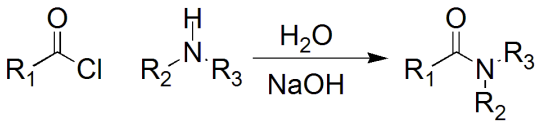

Addition to carbon-carbon multiple bonds

Epoxidation

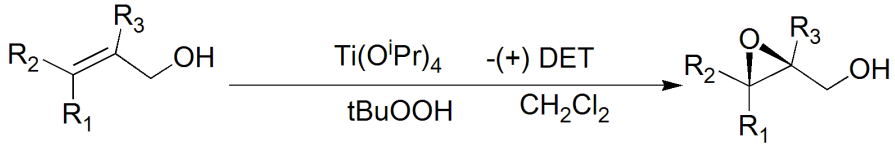

Dihydroxylation

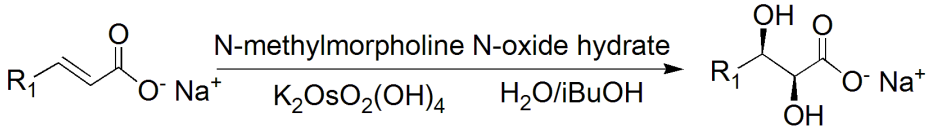

Scheme 2.7 Generalized *click* reaction sequences described in text

The archetypal example of *click* chemistry is undoubtedly the copper catalyzed Huisgen 1,3-dipolar cycloaddition of azides and terminal alkynes. In the absence of an appropriate catalyst, the reaction is usually slow as alkynes are poor 1,3-dipole acceptors. However, in the presence of Cu(I), which can bind to terminal alkynes, cycloaddition reactions are dramatically accelerated, regioselective and highly efficient (yields are often above 95 %). Moreover, the copper-catalyzed azide-alkyne cycloaddition (CuAAC) reaction can be performed in various solvents (including water) and in the presence of numerous other functional groups.

A further popular *click* reaction is the Diels-Alder (DA) reaction. The [4+2] cycloaddition reaction between a diene and a dienophile is one of the most elegant and efficient transformations in organic chemistry. The high regio- and stereo-selectivity typically displayed by this cycloaddition, the ease of execution and the feature that during its course up to four new stereocenters may be created simultaneously, have resulted in innumerable applications for this transformation in the construction of highly complex targets, *e.g.* in the total synthesis of natural products.[136-140] Consequently, various chiral auxiliaries and catalysts for asymmetric Diels-Alder reactions were developed and the steric steering of this important transformation is now possible with very high levels of selectivity and practicability.

The pivotal role which the carbo Diels-Alder reaction often plays in the construction of carbocycles[141-145] is mirrored by the hetero Diels-Alder reaction in the regio- and stereo-selective synthesis of heterocycles. Recently, DA reactions have attracted significant attention in macromolecular chemistry, particularly for providing new materials[146-149,14] and as an exceedingly useful tool for bioconjugation procedures.[150] In addition, Cu(I)-catalyzed Huisgen 1,3-dipolar cycloaddition and Diels–Alder [4+2] reactions are the foremost members of the *click* reaction family and have received growing interest for the preparation of non-linear macromolecular structures with varying composition and topology.[151] However, as discussed earlier both the approaches have certain limitations.

To overcome the limitations of classical *click* reaction, recently our laboratory described the conversion of electron deficient dithioester end-groups of RAFT polymers *via* hetero-Diels-Alder (HDA) cycloaddition with suitable dienes. When diene or

dienophile have a heteroatom like nitrogen, oxygen or sulfur in the conjugated system, they are called heterodynes or heterodienophiles and the reactions are called hetero-Diels-Alder reactions. The RAFT-HDA chemistry is based on a hetero Diels-Alder conjugation in which the dienophile is the thiocarbonyl thio functional RAFT agent. It is used sequentially for two purposes first for controlling the polymerization reactions and subsequently as the reactive heterodienophile in the HDA cycloaddition with an appropriate diene as depicted in **Figure 2.5**.

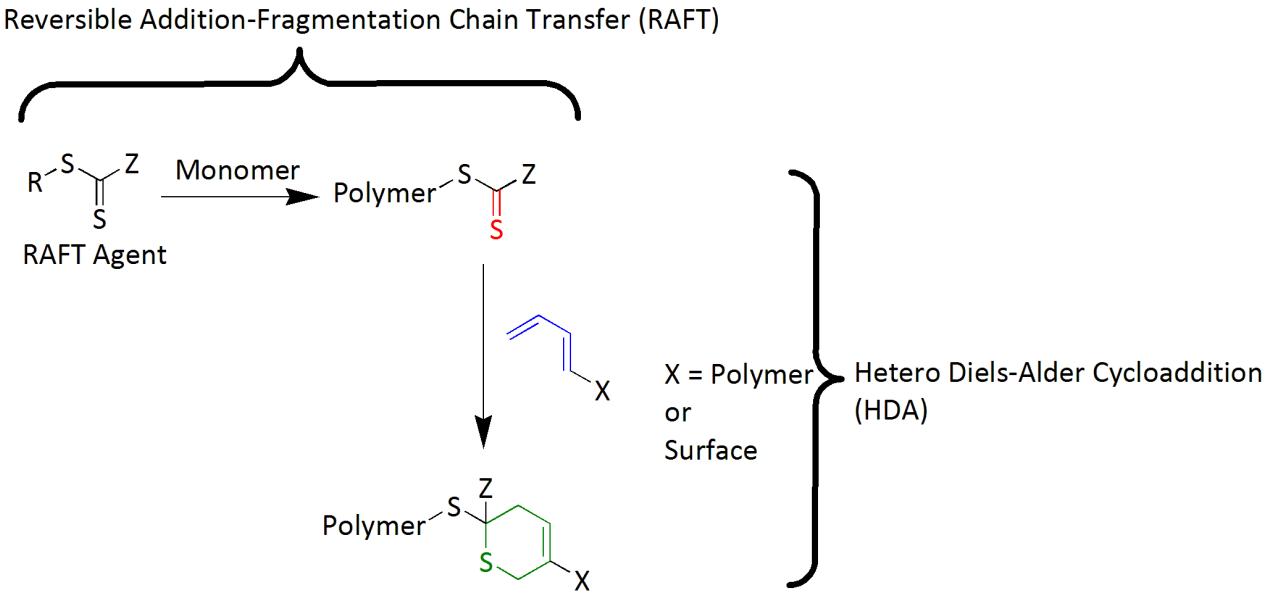

Figure 2.5 General concept for the synthesis of polymer conjugates using the RAFT-HDA approach

The rate of (hetero) Diels-Alder reactions are influenced to a great extent by the substituent which is attached to diene or (hetero) dienophilic moiety. Usually Diels-Alder reactions take place faster if the dienophile has electron-withdrawing groups on it. The electron-donating groups on the diene also have a positive effect on the rate. This is explained most readily from the frontier orbitals. A donor substituent on the diene raises the energy of its HOMO and an electron-withdrawing substituent on the dienophile lowers the energy of its LUMO (as shown in **Figure 2.6**), bringing the two orbitals closer together in energy. The orbitals closer in energy interact more strongly than those far

apart, therefore, the energy of the transition state is lower than it was without the substituents, making the reaction faster.

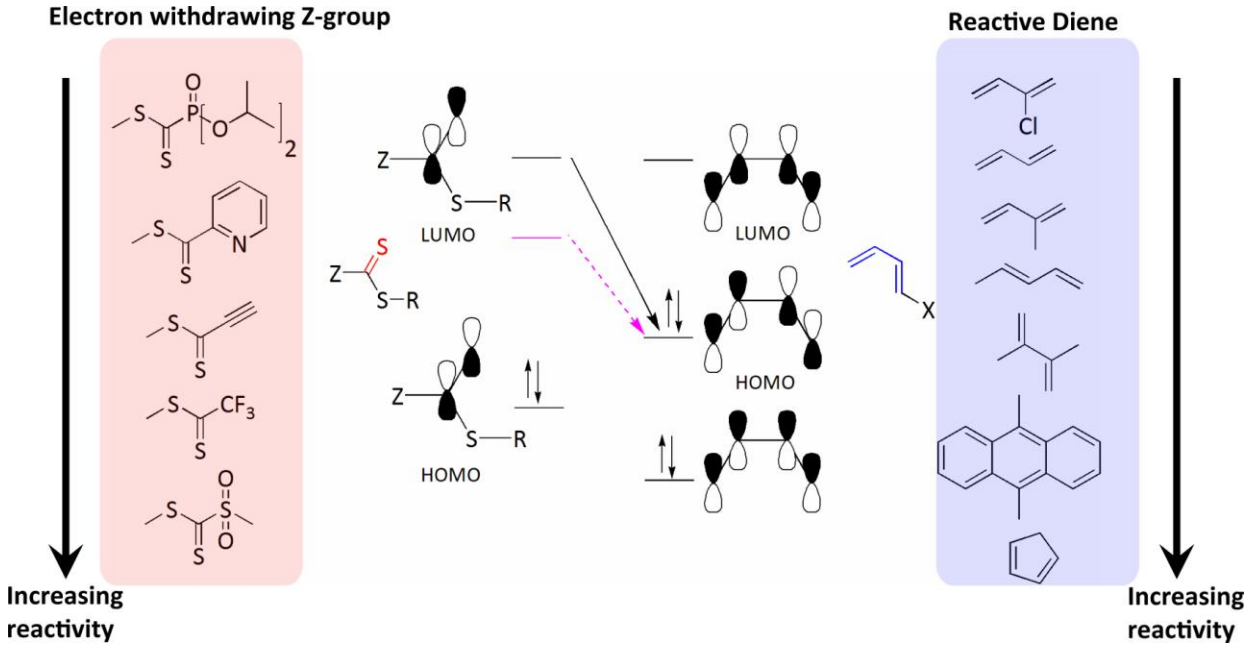

Figure 2.6 Orbital overlap between diene and dienophile in RAFT-HDA approach

Taking into consideration the substituent effects on HDA reactions, the dithioesters for RAFT-HDA reaction have to be suitably chosen as the general ability of dithioesters to undergo HDA cycloadditions, which leads to the formation of 3,6-dihydro-2*H*-thiopyran heterocycles, is rather low.[152] The ability of dipolarophiles containing hetero-atoms to undergo addition is often inferior to structurally analogous C,C-dipolarophiles; however, the highly polarizable C=S double bond frequently constitutes an exception. These thiocarbonyls are efficient dienophiles undergoing Diels-Alder cycloaddition with the reaction occurring preferentially at the C=S π bond. The ability of thiocarbonyl group to act as a dienophile has been shown in several examples involving thioaldehyde, thioketones and dithioesters.[153,154] These cycloadditions which afford dihydrothiopyran derivatives have found interesting applications for the synthesis of natural products or their analogues.[155-157] When the thiocarbonyl group is α-substituted with an electron-withdrawing group (CN,[158] COOEt,[159] CF_3,[160] SO_2R[161]), which lowers its

LUMO, it becomes an efficient heterodienophile. Thus, it can be used as an efficient heterodienophile under mild conditions to obtain functionalized dihydrothiopyran.

In the RAFT-HDA approach, in addition to being a good dienophile for HDA reaction, the dithioesters should function as efficient controlling agent in the RAFT process. The amount of literature on dithioesters which are good dienophile as well as efficient RAFT agent is limited. Two dithioesters (phosphoryldithioformates[162] and pyridyl dithioesters[163]) have been reported to display high heterodienophilicity as well as good controlling agents in RAFT process. In the case of the above thiocarbonyl thio compounds, for small molecule hetero Diels-Alder investigations,[164-166] a 10:1 molar ratio of diene to dienophile was used at temperatures ranging from 25 °C to 50 °C and in the presence of Lewis acid catalyst.

The reactivity of dienes in cycloaddition reactions has been studied by Sauer *et al.*[167] **Figure 2.7** shows the reactivity of a range of dienes towards Diels-Alder reaction with maleic anhydride (dienophile). The reactivities of cyclic and quasi-cyclic dienes have considerably higher reactivity as compared to acyclic dienes. The influence of steric factors is also substantial. Electron-donating substituents on the diene usually accelerate the reaction whereas electron acceptors retard it.

Thus, it is possible to significantly enhance the rate of RAFT-HDA conjugation by using two approaches (as shown in **Figure 2.6**). Firstly, by employing a very reactive diene *i.e.* through the use of novel cyclopentadienyl (Cp) functionalized polymers.[168] By virtue of such Cp-capped polymers it is possible to achieve conjugation under ambient conditions within a few minutes, although a catalyst is in some cases required. Secondly – and this approach is explored in the current research (discussed in detail in **Chapter 4**) – RAFT agents featuring extremely electron withdrawing moieties in the Z-position can be employed so that even less reactive dienes (*e.g.* based on butadiene, which is a much less reactive diene compared to cyclopentadiene) can be conjugated at ambient temperatures and in the absence of catalysts.

Using this atom-economical RAFT-HDA approach, polymer conjugates such as block copolymers,[146] star-shaped polymers,[147] star-shaped block copolymers[148] and surface modified microspheres[14,28] (discussed in detail in **Chapter 5**) as well as silicon surfaces[27] (discussed in detail in **Chapter 7**) are successfully generated.

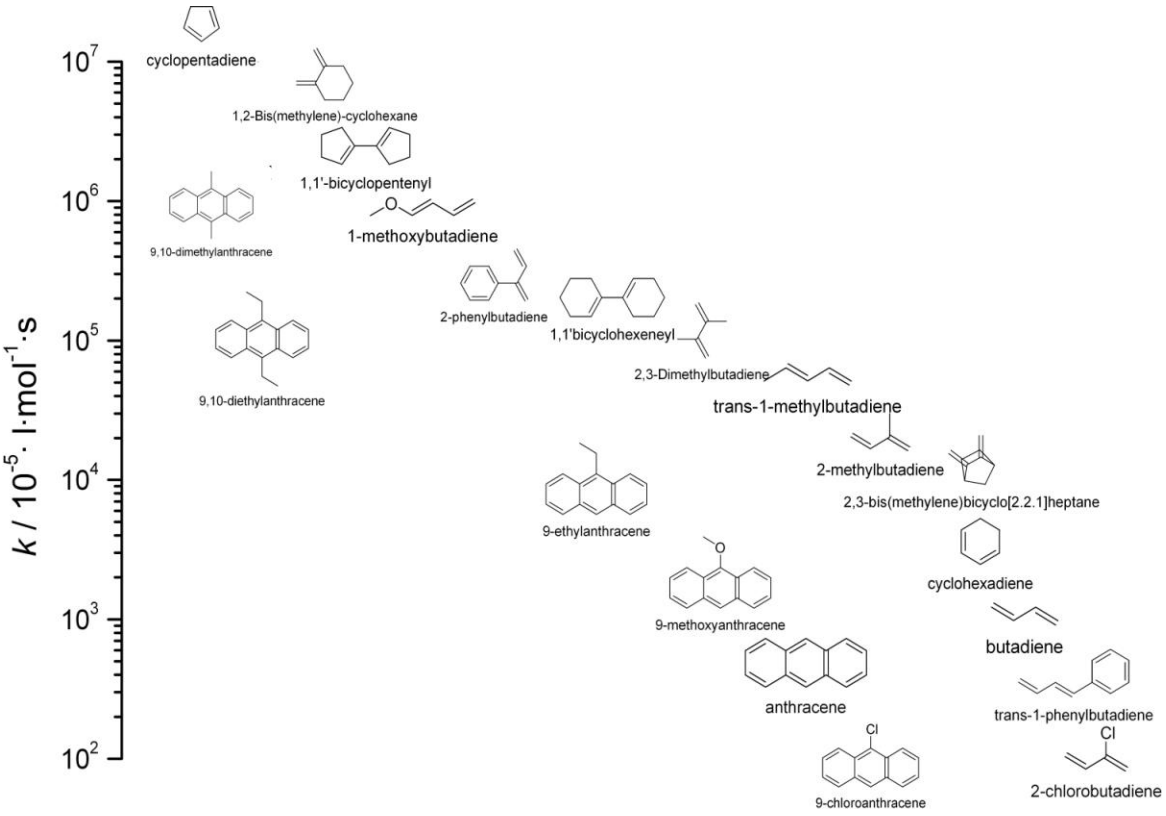

Figure 2.7 Reactivity of variable dienes in Diels-Alder reactions with maleic anhydride (dienophile). The relative rate coefficients are taken from reference 167

2.4.2 Surfaces Modified Using *Click* Chemistry

Click chemistry is widely employed to achieve efficient surface modifications of materials ranging from gold and silica nano-particles, polymeric films and microspheres to fullerenes as well as carbon nanotubes. In addition, the functionalization of surfaces with biomolecules is also possible *via click* chemistry. In the following section, the current state of the art available for the modification of surfaces which are also studied in the current research work is discussed.

2.4.2.1 Polymeric Microspheres

Polymeric microspheres are highly cross-linked particles, having a spherical shape and a narrow size distribution. Polymeric microspheres can be synthesized directly by heterogeneous polymerization techniques, *e.g.* emulsion and dispersion polymerization. In addition, highly crosslinked mono- and narrow-disperse poly(divinyl

benzene) (DVB) microspheres can be synthesised *via* precipitation[169] and distillation precipitation polymerization.[170] The synthesis of monodisperse and highly cross-linked poly(DVB) microspheres *via* precipitation polymerization was reported first time by Stöver and co-workers.[171] A typical precipitation polymerization technique requires a monomer (*e.g.* DVB which also functions as a cross-linker), a radical initiator (*e.g.* AIBN), and a near Θ-solvent for DVB (*e.g.* acetonitrile). The particle formation process involves a nucleation step followed by the growth of the particles. Downey et al.[172] proposed the hypothesis for the particle formation, according to which particle formation consists of two stages: nucleation and growth. Nucleation likely starts by aggregation of soluble oligomers to form swollen microgels which subsequently desolvate to form the particle nuclei. Throughout the polymerization, soluble oligomer radicals are captured from solution by the vinyl groups on the particle surface. In particular, a reactive, entropic capture mechanism, as opposed to one that is solely driven by enthalpic desolvation and deposition of the forming polymer onto the particle surface. This hypothesis implies that the captured oligomers form the new particle surface, and hence even the final particles should contain surface vinyl groups. These residual vinyl groups open the possibility to graft a polymeric shell from or to an existing particle thus constituting an ideal synthetic handle for the preparation of core-shell microspheres and adding further functionalities to the particles. Functional polymeric microspheres have a high potential in medical and biomedical applications, such as drug delivery systems, in medical diagnostics, as contrast agents for X-ray imaging, as stationary phases for chromatography or for the detection of degradation products of chemical weapons.[173]

In general, for the functionalization of microspheres, two grafting techniques are widely used, *i.e. grafting-from* and *grafting-to* (discussed in detail in **section 2.4**). So far, a wide variety of techniques have been used to functionalize these microspheres, including controlled/living radical polymerization,[174] anionic ring-opening polymerization[175] and highly orthogonal *click* chemistry.[176]

Barner *et al.*[174] reported the synthesis of microspheres with RAFT end groups using 1-phenylethyl dithiobenzoate as the RAFT agent in precipitation polymerization.[169] Subsequently, these microspheres were modified with poly(styrene) *via* the *grafting-from* approach. Barner, Barner-Kowollik, Müller and colleagues[177] reported the

functionalization of DVB microspheres using thiol-ene chemistry and azide-alkyne *click* reactions *via* a *grafting-to* approach.

During the current thesis RAFT-HDA chemistry was utilized to successfully generate core-shell microspheres (discussed in detail in **Chapter 5 and 6**). In **Chapter 6**, the quantification of grafting density achieved on the microspheres using *grafting-to* approach is discussed. The grafting densities were obtained after functionalizing the microspheres with polymer chains of different molecular weights using elemental analysis technique. Several authors have reported grafting using surface-initiated living radical polymerization on a variety of surfaces, *e.g.*, inorganic solid surfaces[178-180] and organic polymer surfaces.[181-183] Most of these studies are focused on the control of molecular weight of the grafted polymer, while only limited attention has been paid on the quantification of grafting densities. However, Fukuda and coworkers[184,185] concentrated on the quantification of grafting densities as well as attempts to achieve high grafting densities on solid substrates. Fukuda and colleagues illustrated the advantages of living radical polymerization (LRP) techniques for surface-initiated graft polymerization over other surface grafting techniques. LRP has the advantage that it allows grafting of structures having controlled molecular weights with extremely high surface graft densities. Typically, the grafting densities (relating to the actual surface area and not the nominal surface area as employed in the current study) can be as high as 0.7 chains·nm^{-2} for common polymers such as polystyrene and poly(methyl methacrylate) on inorganic substrates. Such grafting densities are about 1 order of magnitude higher than those achieved using non-controlled techniques for tethering of the chains. In addition to inorganic substrates, Fukuda and coworkers reported the synthesis of high-density polymer brushes on polymer substrates. In this case, 2-hydroxyethyl methacrylate (HEMA) was graft-polymerized from the surface of a poly(tetrafluoroethylene-*co*-hexafluoropropylene) (FEP) film by reversible addition-fragmentation chain transfer (RAFT) mediated LRP. The actual grafting densities obtained in this case (0.3 chains·nm^{-2}) are similar to the graft densities obtained on silicon surfaces *via* RAFT polymerization.[184] Barner and Müller[175] recently reported the functionalization of DVB80 microspheres with poly(ethylene glycol) chains using a *grafting-from* approach *via* anionic polymerization techniques. These resulting

poly(divinylbenzene)-*graft*-poly(ethylene oxide) (PDVB-*g*-PEO) microspheres exhibit a nominal surface grafting density of 1.65-2.09 chains·nm^{-2}. Barner and colleagues estimated the grafting densities using two independent approaches; one approach is based on the particles' weight increase and the other is based on the quantification of the oxygen content of the grafted microspheres *via* elemental analysis. In the current work (discussed in detail in **Chapter 6**), elemental analysis is employed to quantify for the first time the grafting densities on microspheres modified *via* the *grafting-to* approach using RAFT-HDA chemistry. The quantification of the grafting density opens the possibility to investigate the influence of the molecular weight of the grafted chains on the grafting density and therefore to improve the engineering of functional microspheres.

In addition, an in-depth study of microspheres functionalized *via* the RAFT process using *grafting-from* approach using solid-state NMR technique is discussed in detail in **Chapter 8**. Being highly crosslinked, these systems are insoluble and must be characterized in the gel state or the solid-state. To the best of our knowledge, the only characterization of poly(divinyl benzene)-based microspheres in terms of residual vinyl groups was so far carried out qualitatively by infrared spectroscopy (IR).[172] IR spectroscopy detects the residual vinyl groups through resonances at 1 600 and 990 cm^{-1} Crosslinked polystyrene gels were characterized by high-resolution magic-angle spinning (HR-MAS) NMR spectroscopy.[186-189] Well-resolved ^{1}H and ^{13}C NMR spectra were obtained through efficient averaging of chain orientation along the axes between crosslinking points, allowing observing the chemical functionalization. However, it is unclear if the monomer units close to the crosslinking points are[190] contributing to the observed signals due to their slower local dynamics. Residual vinyl groups in poly(divinyl benzene)-based networks were analyzed by ^{13}C solid-state NMR spectroscopy and a wet chemical method, *e.g.* bromination. Noting that ^{13}C cross-polarization NMR is intrinsically not quantitative and that bromination is not quantitative because of side reactions and limited reagents accessibility to highly cross-linked regions, the authors concluded that no method is available yet for accurate, quantitative analysis of the residual vinyl groups. In the current thesis, solid-state NMR spectroscopy was applied for polymer systems exhibiting homogeneous local mobility and

homogeneous ^{1}H density, such as dry poly(divinyl benzene) microspheres, all sample parts contribute to the NMR signal without bias.

2.4.2.2 Silicon Surfaces

Considerable attention has been paid to the modification and control of the physiochemical properties of single-crystal silicon surfaces using the immobilization of dense polymer brushes. Such systems have potential importance within the modern microelectronics industry as well as in sensors and photovoltaic applications.[191]

The synthesis of self-assembled monolayers (SAMs) has been widely used for the modification of silicon surfaces. However, formation of well-defined silicon monolayers typically requires harsh and highly reactive conditions, thus limiting the compounds which can be immobilized. Now days, CuAAC has been widely used for the modification of silicon surfaces as the hydrogen terminated silicon surfaces can be directly functionalized with a number of molecules. Haensch *et al.*[192] reported the reversible and selective functionalization of silicon surfaces with supramolecular building blocks. They utilized the CuAAC reaction to covalently bind an acetylene functionalized Fe(II) bis-complex onto azide-terminated SAMs. This study showed that supramolecular systems can be opened (decomplexed) and closed (complexed) when they are assembled in monolayer systems, thus creating reversible responsive surfaces.

To demonstrate the applicability of CuAAC reactions to mesoporous materials, Ciampi *et al.*[193] reported the modification of porous silicon photonic crystals with the chemically versatile acetylene-terminated SAMs. Porous silicon (PSi) was used, as it can be conveniently tailored to prepare optical materials exhibiting a precise pattern of reflected light[194] (rugate filters) and also has potential for label-free biosensing applications. Cu(I)-catalyzed alkyne-azide cycloaddition reactions were employed to modify the internal pore surfaces through a two-step hydrosilylation/cycloaddition procedure. However, a positive outcome of this catalytic process in a spatially confined environment was only observed in the presence of a ligand-stabilized Cu(I) species. The porous silicon photonic crystal modified by the two-step strategy (as shown in **Figure 2.8**), here with oligoethers moieties on the surface, displayed improved

resistance toward the non-specific adsorption of proteins as determined with fluorescently labelled bovine serum albumin.

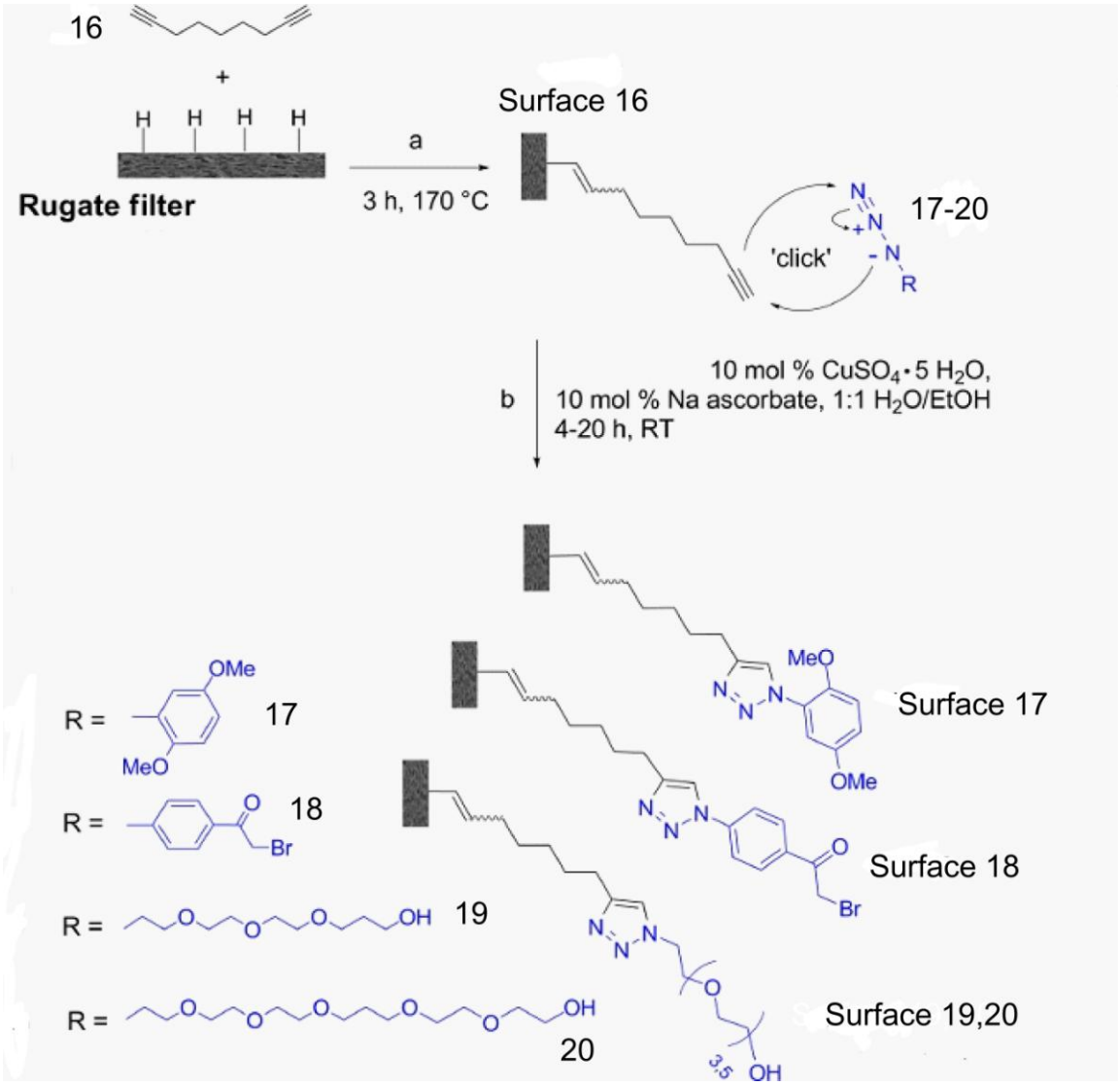

Figure 2.8 *Click* chemistry on acetylenyl PSi rugate filters. The preparation of a monolayer presenting an alkyne functionality (a) was followed by ligand-assisted *click* reaction with substituted azido species (b) to afford a nanostructured network presenting functionalities of interest. The Figure is adapted from reference 193

Ostaci *et al.*[195] presented a versatile method for grafting polymer brushes to passivated silicon surfaces based on the Cu(I)-catalyzed Huisgen 1,3-dipolar cycloaddition of ω-azido polymers and alkynyl-functionalized silicon substrates. Firstly,

silicon wafers were passivated by the deposition of a SAM of a monochlorosilane bearing alkyne functionality. Subsequently, three tailor-made ω-azido linear brush precursors, *i.e.* PEG-N_3, PMMA-N_3, and PS-N_3 (M_n ~ 20,000 g·mol^{-1}), were grafted to alkyne-functionalized SAMs *via click* chemistry.

All the examples shown above utilized CuAAC to achieve functionalization/modification of Si surface. To illustrate the feasibility of highly orthogonal RAFT-HDA approach for the modification of variable surfaces, the silicon wafers were modified with a stimuli responsive polymer using RAFT-HDA chemistry based on highly electron electron-deficient RAFT agents (discussed in detail in **Chapter 7**).

2.4.2.3 Fullerenes

The functionalization of fullerenes (C_{60}) with macromolecular building blocks is an interdisciplinary research area,[196] as the incorporation of fullerene identities into the macromolecular architectures provides an interesting way to combine the unique electronic and optical properties of fullerenes with the highly variable physiochemical properties of polymeric materials. The conjugation of fullerenes with synthetic macromolecules has led to a wide variety of new materials with finely tunable features and with the possibility of tuning their properties by modifying the chemical nature of the components and/or the nature of the chemical linkage between them. The area of fullerene functionalization with synthetic macromolecules is relatively extensive and C_{60} has been modified *via* various approaches.[197-199] Most chemical routes to achieve fullerene containing polymers include thermal- or photo-chemically induced polymerization in the presence of C_{60},[200] the amine addition of amino polymers onto C_{60} double bonds,[201] cycloaddition reactions of functionalized polymers with C_{60},[202,203] the addition of living poly(styryl)lithium chains onto C_{60}[204] as well as the grafting of C_{60} onto nucleophilic lithiated polyethylene surfaces.[205] Recent trends in polymer chemistry demonstrate that *click* chemistry has been an attractive route for the functionalization of fullerenes. CuAAC has been utilized in preparing various C_{60} hexakis adducts[206] and C_{60}-polymer conjugates[207] by equipping the surface of fullerenes with relatively low molecular weight azide or alkyne functionalities.

The [4+2] Diels-Alder reaction is also widely used to prepare stable fullerene adducts.[208,209] Fullerenes readily undergo Diels-Alder cycloadditions with a variety of reactive dienes, including anthracene and cyclopentadiene.[210,211] The applicability of Diels-Alder cycloaddition for the formation of polymer bound fullerenes was explored by Guhr *et al.*[210] They synthesized cyclopentadienyl functionalized polymeric resins which react rapidly with C_{60} under ambient conditions. In addition, they also reported that this Diels-Alder cycloaddition is readily reversible, allowing recovery of C_{60} upon heating of the resin. Most of the Diels-Alder modifications of the fullerenes using cyclopentadiene and anthracene has been carried out using small molecules, yet none of the reports has been concentrated on the functionalization of fullerenes employing cyclopentadiene and anthracene functionalized polymers. In the context of the current thesis, the facile (as well as rapid and ambient temperature) functionalization of fullerenes with cyclopentadienyl and anthracenyl functionalized poly(ethylene glycol) using Diels-Alder cycloadditions (discussed in detail in **Chapter 9**) is reported.

Chapter 3 Experimental and Characterization Techniques

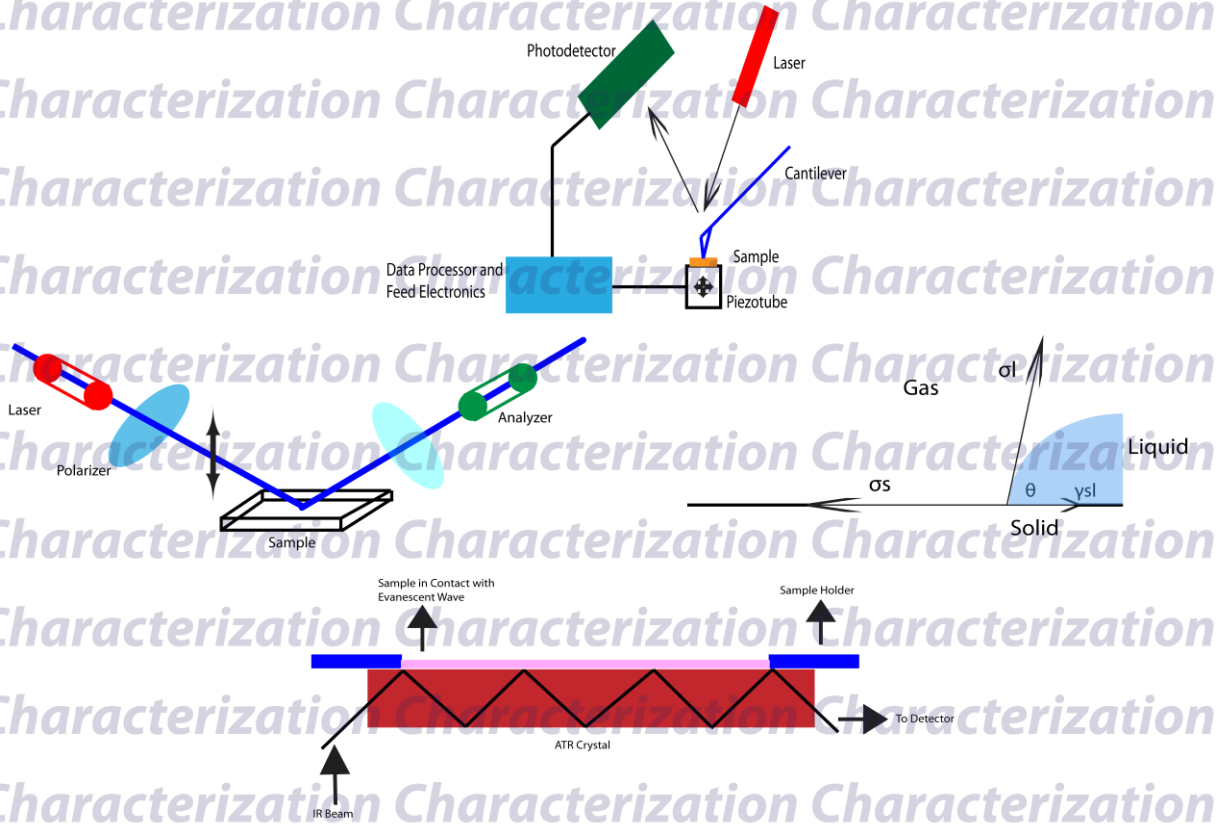

3.1 Materials

Divinyl benzene (tech. 80%, DVB80, Aldrich, divinylbenzene 80 contains 80% divinylbenzene and 20% ethylvinylbenzene), divinyl benzene (tech. 55%, DVB55, Aldrich, divinylbenzene 55 contains 55% divinylbenzene and 45% ethylvinylbenzene) styrene (99.9%, Aldrich), isobornyl acrylate (Technical grade Aldrich), *n*-butyl acrylate (99%, Fluka), methyl methacrylate (99%, Acros) were passed through a column of basic alumina (Brockmann I 50-200 μm, Acros) and stored at -18 °C prior to usage. *ε*-Caprolactone (99%, Alfa Aesar) was distilled over calcium hydride (≥90%, Sigma-Aldrich) and stored over molecular sieves (3 Å, BDH). 2,2'-Azoisobutyronitrile (AIBN, DuPont) was recrystallized twice from methanol before use and stored at -18 °C. Benzyl (diethoxyphosphoryl)dithioformate (BEPTF), cyanopropyl dithiobenzoate (CPDB), ATRP initiator 1,2-bis(bromoisobutyryloxy)ethane was synthesized according to the literature.[162,212,213] Lipase acrylic resin from *Candida antarctica* (≥ 10,000 U/g, Sigma) was stored over phosphorous pentoxide (≥97%, Fluka) at 4 °C, zinc chloride (99.99%, Aldrich) was stored over phosphorous pentoxide (Fluka) at ambient temperature, piranha solution was prepared from 98 wt % concentrated sulfuric acid (70 vol %) and hydrogen peroxide (30 vol %), Copper (I) bromide (≥98%, Sigma-Aldrich) was purified by sequential washing with sulphurous acid, acetic acid and ethanol, followed by drying under reduced pressure.

Thiophosgene (98% Aldrich), benzyl mercaptan (99%, Aldrich), carbon disulfide (anhydrous, ≥99%, Sigma-Aldrich), sodium methanesulfinate (95%, Alfa Aesar), tetrabutylammonium hydrogen sulfate (97%, Sigma-Aldrich), benzenesulfinic acid sodium salt (Technical grade, 85%, Aldrich), *trans,trans*-2,4-hexadien-1-ol (97%, Aldrich), succinic anhydride (Roth), diisopropyl ethylamine (DIPEA) (Roth), citric acid (Roth), poly(ethylene glycol) monomethyl ether 2000 (Aldrich), 4-dimethylamino pyridine (≥99%, Aldrich), *N,N*-dicyclohexylcarbodiimide (99%, Aldrich), *p*-toluenesulfonyl chloride (≥98%, Sigma-Aldrich), sodium cyclopentadienide solution (2.0 M in THF, Aldrich), sodium borohydride (99%, Acros), boron trifluoride diethyl etherate (Sigma), hydrogen peroxide (Roth), 2-bromopropionyl bromide (97%, Aldrich), triethylamine (≥99%, Sigma-Aldrich), fluoresceinamine (Aldrich), trifluoroacetic acid (99%, Sigma-Aldrich), Si wafers [p-type, boron doped (100)] (Siltron INS Korea), 3-(*N*-Styrylmethyl-2-aminoethylamino)-

propyl trimethoxy silane (ABCR GmbH and Co. KG), fullerene-C_{60} (99.5%, Sigma-Aldrich), Benzyl bromide (98%, Aldrich), 9-chloromethylanthracene (Aldrich, ≥98%), sodium hydride (Acros, 60% dispersion in mineral oil), Copper (II) bromide (≥99%, Fluka), *N*,*N*,*N*',*N*',*N*'-pentamethyldiethylenetriamine (Merck), (1-bromoethyl)benzene (97% Aldrich), 2,2'-bipyridyl (≥99%, Sigma-Aldrich), 4-bromomethyl benzoic acid (97%, Acros), 2-(chloromethyl)pyridine hydrochloride (98%, Aldrich), 1,8-diazabicycloundec-7-ene (DBU, ≥99%, Fluka), nickelocene (Strem), potassium *tert*-butoxide (95%, Aldrich), triphenylphosphine (99%, Sigma-Aldrich), sodium iodide (≥99%, Sigma-Aldrich), elemental sulfur (powder, Sigma-Aldrich), *p*-toluenesulfonic acid (98.5%, Sigma-Aldrich), and 1,1,1-tris(hydroxymethyl) propane (98%, Aldrich) were all purchased at the highest available purity and used as received.

Toluene (anhydrous, water <30 ppm, Sigma-Aldrich), tetrahydrofuran (THF, anhydrous, ≥99.9%, Sigma-Aldrich), toluene, diethyl ether, dichloromethane, tetrahydrofuran, ethanol, methanol, n-hexane, acetone, cyclohexane, ethyl acetate and chloroform were purchased in the highest purity and used as received.

3.2 Characterization Techniques

3.2.1 Scanning Electron Microscopy (SEM)

The Scanning Electron Microscope is a microscope that uses electrons rather than light to form an image. The foundation of SEM was laid by Max Knoll in 1930's and was further developed by Prof. Sir Charles Oatley, with first commercial instrument available in 1965. There are many advantages of using SEM over optical microscopy. SEM can magnify objects at upward of 300,000 times the size of the object studied. In contrast, optical microscopes have a magnification power of a few hundred times. SEM also have tremendous depth of field compared to traditional microscopy, which produces a 3-D image to analyze as compared to the flatter image provided by an optical microscopy. In addition, SEM can provide information about sample composition. The basic components (as shown in **Figure 3.1**) present in all SEM equipment are as follows:

1) **Sample chamber:** The samples to be examined are placed in sample chamber after coating with a conductive material (for example, chromium or gold). The sample chamber is usually kept insulated from the vibrations so that the microscope can produce clear images.

2) **Electron gun:** The role of an electron gun is to produce a steady stream of electrons at the sample under examination. The electron guns are located either at the very top or at the very bottom of an SEM. Electron guns are typically one of two types, thermionic guns or field emission guns. The thermionic guns are the most common type and they function by applying thermal energy to a filament (usually made of tungsten, which has a high melting point) which causes electrons to move away from the gun towards the specimen under examination. Field emission guns, on the other hand, create a strong electrical field to pull electrons away from their associated atoms.

3) **Lenses:** The lenses are used to produce clear and detailed images of the samples under examination. The lenses in SEM are not made of glass. Instead, they are made of magnets capable of bending the path of electrons. The use of magnetic lenses makes the electron beam controlled and focused, ensuring that the electrons end up precisely at the sample.

4) **Detectors:** The electron beam produced by an electron gun interacts with the sample in different ways. The role of detector is to detect the various ways in which the electron beam interacts with the sample. The various types of detectors present in the SEM are, for example, secondary electron detectors register secondary electrons, which are electrons removed from the outer surface of a specimen. These detectors are capable of producing the most detailed images of an object's surface. Other detectors, such as backscattered electron detectors and X-ray detectors, give information about the composition of a substance.

5) **Vacuum chamber:** SEM requires a vacuum to operate. Without a vacuum, the electron beam generated by the electron gun would encounter constant interference

from air particles in the atmosphere. This interference is not desirable as it can distort the path of an electron beam which in turn causes interference in scanning the surface of the specimen.

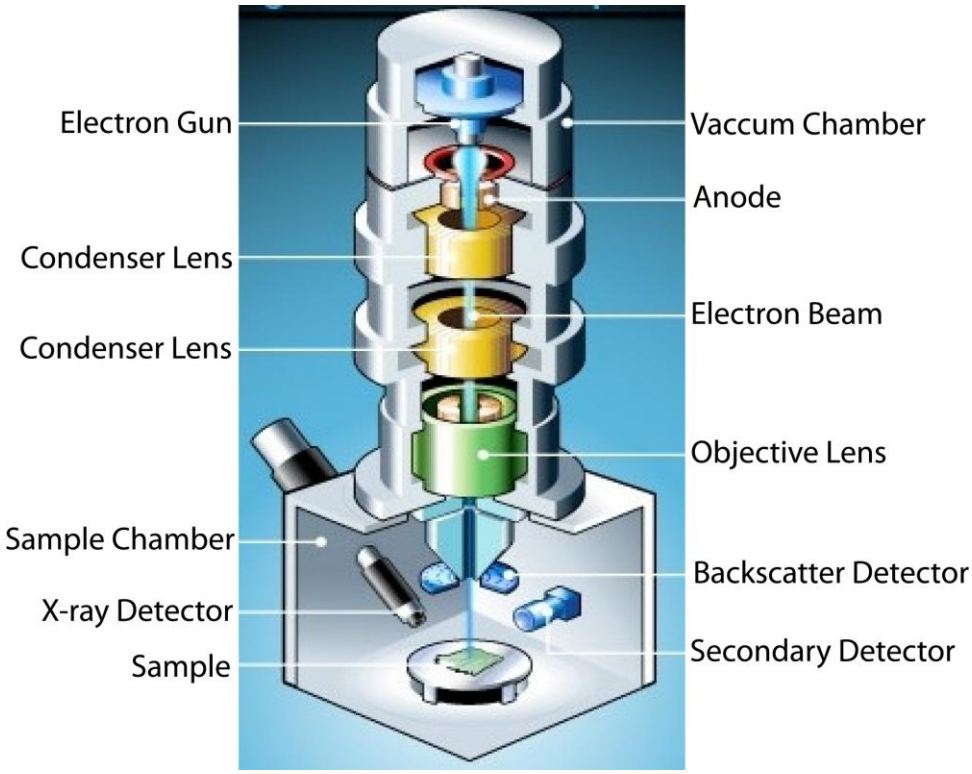

Figure 3.1 Set-up for scanning electron microscope (SEM). The Figure is adapted from http://science.howstuffworks/scnning-electron-microscope2.htm

The SEM works by using an electron beam to trace over the object. The use of magnetic lenses focuses the electron beam at a very fine spot on the sample. As the electron beam hits each spot on the sample, secondary electrons are emitted from the surface of the sample. The final image is built up from the number of electrons emitted from each spot of the sample. Different detectors detect different electrons, for example, a secondary electron detector attracts scattered electrons and depending on the number of electrons that reach the detector, different levels of brightness are registered and displayed on a monitor. Additional sensors detect backscattered electrons (electrons that reflect off the specimen's surface) and X-rays (emitted from beneath the specimen's surface). Dot by dot, row by row, an image of the original object is scanned

and displayed on a monitor for viewing. The microscope can control the movement of an electron beam by using scanning coils, which create variable magnetic fields using fluctuating voltages, to manipulate the electron beam. The scanning coils are able to move the beam precisely back and forth over a defined section of the specimen. The magnification of the image can be increased by setting the electron beam to scan smaller area of the sample.

In the present study, the morphology of the microspheres (**Chapter 5, 6 and 8**) was studied with a Hitachi S900 and LEO 1530 Gemini scanning electron microscope (SEM). The microspheres were dispersed in ethanol; a drop of this particle suspension was cast onto an electron microscope stub covered with a double sided carbon tape which in turn is covered with a 5 mm glass cover slip. Samples were sputter-coated with chromium or gold. Electron micrographs of each sample were recorded at different magnifications. The particle size analysis from SEM micrographs was carried out for an average of 100 microspheres. D_n, D_w and U were calculated using following the equations:[170] $D_n = \Sigma n_i D_i / \Sigma n_i$, $D_w = \Sigma n_i D_i^4 / \Sigma n_i D_i^3$, $U = D_n / D_w$, where D_n is the number average diameter, D_w is the weight average diameter and U is the polydispersity index.

3.2.2 Atomic Force Microscopy (AFM)

An atomic force microscope[214] is an instrument for mapping and measuring surface features of extremely small objects-for example, a carbon atom that is 0.25 nanometers (nm) in diameter. It is one of the foremost tools for imaging and measuring matter at the nanoscale and for performing topographic investigations. The precursor to the AFM, the scanning tunneling microscope, was developed by Gerd Binnig and Heinrich Rohrer in the early 1980's, a development that earned them the Nobel Prize for Physics in 1986. Binnig, Quate and Gerber invented the first atomic force microscope in 1986.[215] In addition to its superior resolution with respect to optical microscopes, the AFM has several advantages as compared to electron microscopes. Compared to SEM, the AFM provides superior topographic contrast, in addition to direct measurement of surface features; it is thus possible to obtain quantitative height information using AFM.

The principle of the AFM relies on the use of a sharp tip to probe the sample surface. AFM tips and cantilevers are usually microfabricated from Si or Si_3N_4. AFM tips often have the shape of a pyramid, with a radius of curvature at the apex between a few and tens of nanometers. The true resolution for imaging is limited by the shape and the radius of the tip. The tip is mounted on a cantilever (100-200 µm in length) which is the most important component in AFM as it is brought into close proximity to the surface where intermolecular forces acting between the tip and the surface cause the cantilever to bend. The most basic setup for an AFM instrument is shown in **Figure 3.2**. Depending on the separation distance between tip and surface, long range or short range forces will dominate the interaction. This force is measured by bending of the cantilever by an optical lever technique; a laser beam is focused on the back of the cantilever and reflected into a photo detector. The small forces between the tip and sample will cause less deflection than large forces. A map of the surface topography and other properties can be generated by scanning the tip across the surface and recording the change in force as a function of position. The data, [*i.e.* topography (height)], can be also be displayed graphically using a color scale to indicate the height observed at each different point.

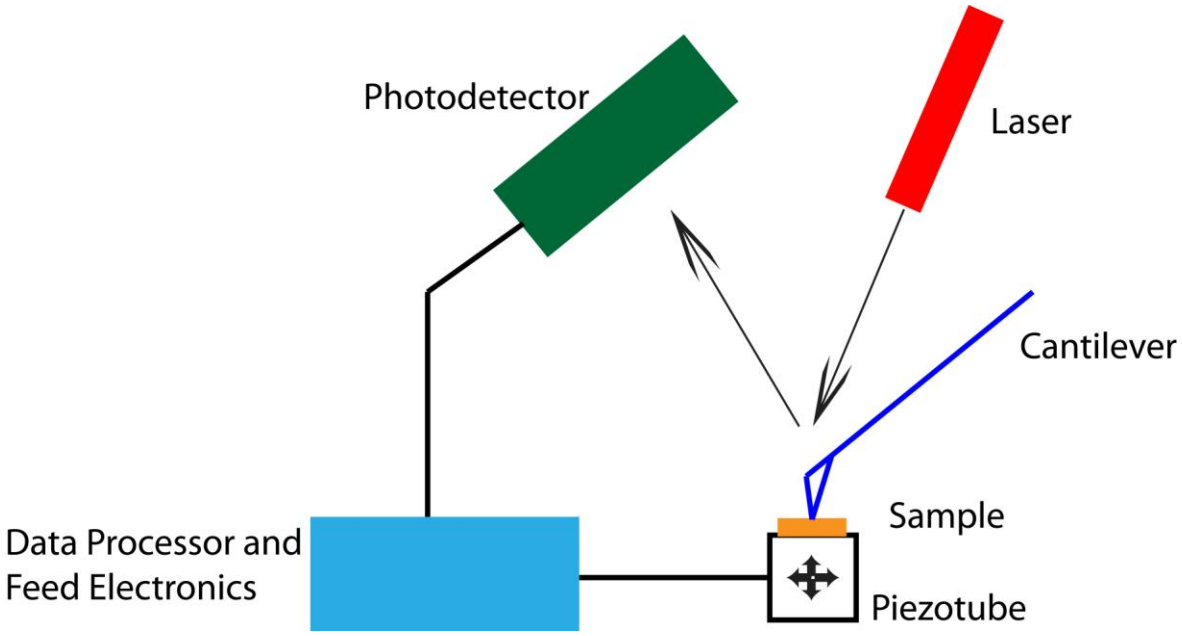

Figure 3.2 Basic setup of an AFM instrument

A number of different modes of operation have been developed in recent years. Contact mode is the most common method of operation of an AFM. In the contact mode, as the name suggests, the tip is brought in direct contact with the surface. One disadvantage of the contact mode is that considerable forces are exerted on the sample, which may cause partial destruction of surface features. This drawback has been circumvented by the tapping mode. In the tapping mode, the tip makes intermittent contact with the surface. As the tip is scanned over the surface, the cantilever is driven at its resonant frequency. As the contact time is a small fraction of its oscillation period, the lateral forces are reduced. Tapping mode is usually preferred to images samples in which the structures are weakly bound to the surface or samples that are soft, for examples, polymers or thin films.

In the present thesis, the AFM measurements (**Chapter 7**) were performed on Digital instruments Nanoscope III in tapping mode by Dr Petia Atanasova at Max Planck Institute for Metals Research, Stuttgart. For the measurement standard Si cantilevers with ~ 15 nm tip radius were used to scan the sample size of 1 μm at a scan rate of 0.984 Hz.

3.2.3 Confocal Microscopy

Confocal microscopy is a powerful technique to obtain high resolution images of a specimen that would otherwise appear blurred when viewed with a conventional optical microscope. The image has less haze and better contrast than that of a conventional microscope and represents a thin cross-section of the specimen. This is achieved by excluding most of the light from the specimen that is not from the microscope's focal plane. The principle of confocal microscopy was originally patented by Marvin Minsky in 1955,[216] but it took another thirty years and the development of lasers for confocal microscopy to become a standard technique toward the end of the 1980s.

The confocal microscope detects only the in-focus light while the out-of-focus light is blocked out. This is achieved by the use of a pinhole (as shown in **Figure 3.3**). In the confocal microscope a pinhole and laser scanning are used in order to produce high resolution images of sample which is inherently fluorescent or is being labelled with

fluorescent molecules. The emitted light from the fluorescent molecule is sent to a detector that is placed behind the pinhole instead of being emitted back through an eyepiece. The detector is able to detect the light that is able to make it through the pinhole, thus producing an image only from the emitted light from one point in the specimen. An entire area or plane is scanned through the use of scanning mirrors. This enables users to see a thin section of the entire specimen with a small depth of field. If many of these thin slices of an image are taken at different depth of fields within the sample, it is possible to reconstruct a 3D image of the entire specimen.

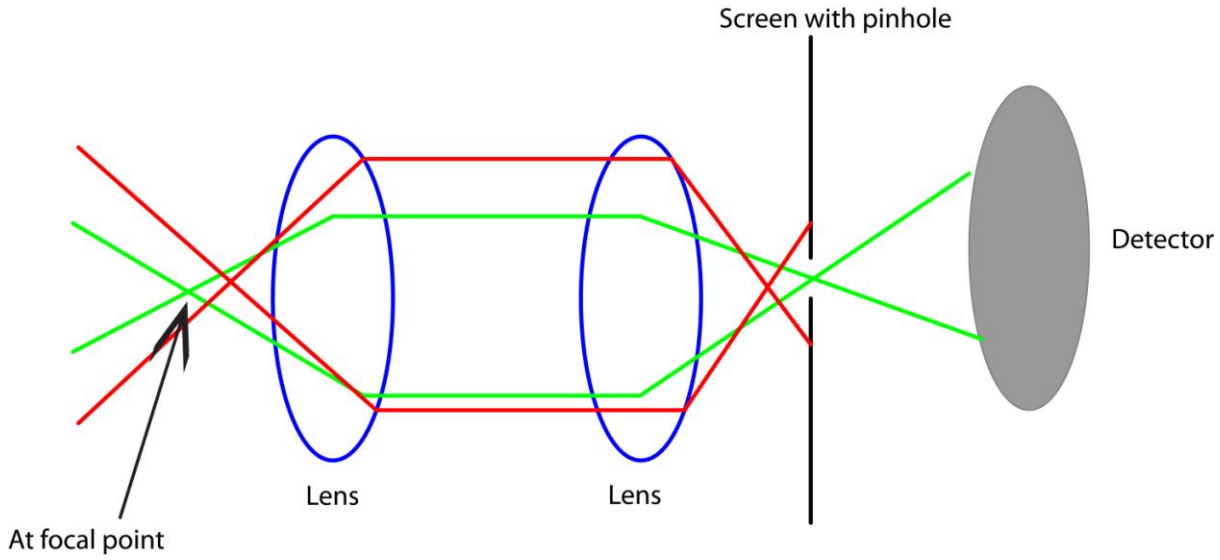

Figure 3.3 Basic principle of operation of a confocal microscope

In the current thesis, confocal microscopy images were captured using an Olympus FV1000 inverted confocal scanning laser microscope (Tokyo, Japan) (**Chapter 5**), using a UPLSAPO 100x oil immersion lens NA 1.40. Rhodamine B was excited by a 514 nm Argon laser, with a DM 405-440/515 excitation dichroic mirror. Emission was captured by a spectral detection unit set to 530-630 nm. In addition, a LSM 510 meta microscope (Zeiss) (**Chapter 6**) was also used in the current study. In this case, all images were captured using 'Plan-Apochromat' (Zeiss) 63 x/1.4 oil DIC (Differential Interference Contrast). Fluoresceinamine was excited by a 514 nm Argon laser, with a DM 405-440/515 excitation dichroic mirror. The absorption and emission was detected by a spectral detection unit set to 485 and 514 nm, respectively.

3.2.4 IR Spectroscopy

IR spectroscopy is an important analytical tool to obtain information about structure of a compound. IR spectroscopic analysis is largely used to determine chemical functional groups in the sample. This is due to the reason that different functional groups absorb characteristic frequencies in IR radiation. IR radiation spans a section of the electromagnetic spectrum having a wavenumber from roughly 13,000 to 10 cm^{-1}. IR spectra are obtained by detecting changes in transmittance (or absorption) intensity as a function of frequency. Nowadays, most commercial instruments separate and measure IR radiation using Fourier transform (FT) spectrometers. The three basic components in a FT system are: radiation source, interferometer and detector. The IR radiation from a broadband source is first directed into an interferometer, where it is divided and then recombined after the spilt beams travel different optical paths to generate constructive and destructive interference. Next, the resulting beam passes through the sample compartment and finally it reaches the detector. Most of the benchtop FT-IR spectrometers are single-beam instruments. A typical operating procedure to obtain the FT-IR spectrum is described as follows:

1) Firstly a background spectrum is obtained by collecting interferograms (raw data), followed by processing the data by FT conversion. This is a response curve of the spectrometer and takes account of the combined performance of source, interferometer, and detector. The background spectrum also includes the peaks arising from any ambient water (observed as two irregular groups of vibrations at about 3600 cm^{-1} and about 1600 cm^{-1}) and carbon dioxide (a doublet at 2360 cm^{-1} and sharp peak at 667 cm^{-1}) present in the optical bench.

2) A single beam sample spectrum is collected. It contains absorption bands from the sample and the background (air or solvent).

3) The ratio of the single-beam sample spectrum against the single beam background spectrum results in a double-beam spectrum of the sample.

Wide ranges of sampling accessories are available to take advantage of the capabilities of the FT-IR instrument. Two of the accessories used in the current thesis (**Chapter 5, 6 and 7**) are described in following paragraph.

Attenuated total reflectance (ATR) accessories are especially useful for obtaining IR spectra of samples which are difficult to be examined by the normal transmission method. The ATR accessory is suitable for studying thick or highly absorbing solid and liquid materials, including films, coatings, powders, adhesives, polymers, and aqueous samples. ATR requires little or no sample preparation in most cases and is one of the most versatile sampling techniques.

The ATR technique is based on the propagation of IR radiation through a material (internal reflection medium) (as shown in **Figure 3.4**) which has a high refractive index such as zinc selenide, thallium bromide–thallium iodide (KRS-5), or germanium. The reflection of IR radiation occurs at the interface between the material of high refractive index and the sample with which it makes contact. Two important conditions should usually be satisfied in order to achieve internal reflection. The first is that the angle of incidence of the IR radiation must be larger than the critical angle of material of high refractive index (which is characteristic for each material) and the refractive index of the internal reflection material used should be greater than refractive index of the sample to be examined. When the IR radiation penetrates into the sample, an evanescent electromagnetic wave is generated at the interface and the radiation propagates through the material of high refractive index upon successive internal reflections. The extent of penetration of the IR radiation into the sample depends on the wavelength and the optical properties (refractive indices and angle of incidence of the sample as well as of the internal reflection element).

The ATR-IR spectrum resembles the conventional IR spectrum, but with some differences: The absorption band positions are identical in the two spectra, but the relative intensities of corresponding bands are different. Although ATR spectra can be obtained using either dispersive or FT instruments, higher quality spectra are obtained using FT-IR spectrometers.

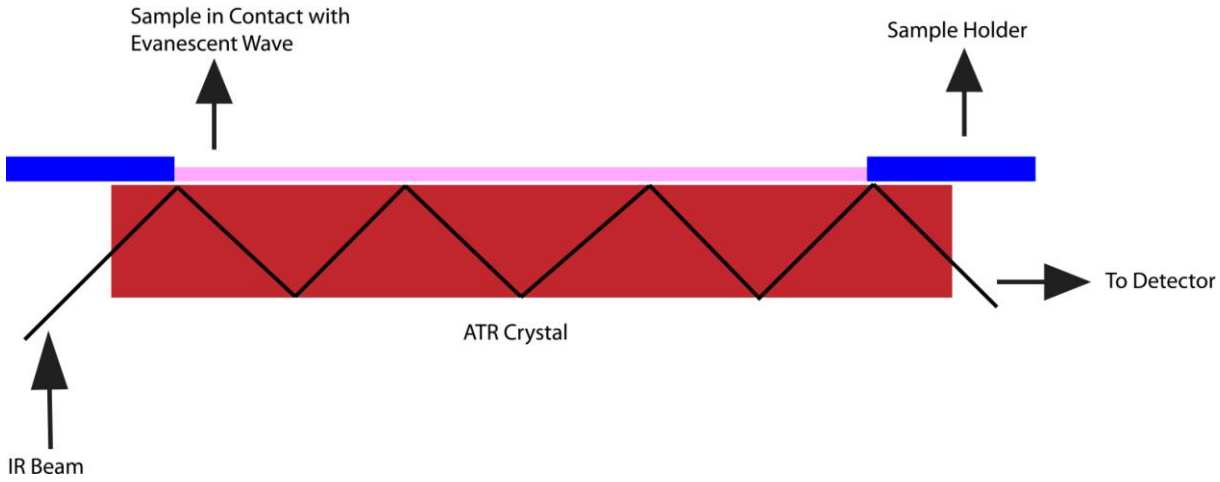

Figure 3.4 Schematic of a multiple refection ATR system

Other than ATR-FT-IR spectroscopy, infrared microscopy was utilized to study the modification of Si wafers with poly(isobornyl acrylate) as discussed in detail in **Chapter 7**. The power of infrared microscopy lies in its ability to obtain molecular information on a microscopic scale. Infrared microscopy is a combination of infrared spectroscopic data collection with optical visualization using optical microscopy. The infrared spectroscopic data collection employs focal plane array (FPA) detection for infrared chemical imaging where the image contrast is determined by the response of individual sample regions to particular selected IR wavelength.

3.2.4.1 Fourier-Transform Near Infra Red (FT-NIR) Spectroscopy

Monomer conversions were determined (**Chapter 4**) using on-line FT-NIR spectroscopy by following the decrease of the intensity of the first vinylic stretching overtone of the monomer [υ_{max} (isobornyl acrylate)/cm^{-1} 6142]. The FT-NIR measurements were performed using a Bruker Vertex 70 Fourier-transform spectrometer equipped with a tungsten halogen lamp, a CaF_2 beam splitter and a liquid nitrogen-cooled InSb detector. Each spectrum in the spectroscopic region of 8000-4000 cm^{-1} was calculated from the co-added interferograms of 32 scans with resolution of 4 cm^{-1}. For the conversion determination, a linear baseline was selected between 6200 and 6100 cm^{-1}. The integrated absorbance between these two points was subsequently used to calculate the monomer-to-polymer conversion.

3.2.4.2 Attenuated Total Reflectance-Infra Red Spectroscopy (ATR-IR)

Solid-state Fourier transform infrared spectra (**Chapter 5, 6 and 7**) were recorded with an attenuated total reflectance spectrometer (Bruker IFS66\S, *Golden Gate*) and also on Bruker Vertex 70 fourier-transform spectrometer, equipped with a tungsten halogen lamp, a KBr beam splitter and DTGS detector. Each spectrum in the spectroscopic region of 4000-400 cm^{-1} was calculated from the co-added interferograms of 32 scans with resolution of 4 cm^{-1}.

3.2.4.3 Infra Red Microscope

Measurements using infra red microscope were carried out on Si wafers modified with poly(isobornyl acrylate) (**Chapter 7**). The experiments were performed at the Bruker application laboratories in Ettlingen, Germany, utilizing an IFS 66 step scan FT-IR spectrometer connected to an infrared microscope IRscope II (HYPERION 3000). The microscope was equipped with a 64 x 64 MCT, FPA detector, which allows the simultaneous acquisition of 4096 spectra from an area of 32 x 32 µm with a pixel resolution of 0.5 µm. Spectra were recorded in transmission mode at a sampling rate of 250 kHz with a spectral resolution of 4 cm^{-1} and a data acquisition time of approximately 11.6 min for the sample and 11.6 min for background measurements.

3.2.5 Ultraviolet-Visible (UV-Vis) Spectroscopy

UV-Visible spectrophotometers are used to measure absorption in the UV-Visible wavelength range. The UV-Visible region extends from 200-800 nm. For the solution of an absorbing substance, it measures the intensity of light passing through a sample (I), and compares it to the intensity of light before it passes through the sample (I_0). The transmittance, usually expressed as a percentage ($\%T$), is ratio of I / I_0 .The absorbance, A, can be calculated from the transmittance using the following equation:

$$A = - \log (\%T / 100\%) \quad (3.1)$$

The absorbance is related to the concentration of the absorbing substance and optical path-length by the Beer Lambert law which is described by following equation:

$$A = - \log (I / I_0) = \varepsilon \cdot c \cdot l \quad (3.2)$$

where ε is molar absorptivity (usually expressed in $L \cdot mol^{-1} \cdot cm^{-1}$), c is the concentration of absorbing substance in $mol \cdot L^{-1}$ and l is the path length in cm. The basic components of an UV-Visible spectrophotometer are a light source, sample holder, a diffraction grating or monochromator to separate the different wavelengths of light, and a detector. The light source is often a tungsten filament (300-2500 nm), a deuterium arc lamp which is continuous over the ultraviolet region (190-400 nm), and more recently light emitting diodes (LED) and Xenon Arc Lamps for the visible wavelengths. A photodiode or a charged coupled device (CCD) are typically used a detector. Photodiodes are used with a monochromator, which filters the light so that only light of a single wavelength reaches the detector. Diffraction gratings are used with CCDs, which collects light of different wavelengths on different pixels.

A UV-Visible spectrophotometer can be either *single beam* or *double beam*. In a single beam instrument, all of the light passes through the sample cell. I_0 is measured by removing the sample. In a double-beam instrument, the light is split into two beams before it reaches the sample. One beam is used as the reference; the other beam passes through the sample. Some double-beam instruments have two detectors (photodiodes), and the sample and reference beam are measured at the same time. In other instruments, the two beams pass through a beam chopper, which blocks one beam at a time. The detector alternates between measuring the sample beam and the reference beam.

In the current study, UV-Visible spectroscopy (**Chapter 4 and 9**) was performed using a Cary 300 Bio UV-Visible spectrophotometer (Varian) featuring a thermostated sample cell holder. Absorption was measured in $CHCl_3$ solution from 200 to 800 nm with a resolution of 1 nm and slit width of 2 nm in a 10 mm UV cuvette.

3.2.6 X-Ray Photoelectron Spectroscopy (XPS)

XPS is a very important technique to study the composition and electronic state of the surface region of a sample by exposing it to soft X-rays (with photon energy of

200-2000 eV) to examine core levels *via* analysis of the kinetic energy distribution of the emitted photoelectrons.

The process of photoemission is shown schematically in **Figure 3.5** where an electron from the K shell is ejected from the atom (a 1s photoelectron).[217] The photoelectron spectrum will reproduce the electronic structure of an element quite accurately since all electrons with a binding energy less than the photon energy will feature in the spectrum. The electrons which are excited and escape without energy loss contribute to the characteristic peaks in the spectrum; those which undergo inelastic scattering and suffer energy loss contribute to the background of the spectrum. Once a photoelectron has been emitted, the ionized atom must relax in some way. This can be achieved by the emission of an X-ray photon, known as X-ray fluorescence. The other possibility is the ejection of an Auger electron (When an electron is removed from a core level of an atom, leaving a vacancy, an electron from a higher energy level may fall into the vacancy, resulting in a release of energy. Although sometimes this energy is released in the form of an emitted photon, the energy can also be transferred to another electron, which is ejected from the atom. This second ejected electron is called an Auger electron). Thus Auger electrons are produced as a consequence of the XPS process often referred to as X-AES (X-ray induced Auger electron spectroscopy). X-AES, although not widely practiced, can yield valuable chemical information about an atom.

The basic components of XPS equipment are: a source of fixed energy radiation (an X-ray source for XPS), an electron energy analyzer (which can disperse the emitted electrons according to their kinetic energy and thereby measure the flux of emitted electrons of a particular energy) and a high vaccum environment which is important to enable the emitted photoelectron to be analyzed without interference. The most commonly employed X-ray source is Mg K_α radiation with photon energy of 1253.6 eV or Al K_α radiation with photon energy of 1486.6 eV. The emitted photoelectron will therefore have kinetic energies in the range of 0-1250 eV or 0-1480 eV.

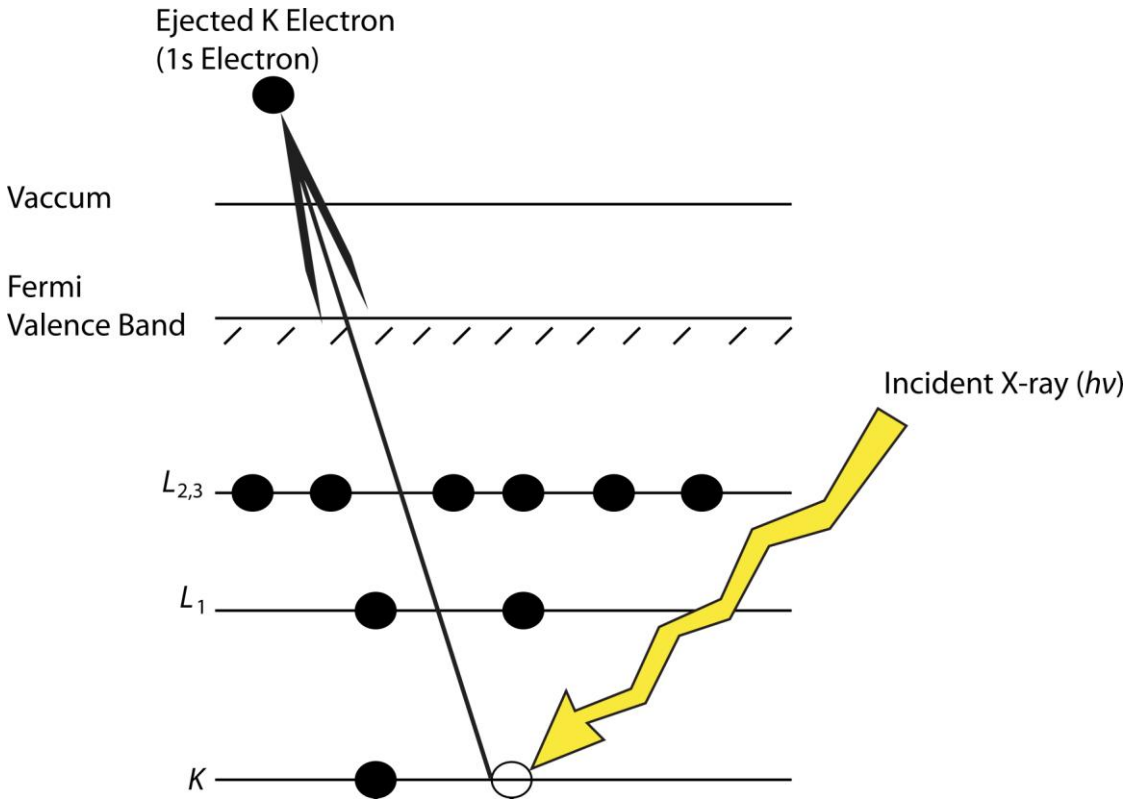

Figure 3.5 Schematic diagram of the XPS process, showing the photoionization of an atom by the ejection of a 1s electron.

In XPS, the kinetic energy (E_K) of the electron is the experimental quantity measured by the spectrometer but this is dependent on the photon energy of the X-rays employed and is therefore not an intrinsic material property. The binding energy of the electron (E_B) is the parameter which identifies the electron specifically, both in terms of its parent element and atomic energy level. The relationship between the parameters involved in the XPS experiment is:

$$E_B = hv - E_K - W \tag{3.3}$$

where hv is the photon energy, E_K is the kinetic energy of the electron and W is the spectrometer work function. As all three quantities on the right-hand side of the equation are known or measurable, it is a simple matter to calculate the binding energy of the electron. In practice, this task will be performed by the control electronics or data

acquisition system associated with the spectrometer and the operator merely selects a binding or kinetic energy scale whichever is considered the more appropriate.

In the present study, XPS investigation (**Chapter 5**) was performed on ESCALAB220i-XL surface analysis instrument with a mono-chromatized Al K_α X-ray source (1486.6 eV photons) at a constant dwelling time of 100 ms for several scans and a pass energy of 20 eV for region scan spectra and 100 eV for survey scan spectra. The power of the source was 150 W (15 mA and 10 kV). The pressure in the analysis chamber was maintained at $2 \cdot 10^{-9}$ Torr or lower during each measurement. The microsphere samples were mounted on standard sample stubs by means of double-sided adhesive tapes. Peak splitting of the XPS spectra was performed using the deconvolution method of the peak fit program (PeakFit v4.12 SeaSolve Software Inc.) or a K-Alpha spectrometer (ThermoFisher Scientific, East Grinstead, UK) (**Chapter 7**) using a microfocused, monochromatic Al K_α X-ray source (200 µm spot size). The samples were measured by Dr. Michael Bruns at Institute of Materials Research III, KIT (campus north). Up to 30 separated spots were measured in order to prevent the samples from X-ray damage, each at minimum acquisition time. All spectra were finally collapsed to one single spectrum with a sufficient signal/noise ratio. The kinetic energy of the electrons was measured by a 180° hemispherical energy analyzer operated in the constant analyzer energy mode (CAE) at 50 eV pass energy for elemental spectra. Data acquisition and processing using the Thermo Avantage software is described elsewhere.[218] The spectra were fitted with one or more Voigt profiles (BE uncertainty: +/- 0.2 eV) and Scofield[219] sensitivity factors were applied for quantification. All spectra were referenced to the C 1s peak assumed to originate from surface hydrocarbon contamination at 285.0 eV binding energy controlled by means of the well known photoelectron peaks of Cu, Ag and Au respectively.

3.2.7 Solution Nuclear Magnetic Resonance (NMR) Spectroscopy

The structures of the synthesized compounds in the present study were confirmed by ^{1}H-NMR and ^{13}C-NMR spectroscopy using a Bruker AM 400 MHz spectrometer for hydrogen nuclei and 100 MHz for carbon nuclei. All samples were

dissolved in $CDCl_3$ or DMSO-d_6 The δ–scale is referenced to tetramethylsilane (δ = 0.00) as internal standard.

3.2.8 Solid-State Nuclear Magnetic Resonance (NMR) Spectroscopy

Solid-state NMR spectroscopy is an important method for polymer characterization as most polymers are used in the solid-state and these NMR methods provide the link between the chemical structure and microstructure of polymers.[220] Solid-state NMR has developed more slowly than solution NMR spectroscopy, in part because in solids the lines are broader and it is more difficult to observe a high-resolution spectrum.[221] In order to obtain molecular-level information about the structure of polymers in the solid state, it is necessary to average the local interactions (chemical-shift anisotropy, dipolar coupling) to obtain a high-resolution spectrum. This can be accomplished with the combination of magic-angle sample spinning to average the chemical-shift anisotropy and high-power decoupling to remove the dipolar broadening. High-resolution spectra can also be observed when the spinning rate is fast compared to the breadth of the chemical-shift anisotropy lineshape and the dipolar broadening.

As the molecular dynamics of polymers are much slower in solids compared to solutions, large differences in relaxation times are often observed for solid polymers and polymers in solution. For carbon, nitrogen, and silicon atoms this frequently leads to extremely long relaxation times. This lowers the signal-to-noise ratios, since long waiting times are required between the scans. It is often possible to overcome this limitation by using cross-polarization between the protons and the nuclei of interest since the time between acquisitions depends on the proton relaxation times, which are typically only a few seconds. There is also a sensitivity enhancement for cross-polarization, since the experiment begins with proton magnetization, which has the highest sensitivity. One of the limitations of cross-polarization is that it is generally not quantitative, since the rate of cross-polarization may be different for different parts of the molecule.

3.2.8.1 Heteronuclear Dipolar Coupling

The heteronuclear dipolar coupling arises from an interaction between the nuclear magnetic moments of two different nuclear spins. The most common heteronuclear coupling is the ^{1}H-^{13}C coupling. The heteronuclear coupling is responsible for much of the peak broadening in solid-state NMR spectroscopy. However, this heteronuclear coupling can be eliminated by taking advantage of the fact that the dipolar coupling is zero when the internuclear vector is oriented at the magic angle with respect to the magnetic field. This is implemented in a technique known as magic-angle spinning (MAS).

3.2.8.2 Chemical-Shift Anisotropy (CSA)

The origin of the chemical-shift can be understood by examining the effect of the external magnetic field on the electrons around a nucleus. When an external magnetic field is applied to an atom, not only are the nuclear spins are perturbed but the surrounding electrons are also affected since they, too, have magnetic moments. The external field induces circulating currents of electrons that in turn produce small magnetic fields (typically ~ $1 \cdot 10^{6}$ times smaller than external magnetic field), which either add to or subtract from the external field felt by the nucleus. Therefore, the effective magnetic field experienced by the nucleus is altered as is its resonance frequency. The CSA results from the fact that the atoms in molecules rarely possess spherically symmetric electron distributions; instead, the electron density can be thought of as an ellipsoid, typically elongated along bonds or nonbonding p-orbitals. The degree to which the electron density affects the resonance frequency of a nucleus depends on the orientation of the electron cloud (and hence the orientation of the molecule) with respect to external magnetic field. The chemical-shift anisotropy can be eliminated by spinning the sample around a unique well-chosen axis (magic-angle spinning).

3.2.8.3 Magic-Angle Spinning (MAS)

In the case of solid samples, a nuclear spin experiences a great number of interactions. The main interactions (dipolar coupling, chemical-shift anisotropy) often lead to very broad and featureless signals. However, these interactions in solids can be

averaged by magic-angle spinning. The MAS procedure involves rotating the solid sample uniformly about an axis inclined at the angle 54°44' (θ_m) to the direction of the static magnetic field of the NMR magnet. Very fast rotation compared to the line width is needed and rotation speeds of more than 25 kHz can be achieved. The nuclear dipole-dipole interaction, between magnetic moments of nuclei averages to zero only at the magic-angle. The chemical-shift anisotropy, a nuclear-electron interaction, also averages to a zero value.

3.2.8.4 Single Pulse Excitation

3.2.8.4.1 ^{1}H-NMR Spectra

The pulse sequence to obtain ^{1}H single pulse excitation spectrum is shown in **Figure 3.1.**[222] The sequence to obtain ^{1}H single pulse excitation spectrum is as follows:

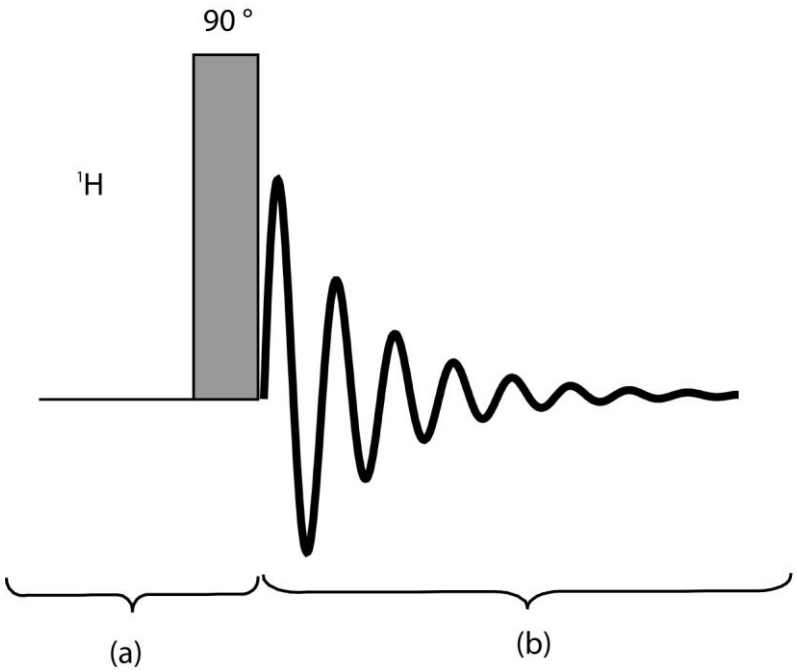

Figure 3.6 Pulse sequence to obtain ^{1}H single pulse excitation spectra consisting of 90° pulse excitation (a) and the detection of magnetization (b). The Figure is adapted from reference 222

(a) The pulse program consists of one 90° pulse which flips the magnetization of ^{1}H nuclei in the plane perpendicular to B_0 (external magnetic field).

(b) The detection of magnetization is done in the xy plane (having magnetic component B_1 orthogonal to the constant external magnetic field B_0), leading to the free induction decay and to the spectrum after Fourier transformation.

3.2.8.4.2 ^{13}C-NMR Spectra

There are two methods to obtain one-dimensional ^{13}C spectra: single pulse excitation (SPE) and cross-polarization (CP) (discussed in detail in **section 3.2.8.5**). The pulse sequence to obtain ^{13}C SPE spectrum is shown in **Figure 3.7**. The sequence of events to obtain ^{13}C SPE is as follows:

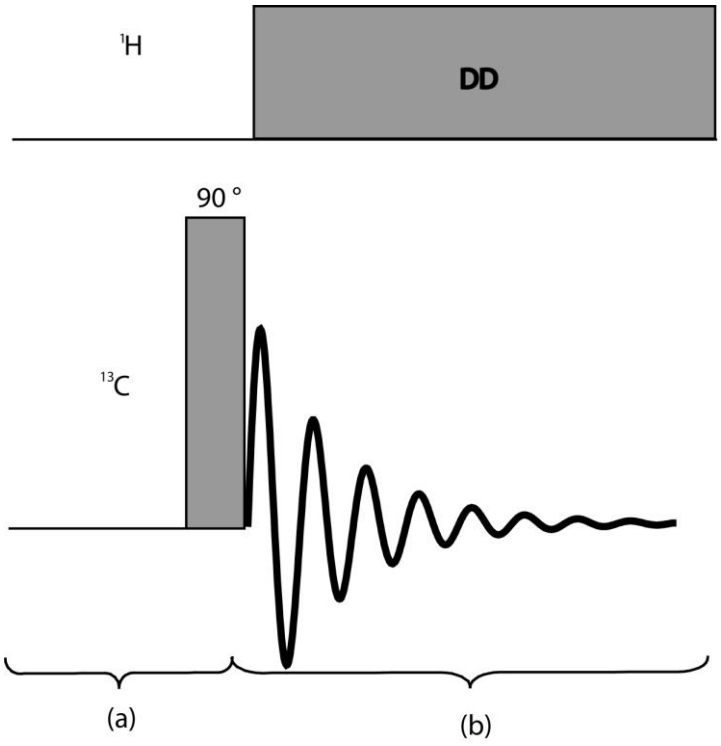

Figure 3.7 Pulse sequence to obtain ^{13}C single pulse excitation spectra consisting of 90° pulse excitation (a) and the detection of magnetization (b). The Figure is adapted from reference 222

(a) The pulse program consists of one 90° pulse which flips the magnetization of ^{13}C nuclei in the plane perpendicular to B_0 (external magnetic field).

(b) The detection of magnetization is done in the xy plane (having magnetic component B_1 orthogonal to the constant external magnetic field B_0), leading to the free induction decay and to the spectrum after Fourier transformation.

During the data acquisition, the ^{13}C nuclei are decoupled from the surrounding ^{1}H nuclei by irradiating the ^{1}H nuclei with continuous radiofrequency (rf) field. The heteronuclear decoupling procedure eliminates the broadening of the ^{13}C lines due to strong heteronuclear dipole-dipole coupling between ^{1}H and ^{13}C.

3.2.8.5 Cross-Polarization (CP) ^{13}C-NMR Spectra

As the result of the difficulties involved in obtaining high-resolution solid-state ^{1}H-NMR spectra, the majority of solid-state NMR experiments detect the magnetization of other nuclei such as ^{13}C, ^{31}P, and ^{15}N. The drawbacks of directly detecting low magnetogyric ratio (γ) nuclei such as ^{13}C are low isotopic abundances, low spin polarization, and low signal intensity. These drawbacks can be circumvented by solid-state NMR technique that combines both the high polarization and short relaxation time that is typical of ^{1}H-NMR spectroscopy with high resolution (e.g. of ^{13}C). To enhance the signals from rare nuclei such as ^{13}C, solid-state NMR experiments routinely involve the transfer of polarization from abundant nuclei (usually ^{1}H nuclei) by using a technique called cross-polarization (CP). The process of CP occurs through the tendency of the magnetization flow from highly polarized nuclei to nuclei with lower polarizations when the two are brought into contact. CP is a method used to obtain ^{13}C magnetization not directly from T_1 relaxation (like in the case of single pulse excitation), but indirectly *via* ^{1}H magnetization. It usually provides a higher polarization (and therefore more signals) and allows more frequent measurements (because the T_1 relaxation is faster for the hydrogen than for the carbon nuclei). Thus, spectra similar to single pulse ^{13}C spectra can be obtained within a shorter measurement time provided the sample has only a limited mobility. The CP experiment is divided in three parts (**Figure 3.8**):

In the first part of the experiment (a), the ^{1}H magnetization is driven to the xy plane through a 90° pulse. In the part (b) of the experiment, the CP is realized during a defined contact time T_{CP}. During this time T_{CP}, the magnetization is exchanged between ^{1}H and ^{13}C nuclei. The detection of the FID of the ^{13}C nuclei takes place in the part (c) with dipolar decoupling of the ^{1}H nuclei.

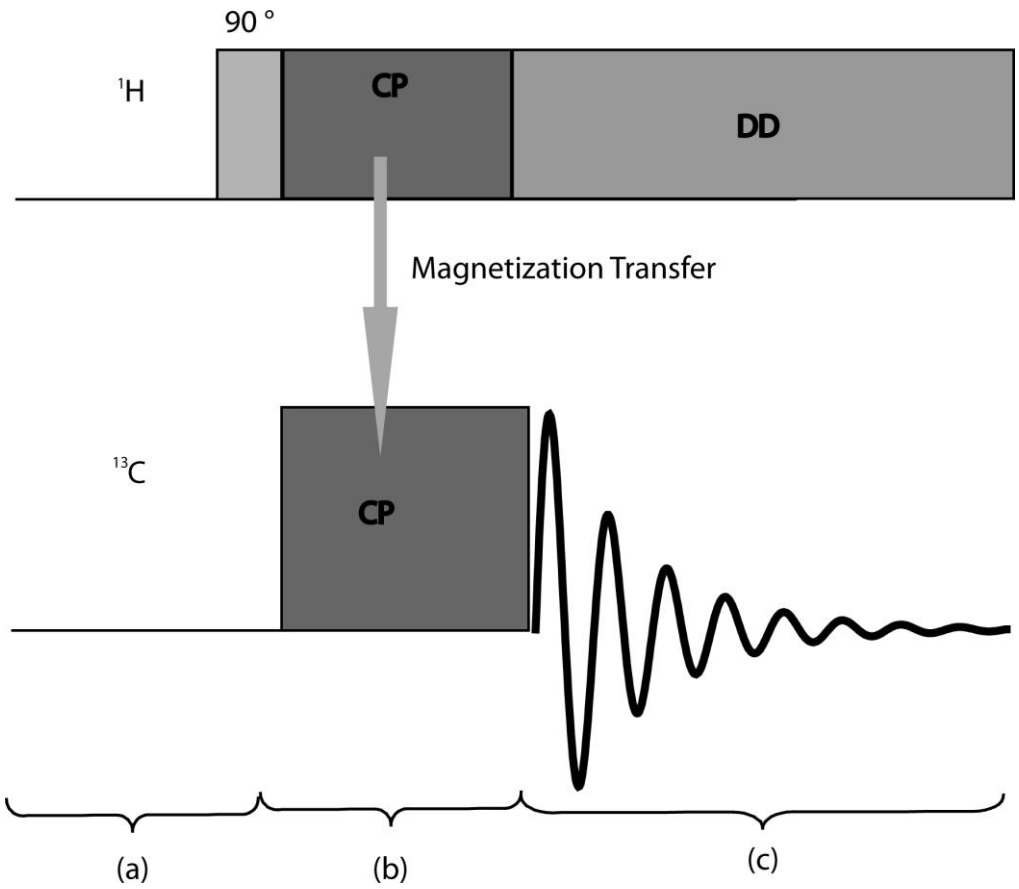

Figure 3.8 Pulse sequence to obtain ^{13}C cross-polarization spectra consisting of 90° pulse excitation (a), transfer of polarization (b) and the detection of magnetization (c). The Figure is adapted from reference 222

In this work, ^{1}H MAS NMR spectroscopy was carried out on a Bruker Avance spectrometer (Bruker BioSpin, Germany) operating at a ^{1}H Larmor frequency of 700.13 MHz using a 2.5 mm solid-state MAS NMR probehead and a MAS rotational frequency of 30 kHz by Dr. Marianne Gaborieau at Max Planck Institute of Polymer Research, Mainz. Spectra were recorded using a 2.5 µs 90° pulse, 16 transients and 5 s

repetition delay. ^{13}C SPE-MAS NMR was carried out on a Bruker Avance spectrometer (Bruker BioSpin, Germany) operating at a ^{13}C Larmor frequency of 175 MHz using a 4 mm solid-state MAS NMR probehead and a MAS rotational frequency of 18 kHz. Spectra were recorded using a 4 µs 90° pulse, 7062 transients (8064 transients for background) and 60 s repetition delay. ^{13}C CP-MAS NMR spectroscopy was carried out on a Bruker Avance spectrometer (Bruker BioSpin, Germany) operating at a ^{13}C Larmor frequency of 125.75 MHz using a 2.5 mm solid-state MAS NMR probehead and a MAS rotational frequency of 18 kHz. Spectra were recorded using a 2.5 µs 90° pulse, 2 ms contact time, 5 632 transients (1 024 transients for experiments with variable contact time) and 5 s repetition delay.

3.2.9 Size Exclusion Chromatography (SEC)

SEC measurements were performed on a Polymer Laboratories PL-GPC 50 Plus Integrated System, comprising an autosampler, a PLgel 5 µm bead-size guard column (50 × 7.5 mm) followed by the three PLgel 5 µm MixedC columns (300 × 7.5 mm) and a differential refractive index detector using THF as the eluent at 35 °C with a flow rate of 1 mL·min^{-1}. The SEC system was calibrated using linear polystyrene standards ranging from 160 to 6·10^6 g·mol^{-1} and linear poly(methyl methacrylate) standards ranging from 700 to 2·10^6 g·mol^{-1}. The resulting molecular weight distribution has been corrected using the Mark-Houwink relationship with K = 14.1·10^{-5} dL·g^{-1}, α = 0.7 for polystyrene[223] K = 12.8·10^{-5} dL·g^{-1}, α = 0.69 for poly(methyl methacrylate),and K = 12.2·10^{-5} dL·g^{-1}, α = 0.70 for poly(*n*-butyl acrylate),[224,225] K = 13.95·10^{-5} dL·g^{-1}, α = 0.786 for poly(ε-caprolactone),[226] and K = 5.00·10^{-5} dL·g^{-1} and α = 0.75 for poly(isobornyl acrylate).[227]

3.2.10 Electrospray Ionization-Mass Spectrometry (ESI-MS) Measurements

Electrospray Ionization (ESI)[228,229] is a technique used in mass spectrometry to produce intact ions *in vacuo* from solution of large and complex species. It is especially useful in producing ions from macromolecules because it overcomes the propensity of these molecules to fragment when ionized. John Bennett was awarded with Nobel Prize in chemistry in 2002 for the development of electrospray ionization for the analysis of biological macromolecules.[228] ESI-MS is now a basic method used in biological

chemistry laboratory and in addition is extensively being used for the analysis of macromolecules.

The basic set-up of an ESI-MS is shown in **Figure 3.9**. The analyte is introduced to the source in solution either from a syringe pump or as the eluent flow from liquid chromatography. Flow rates are typically of the order of 5-10 $\mu L \cdot min^{-1}$. The analyte solution passes through the electrospray needle that has a high potential difference (with respect to the counter electrode) applied to it (typically in the range from 2.5 to 4 kV). This forces the spraying of charged droplets from the needle with a surface charge of the same polarity to the charge on the needle. The droplets are repelled from the needle towards the source sampling cone on the counter electrode. As the droplets traverse the space between the needle tip and the cone and solvent evaporation occurs.

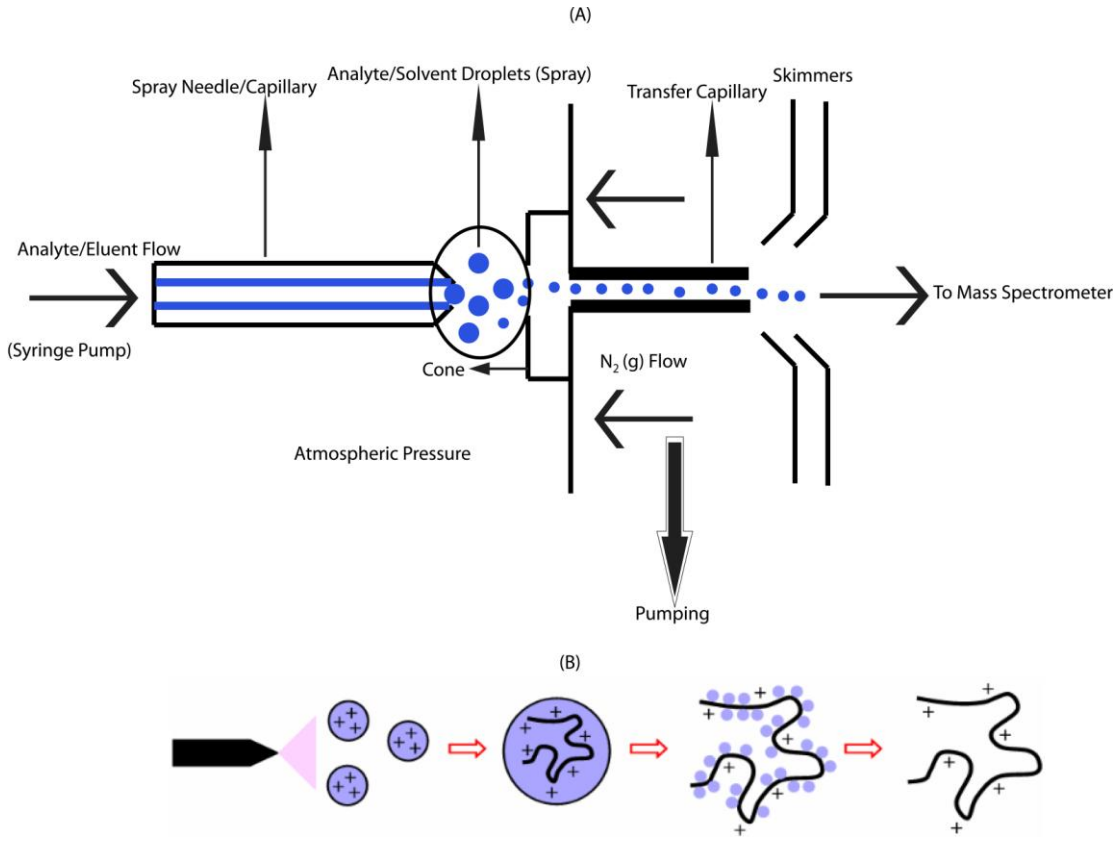

Figure 3.9 Basic setup of ESI-MS and schematic mechanism of the ion formation in ESI. Figure B is adapted from the lecture script of Prof. Dr. Christopher Barner-Kowollik "Modern Methods for Synthesis and Characterization of Macromolecules"

As the solvent evaporation occurs, the droplet shrinks until it reaches the point that the surface tension can no longer sustain the charge (the Rayleigh limit) at which point a "Columbic explosion" occurs and the droplet is ripped apart. This produces smaller droplets that can repeat the process as well as naked charged analyte molecules. These charged analyte molecules (they are not strictly ions) can be singly or multiply charged. ESI is a very soft method of ionization and is an important technique in biological and macromolecular studies where it is required that non-covalent molecule-protein or protein-protein interactions are representatively transferred into the gas-phase. The major disadvantage of the technique is that very little (usually no) fragmentation is produced. This leads to the requirement for tandem mass spectrometry for structural elucidation studies where the analyte molecules can be fragmented.

In the present thesis (**Chapter 4, 9 and 10**), mass spectra were recorded on an LXQ mass spectrometer (ThermoFisher Scientific, San Jose, CA, USA) equipped with an atmospheric pressure ionization source operating in the nebulizer assisted electrospray mode. The instrument was calibrated in the *m*/*z* range 195-1822 using a standard containing caffeine, Met-Arg-Phe-Ala acetate (MRFA) and a mixture of fluorinated phosphazenes (Ultramark 1621) (all from Aldrich). A constant spray voltage of 3.5 kV and a dimensionless sheath gas of 8 and a sweep gas flow rate of 2 were applied. The capillary voltage, the tube lens offset voltage, and the capillary temperature, were set to 60 V, 120 V and 275 °C, respectively. The LXQ was coupled to a Series 1200 HPLC-system (Agilent, Santa Clara, CA, USA) consisting of a solvent degasser (G1322A), a binary pump (G1312A), a high-performance autosampler (G1367B), followed by a thermostated column compartment (G1316A). Separation was performed on two mixed bed size exclusion chromatography columns (Polymer Laboratories, Mesopore 250 × 4.6 mm, particle diameter. 3 µm) with pre-column (Mesopore 50 x 4.6 mm) operating at 30°C. THF at a flow rate of 0.30 mL·min^{-1} was used as eluent. The mass spectrometer was coupled to the column in parallel to an RI-detector (G1362A with SS420x A/D) in a setup described earlier.[230] 0.27 mL·min^{-1} of the eluent were directed through the RI-detector and 30 µL·min^{-1} infused into the electrospray source after post-column addition of a 100 µM solution of sodium iodide in methanol at 20 µL·min^{-1} by a micro-flow HPLC syringe pump (Teledyne ISCO, Model

100DM). Flow-rates, instrument settings and salt concentrations were optimized to yield maximum ionization efficiency while keeping salt cluster formation to a minimum.[231] 20 µL of a polymer solution with a concentration of 6 $mg \cdot mL^{-1}$ were injected onto the HPLC system.

3.2.11 Contact Angle (CA) Measurement

Contact angle (CA) measurement is an important method for surface analysis related to surface energy and tension. Contact angle is a quantitative measure of the degree of wetting of a solid by a liquid. It is defined geometrically as the angle formed by a liquid at the three phase boundary where a liquid, gas and solid intersect as shown in **Figure 3.10**.

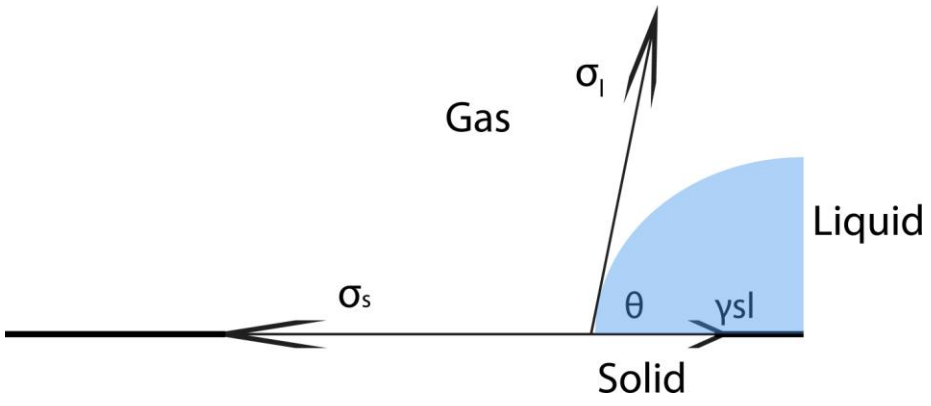

Figure 3.10 Contact angle formation on solid surfaces

Indices s and l stands for solid and liquid, the σ_s and σ_l describe the surface tension components, γ_{sl} represents the interfacial tension between the two phases and θ is the contact angle corresponding to the angle between vectors σ_l and γ_{sl}. The low value of θ indicates that the liquid spreads well while high value of θ indicate poor wetting. Because of its simplicity, contact angle measurement has been broadly accepted for material surface analysis related to wetting, adhesion, and absorption. The performance of contact angle analysis has been made easier, quicker, and more precise with the availability of modern contact angle systems which make use of precision optics and charge-couple device (CCD) cameras with image processing

hardware and software. A droplet of liquid is dispensed onto the substrate surface (manually or automatically), and a CCD camera reveals the profile of the droplet on a monitor. Software calculates the tangent to the droplet shape and the contact angle.

In this present thesis (**Chapter 7**), the contact angle measurements were performed at the Max Planck Institute of Metals Research, Stuttgart on Krüss contact angle measuring system G10.

3.2.12 Ellipsometry

Ellipsometry is a non-destructive optical method for determining thickness and optical properties of thin films, surfaces and material's microstructures. It measures changes in the state of polarization of the light reflected or transmitted from the material's surface. The polarization change is represented as an amplitude ratio, Ψ, and the phase difference, Δ. The basic components for collecting ellipsometry data are: light source, a polarizer, which polarizes the light, a compensator, introducing a defined phase retardation of one field component with respect to the orthogonal one, a sample, an analyzer and a detector. The set-up of a typical ellipsometer is shown in **Figure 3.11**.

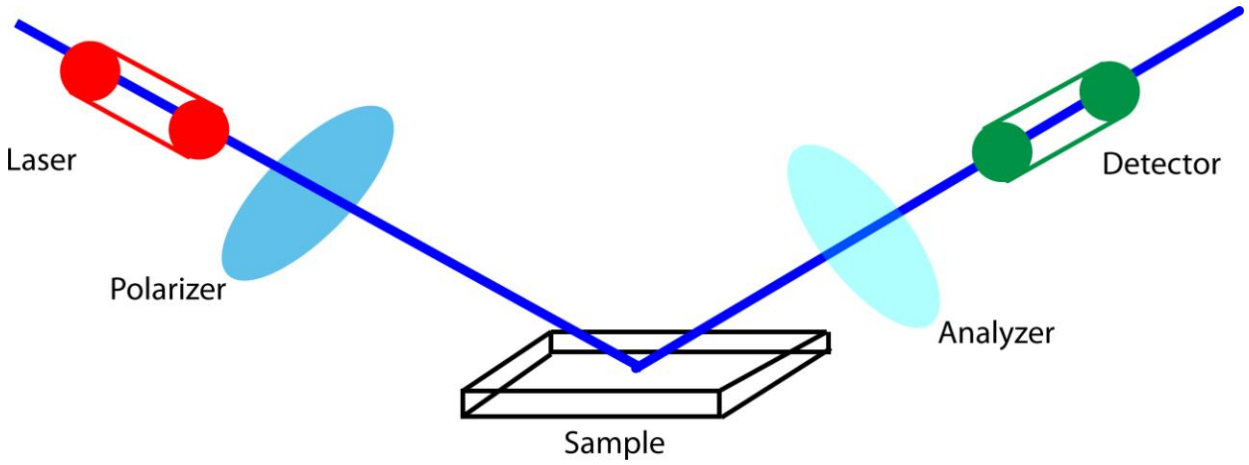

Figure 3.11 Schematic setup for an ellipsometry measurement

In spite of its extreme sensitivity, ellipsometry has not been widely used because it is an indirect measurement requiring the computational power of modern computers. Ellipsometry does not measure directly the optical constants or film thickness, but an amplitude ratio (Ψ) and the phase difference (Δ) which, however, are functions of these

characteristics. The film thickness and all optical constants must be extracted through a careful and rather sophisticated analysis based on different models.

All the measurements in the current thesis (**Chapter 7**) were carried out on submonolayer-ellipsometer EL-X-02C (DRE GmbH). As a light source, a He-Ne laser with λ = 632.8 nm was applied and the angle of incidence was set to 65 °. A four-layer model (silicon substrate + silicon oxide layer + SM-TMS monolayer + polymer layer) was employed to simulate the experimental data. The refractive indices used to calculate the thickness of silicon substrate, silicon substrate with oxide layer, silicon substrate with SM-TMS, silicon substrate with polymer (PAA) were 3.858-i0.018, 1.4598, 1.402 and 1.527, respectively.[232]

3.2.13 Density Measurement

The measurement of density is based on the oscillating U-tube method. The sample is introduced into U-shaped borosilicate glass tube that is electronically excited to vibrate at its characteristic frequency. The characteristic frequency changes depending on the density of the sample. Through a precise determination of the characteristic frequency and mathematical conversion, the density of the sample can be determined. Due to the high temperature dependency of the density value, the measuring cell has to be thermostated precisely.

In the binary mixtures, the density of the mixture is a function of its composition. Thus, by using density/concentration tables, the density value of a binary mixture can be used to calculate its composition. The accuracy of the concentration measurement is dependent not only on the accuracy of the instrument, but also on the gradient of the density/concentration correlation.

The density of the PDVB microspheres (**Chapter 8**) in ethanol was determined using a density meter (DMA 5000 M, Anton Paar) at 293K. The particle density was found to be 1.82 $g \cdot cm^{-3}$ and 1.12 $g \cdot cm^{-3}$ for PDVB80 and PDVB55 microspheres, respectively (as shown in **Figure 3.12** and **3.13**). If the analysed solutions are diluted enough, a linear dependence of the density ρ on the concentration of the solute c can be observed:

$$\rho = \frac{\partial \rho}{\partial c} c + \rho_1 \tag{3.4}$$

where ρ_1 denotes the density of the solvent.

If this linear dependence is experimentally confirmed, the gradient and the intercept of the straight line give respectively $\partial\rho/\partial c$ and ρ_1. Finally, the density of the polymer ρ_2 in the given solvent can be expressed as follows:

$$\rho_2 = \frac{\rho_1}{1-\frac{\partial\rho}{\partial c}} \tag{3.5}$$

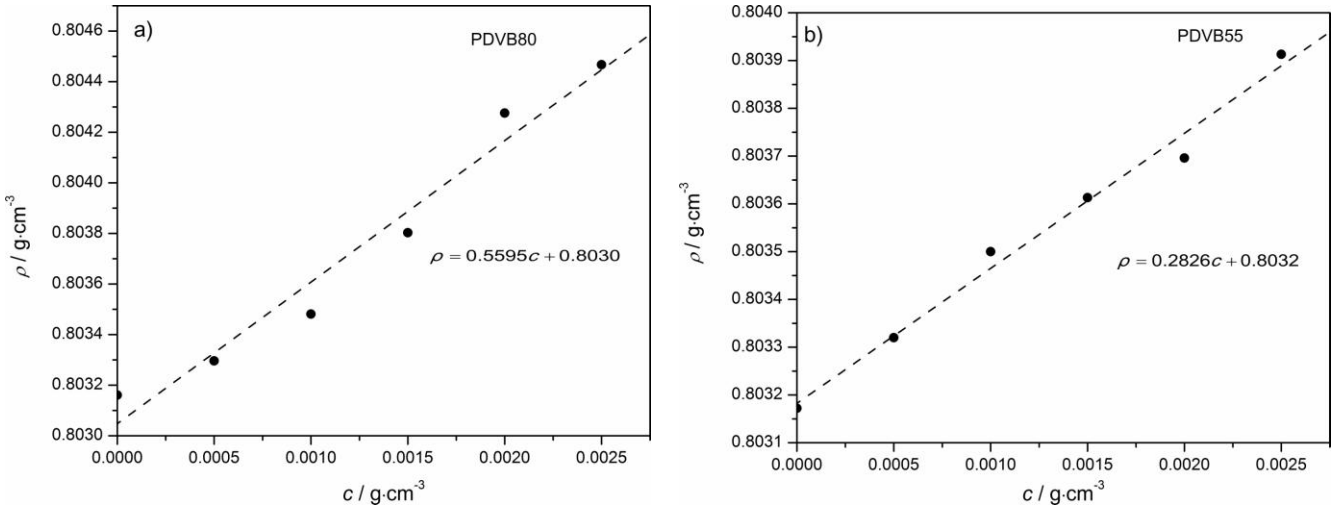

Figure 3.12 Determination of the density of a) poly(divinylbenzene) 80 and b) poly(divinylbenzene) 55 microspheres by linear fitting (solid line)

3.2.14 Elemental Analysis

Elemental analysis is an important analytical to obtain information concerning the elemental composition of a sample. The elemental analysis can not only determine what elements are present in a sample but can be used to quantify the percentages of different elements present in any sample. Therefore, elemental analysis is useful in determining the structure as well as to obtain information about structure and purity of an unknown compound. The most common form of elemental analysis, CHN analysis, is accomplished by combustion analysis. In this technique, a sample is burned in an excess of oxygen, and various traps collect the combustion products — carbon dioxide,

water, and nitric oxide. The weights of these combustion products can be used to calculate the composition of the unknown sample.

In the present thesis (Chapter 6), the elemental composition of the microspheres was analysed using an automatic elemental analyser Flash EA 1112 from Thermo Scientific, which was equipped with a MAS 200R auto sampler by Dr. Detlef Schmiedl at Fraunhofer Institute for Chemical Technology. The calibration standards methionine, and 2,5-bis-5-tert-butyl-2-benzoxazolylthiophene (BBOT), and vanadium pentoxide, tin capsules, and silver containers were purchased from IVA Analysentechnik e. K., Germany. Helium 5.0 for the GC-TCD analysis was purchased from Linde, Germany. The exact details for the calibration of the equipment are described in following paragraphs.

Prior to the determination of the elemental composition, the samples, standards, capsules and chemicals were conditioned as follows: The samples, calibration standards and vanadium pentoxide were allowed to stand for 5 days at ambient temperature in a dessicator over phosphorous pentoxide. The tin capsules and silver containers were stored at ambient temperature in a drying chamber at 24 °C with an air humidity of 30%.

For the accurate, simultaneous determination of carbon, hydrogen, nitrogen and sulphur (CHNS) a calibration of the system was carried out using methionine. Methionine was accurately weighed (0.200 to 2.250 mg) into tin containers in duplicate with a microbalance XP26 DR (METTLER TOLEDO, Germany). Vanadium pentoxide (2.5-3.5 mg) was added to the sample. The tin containers were subsequently accurately sealed (air free).

A six point linear calibration curve was generated for each element by combustion of the standard samples and simultaneous gas chromatographic separation of the generated combustion gases N_2, CO_2, H_2O and SO_2. The gases were determined by thermal conductivity detection (TCD). The peak areas were calculated by the software Eager300 (Thermo Scientific). The calculation of the linear function ($y = f(x) = a \cdot x + b$), slope, axis intercept, the coefficient of determination) were performed using Microsoft Excel 2000. The coefficients of determination were 0.9998 for N, C and H, and 0.9999 for S, respectively.

Table 3.1 Calibration of elemental analysis equipment using methionine and BBOT for the simultaneous determination of CHNS

Standard	Composition in wt.-% (mean ±SD; *n* = 6)			
	N	C	H	S
Methionine (theo.)	9.39	40.25	7.43	21.49
Methionine (exp.)	9.34 ±0.12	40.49 ±0.44	7.44 ±0.09	21.54 ±0.19
BBOT (theo.)	6.51	72.53	6.05	7.44
BBOT (exp.)	6.79 ±0.06	72.96 ±0.48	6.10 ±0.04	7.74 ±0.07

The retrieval and accuracy of the method was determined using the standards methionine and BBOT. 1.000 mg of the standards were weighed six-fold into tin containers, vanadium pentoxide was subsequently added. The containers were sealed and the retrieval of the elements CHNS was determined as described above.

To determine the CNHS composition of the microspheres samples, known amounts (1 to 2 mg) of each sample and vanadium pentoxide were weighed into tin capsules using a microbalance XP26 DR (METTLER TOLEDO, Germany). After sealing the capsules, they were placed inside the MAS 200R auto sampler, and then dropped into an oxidation/reduction reactor kept at 900 °C. The exact amount of oxygen required for the optimum combustion of the sample was delivered into the combustion reactor at a known time. The reaction of oxygen with the tin capsule at elevated temperature generates an exothermic reaction which raises the temperature to 1 800 °C for a few seconds. At this high temperature organic substances are converted into gases.

Reliable oxygen determination is achieved through an oxygen-specific pyrolysis reactor heated to 1 065 °C. This allows for a complete pyrolysis of the sample in an oxidant-free environment. A “nickel plated carbon” catalyst ensures a high precision of oxygen determination by generation of carbon monoxide (CO). The formed gas is measured by simultaneous GC-TCD. For the accurate oxygen determination a calibration of the system was performed with methionine. Methionine was accurately weighed (0.200 to 2.250 mg) into silver containers in duplicate with a microbalance XP26 DR (METTLER TOLEDO, Germany). The silver containers were accurately sealed (air free). A six point linear calibration curve was generated for oxygen by

pyrolysis of the standard samples and simultaneous gas chromatographic separation of the generated CO. The gas was determined by TCD. The peak area was calculated by the software Eager300 (Thermo Scientific). The calculation of the linear function ($y = f(x) = a \cdot x + b$), gradient, axis intercept, the coefficient of determination) was done using Microsoft Excel 2000. The coefficient of determination was 0.9997 for O.

Table 3.2 Calibration of elemental analysis equipment using methionine and BBOT for the determination of O

Standard	Composition in wt.-% (mean ±SD; n = 6)
	O
Methionine (theo.)	21.45
Methionine (exp.)	21.57 ±0.16
BBOT (theo.)	7.43
BBOT (exp.)	7.30 ±0.1

The retrieval and accuracy of the method was determined using the standards methionine and BBOT. 1.000 mg of the standards was weighed six-fold into silver containers. The containers were sealed and the retrieval of the element O was determined as described above.

The determination of the elemental composition CHONS of the samples was carried out as described above. The determination was performed within the calibration range, i.e. the peak areas of the combustion gases (N_2, CO_2, H_2O, SO_2) and the pyrolysis gas (CO) were inside the calibration range. Generally an amount of 1.000 to 2.000 mg of the microspheres samples was weighed into tin or silver containers and the composition was determined.

3.2.15 Thermogravimetric Analysis (TGA)

Thermogravimetric analysis is used to determine changes in weight of the sample as a function of temperature. TGA is commonly used to study decomposition temperature and thermal stability of a material. In the field of polymers, TGA is largely

used to determine polymer degradation temperatures, and also to determine the amount of inorganic (noncombustible) filler in polymer or polymer composites.

A typical TGA includes the following operations: a sample is placed into a high-precision balance with a pan. The pan is subsequently placed into a small electrically heated furnace with a thermocouple to accurately measure the temperature. The atmosphere may be purged with an inert gas to prevent oxidation or other undesired reactions. A computer is generally used to control the instrument. Analysis is carried out by raising the temperature gradually and monitoring changes in sample weight as temperature is increased. After the data are obtained, curve smoothing and other operations are usually done to obtain exact points of inflection.

In the present thesis (**Chapter 9**), thermogravimetric measurements were carried out on a with a 951 Thermogravimetric analyzer from DuPont. Approximately 6 mg of sample was heated from 5 $K \cdot min^{-1}$ from ambient temperature to 800 °C in a dynamic nitrogen atmosphere (*flow rate* = 100 $mL \cdot min^{-1}$).

Chapter 4 Strongly Electron Deficient Sulfonyldithioformate Based RAFT Agents for Hetero Diels-Alder (HDA) Conjugation: Computational Design and Experimental Evaluation

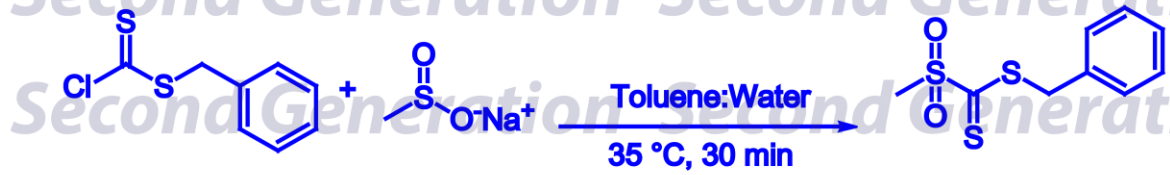

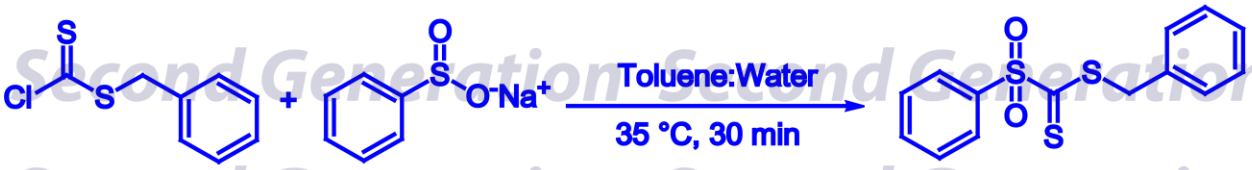

4.1 Introduction

As discussed in detail in **Chapter 2**, attempts to address the existing shortcomings of classical *click* and Diels-Alder conjugation and to provide a convenient methodology using RAFT generated polymers directly (*i.e.* without any further modification) as a heterodienophile have been attempted in a RAFT-HDA approach. A combination of RAFT polymerization and HDA chemistry can be employed as a versatile method for the synthesis of complex polymer architectures such as block copolymers,[146] stars,[147] as well as functional surfaces (discussed in detail in **Chapter 5**, **6** and **7**). The tendency of electron deficient dithioesters to undergo HDA cycloaddition can be successfully used for the formation of block copolymers constituted of monomers from different families. However, the previously discussed RAFT-HDA conjugations were facilitated by the use of a catalyst which enhances the electron-withdrawing nature of the RAFT Z-group allowing the reactions to be carried out at 50 °C and achieve near quantitative completion within several hours.

While such reaction times and temperatures compare very favorably with the reaction times observed in the Cu(I) catalyzed azide/alkyne coupling, a further rate enhancement and temperature decrease is highly desirable, especially in applications that involve the coupling or grafting of biological moieties. It is indeed possible to dramatically enhance the rate of RAFT-HDA conjugation by using two approaches. Firstly by employing a very reactive diene, *i.e.* through the use of novel cyclopentadienyl (Cp) functionalized polymers.[168] By virtue of such Cp-capped polymers it is possible to achieve conjugation under ambient conditions within a few minutes, although a catalyst is required in some cases. Secondly - and this approach is explored in the current contribution – RAFT agents featuring extremely electron withdrawing moieties in the Z-position can be employed so that even less reactive dienes (*e.g.* based on butadiene) can be conjugated at ambient temperatures and in the absence of catalysts. The approach taken in the current study is as follows: The ability to function as RAFT agents of these suitable thiocarbonyl thio compounds which are reported in the literature to be excellent electron deficient dienophiles[233] is assessed *via ab-initio* quantum mechanical calculations. These quantum mechanical calculations were carried out in the group of A/Prof. Michelle Coote at the Australian National University (ANU) in Canberra. Based

on these quantum mechanical calculations the corresponding RAFT agent is synthesized and evaluated for its ability to mediate the controlled radical polymerization of variable monomers. In parallel studies, the reactivity of these RAFT agents in HDA reactions is assessed by reacting them with a series of low molecular weight dienes. The progress of these model reactions is followed *via* electrospray ionization mass spectrometry (ESI-MS). Finally, polymers prepared *via* the novel RAFT agent class are conjugated to diene carrying polymers to assess the efficiency of the HDA cycloaddition for block copolymer formation.

4.2 Experimental

4.2.1 Synthesis of Benzyl chlorodithioformate (3)

Thiophosgene (25.0 g, 220 mmol) and benzyl mercaptan (26.0 mL, 220 mmol) were dissolved in 50 ml of carbon disulfide. The solution was stirred in a flask with a gas outlet for 48 h at ambient temperature. The HCl gas produced was passed through a bubble counter and subsequently neutralized in alkaline sodium hydroxide solution. After the reaction had finished, the solvent was evaporated and the product was distilled under vaccum to yield (17.5 g, 86 mmol) of benzyl chlorodithioformate in 40% yield.^{1}H-NMR (400 MHz, $CDCl_3$, δ / ppm) (shown in **Figure S.4.1** in SI): 4.74 (s, 2H, CH_2^{b}), 7.52-7.58 (m, 5H,$C_6H_5^{a}$).^{13}C-NMR (75 MHz, $CDCl_3$, δ / ppm) (shown in **Figure S.4.2** in SI): 46.22 (1C, CH_2^{e}), 128.34-128.85 (4C, $C_6H_5^{b,c}$), 129.25 (1C, $C_6H_5^{a}$), 137.46 (1C, $C_6H_5^{d}$), 196.37 (1C, C=S^{f}).

4.2.3 Synthesis of Benzyl methylsulfonyldithioformate (5)

The two-phase mixture of the benzyl chlorodithioformate (7.5 g, 37 mmol), sodium methane sulfinate (3.8 g, 37 mmol), tetrabutylammonium hydrogen sulfate 0.5 g, 0.19 mmol), 60 mL toluene and 60 mL water was stirred at 35 °C for 30 min. After 30 min the toluene phase was washed with water (3 times), dried over $MgSO_4$ and evaporated *in vacuo*. The red oily residue was purified by column chromatography using a 1:1 mixture of petroleum spirit (40 °C - 60 °C) and diethyl ether. The red fraction was collected and concentrated *in vacuo* to give orange crystals (1g, 4 mmol, 11% yield).

^{1}H-NMR (400 MHz, $CDCl_3$, δ / ppm) (shown in **Figure S.4.3** in SI): 3.20 (s, 3H, CH_3^a), 4.44 (s, 2H, CH_2^b), 7.34 (m, 5H, $C_6H_5^c$). ^{13}C-NMR (75 MHz, $CDCl_3$, δ / ppm) (shown in **Figure S.4.4** in SI): 38.28 (1C, CH_3^a), 41.56 (1C, CH_2^b), 127.3 (1C, $C_6H_5^c$), 127.71 (2C, $C_6H_5^d$), 128.09 (2C, $C_6H_5^e$), 131.01 (1C, $C_6H_5^f$), 220 (1C; C=S^g).

4.2.4 Synthesis of Benzyl phenylsulfonyldithioformate (7)

A two-phase mixture of benzyl chlorodithioformate (7.5 g, 37 mmol), benzenesulfinic acid sodium salt (3.8 g, 37 mmol), tetrabutylammonium hydrogen sulfate (0.5 g, 0.19 mmol), 60 mL of toluene and 60 mL water was stirred at 35 °C for 30 min. After 30 min the toluene phase was washed with water (3 times), dried over $MgSO_4$ and evaporated *in vacuo*. The pink oily residue was purified by column chromatography using 1:1 mixture of petroleum spirit (40 °C - 60 °C) and diethyl ether. The pink fraction was collected and concentrated *in vacuo* to give pink crystals (8g, 26 mmol, 70% yield). ^{1}H-NMR (400 MHz, $CDCl_3$, δ / ppm) (shown in **Figure S.4.5** in SI): 4.35 (s, 2H, CH_2^d), 7.31 (m, 5H, $C_6H_5^e$), 7.54 (m, 2H, $C_6H_5^b$), 7.67 (m, 1H, $C_6H_5^c$), 8.02 (m, 2H, $C_6H_5^a$). ^{13}C-NMR (75 MHz, $CDCl_3$, δ / ppm) (shown in **Figure S.4.6** in SI): 43.5 (1C, CH_2^f), 128.52-129.91 (5C, $C_6H_5^{b,c,h,i,j}$), 132.46 (1C, $C_6H_5^a$), 134.63 (1C, $C_6H_5^d$), 136.50 (1C, $C_6H_5^g$), 222.2 (1C, C=S^e).

4.2.5 Monitoring the Reaction between (7) and Butyl Acrylate by UV-Visible Spectroscopy

Butyl acrylate (1.4 g, 10.88 mmol) and Benzyl phenylsulfonyl dithioformate (0.02 g, 0.063 mmol) were mixed and 1 mL of this mixture was dissolved in 4 mL of chloroform. The resulting solution was transferred to a UV cuvette immediately prior to placing in the preheated (60 °C) cuvette holder of the UV-Visible spectrophotometer. The reaction was allowed to proceed at this temperature for 13 h.

4.2.6 Polymerizations

A master batch of isobornyl acrylate, AIBN and (**7**) (at concentrations of 0.016 mol·L^{-1} and 0.027 mol·L^{-1} as shown in **Table 4.3**, see the *Results and Discussion* section) was prepared, and aliquots of 2 mL were placed in separate sample vials. The

reaction mixtures were subsequently purged with nitrogen to remove residual oxygen. The polymerizations were performed at 60 °C for required time intervals. The reaction was stopped by exposing the reactants to oxygen and chilling in an ice bath.

4.2.7 Synthesis of Hexadiene-1-ol Derivative (12)

A mixture of *trans*,*trans*-2,4-hexadien-ol (2.55 g, 26 mmol), succinic anhydride (3.0 g, 30 mmol), and DiPEA (3.4 g, 26 mmol) in diethyl ether (10 mL) was stirred for 2 days at ambient temperature. The solvent was removed under reduced pressure and the residue dissolved in CH_2Cl_2 and washed with aqueous solution of 5% w/w citric acid. The organic layer was dried over $MgSO_4$, filtered and the solvent was removed under reduced pressure to give (**12**). ^{1}H-NMR (400 MHz, $CDCl_3$, δ / ppm) (as shown in **Figure S.4.11** in SI): 1.70 (d, 3H, CH_3^a), 2.61 (t, 4H, CH_2^g), 4.54 (d, 2H, CH_2^f), 5.58 (dt, 1H, CH^e), 5.71 (dq, 1H, CH^b), 6.01 (ddq, 1H, CH^c), 6.21 (dd, 1H, CH^d).

4.2.8 Synthesis of Open Chain Diene Functionalized Poly(ethylene glycol) monomethylether (14)

Poly(ethylene glycol) monomethylether (2 g, 1 mmol), (**12**) (1.8 g, 9 mmol) and 4-dimethylamino pyridine (0.07 g, 0.6 mmol) was dissolved in 48 mL CH_2Cl_2 and was cooled in ice bath. *N*,*N*-dicyclohexylcarbodiimide (1.8 g, 9 mmol) dissolved in 24 mL CH_2Cl_2 was added dropwise to above mixture. The resulting solution was stirred at ambient temperature for 12 h. The solution was filtered through a cotton fitted Pasteur pipette and the polymer was precipitated in cooled diethyl ether. M_n (NMR) = 2061 g·mol^{-1}. ^{1}H-NMR (400 MHz, $CDCl_3$, δ / ppm) (as shown in **Figure S.4.12** in SI): 1.70 (d, CH_3^a), 2.61 (t, CH_2^g), 3.36 (s, CH_3^i), 3.61 (m, CH_2^h), 4.23 (t, CH_2^h), 4.58 (d, CH_2^f), 5.58 (dt, CH^e), 5.71 (dq, CH^b), 6.01 (ddq, CH^c), 6.21 (dd, CH^d).

4.2.9 Synthesis of Tosylated Poly(ethylene glycol) monomethylether (16)

NaOH (1.4 g) was dissolved in 7.5 mL of H_2O. A solution of poly(ethylene glycol) monomethyl ether (5.0 g, 2.5 mmol) in 6.2 mL THF was subsequently added. The resulting mixture was cooled in an ice bath. To this was added solution of *p*-toluenesulfonyl chloride (4.3 g, 2.2 mmol) in 6.2 mL THF. The mixture was stirred

overnight at ambient temperature. The mixture was extracted with CH_2Cl_2 and the CH_2Cl_2 phase was washed three times with water. The CH_2Cl_2 phase was dried over $MgSO_4$, filtered and concentrated. The concentrated solution was precipitated in cold diethyl ether. M_n (NMR) = 2167 g·mol^{-1}. ^{1}H-NMR (400 MHz, $CDCl_3$, δ / ppm) (as shown in **Figure S.4.13** in SI): 2.45 (s, CH_3^a), 3.38 (s, CH_3^e), 3.63 (m, CH_2^d), 4.15 (t, $CH_2^{d'}$), 7.36 (m, $C_6H_5^b$), 7.81 (m., $C_6H_5^c$).

4.2.10 Synthesis of Cyclopentadienyl Functionalized Poly(ethylene glycol) monomethylether (17)

Tosylated poly(ethylene glycol) monomethyl ether (1.0 g, 0.45 mmol) was dissolved in anhydrous THF (5 mL) and cooled to 0 °C in an ice-salt bath. To this solution sodium cyclopentadienide solution (2.0 M in THF) (0.7 mL, 1.36 mmol, 3 equiv.) was slowly added. The mixture was stirred overnight at ambient temperature. The resulting mixture was filtered through a pad of silica gel and washed with THF. The filterate was concentrated *in vacuo* and the polymer was precipitated in cold diethyl ether. M_n (NMR) = 2200 g mol^{-1}. ^{1}H-NMR (400 MHz, $CDCl_3$, δ / ppm) (as shown in **Figure S.4.14** in SI): 2.71 (m, -CH_2^c), 2.95 (m, CH_2^d), 3.38 (s, CH_3^a), 6.47-6.08 (m, $C_5H_5^{e,f,g}$).

4.2.11 Model Reaction between Open Chain Diene Functionalized PEG (14) and Benzyl methylsulfonyldithioformate (5)

A solution of (**14**) (0.2 g, 0.097 mmol) and benzyl methylsulfonyldithioformate (0.03 g, 0.123 mmol, 2 equiv.) in 1 mL chloroform was kept at room temperature for 1h and 24 h, respectively. The resulting mixture was analyzed by direct infusion ESI-MS.

4.2.12 Model Reaction between Open Chain Diene Functionalized PEG (14) and Benzyl phenylsulfonyldithioformate (7)

A solution of (**14**) (0.2 g, 0.097 mmol) and benzyl phenylsulfonyldithioformate (0.04 g, 0.123 mmol, 2 equiv.) in 1 mL chloroform was kept at ambient temperature for 1 h and 24 h, respectively. The resulting mixture was analyzed by direct infusion ESI-MS.

4.2.13 Model Reaction between PEG-Cp (17) and Benzyl methylsulfonyldithioformate (5)

A solution of (**17**) (0.2 g, 0.088 mmol) and benzyl methylsulfonyldithioformate (0.04 g, 0.1818 mmol, 2 equiv.) in 1 mL chloroform was kept at ambient temperature for 1 h and 24 h respectively. The resulting mixture was analyzed by direct infusion ESI-MS.

4.2.14 Synthesis of Bromide-Terminated Polystyrene (28)

To a dried Schlenk tube was added copper (I) bromide. The tube was then sealed with a septum, evacuated and back filled with nitrogen. In another Schlenk tube was added styrene and PMDETA. The resulting monomer solution was then deoxygenated by three freeze-pump-thaw cycles and subsequently transferred to the Schlenk tube containing the copper (I) bromide *via* cannula. The tube was then sealed under a nitrogen atmosphere and placed in a thermostatic oil bath held at 90 °C. After the polymerization mixture reached the desired temperature, 1-phenylethyl bromide (1-PEBr) was added. The initial ratio of [Styrene]: [1-PEBr]:[CuBr]:[PMDETA] was 100:1:1:1. The polymerization was stopped by cooling the tube in an ice-bath and exposing the contents to oxygen. The resulting mixture was then diluted with THF and passed through a column of neutral alumina to remove the copper catalyst. The polymer was isolated by two-fold precipitation in cold methanol.

4.2.15 Synthesis of Cyclopentadienyl-Terminated Polystyrene (28)

To a stirred solution of bromide terminated polystyrene (**27**) dissolved in THF, cooled in an ice-salt bath, a 10-fold excess of sodium cyclopentadienide (2.0 M in THF) was added dropwise. After the addition was completed, the reaction mixture was allowed to gradually warm to ambient temperature and stirred over night. The cyclopentadienyl functionalized polymer was subsequently isolated by precipitation in cold methanol. M_n (SEC) = 3400 and 4900 g·mol^{-1}. ^{1}H-NMR (400 MHz, $CDCl_3$, δ / ppm) (as shown in **Figure S.4.15** in SI): 1.04 (m, -CH_3^c), 1.13-2.5 (m, CH^b, CH_2^d, CH^e, CH_2^f), 2.83 (m, CH_2^i), 3.28 (m, CH^g), 5.78-6.19 (m, $C_5H_5^{j,k,l}$), 6.51-7.16 (m, $C_6H_5^{a,h}$).

4.2.16 Hetero Diels-Alder Cycloaddition Between Benzyl phenylsulfonyldithioformate Terminated Poly(isobornyl acrylate) (9) and Cyclopentadienyl Terminated Polystyrene (28)

A solution of poly(isobornyl acrylate) (6.3 mg, 1.25 μmol), polystyrene (4.3 mg, 1.25 μmol) or (6.3 mg, 1.25 μmol), weight depending on M_n) in 40 μL chloroform was kept at ambient temperature for 10 minutes. The solvent was subsequently removed under reduced pressure and the residue analyzed by SEC employing THF as the solvent.

4.2.17 Computational Procedures (A/Prof. M. L. Coote, ANU)

Standard *ab-initio* molecular orbital theory and density functional theory calculations were performed using Gaussian 03[234] and Molpro 2002.1[235] software, using a high-level of theory, previously shown to reproduce experimental equilibrium constants for radical addition to C=S double bonds to within an order of magnitude.[236] Geometries of all species were optimized at the B3-LYP/6-31G(d) level of theory and scaled frequency calculations were also performed at that level. Conformations of all species were systematically screened at the B3-LYP/6-31G(d) level of theory. Improved energies were then obtained using our W1-ONIOM method, as defined and evaluated in our previous papers.[237] In each case the G3 core was taken as the corresponding reaction of the $S=C(Z)SCH_3$ agent, the W1 inner core was taken as the reaction of methyl radical with $S=CH_2$, and the outer layer (where this differed from our core) was calculated at the ROMP2/6-311+G(3df,2p) level of theory. For the equilibrium constants, results are shown both using the harmonic oscillator approximation, and also the more accurate hindered rotor model. The hindered rotor calculations were performed using the TES 60° method, as described previously.[238] Comparison calculations for the Z = H, F, CH_3, Ph and OCH_3 RAFT agents are taken from ref.[239] These computational calculations carried out at the ARC Centre of Excellence for Free Radical Chemistry and Biotechnology, Research School of Chemistry, Australian National University, Australia by C.Y. Lin and A/Prof. M. L. Coote.

4.3 Results and Discussion

4.3.1 Quantum Mechanical Assessment (A/Prof. M. L. Coote, ANU)

Based on observations in the literature, RAFT agents carrying methylsulfonyl and phenylsulfonyl Z-groups should be excellent and extremely electron deficient dienophiles in the context of Diels-Alder conjugation.[240] However, these sulfonyl dithioformates have never been assessed in their ability to function as RAFT agents. Thus, as a first step, we evaluate the ability of these thiocarbonyl thio compounds to act as potential RAFT agents, before progressing to their synthesis. Below, we also include other Z-groups – that are also strongly electron withdrawing such as CF_3 – into our quantum mechanical assessment, although the current study only considers sulfonyl type leaving groups from a synthetic perspective. In our earlier theoretical studies of the RAFT process, we identified a number of key thermodynamic quantities that could be employed to rank RAFT agents for the rapid qualitative assessment of their suitability as control agents in practical settings.[241] The effect of the Z-group on the stability of the RAFT agent is assessed as the energy change of the isodesmic reaction (equation 4.1).

$$S{=}C(Z)SCH_3 + H{-}CH_3 \rightarrow S{=}C(H)SCH_3 + Z{-}CH_3 \qquad (4.1)$$

The effect of the Z group on the stability of the RAFT adduct radical is assessed as the energy change of the isodesmic reaction (equation 4.2), which is more commonly known as the radical stabilization energy.

$$CH_3SC{\bullet}(Z)SCH_3 + H{-}CH_3 \rightarrow CH_3SCH(Z)SCH_3 + {\bullet}CH_3 \qquad (4.2)$$

The effect of the Z group on the fragmentation efficiency (ΔH_{frag}) of the RAFT adduct radical is assessed as the energy change of the isodesmic reaction (equation 4.3).

$$CH_3SC{\bullet}(Z)SCH_3 + S{=}C(H)SCH_3 \rightarrow CH_3SC{\bullet}(H)SCH_3 + S{=}C(Z)SCH_3 \qquad (4.3)$$

Values of these thermodynamic quantities for Z = CF_3 and SO_2CH_3 are provided in **Table 4.1**, together with corresponding values for other prototypical RAFT agent substituents (Z = H, F, CH_3, Ph and OCH_3), taken from the literature.[239] The corresponding actual equilibrium constants at 333.15 K (K_{333}) for the addition-fragmentation reactions, (equation 4.4), have also been calculated for Z = CF_3 and SO_2CH_3, for two model leaving groups, R = $CH(CH_3)Ph$ and $C(CH_3)_2CN$, and are provided in **Table 4.2** and compared with the corresponding data for the known RAFT agent substituent, Z = Ph, taken from the literature.[239]

$$R\bullet + S{=}C(Z)SCH(CH_3)_2 \rightarrow RSC\bullet(Z)SCH(CH_3)_2 \qquad (4.4)$$

Table 4.1 Effect of Z-Group on the Stabilities (0 K; $kJ{\cdot}mol^{-1}$) of $S{=}C(Z)SCH_3$ and $CH_3SC\bullet(Z)SCH_3$

Z-Group	Stability $S{=}C(Z)SCH_3$	Stability $CH_3SC\bullet(Z)SCH_3$	ΔH_{frag}
SO_2CH_3	5.8	75.3	30.9
Ph	41.3	96.3	21.0
CF_3	–17.3	62.6	17.8
H	0	61.1	0
CH_3	35.1	59.9	-10.0
F	43.5	46.9	-24.0
OCH_3	85.9	58.5	-45.0

From **Table 4.1** it is seen that the effect of the CF_3 and SO_2CH_3 Z-groups on the fragmentation efficiency of the RAFT agents is similar to that of a phenyl group; in the case of Z = CF_3 the efficiency is marginally lower, for Z= SO_2CH_3 it is marginally higher. On this basis one might expect these two RAFT agents to show similar degrees of rate retardation to dithiobenzoates, and this is also suggested by the equilibrium constants for their radical addition reactions in **Table 4.2**.

The exact ordering of the equilibrium constants is affected by the nature of the leaving group. In particular, as discussed previously,[242] cyanoisopropyl is a particularly efficient leaving group and this is due not only to the high stability of the cyanoisopropyl radical but also to a homoanomeric effect in the corresponding RAFT-adduct radical. This latter effect is stronger for the SO_2CH_3 Z-group and its equilibrium constant is thus marginally lower than for the other species. For the $CH(CH_3)Ph$ leaving group, the homoanomeric effect is now absent and the equilibrium constants thus follow their fragmentation efficiencies, with the CF_3 Z-group giving rise to the lowest equilibrium constants. Despite these minor differences, the main conclusion is that the equilibrium constants for reactions of the Z = CF_3 and SO_2CH_3 RAFT agents are similar to those of Z = Ph. Hence, when used under the same conditions with the same monomers and leaving groups, one might expect the Z = CF_3 and SO_2CH_3 RAFT agents to display similar degrees of rate retardation to analogous dithiobenzoates.

Table 4.2 Equilibrium Constants and Associated Thermodynamic Parameters at 333.15 K for R• + S=C(Z)SCH$(CH_3)_2$→RSC•(Z)SCH$(CH_3)_2$

Z-Group	Harmonic Oscillator				Hindered Rotor			
	ΔS (J/mol)	ΔH (kJ/mol)	ΔG (kJ/mol)	K (L/mol)	ΔS (J/mol)	ΔH (kJ/mol)	ΔG (kJ/mol)	K (L/mol)
R = $C(CH_3)_2CN$								
SO_2CH_3	-183.3	-77.3	-16.2	9.4×10^3	-171.1	-75.7	-14.6	5.4×10^3
CF_3	-184.0	-82. 6	-21.3	5.9×10^4	-172.9	-81.0	-19.7	3.4×10^4
Ph	-190.5	-86.4	-23.0	1.1×10^5	-177.8	-81.1	-21.9	7.4×10^4
R = $CH(CH_3)Ph$								
SO_2CH_3	-165.0	-90.7	-35.7	1.1×10^7	-141.7	-88.7	-33.7	5.3×10^6
CF_3	-167.5	-75. 7	-19.9	3.6×10^4	-159.9	-73.9	-18.1	1.9×10^4
Ph	-164.3	-80.4	-25.7	2.9×10^5	-142.8	-75.5	-28.0	6.6×10^5

Although the thermodynamics of the addition-fragmentation equilibrium are similar for Z = CF_3, SO_2CH_3 and Ph, the stability calculations in **Table 4.1** indicate that their addition and fragmentation kinetics are likely to be very different. In particular, both

Z = CF_3 and Z = SO_2CH_3 significantly destabilize the RAFT agent when compared with Z = Ph, CH_3, F and OCH_3. This is not unexpected, as both CF_3 and SO_2CH_3 are significantly more electron withdrawing than the other Z-groups considered and as such interfere with the resonance stabilization of $S=C(Z)SCH_3$. At the same time both CF_3 and SO_2CH_3 are less effective at stabilizing the RAFT adduct radical than the phenyl group, which is a strong resonance stabilizer. As a result, one would expect the Z= CF_3 and Z= SO_2CH_3 RAFT agents to show both faster addition and fragmentation rates than Z = Ph. These increases in the forward and reverse reaction rates counterbalance each other and the net effect is that their equilibrium constants are relatively similar; however, as is well known, the faster exchange rates are expected to give rise to narrower polydispersities and better overall control of the polymerization.[243]

In summary, the above computational study predicts that RAFT agents having CF_3 or SO_2CH_3 Z-groups should be effective RAFT agents. They may show similar degrees of rate retardation to corresponding dithiobenzoate reactions under the same conditions, but are expected to show much faster exchange rates and hence better control of polymerization.

4.3.2 Synthesis of Benzyl methylsulfonyldithioformate (5) and Benzyl phenylsulfonyldithioformate (7) and their Suitability as Potential RAFT Agents

Based on the above *ab initio* quantum mechanical calculations, it seemed promising to synthesize two sulfonyl type RAFT agents, *i.e.* benzyl methylsulfonyldithioformate (**5**) and benzyl phenylsulfonyldithioformate (**7**), which can be achieved in a two step procedure. Note that both (**5**) and (**7**) possess a benzyl leaving group. Although the quantum chemical recommendation would be a cyanoisopropyl leaving group, the target RAFT agents are synthetically simpler to access when they carry a benzyl R-group. The first step – which is common to the synthesis of both – involves the reaction of thiophosgene with equivalent amounts of benzyl mercaptan.[244] Subsequently, the remaining chloride function was substituted by a methylsulfonyl or phenylsulfonyl moiety *via* a two-phase reaction between an aqueous solution of sodium methanesulfinate and benzyl chlorodithioformate (dissolved in toluene) employing tetrabutylammonium hydrogen sulfate as phase transfer catalyst.[245]

The entire reaction sequence is depicted in **Scheme 4.1**. The yield for the synthesis of the intermediate benzyl chlorodithioformate (**3**) is close to 40%, whereas the subsequent yield for (**5**) is very low (less then 11%), in agreement with previous observations by Senning *et al.* for the synthesis of similar electron depleted thiocarbonyl compounds.[246] In contrast, (**7**) could be obtained with yields close to 70%. It is for this reason that (**7**) is preferentially employed in the current study. The resulting ^{1}H and ^{13}C-NMR of (**3**), (**5**), (**7**) are shown in **Figure S.4.1- S.4.7** in the supporting information section.

In a subsequent step, the ability of the prepared C-sulfonyldithioformate to induce living characteristics in a free radical polymerization was assessed. For this purpose (**7**) was chosen as control agent, as large amounts (see above) could be readily prepared. Using (**7**) styrene was polymerized first using $5 \cdot 10^{-2}$ mol·L^{-1} of (**7**) and AIBN (5.10^{-3} mol·L^{-1}) as initiator.

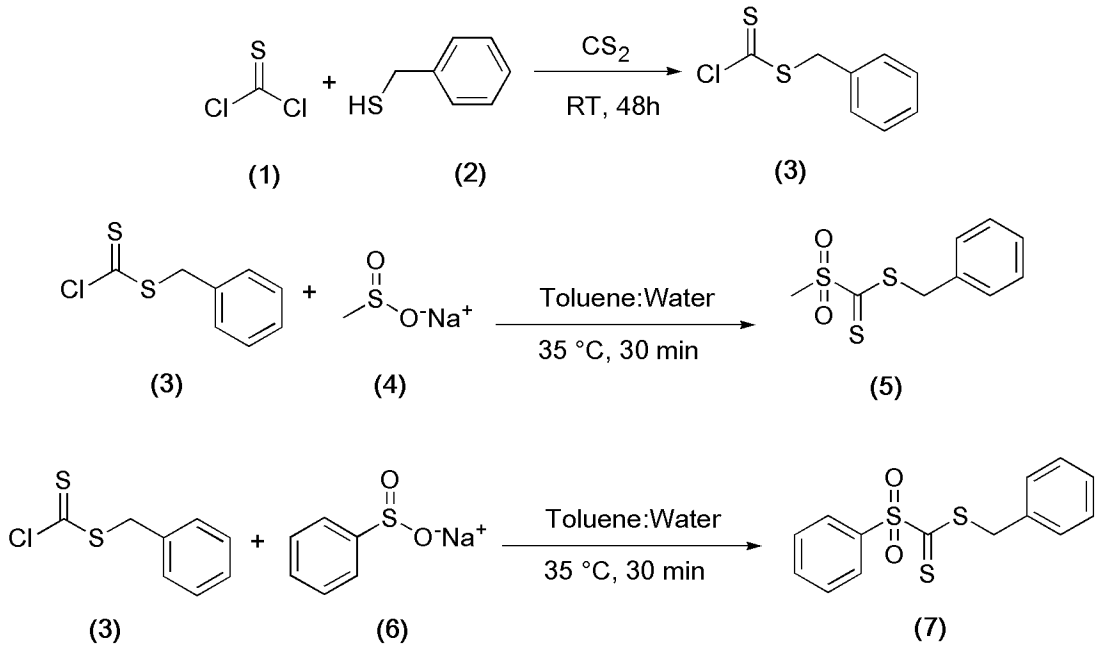

(1) (2) (3) (3) (4) (5) (3) (6) (7)

Scheme 4.1 Reaction of benzyl chlorodithioformate (obtained by reaction of thiophosgene and benzyl mercaptan) with sodium methane sulfinate and benzene sulfinic acid sodium salt to synthesize benzyl methylsulfonyldithioformate (**5**) and benzyl phenylsulfonyldithioformate (**7**) respectively

Interestingly, only partial living behaviour is observed: The molecular weight distributions each depict a signal for polymer (which increases in number average molecular weight but also polydispersity with time) as well as one additional well-defined peak at lower molecular weight of close to 430 g·mol^{-1}, which is stationary over time. Concomitantly, the reaction solution loses its characteristic pink color. Subsequently, a range of (meth)acrylates were assessed for their ability to be mediated by (**7**), including butyl acrylate, methyl acrylate, *tert*-butyl acrylate and methyl methacrylate. For all these monomers a similar result is observed: A loss of color of the reaction solution and only initially some limited control over the polymerization with an additional sharp peak in the chromatogram at high retention times. In order to test the origin of the inability of the RAFT agent to induce a well-controlled process with living characteristics, butyl acrylate – in the presence of (**7**) – was heated at 60 °C for a period of 13 h and UV/Vis spectra were recorded at pre-set time intervals (see **Figure 4.1**). As the on-line UV/Vis monitoring was carried out in the absence of a radical initiator, the color loss must be due to a reaction between the monomer and the RAFT agent in which the choromophore (*i.e.* the dithioester unit) is converted.

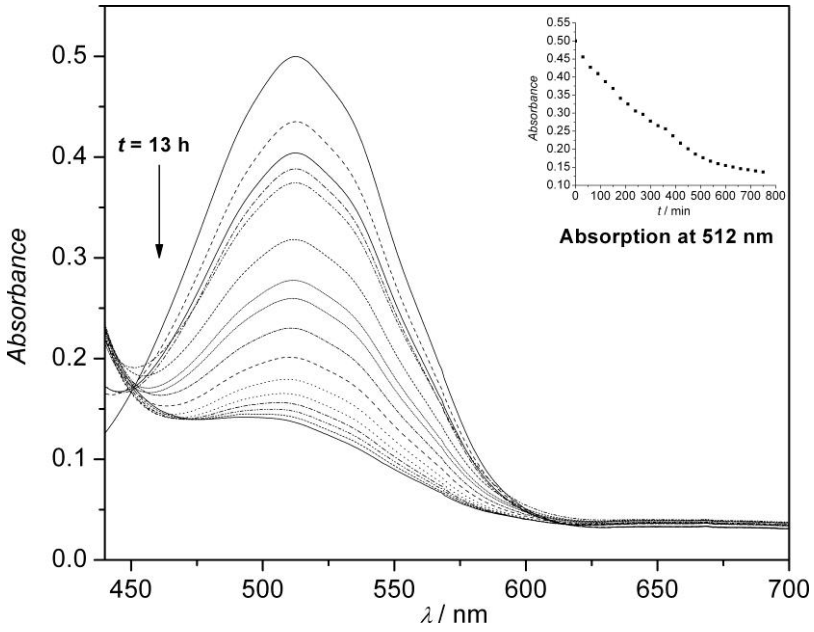

Figure 4.1 Evolution of the UV absorbance (on-line monitoring) during the reaction between butyl acrylate (BA) and PSDTF (**7**) (c_0^{BA} = 10.88 mol·L^{-1} and c_0^{PSDTF} = 0.063

mol·L^{-1}) carried out at T = 60 °C in chloroform in the absence of a radical source. The figure in set depicts the peak absorption intensity as a function of time

A simple explanation for such behavior is the hypothesis that the dithioester undergoes a hetero Diels-Alder reaction with the respective monomer, which functions as a diene. Such a reaction can take place as (**7**) is highly electron deficient and a potent dienophile. With this assumption, the observed well-defined peak in the SEC elugrams is understandable. The molecular weight of the hetero Diels-Alder adduct between (**7**) and styrene is 412 g·mol^{-1}, which is – within experimental uncertainty – close to the molecular weight of the peak observed in the SEC traces. A similarly good agreement is observed between the potential butyl acrylate-HDA adduct and the observed sharp peak in the SEC distribution of reaction mixtures taken from (**7**) mediated butyl acrylate polymerization (M_n^{SEC} = 480 g·mol^{-1}, $M_n^{BA\text{-}HDA\ adduct}$ = 436 g·mol^{-1}). The SEC elugrams for the polymerization of styrene and butyl acrylate in the presence of (**7**) are depicted in **Figure S.4.8** and **S.4.9** in the supporting information section. However, the reaction of (**7**) with butyl acrylate may be alternatively (and possibly more plausibly) explained by considering that the sulfur atom in (**7**) is a good nucleophile that can undergo Michael-type additions with acrylates, resulting in the formation of a heterocyclic compound with the same structure as the HDA adduct.[247]

The detailed mechanism of the reaction between (**7**) and butyl acrylate is provided in **Figure S.4.7** in the supporting information section. ^{1}H-NMR spectra of the products obtained after reaction of styrene and butyl acrylate with (**7**) are highly complex as the chemical shifts of the protons associated with the thiopyran rings are in variable axial and equatorial positions and have different shifts. Employing the high dienophilicity of (**7**) towards variable monomer units, the reaction of a dithioester with styrene in a hetero Diels-Alder reaction is readily employed to conjugate polymer strands to the surface of silicon wafers, where the wafer is functionalized with the styrene units and reacted with linear polymer chains capped with sulfonyldithioformate units (discussed in detail in **Chapter 7**).

To circumvent side reactions of the thiocarbonyl group in (**7**) with monomer units, an acrylate monomer with a considerably bulky ester group was selected, which

provides a steric hindrance to possible reaction partners. Indeed, isobornyl acrylate does not show any decolorization during polymerization in the presence of (**7**). The reaction scheme for the polymerization of isobornyl acrylate using (**7**) is shown in **Scheme 4.2**. In order to assess the effectiveness of the reaction, a series of RAFT agent concentrations was employed. The results of the individual reaction runs are collated in **Table 4.3**.

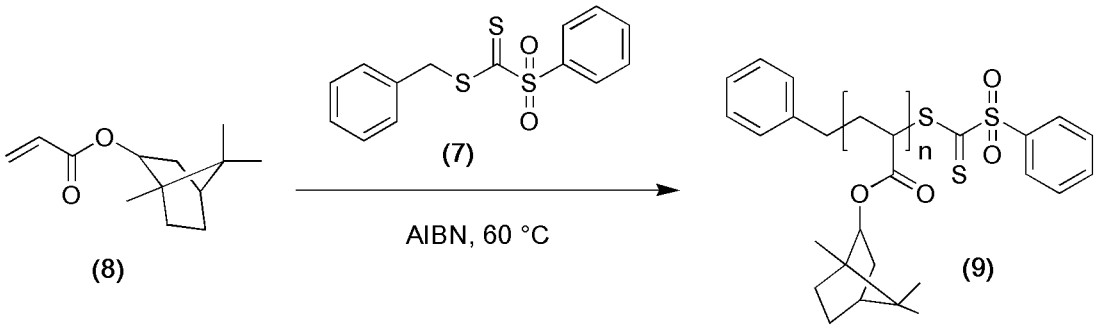

Scheme 4.2 Reaction scheme for the bulk polymerization of iBA using (**7**) and AIBN at 60 °C. The polymerization was carried out employing different concentrations of (**7**), which are collated in **Table 4.3**

Figure 4.2 depicts the number average molecular weight (theoretical as well as experimental) and polydispersity *vs* conversion plot for the polymerization of isobornyl acrylate employing both the higher concentration of (**7**) ($c_{\mathbf{7}0}$ = 1.6·10^{-2} mol·L^{-1}) as well as the lower one ($c_{\mathbf{7}0}$ = 2.7·10^{-2} mol·L^{-1}). The associated conversion *vs* time plots are included in the supporting information section (see **Figure S.4.10**).

The polymerization is both inhibited (*i.e.* there exists a time period in which no polymerization activity is recorded) and rate retarded (*i.e.* the polymerization is significantly slower as the corresponding non-RAFT mediated process or a polymerization at lower initial RAFT agent concentration), in agreement with the *ab-initio* quantum mechanical calculations which predict a considerable rate retardation. Inspection of **Figure 4.2** and **Table 4.3** indicates that the experimental molecular weights are in close agreement with those predicted theoretically. The polydispersities are relatively low and support the notion that a polymerization with living characteristics is occurring.

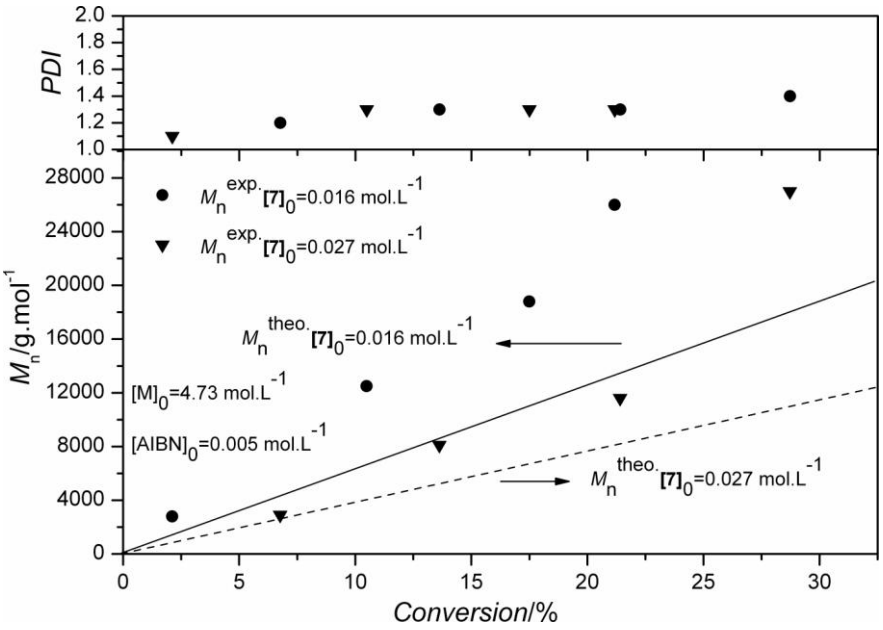

Figure 4.2 Monomer to polymer conversion *vs* theoretical, M_n^{theo}, and experimental, M_n^{exp}, number average molecular weights and *PDI* for the bulk polymerization of iBA (T = 60 °C) using (**7**) at two concentrations as indicated within the figure

Table 4.3 Molar mass and conversion data for poly(isobornyl acrylate) samples synthesized *via* AIBN initiated RAFT polymerization using (**7**) as RAFT agent at 60 °C

Sample	*time* /h	$[M]_0$	$[7]_0$	$[AIBN]_0$	*Conversion*[a] / %	M_n^{exp}/ g mol^{-1}	*PDI*	M_n^{theo}/ g mol^{-1}
PiBA 1	8	4.73	0.016	0.005	2.1	2800	1.1	1600
PiBA 2	13	4.73	0.016	0.005	10.5	12500	1.3	6800
PiBA 3	14	4.73	0.016	0.005	17.5	18800	1.3	11000
PiBA 4	16	4.73	0.016	0.005	21.1	26000	1.3	13300
PiBA 5	24	4.73	0.027	0.005	6.8	2900	1.2	2700
PiBA 6	26	4.73	0.027	0.005	13.6	8100	1.3	5200
PiBA 7	28	4.73	0.027	0.005	21.4	11600	1.3	8100
PiBA 8	30	4.73	0.027	0.005	28.7	24000	1.4	10700

[a]Conversions were derived *via* on-line FT-NIR experiments; the theoretical molecular weight, M_n^{theo}, was calculated *via* the following equation: $M_n^{theo} = ([M]_0/[PSDTF]_0) \cdot M^{Mon} \cdot Conversion + M^{PSDTF}$

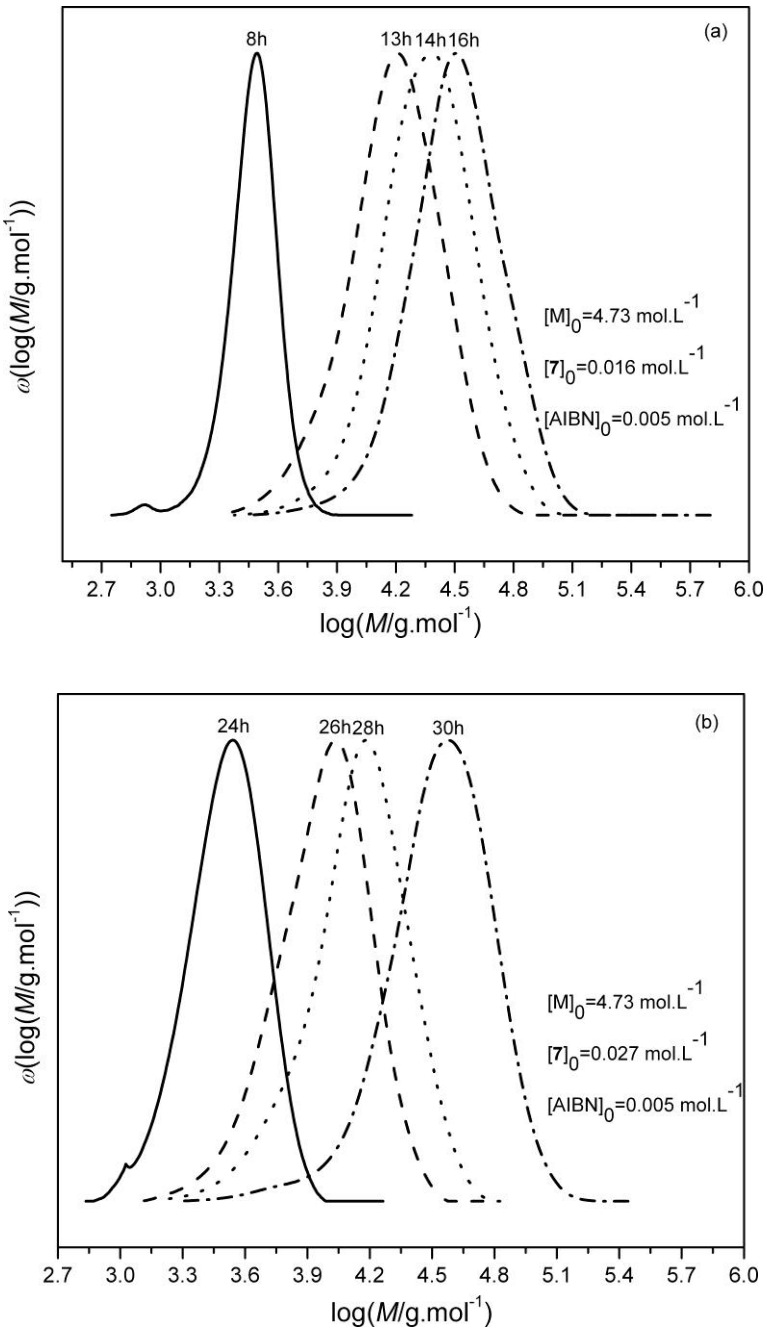

Figure 4.3 Molecular weight distribution evolution with increasing reaction time for the bulk polymerization of iBA using AIBN as initiator and two concentrations of RAFT agent (**7**) (provided within the Figure) at 60 °C

Figure 4.3 (a) depicts the evolution of molecular weight using the lower concentration of (**7**), while **Figure 4.3** (b) shows a similar plot for the higher concentration of (**7**). For each concentration, mono-modal molecular weight

distributions, *w*(log *M*) vs log *M*, are observed which shift to higher molecular weight without any tailing or bimodalities with increasing monomer to polymer conversion (*i.e.* reaction time). The results depicted in **Figure 4.3** support the notion that selecting isobornyl acrylate as monomer can – due to its bulky ester side chain – effectively prevent the *in-situ* Diels-Alder and/or Michael-type reactions between the RAFT agent and the monomer.

4.3.3 Synthesis of Diene Functionalized Polymers

The RAFT agent (**7**) was prepared with regard to its strongly electron deficient nature and it should thus be an excellent dienophile in conjugation reactions with suitable diene carrying polymer chains. Such conjugations should proceed without the addition of catalyst and under mild reaction conditions. To generate suitable macro-dienes, poly(ethylene glycol) monomethylether (PEG) was functionalized with two types of dienes that are different in their reactivity, *i.e.* an open chain diene, which displays a reduced reactivity towards the ene, and cyclopentadiene (Cp), which is highly reactive in HDA reactions. The molecular weight of the PEG was selected such that the progress of the conjugation reaction could be easily monitored *via* ESI-MS analysis of the product mixtures. The synthesis of the hexadiene functionalized PEG was carried out in a two step process as depicted in **Scheme 4.3**. The first step involves the reaction between a hexadiene-ol with succinic anhydride, which results in the formation of a diene having carboxyl end groups (**12**). Subsequently, this diene is reacted with poly(ethylene glycol) monomethylether *via* DCC coupling to form the open chain diene functionalized PEG (**14**). The ^{1}H-NMR spectra for (**12**) and (**14**) are shown in **Figure S.4.11** and **S.4.12**, respectively, in the supporting information section.

The synthesis of the cyclopentadienyl functionalized PEG is also a two step process, where the first step involves the synthesis of the tosylated PEG derivative (**16**), which is obtained *via* the reaction of poly(ethylene glycol) monomethyl ether with *p*-toluenesulfonyl chloride. The subsequent step involves the reaction of tosylated PEG (**16**) with sodium cyclopentadienide solution to result in the formation of the cyclopentadienyl functionalized PEG (**17**). The reaction sequence is provided in

Scheme 4.3 and ^{1}H-NMR spectra for (**16**) and (**17**) are depicted in **Figure S.4.13** and **S.4.14**, respectively, in the supporting information section.

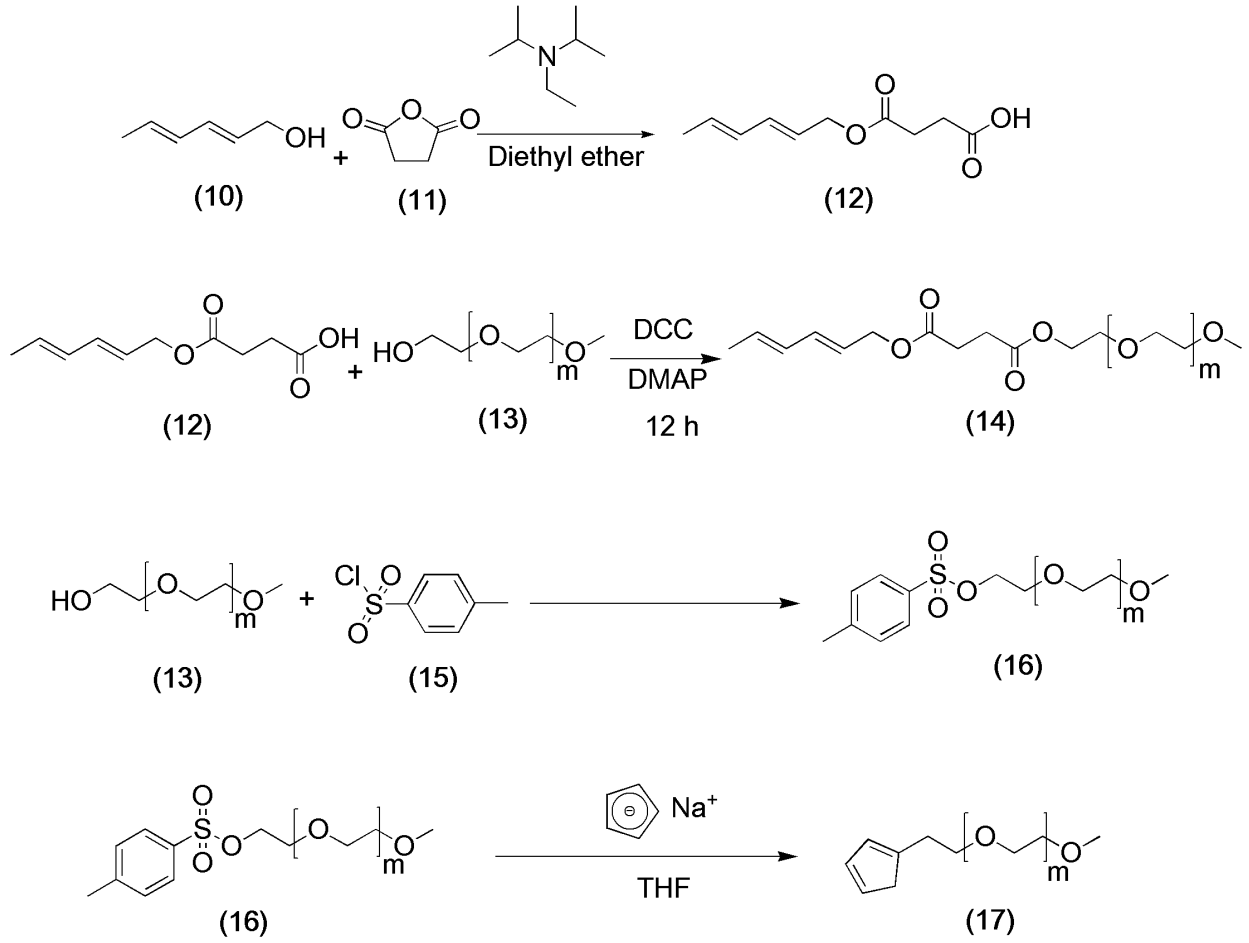

Scheme 4.3 Synthesis of the hexadiene-1-ol derivative (**12**) from *trans*, *trans*-hexadiene-ol (**10**) and succinic anhydride (**11**) to subsequently provide the open chain diene functionalized PEG (**14**) from the reaction of (**12**) with PEG monomethyl ether (**13**). Also depicted is the reaction of PEG monomethyl ether (**13**) with *p*-toluenesulfonyl chloride (**15**) to obtain the tosylated functionalized PEG (**16**), which is subsequently reacted with sodium cyclopentadienide solution to obtain the cyclopentadienyl functionalized PEG (**17**)

4.3.4 Model Reactions between Benzyl methylsulfonyldithioformate and Benzyl phenylsulfonyldithioformate with PEG Functionalized Dienes

To establish the efficiency of the RAFT-HDA conjugation chemistry of the two prepared RAFT agents, various model studies were performed between (**5**) and (**7**) and the diene functionalized PEGs. The reaction sequence for the reaction between open chain and cyclopentadienyl functionalized PEG and (**5**) and (**7**) is shown in **Scheme 4.4**. The dithioformates (**5**) and the PEG-type diene (**14**) were dissolved in chloroform under ambient conditions (in the absence of any catalyst) and the reaction mixture was analyzed *via* ESI-MS after 1 and 24 h, respectively.

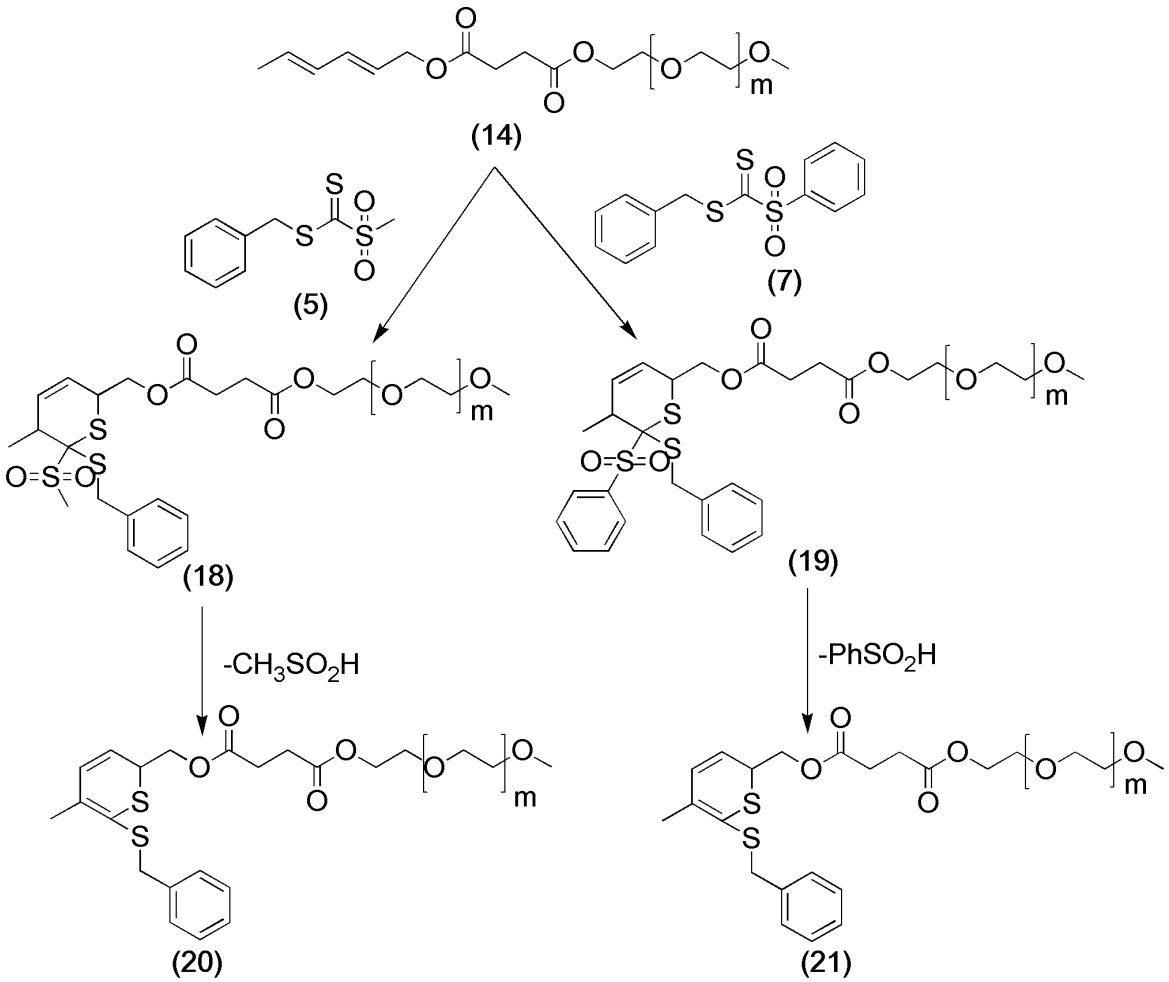

Scheme 4.4 Model reaction between the open chain diene functionalized PEG (**14**) with (**5**) and (**7**) resulting in the formation of the cycloadduct (**18** and **19**) and the subsequent loss of sulfinic acid (**20** and **21**)

Figure 4.4 shows the ESI-MS spectra (expanded in the region between 1800 and 1860 Da) for the reaction between the PEG diene (**14**) and the dithioformate (**5**). The assignment of the spectra is provided in **Table 4.4**. In the reaction of the dithioformate (**5**) with the open chain diene, the main product which can be assigned is generated after the loss of sulfinic acid from the formed thiopyran ring. Such a quantitative loss of sulfinic acid after the cycloaddition has previously been reported in the literature.[248] It should be noted that the loss of sulfinic acid does not affect the covalent linkage between two macromolecular building blocks, when a polymer carrying a dithioformate end group is employed instead of the initial RAFT agent itself. After 1 h the spectrum shows the signals for the starting material and product, while after 24 h the main signal which is observed can be assigned to PEG conjugated to (**5**) through the formation of the 3,6-dihyro-2*H*-thiopyran ring. The individual peak assignments are provided in **Table 4.4**. Inspection of **Table 4.4** shows that the assigned peaks correspond well with the theoretically expected molecular weights.

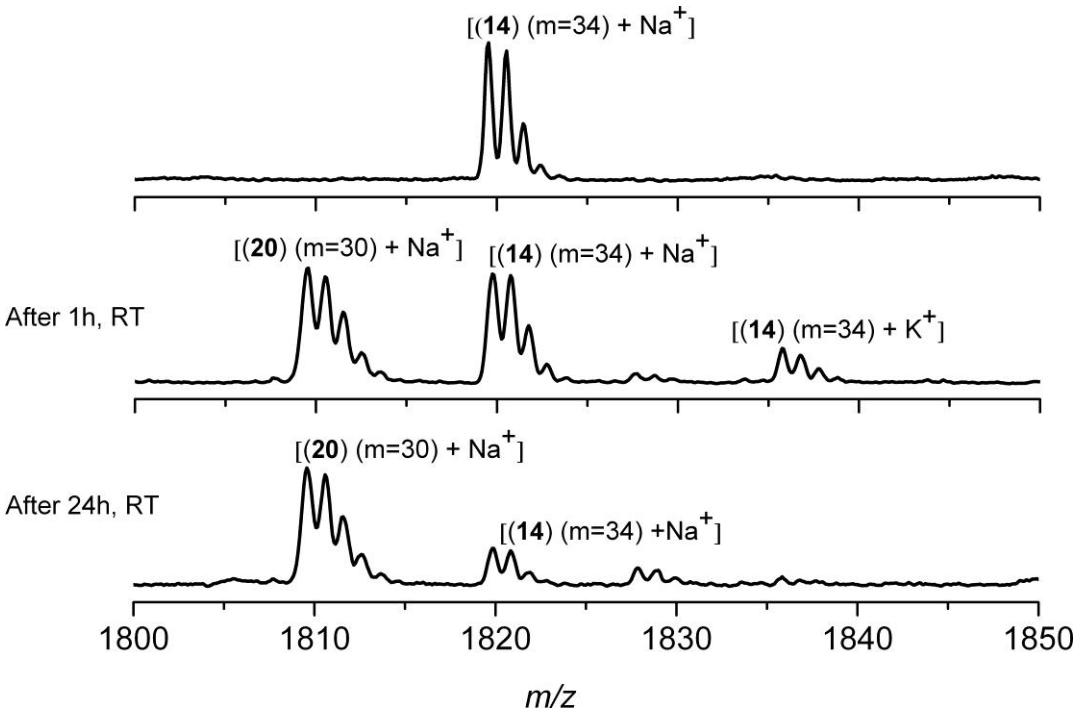

Figure 4.4 Model reaction between open chain diene functionalized PEG (**14**) and (**5**). The conjugation is possible under ambient conditions without any catalyst. The ESI-MS spectra are recorded *via* direct infusion

However, it is also is also evident that some starting material (**14**) is either not reacted to completion or the retro-Diels-Alder reaction occurs under conditions of elevated temperature in the ionization source (275 °C). The amount of (**14**) observable in the mass spectrum is constant even after extending the reaction time beyond 24 h. Neither does elevating the reaction temperature above ambient alter its amount. Such an observation suggests that the residual (**14**) present in the mass spectra may be generated during the ionization process.

Table 4.4 Theoretical and experimental *m/z* values for the first peak in the isotopic distributions of (**14**) and (**20**) in the *m/z* range between 1800 and 1860

m/z^{exp}	Ion Assignment	Molecular Formula	m/z^{theo}	$\Delta m/z$
1809.6	(**20**) (m=30)+Na^+	$[C_{83}H_{150}O_{36}S_2Na]^+$	1809.9	0.3
1819.8	(**14**) (m=34)+Na^+	$[C_{83}H_{160}O_{40}Na]^+$	1820.0	0.2
1835.8	(**14**) (m=34)+K^+	$[C_{83}H_{160}O_{40}K]^+$	1836.0	0.2

Similarly, **Figure 4.5** shows the ESI-MS spectra (expanded in the region between 1800 and 1850 Da) recorded from reaction mixtures between PEG diene (**14**) with (**7**) after 1 and 24 h reaction time at ambient temperature. The individual peak assignments of the spectra are collated in **Table 4.5**, indicating good agreement between the experimental and theoretically expected values. Similar to the reaction between (**14**) and (**5**), the main product which can be assigned is generated after the loss of sulfinic acid. As can be seen in **Figure 4.5**, the reaction between (**7**) and (**14**) is completed after 24 h under ambient conditions. After 1 h the spectra shows mainly the signals from the starting material as well as the emerging product signal.

Again, a small yet significant amount of (**14**) remains even after 24 h of reaction. Identical to what has been observed in the case of the reaction between (**14**) and (**5**), no extension of the reaction time nor an elevation of the reaction temperature or the addition of catalyst can decrease the amount of (**14**) remaining in the mass spectra. Again, it cannot be excluded that the retro Diels-Alder reaction occurs to some extent during ionization.

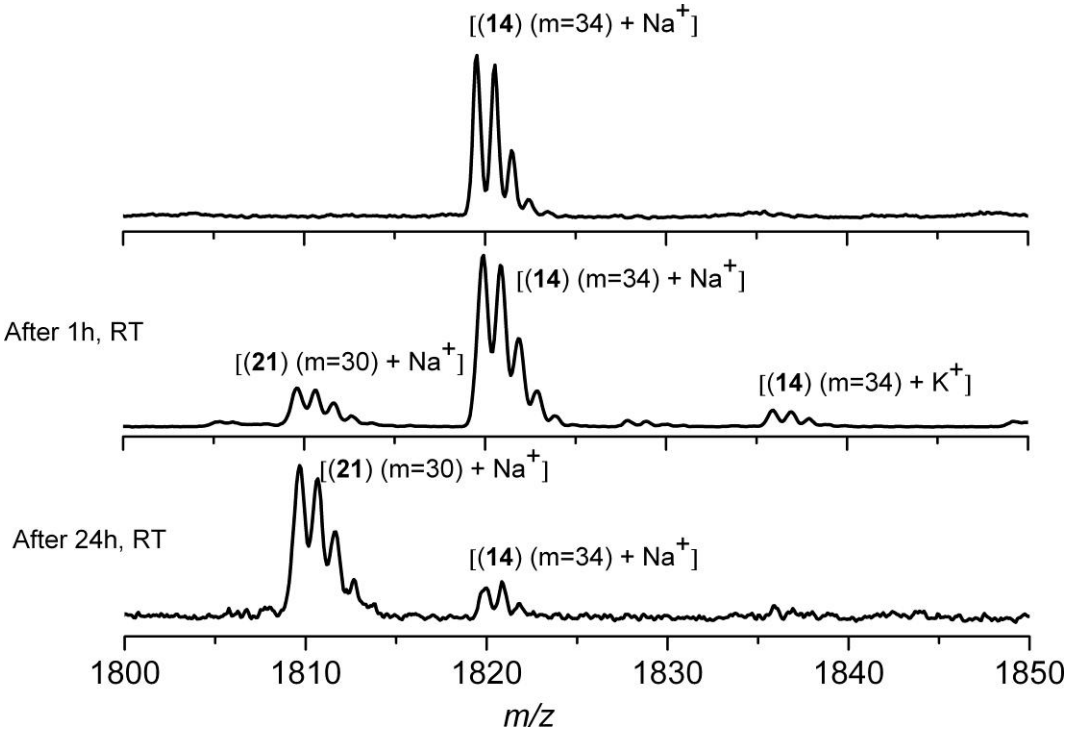

Figure 4.5 Model reaction between the open chain diene functionalized PEG (**14**) and (**7**). The conjugation is possible under ambient conditions without any catalyst. The ESI-MS spectra are recorded *via* direct infusion

Table 4.5 Theoretical and experimental *m/z* values for the first peak in the isotopic distributions of (**14**) and (**21**) in the *m/z* range between 1800 and 1850

m/z^{exp}	Ion Assignment	Molecular Formula	m/z^{theo}	$\Delta m/z$
1809.7	(**21**) (m=30)+Na^+	$[C_{83}H_{150}O_{36}S_2Na]^+$	1809.9	0.2
1819.9	(**14**) (m=34)+Na^+	$[C_{83}H_{160}O_{40}Na]^+$	1820.0	0.1
1835.9	(**14**) (m=34)+K^+	$[C_{83}H_{160}O_{40}K]^+$	1836.0	0.1

In the above model experiments it has been demonstrated that the highly electron deficient dithioformates can react at ambient temperatures in an efficient fashion with open chain dienes. The use of these strongly electron deficient dienophiles allowed the decrease of the reaction temperature without the presence of any catalyst to prepare PEG conjugates. This is a substantial improvement in the reaction conditions

employed previously when benzyl (diethoxyphosphoryl) dithioformate and benzyl pyridine-2-yl dithioformate capped polymers were reacted with identical dienes but required reaction temperatures of 50 °C and the presence of a Lewis acid to increase the reactivity of the dienophile.[146] Recently cyclopentadienyl capped polymers have been reported to improve the reaction rates with benzyl (diethoxyphosphoryl) dithioformate and benzyl pyridine-2-yl dithioformate capped polymers, enabling conjugation times of under a few minutes at ambient conditions.[147] It thus seems a matter of priority to assess whether the dithioformates employed in the present study react in a similar rapid fashion with Cp-capped polymer chains. Similar to the model reactions carried out above with the open chain diene, the cyclopentadiene functionalized PEG (**17**) and (**5**) were reacted at ambient temperatures in the absence of any catalyst. Reaction of (**17**) with (**7**) yields a conjugate product which is isobaric (within the resolution limits of the employed linear quadrupole ion trap) with (**17**) [*m/z* (**17**, n=35+Na^+) = 1732.0 and *m/z* (**17+7**, n=35+Na^+) = 1731.0]. For this reason the mass spectrometric investigation concentrates on the reaction between (**17**) and (**5**). **Figure 4.6** depicts the ESI-MS spectra (expanded in the region between 1700 and 1750 *m/z*) of the reaction between (**17**) and (**5**) after 1 and 24 h, respectively. The assignment of the individual peaks is provided in **Table 4.6** alongside the experimental and theoretically expected *m/z* ratios. In contrast to observations made in the conjugation of the open chain dienes, the conjugate does not loose sulfinic acid in agreement with existing literature reports on the relatively high stabilities of Cp-dithioester adducts.[248] Employing the cyclopentadienyl functionalized polymer, the reaction reaches its final state within a few minutes and a further extension of the reaction time does not lead to a change in the product distribution. The mass spectroscopic observation reveals two facts: Firstly, the conjugation time (at ambient temperature and in the absence of any catalyst) is greatly decreased compared to the reaction rate observed in the case of the open chain dienes. Such an observation does not come as a surprise, as the cyclopentadiene is a more reactive diene than alkyl-substituted butadiene derivatives. Secondly – although the reaction rate of (**17**) and (**5**) is very rapid – again some minor amount of (**17**) is seen in the mass spectra. It is noteworthy that the residual amount of (**17**) does not change at pro-longed reaction times, again supporting the hypothesis that

the retro-Diels-Alder reaction occurs to some extent under the present source conditions. To test this hypothesis, the source conditions, *i.e.* the source temperature, was varied from 100 to 350 °C to assess whether the amount of (**17**) can be influenced. The results indicated that at a source temperature exceeding 300 °C large amounts of (**17**) are found, providing some indication that high temperature during the ionization can potentially contribute to the product peak.

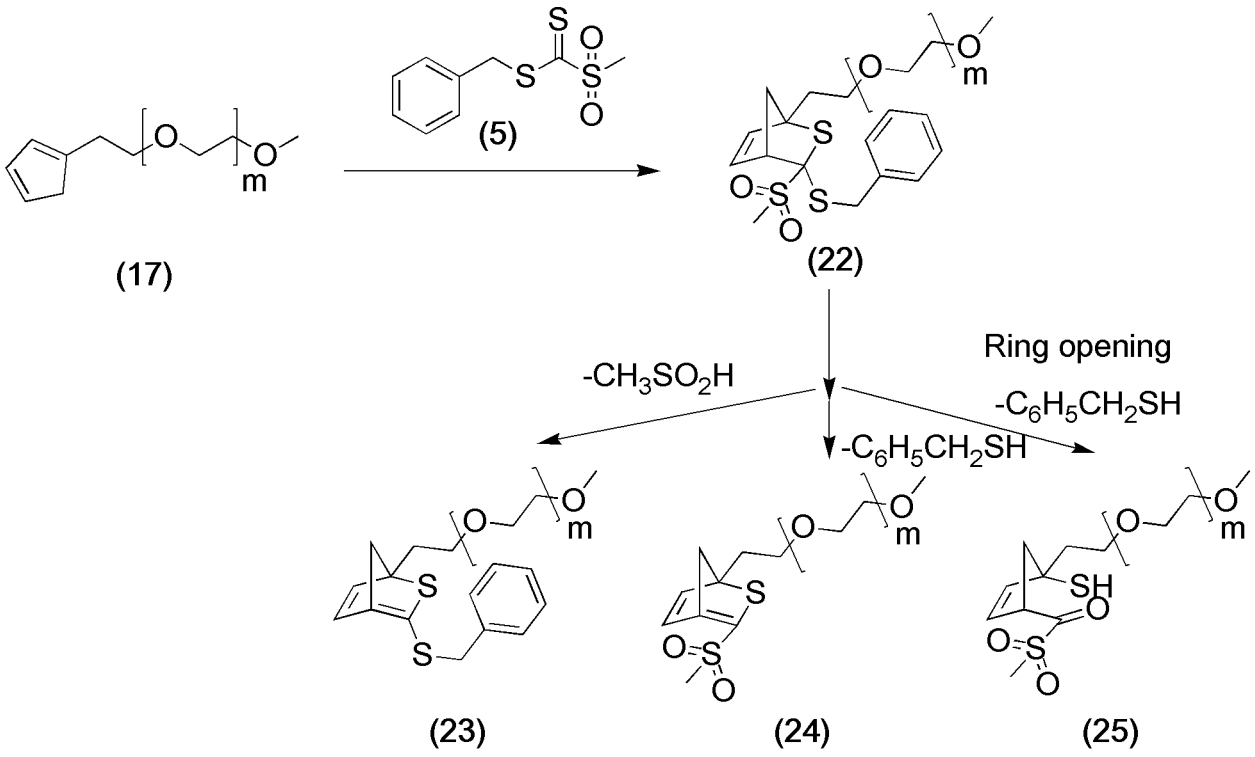

Scheme 4.5 Conjugation of the cyclopentadienyl functionalized PEG (**17**) with (**5**), resulting in the formation of a relatively stable cycloadduct (**22**) without the loss of sulfinic acid, as well as other possible products generated from (**22**) *via* the loss of sulfinic acid (**23**), benzyl mercaptan (**24**) and *via* the oxidative opening of the thiopyran ring and subsequent loss of benzyl mercaptan

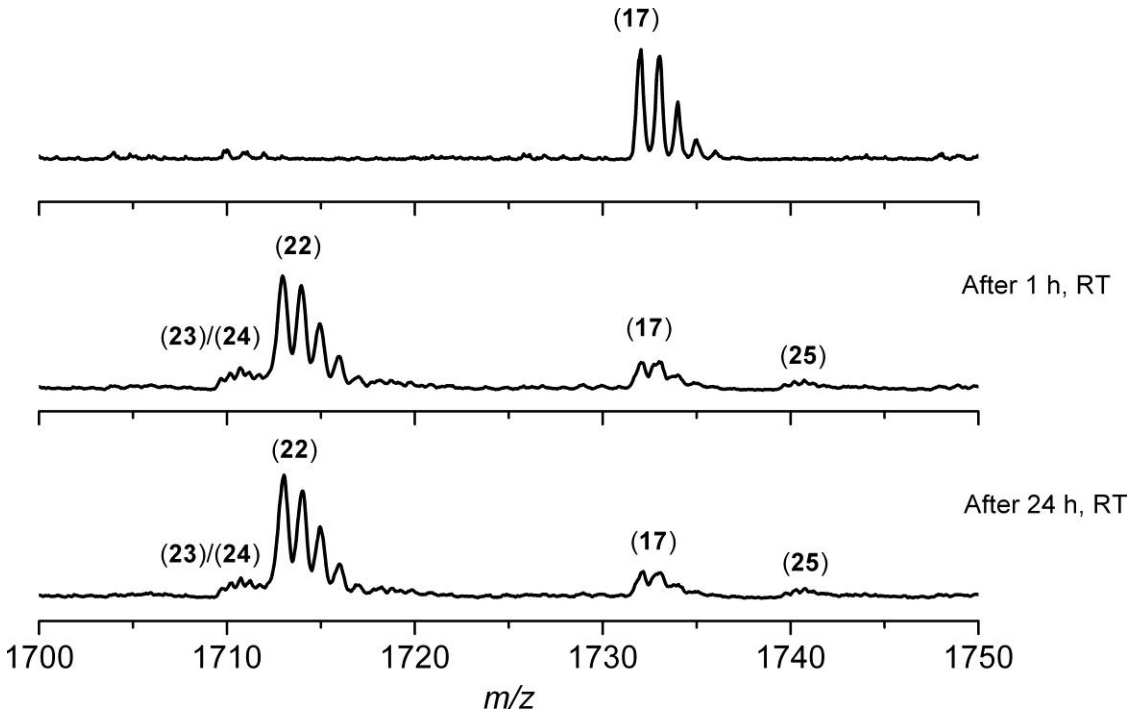

Figure 4.6 Model reaction between cyclopentadienyl functionalized PEG (**17**) and (**5**). The conjugation is possible under ambient conditions without any catalyst. The ESI-MS spectra are recorded *via* direct infusion

Closer inspection of **Figure 4.6** reveals, in addition to the main product and some residual (or reformed) (**17**), that additional minor peaks are present in the product mass spectra, these peaks are labeled (**23**), (**24**) and (**25**) in **Figure 4.6**. The numbers assigned to these peaks represent possible structures that have formed during the reaction and are depicted in **Scheme 4.5**. Structure (**23**) and (**24**) are isobaric and can thus not be differentiated from each other within the resolution of the employed quadrupole ion trap analyzer. Structure (**23**) corresponds to the potential loss of sulfinic acid. However, it is known from the literature that such a reaction should not occur to any significant extent in the Cp-system.[248] More likely is the elimination of benzyl thiol, which leads to species (**24**). However, within the accuracy of the mass spectrometric analysis, neither can be excluded. Species (**25**) can be assigned to a product that is formed *via* the oxidative ring opening of the thio-norbornene ring and the loss of benzyl thiol. Both the formation of species (**24**) and (**25**) have – in contrast to the loss of sulfinic acid – a significant consequence: Since the part of the structure that contains the R-

group of the RAFT agent is lost, a polymer conjugate (based on a RAFT polymer containing (**7**) or (**5**) as well as a Cp-capped counter part) has the potential to lose at least some if its integrity. It will be demonstrated below how the mass spectral results shown in **Figure 4.6** may be of consequence for the preparation of polymer conjugates.

Table 4.6 Theoretical and experimental *m/z* values for the first peak in the isotopic distributions of (**17**) and (**22**) in the *m/z* range between 1700 and 1800

m/z^{exp}	Ion Assignment	Molecular Formula	m/z^{theo}	$\Delta m/z$
1709.7	(**23**) (m=69)+2Na$^+$	$[C_{156}H_{298}O_{71}S_2Na_2]^{++}$	1709.0	0.7[a]
1709.7	(**24**) (m=70)+2Na$^+$	$[C_{152}H_{298}O_{74}S_2Na_2]^{++}$	1708.9	0.8[a]
1713.0	(**22**) (m=29)+Na$^+$	$[C_{77}H_{142}O_{33}S_3Na]^+$	1713.8	0.8[a]
1732.0	(**17**) (m=35)+Na$^+$	$[C_{80}H_{156}O_{37}Na]^+$	1732.0	0.0
1739.7	(**25**) (m=71)+2Na$^+$	$[C_{154}H_{304}O_{76}S_2Na_2]^{++}$	1740.0	0.3

[a]The difference between the theoretical assignments and the experimentally found *m/z* is elevated for these peaks. Such deviations can occur at higher *m/z* ratios and have been observed before in PEG systems.[249] At lower masses (below 1000 *m/z*), the deviations for the same structures are within the error limits of the quadrupole ion trap analyzer (*i.e.* below 0.3 to 0.4 Da).

4.3.5 Synthesis of Polymer Conjugates

The above model reactions serve the purpose of demonstrating that the proposed RAFT agents can indeed afford straightforward conjugation under ambient conditions for both open and cyclic dienes. To assess their efficacy for block copolymer generation, sulfonyl dithioformate functionalized poly(isobornyl acrylate) and cyclopentadienyl functionalized polystyrene are conjugated. The cyclopentadienyl functionalized polystyrene was synthesized from bromide terminated polystyrene prepared *via* the ATRP technique as illustrated in **Scheme 4.6**. The ^{1}H-NMR spectra of bromide functionalized and cyclopentadienyl functionalized polystyrene are shown in **Figure S.4.14** and **S.4.15** in the supporting information section.

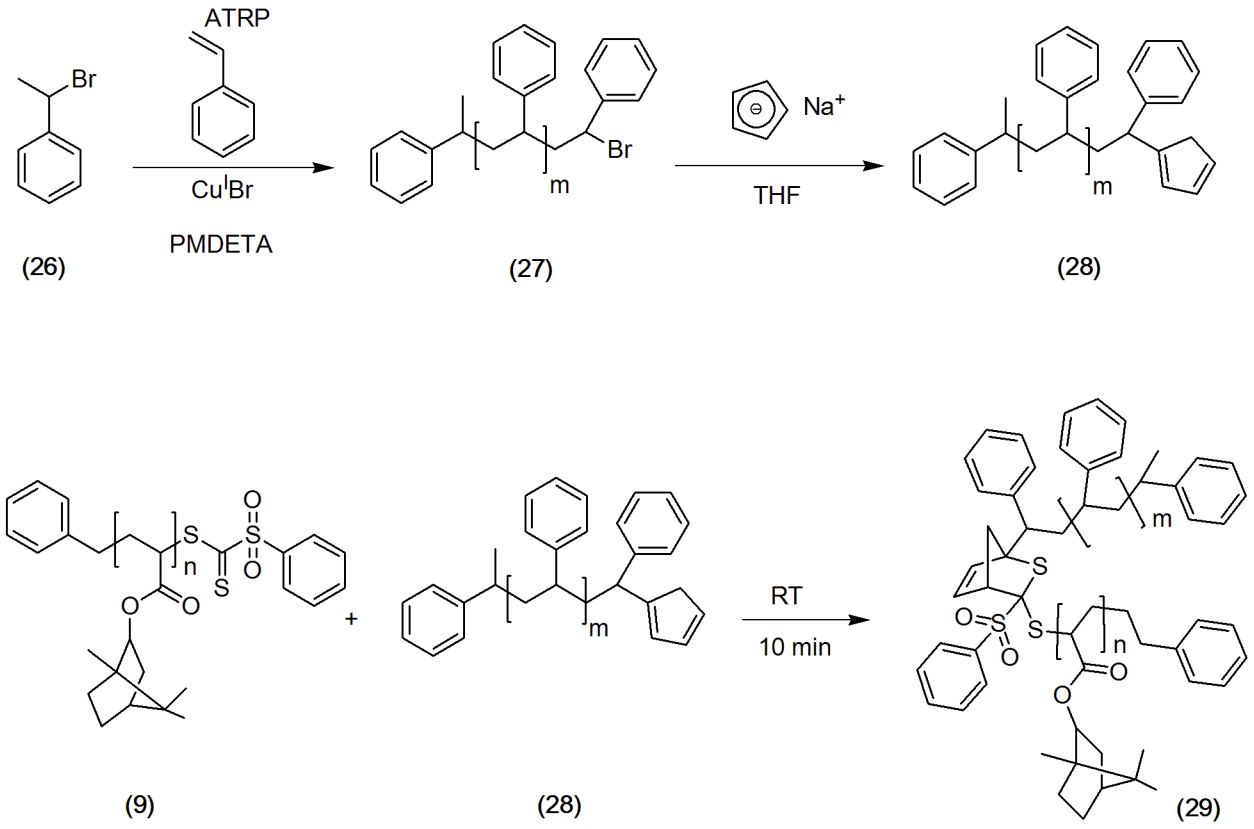

Scheme 4.6 Synthesis of cyclopentadienyl functionalized polystyrene (**28**) from bromide functionalized polystyrene (**27**) synthesized *via* ATRP as well as its subsequent conjugation with sulfonyl dithioformate capped poly(isobornyl acrylate) (**9**) under ambient conditions and in the absence of any catalyst

For the synthesis of the block copolymers equimolar ratios of sulfonyl dithioformate functionalized poly(isobornyl acrylate) and cyclopentadienyl functionalized polystyrene were mixed in $CHCl_3$ under ambient conditions. The solvent was removed under vaccum after 10 min of reaction time and the reaction mixture was immediately analyzed *via* SEC. **Figure 4.7** depicts the molar mass distribution of the obtained PiBA-*b*-PS copolymer (**29**). In comparison to the starting materials (**9**) and (**28**), the reaction product (**29**) is shifted to higher molecular weights, consistent with the calculated number average molecular weight, M_n, of the generated block copolymer. For the two conjugations, the conjugate molecular weight (on the basis of a linear polystyrene calibration) is 6600 g·mol^{-1} (theoretical 7700 g·mol^{-1}) and 5800 g·mol^{-1} (theoretical 6200 g·mol^{-1}), respectively.

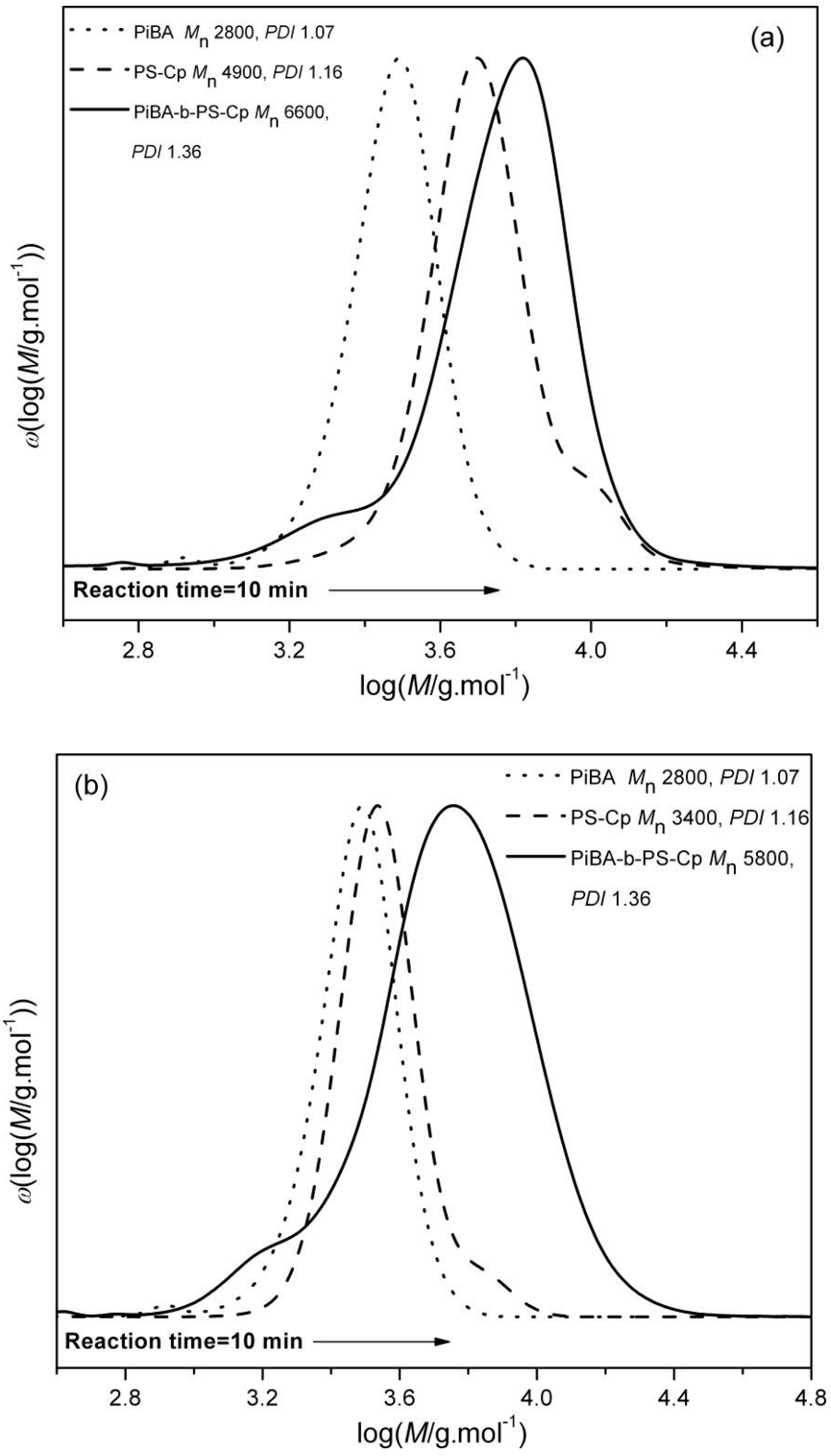

Figure 4.7 Ambient temperature block copolymer formation of poly(isobornyl acrylate) and polystyrene *via* RAFT-HDA chemistry. Depicted are the SEC traces of PiBA functionalized with sulfonyl dithioformate, PS functionalized with cyclopentadiene as well as the resultant PiBA-*b*-PS block copolymer distributions

Inspection of the initial PS molecular weight distributions indicates a small shoulder at the high molecular weight side, which is due to bimolecular termination events occurring during the ATRP process, which can not be fully excluded.[250] Significantly more interesting is the slight amount of low molecular weight material that is observed in the conjugate molecular weight distribution, which coincides in molecular weight with the thiocarbonyl thio functionalized poly(isobornyl acrylate). One is tempted to correlate the presence of the residual polymer to the mass spectrometric observation that some of the diene functional polymer (whose conjugation ability in the ESI-MS assessment exercise is described above) seems to remain even after prolonged conjugation times. However, such a hypothesis is not tenable as the remaining polymeric material on the low molecular weight side of the conjugate distribution coincides with the molecular weight of the isobornyl acrylate polymer (*i.e.* the dienophile).

A more likely explanation thus comes from the detailed analysis of the mass spectra provided in **Figure 4.6**, which has been discussed above. The formation of structures analogous to (**24**) and (**25**) – implying the loss of the RAFT part of the conjugate – is a viable hypothesis for the observed low molecular weight shoulder, especially since its molecular weight is similar to that of the initial RAFT polymer. It is important to note that the obtained conjugates are stable (in solution (chloroform) and the solid state) for several days with no signs of changes in the molecular weight distributions (*i.e.* no increase in the low molecular weight shoulder). Such an observation is congruent with the results of a recent study, where the stability of thiopyran rings in polymer conjugates was assessed under conditions of heat and hydrolysis.[249] A detailed stability assessment of the specific thiopyran conjugates (derived from open and cyclic dienes) described in the current contribution will be provided in a forthcoming study. It will also be a matter of priority to establish how other substitution patterns on the SO_2 unit or alternative dienes behave under similar reaction conditions. To obtain an even purer conjugate in the present case, one has to perform a preparative purification step, as has been carried out before in the context of Cu(I) catalyzed azide-acetylene conjugations.[251,252]

4.4 Conclusions

In the present chapter, the behaviour of strongly electron deficient RAFT agents, *i.e.* benzyl methylsulfonyldithioformate (MSDTF) and benzyl phenylsulfonyldithioformate (PSDTF), has been explored in their ability to mediate radical polymerizations as well as serve as conjugation entities in orthogonal reactions. Sulfonyldithioformate type RAFT agents can indeed mediate the polymerization process and induce living characteristics in agreement with *ab-initio* quantum mechanical calculations, however, the highly electron deficient nature of the C=S double bond leads to a competition reaction between monomer and RAFT agent and concurrent polymerization. The competitive side reaction can be suppressed by employing a monomer with highly bulky substituent group such as isobornyl acrylate. With such a monomer, an efficient RAFT process is observed leading to low polydispersity polymers of variable molecular weight. In model experiments – assessed *via* ESI-MS – of poly(ethylene glycol) chains carrying either butadiene or cyclopentadiene moieties as dienes, it is demonstrated that the strongly electron withdrawing RAFT agents can be conjugated to open chain dienes at ambient temperatures in the absence of catalysts in contrast to the corresponding first generation RAFT-HDA agents (benzyl (diethoxyphosphoryl)dithioformate and benzyl pyridine-2-yl dithioformate), which required catalysts and elevated temperatures. In addition, the conjugation of the sulfonyldithioformate RAFT agents with Cp-capped polymers proceeds at similar rates as those reported earlier for the first generation RAFT-HDA agents, however with the sulfonyl dithioformates no additional catalyst is required to reach these rates. The mass spectrometric investigations also reveal that in the case when Cp is employed as a diene, a slight amount of conjugate functionality is lost due to secondary reactions involving the thionorbornene ring. These observations are confirmed in the conjugate distributions of Cp-capped polystyrene with sulfonyldithioformate capped poly(isobornyl acrylate). Despite these limitations, the present exploration has provided evidence that sulfonyldithioformates are powerful and promising dienophiles that can react under mild reaction conditions with variable dienes. Their main potential is seen as conjugation sites for variable diene carrying polymers onto surfaces (ranging from microspheres to silicon wafers but also in biological

contexts), where rapid conjugations under mild reaction are essential and high grafting densities *via grafting-to* approaches may be desirable.

4.5 Supporting Information

TABLE S1 Temperature corrections (*TC*), zero-point vibrational energies (*ZPVE*), Temperature entropies (*TS*), absolute energies at various levels of theory (ROMP2, G3(MP2)-RAD and W1), enthalpies (*H*, with ZPVE), and Gibbs free energies (*G*) in the gas phase for the species in this study at 333.15K, under the Hindered rotor (HR) approximations (all units are in Hartrees). For the detailed description, the readers are referred to read *J. Polym. Sci. Part A: Polym. Chem.* **2009**, *47*, 6065

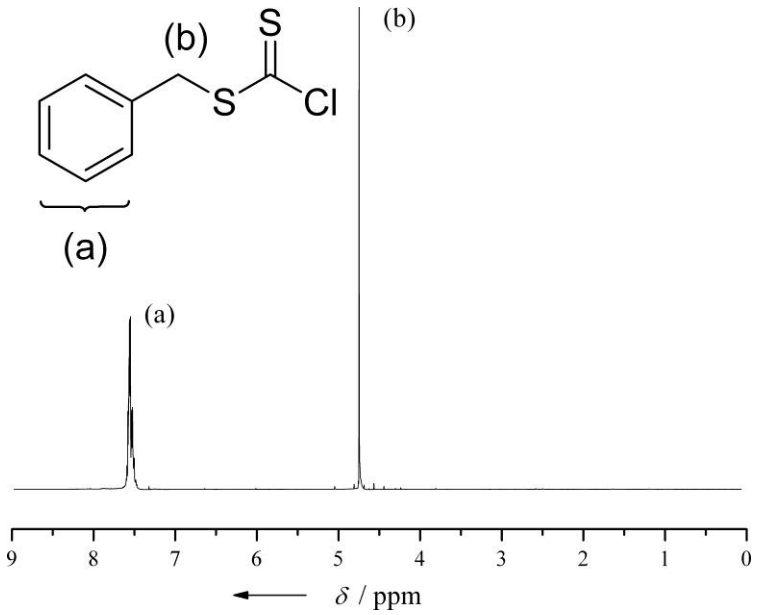

Figure S.4.1 ^{1}H NMR spectrum of benzyl chlorodithioformate (**3**) obtained by reaction of thiophosgene (**1**) and benzyl mercaptan (**2**)

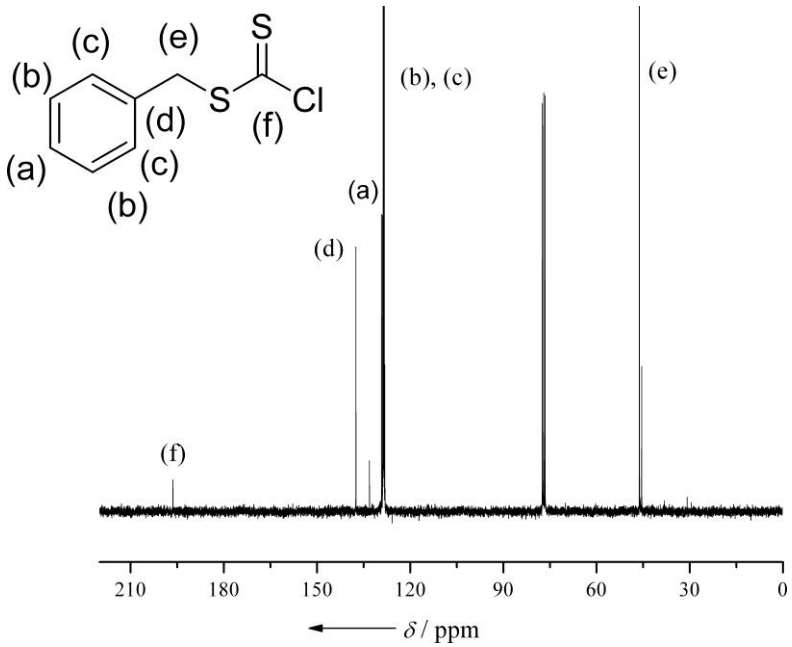

Figure S.4.2 ^{13}C NMR spectrum of benzyl chlorodithioformate (**3**) obtained by reaction of thiophosgene (**1**) and benzyl mercaptan (**2**)

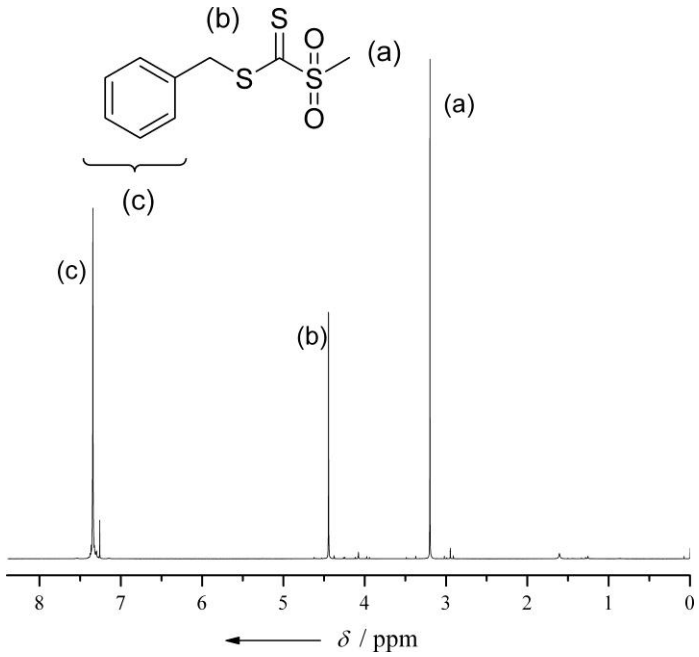

Figure S.4.3 ^{1}H NMR spectrum of benzyl methylsulfonyldithioformate (**5**) obtained by reaction of benzyl chlorodithioformate (**3**) and sodium methanesulfinate (**4**)

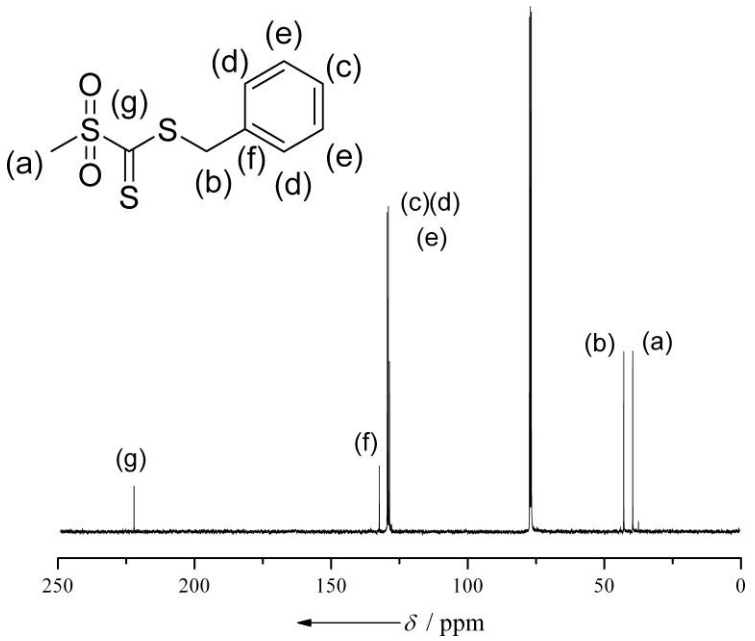

Figure S.4.4 ^{13}C NMR spectrum of benzyl methylsulfonyldithioformate (**5**) obtained by reaction of benzyl chlorodithioformate (**3**) and sodium methanesulfinate (**4**)

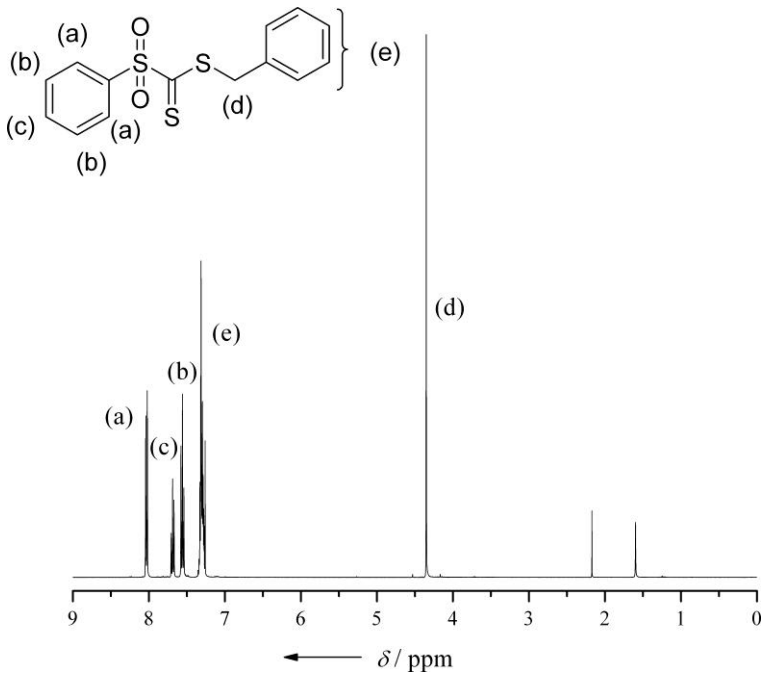

Figure S.4.5 ^{1}H NMR spectrum of benzyl phenylsulfonyldithioformate (**7**) obtained by reaction of benzyl chlorodithioformate (**3**) and benzene sulfinic acid sodium salt (**6**)

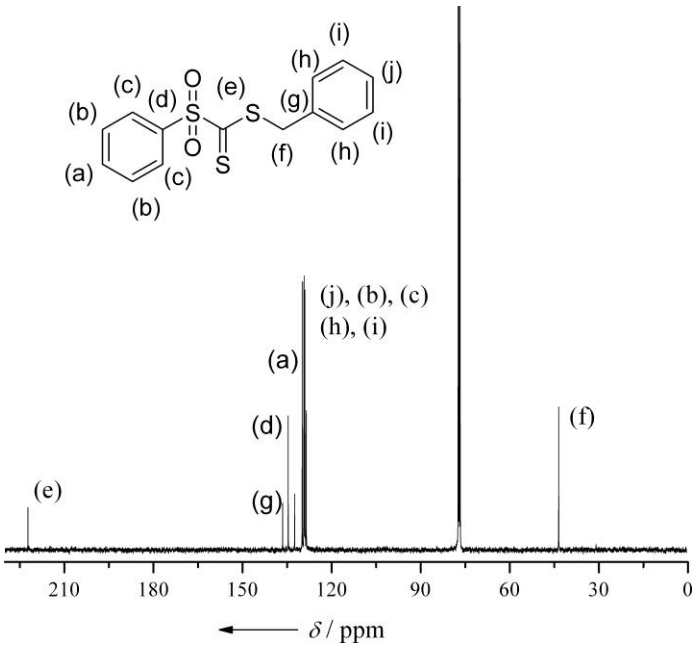

Figure S.4.6 ^{13}C NMR spectrum of benzyl phenylsulfonyldithioformate (**7**) obtained by reaction of benzyl chlorodithioformate (**3**) and benzene sulfinic acid sodium salt (**6**)

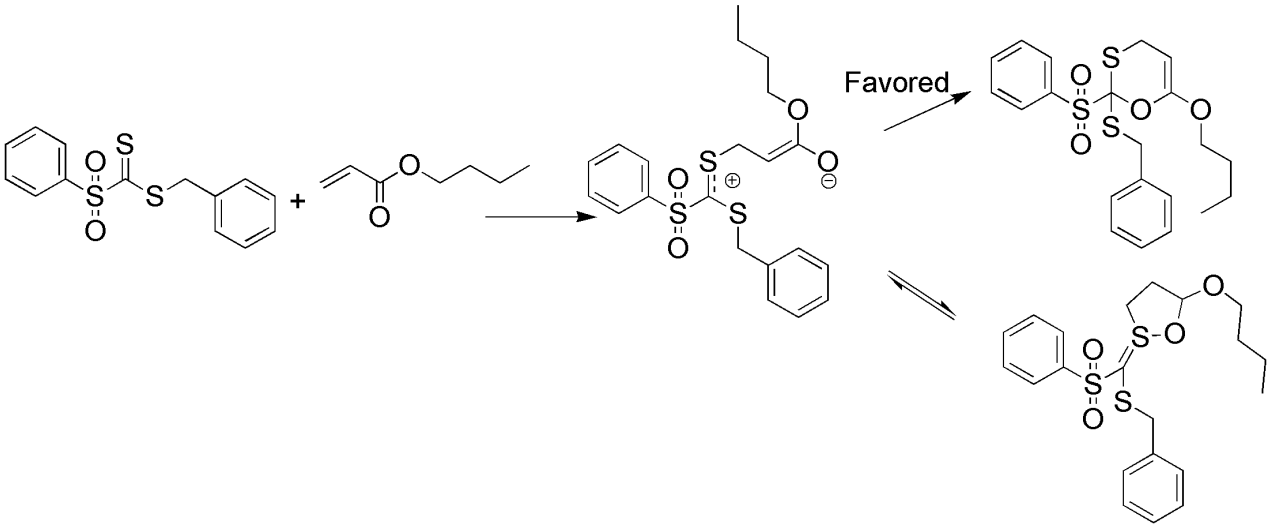

Scheme S.4.1 Possible reaction mechanism for the reaction of benzyl phenylsulfonyldithioformate with butyl acrylate

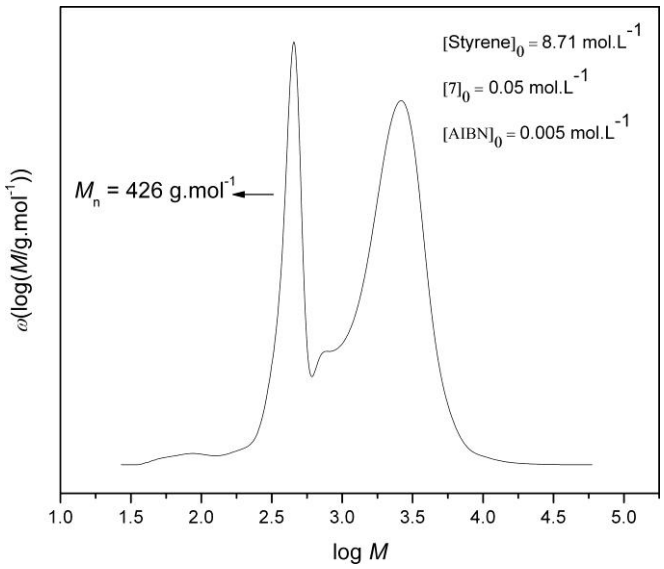

Figure S.4.7 Typical SEC elugram for the bulk polymerization of styrene (T = 60 °C) using (**7**) at the concentrations indicated within the figure

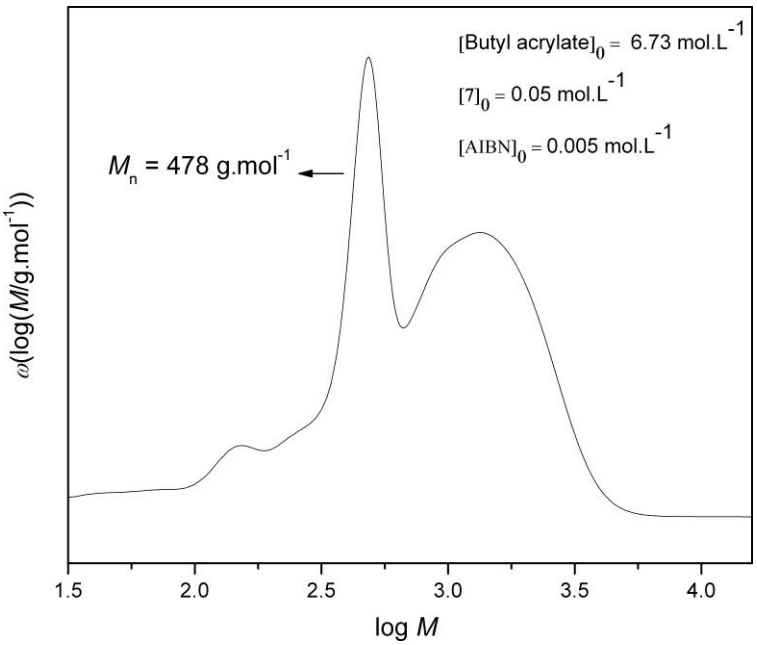

Figure S.4.8 Typical SEC elugram for the bulk polymerization of butyl acrylate (T = 60 °C) using (**7**) at the concentrations indicated within the figure

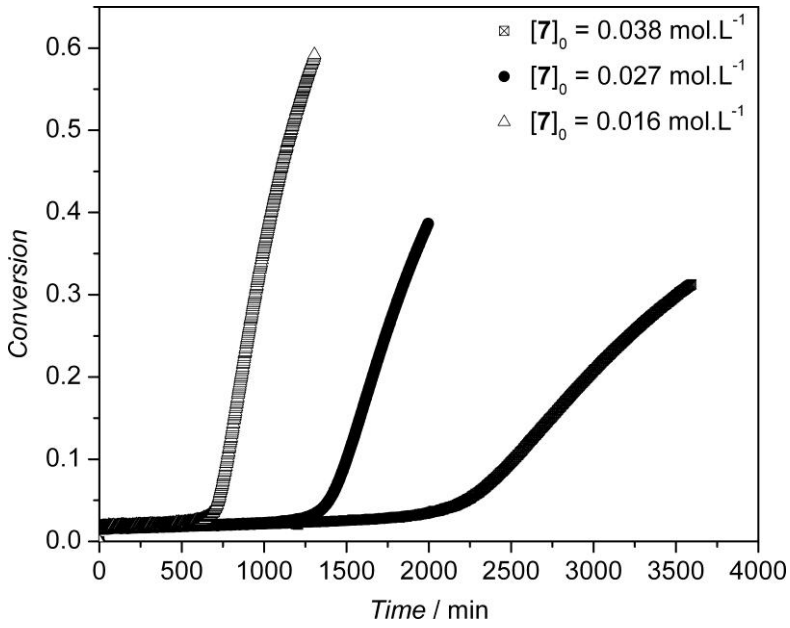

Figure S.4.9 Monomer conversion *vs* time evolution for the bulk polymerization of isobornyl acrylate (T = 60 °C) using (**7**) at three initial concentrations as indicated within the figure. The concentrations of monomer and AIBN are 4.73 and 0.005 mol·L^{-1}, respectively

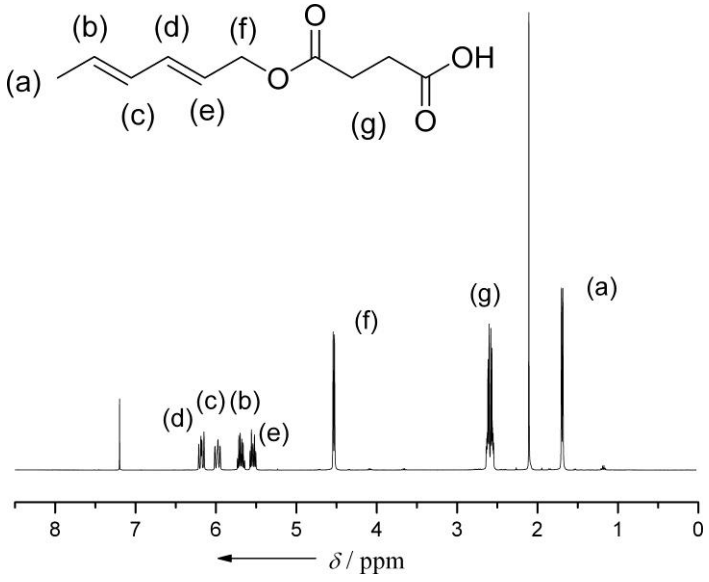

Figure S.4.10 ^{1}H NMR spectrum of hexadiene-1-ol derivative (**12**) obtained by reaction of *trans*, *trans*-hexadiene-1-ol (**10**) and succinic anhydride (**11**)

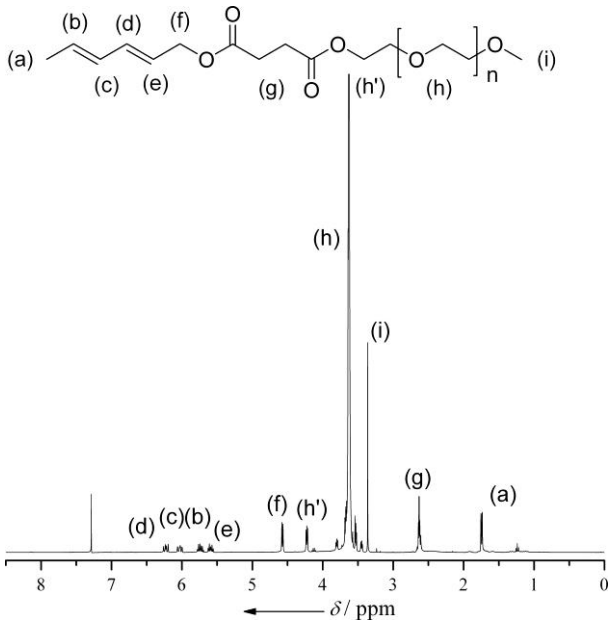

Figure S.4.11 ^{1}H NMR spectrum of the open chain diene functionalized PEG monomethyl ether (**14**) obtained by reaction of poly(ethylene glycol) monomethylether (**13**) and hexadiene-1-ol derivative (**12**)

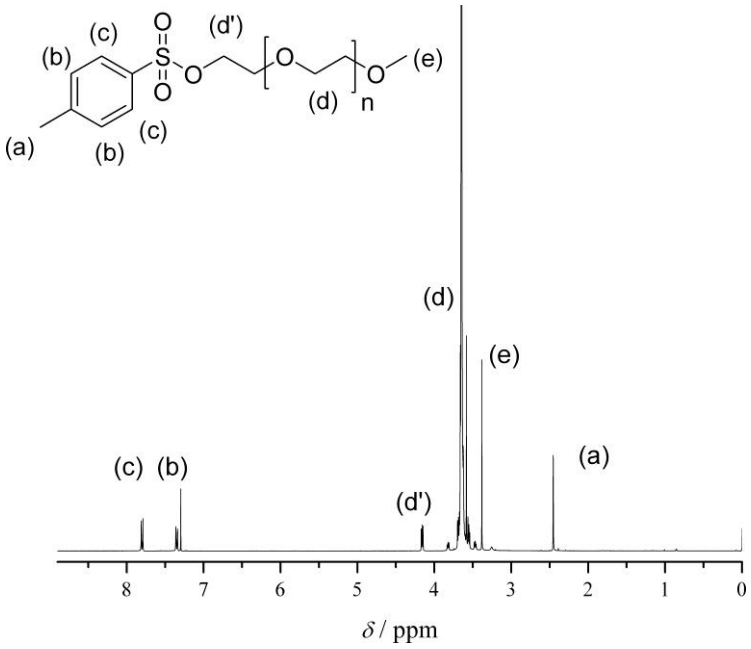

Figure S.4.12 ^{1}H NMR spectrum of tosylated poly(ethylene glycol) monomethylether (**16**) obtained by reaction of poly(ethylene glycol) monomethylether (**13**) and *p*-toluene sulfonyl chloride (**15**)

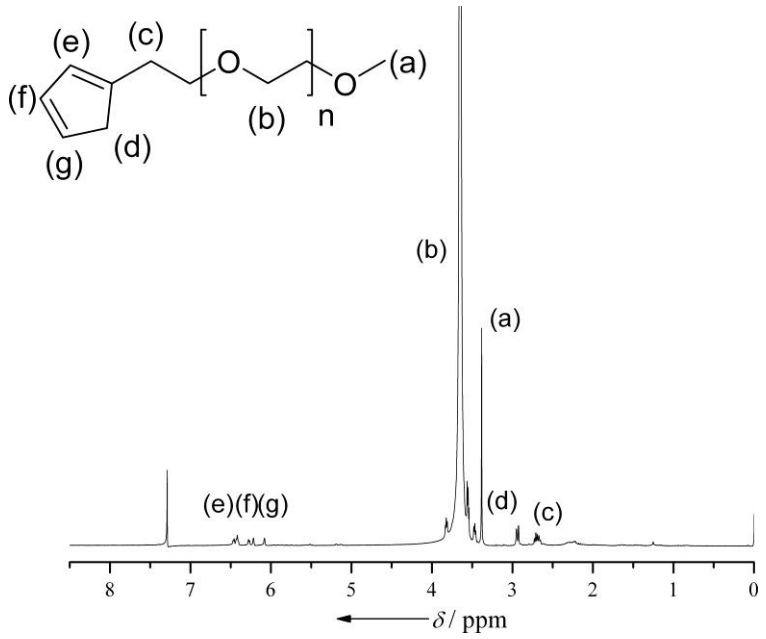

Figure S.4.13 ^{1}H NMR spectrum of cyclopentadienyl functionalized PEG monomethylether (**17**) obtained by reaction of tosylated PEG monomethyl ether (**16**) with sodium cyclopentadienide solution

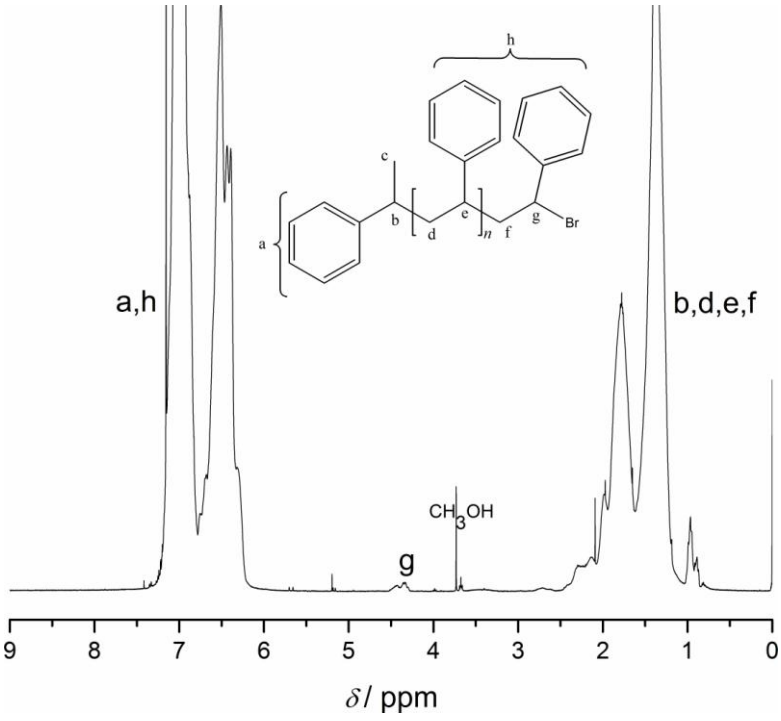

Figure S.4.14 ^{1}H NMR spectrum of bromide functionalized polystyrene (**27**)

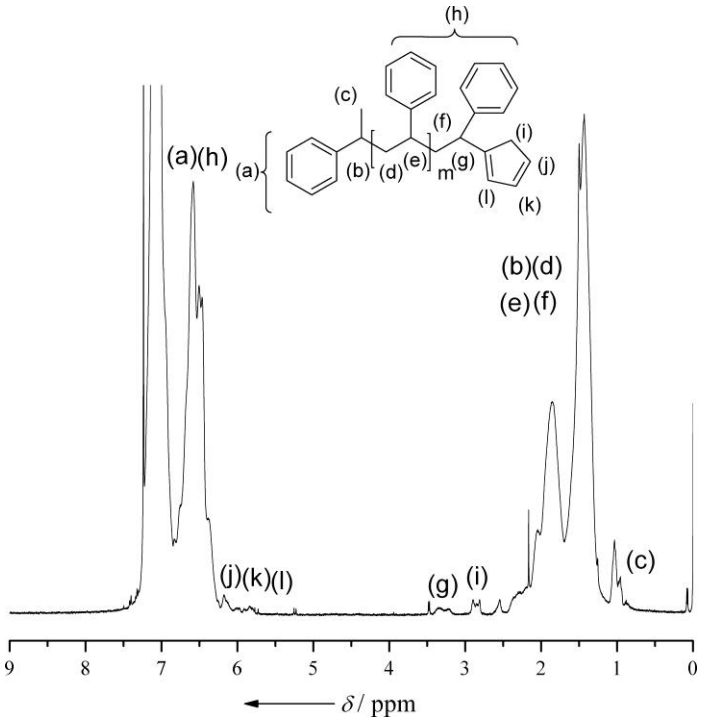

Figure S.4.15 ^{1}H NMR spectrum of cyclopentadienyl functionalized polystyrene (**28**) obtained by reaction of bromide terminated polystyrene (**27**) with sodium cyclopentadienide solution

Chapter 5 Efficient Surface Modification of Divinylbenzene Microspheres *via* a Combination of RAFT and Hetero Diels-Alder Chemistry

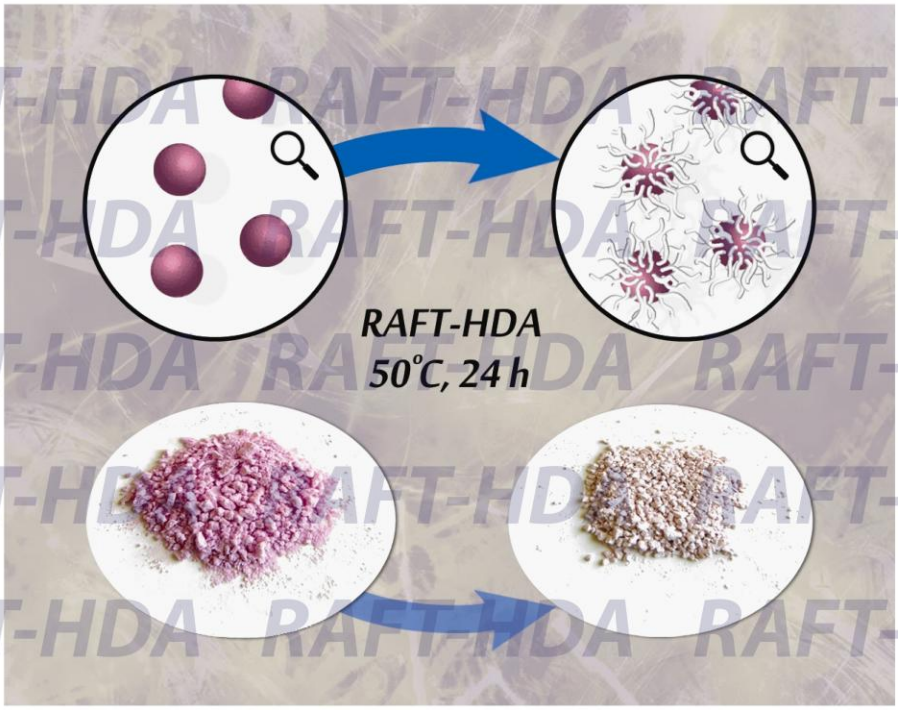

5.1 Introduction

In **Chapter 4**, the synthesis and efficiency of sulfonyl dithioformates as potential RAFT agents as well as heterodienophiles was discussed. These sulfonyldithioformates showed to be powerful and promising dienophiles that can react under mild reaction conditions with a variety of dienes. These extremely reactive thiocarbonyl thio compounds can be used for the efficient and mild modification of surfaces such as microspheres (discussed in detail in **Chapter 6**) and silicon wafers (discussed in detail in **Chapter 7**). Before investigating the use of sulfonyl dithioformates for the efficient modification of surfaces, first generation thiocarbonyl thio compounds were examined in this context for the modification of microspheres. In particular, the present chapter discusses the surface modification of divinylbenzene microspheres having surface expressed RAFT groups with diene functionalized poly(*ε*-caprolactone) chains *via* RAFT-HDA chemistry.

Grafting techniques in combination with controlled radical polymerization methods have largely been used for the modification of a number of surfaces. These grafting techniques have been discussed in detail in **Chapter 2**. In the present chapter, it is now demonstrated that microspheres with electron-deficient, surface expressed RAFT groups can also open the possibility of efficient modification and functionalization of these microspheres *via* the *grafting-to* approach. The *grafting-to* approach used here is based on RAFT-HDA chemistry described previously in **Chapter 2** and **4**. In the RAFT-HDA concept, the dithioester function of a RAFT agent serves two purposes: Initially, the dithioester moiety functions as a RAFT agent in the synthesis of the DVB microspheres, on which it is surface expressed (see reaction (a) in **Scheme 5.1**). It is subsequently employed as a reactive heterodienophile for the HDA reaction with a functionalized diene, resulting in facile microsphere-polymer conjugation (see reaction (c) in **Scheme 5.1**). The polymer which is used for functionalizing divinylbenzene microspheres in the present work is a diene functionalized poly(*ε*-caprolactone) (PCL). The diene functionalized PCL was obtained by enzymatic ROP of *ε*-caprolactone in the presence of *trans,trans*-2,4-hexadien-1-ol (see reaction (b) in **Scheme 5.1**). Benzyl (diethoxyphosphoryl)dithioformate (**1**) was selected as the RAFT agent in the precipitation polymerization process to synthesize RAFT functionalized microspheres.

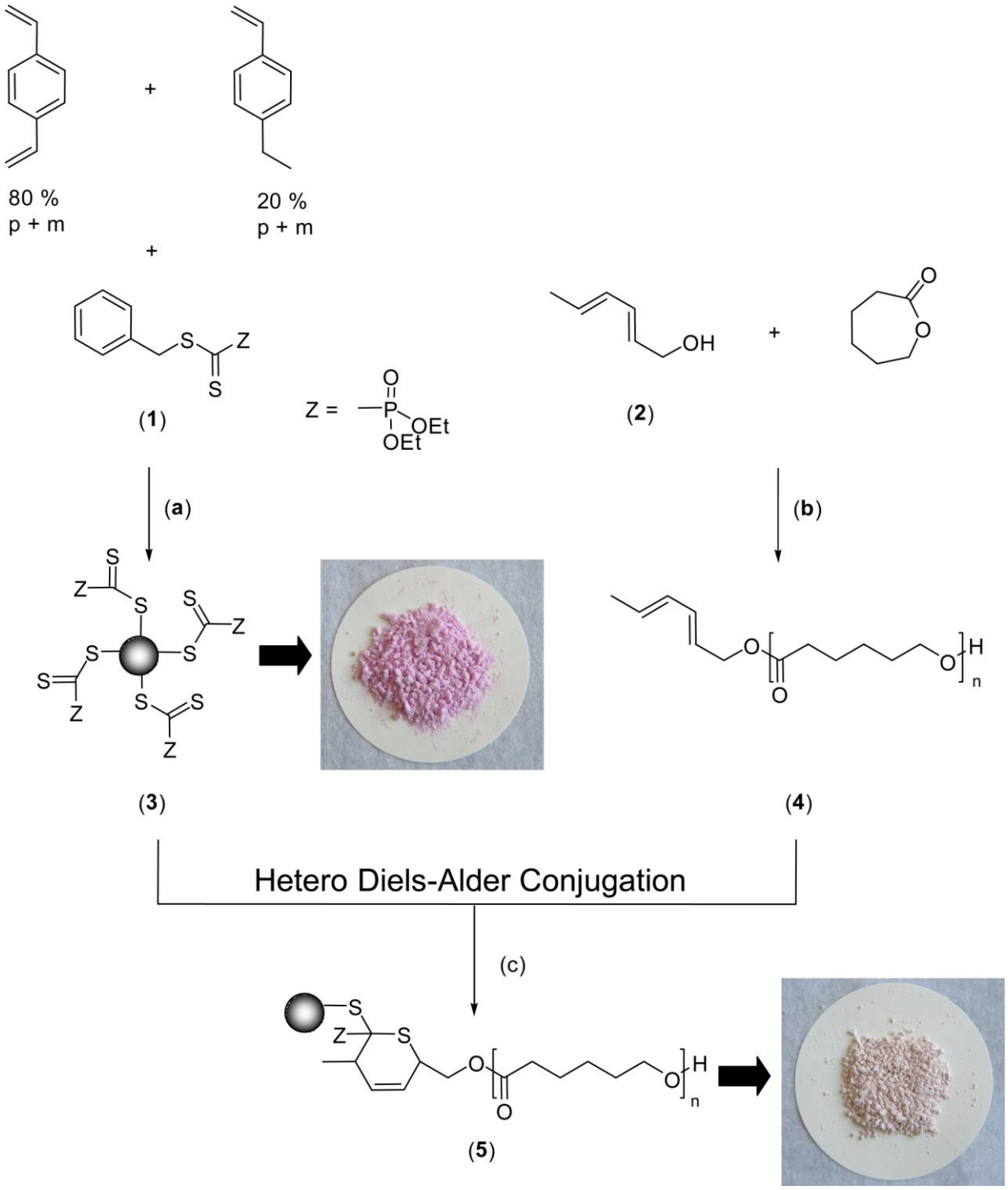

Scheme 5.1 General synthetic approach for the generation of microspheres with BEPTF derived and surface expressed dithioester groups (**3**) as well as 2,4-hexadienoyl terminated PCL (**4**) followed by their coupling *via* HDA cycloaddition. a) Precipitation polymerization in the presence of RAFT agent (**1**), AIBN, 70 °C; b) ROP, lipase, 70 °C; c) $ZnCl_2$, 50 °C, 24 h, chloroform

5.2 Experimental

5.2.1 Synthesis of Benzyl (diethoxyphosphoryl)dithioformate (1)

To a suspension of NaH (0.46g, 19.4 mmol) in THF (20 mL) was added a solution of diethyl phosphite (2.5 mL, 19.4 mmol) in THF (10 mL) dropwise under nitrogen. After the evolution of hydrogen ceased, the reaction mixture was refluxed for 5 minutes. The reaction mixture was then cooled in liquid nitrogen/acetone bath before dry carbon disulfide (5.8 mL, 96 mmol) was added. At the end of the addition, the temperature of the mixture was allowed to rise to 25 °C under rigorous stirring. Stirring was continued for 30 min, at which point benzyl bromide (2.6 mL, 22 mmol) was added dropwise. Stirring continued for further 30 min before *n*-hexane (60 mL) was added, the mixture was filtered and the solvent removed *in vacuo*. The residue was dissolved in minimum amount of cyclohexane and chromatographed over silica gel using first cyclohexane as eluent to remove impurities and then diethyl ether to collect the red fraction. The diethyl ether was removed *in vacuo* to obtain purple viscous liquid (4.6 g, 78% yield). ^{1}H-NMR (300 MHz, $CDCl_3$, δ / ppm) (as shown in **Figure S.5.2** in SI): 1.33 (t, 6H, CH_3^a), 4.24 (m, 4H, CH_2^b), 4.44 (s, 2H, CH_2^c), 7.3 (s, 5H, $C_6H_5^d$).

5.2.2 Synthesis of Core Microspheres with Surface Expressed RAFT End Groups (3)

Core microspheres with RAFT end groups were prepared by precipitation polymerization in neat acetonitrile. DVB80 (5 ml, 35.35 mmol), acetonitrile (200 ml), AIBN (0.092 g, 0.56 mmol) and benzyl (diethoxyphosphoryl)dithioformate (0.3044 g, 1 mmol) were placed in 250 ml polypropylene bottle and subsequently purged with nitrogen. The mixture was stirred at ambient temperature until all AIBN was dissolved completely and the whole mixture was degassed again for 30 minutes. The polymerization was performed in oscillating water bath in which the temperature was increased from ambient temperature to 60 °C within 1 h followed by a ramp to 70 °C within 1 hour and then a kept at 70 °C for 24 hours. The core microspheres with RAFT end groups were isolated by filtration through a 0.45 µm membrane washed and resuspended twice each in tetrahydrofuran, acetone and diethylether sequentially. The polymeric particles were dried in vaccum oven to afford polymeric microspheres with

RAFT end groups in 27% yield. The scanning electron micrograph of microspheres (3) is shown in **Figure S.5.1** in the supporting information section.

5.2.3 Synthesis of Diene Functionalized 2,4-Hexadienoyl Terminated PCL (4)

Under nitrogen atmosphere, a mixture of *trans,trans*-2,4-hexadien-1-ol (430 mg, 4.4 mmol), *ε*-caprolactone (9.3 mL, 10 g, 88 mmol), toluene (10 mL) and lipase acrylic resin (250 mg) were placed in a dried schlenk flask. The solution was stirred at 70 °C for 1.5 h. After cooling down to room temperature, the lipase acrylic resin was removed by filtration. The polymer was precipitated from the filtrate in a cold mixture of diethylether/n-hexane (1:1) (9.34 g, 90% yield). SEC (THF): M_n: 3163 g·mol^{-1}, *PDI* = 1.69. ^{1}H-NMR (as shown in **Figure S.5.2** in SI) (300 MHz, $CDCl_3$, δ / ppm) 6.21 (dd, CH^d), 6.01 (ddq, CH^c), 5.71 (dq, CH^b), 5.58 (dt, CH^a), 4.53 (d, CH_2^f), 4.03(t; CH_2^k), 3.60(t, $CH_2^{k'}$), 2.7 (t, CH_2^g), 1.5-1.7 (m, CH_2^{h+j}), 1.25-1.45 (m, CH_2^i).

5.2.4 Synthesis of PCL Functionalized Microspheres (5)

A solution of 2,4-hexadienoyl terminated PCL (**4**) (1.88 g, 0.6 mmol), 300 mg of poly(DVB80)-BEPTF microspheres and $ZnCl_2$ (0.08 g, 0.6 mmol) in 6 mL chloroform was stirred at 50 °C for 24 h. The poly(DVB80) PCL functionalized microspheres (**5**) were then isolated by filtration through a 0.45 µm membrane, washed and re-suspended twice in chloroform. The microspheres were dried in a vacuum oven at 30 ºC for 12 h before characterization.

5.2.5 Fluorescent Labelling of PCL-Functionalized Microspheres (5)

PCL-functionalized microspheres (50 mg) (**5**) were added to a solution of *N*,*N*-dicyclohexylcarbodiimide (DCC) (0.06 g, 0.29 mmol), 4-dimethylaminopyridine (0.012 g, 0.10 mmol) and rhodamine B (0.14 g, 0.29 mmol) in 50 mL tetrahydrofuran. The resulting mixture was stirred for 24 h at room temperature. The microspheres were isolated by centrifugation at 7 000 rpm for 10 min. The excess rhodamine B was removed by washing repetitively with ethanol until the filtrate showed no sign of fluorescence. The microspheres were dried overnight in vacuum oven before

characterization *via* confocal microscopy. As a control experiment, poly(DVB80)-BEPTF microspheres (**3**) were submitted to the same reaction conditions.

5.2.6 Thermal Treatment of PCL-functionalized Microspheres (5)

300 mg of PCL-functionalized microspheres (**5**) were suspended in 5 mL toluene in a pressure tube and kept at 160 °C for 24 h. The microspheres were isolated by filtration through a 0.45 µm membrane, washed and resuspended twice in toluene. Subsequently, the microspheres were dried in vacuum oven at 30 ºC for 12 h before characterization.

5.3 Results and Discussion

In the following, the characterization of the RAFT-HDA obtained microspheres *via* a series of experimental approaches is discussed in detail. Initially, the state of the core microspheres is discussed prior to the HDA functionalization: The precipitation polymerization of DVB80 in the presence of benzyl (diethoxyphosphoryl)dithioformate resulted in narrow disperse poly(DVB80)-BEPTF microspheres (see **section 5.2.2**), which are – in contrast to conventional poly(DVB80) microspheres – purple (see **Figure 5.2** for an optical image of the obtained material). Prior to the HDA surface modification, the morphology of the microspheres was studied *via* SEM. The number average, D_n, and weight average, D_w, diameter of the microspheres with BEPTF derived surface expressed dithioester groups were 6.26 µm and 8.01 µm, respectively, featuring a *PDI* of 1.28. Furthermore, the surface of the dithioester surface expressed microspheres was studied *via* XPS. The results of the XPS investigations (for the core and core-shell microspheres) are collated in **Figure 5.1**.

Figures 5.1 (a) and (b) depicts XPS spectra of poly(DVB80) microspheres with and without BEPTF derived surface groups, respectively. Inspection of the figures clearly indicates that microspheres with dithioester groups display signals for P, S and O atoms while microspheres prepared as a control with no dithioester groups have no signals corresponding to P, S and O atoms. As the Z-group of the employed RAFT agent contains phosphorous, the microspheres with surface expressed dithioester groups should display phosphorous atoms on their surface.

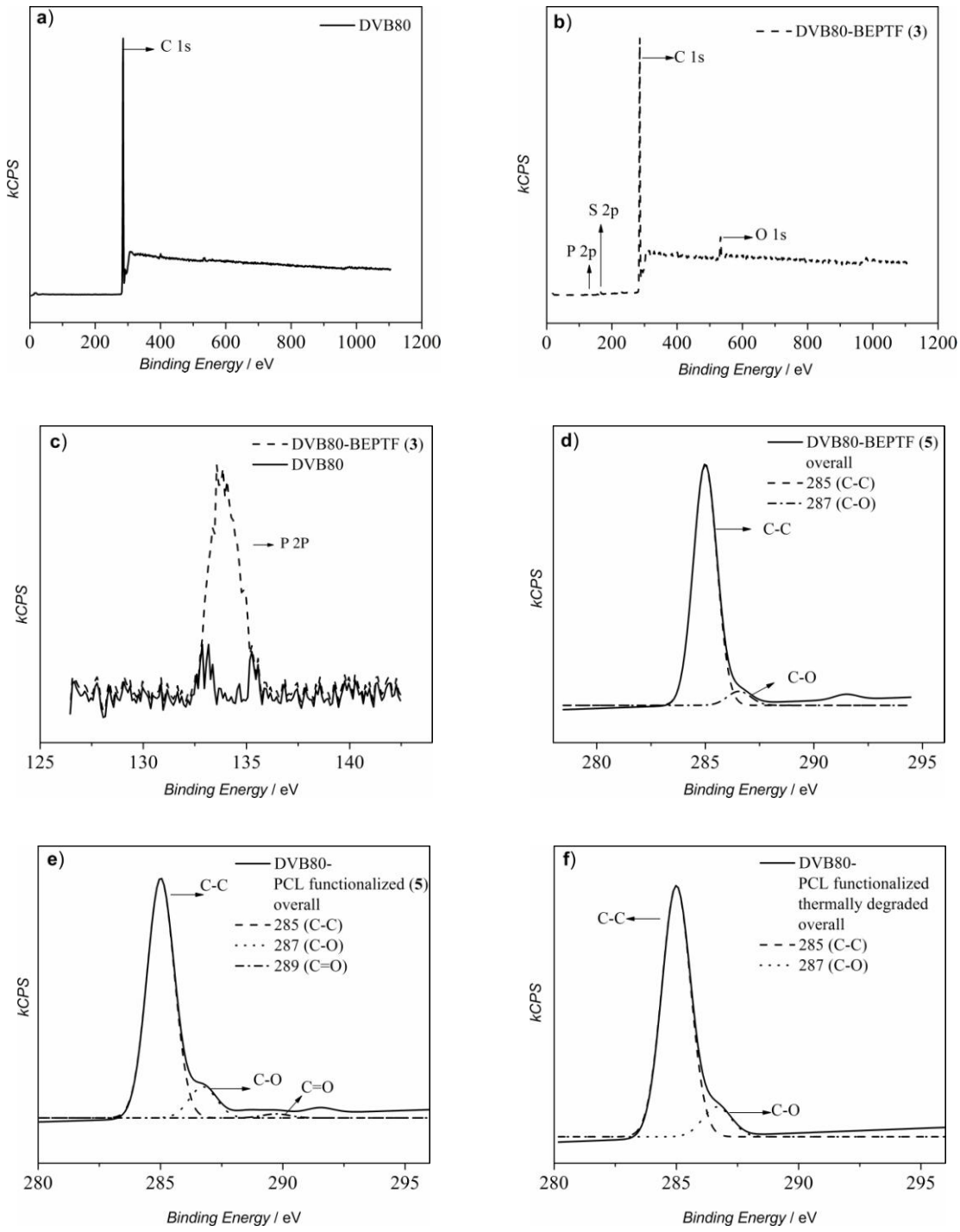

Figure 5.1 XPS spectra of a) poly(DVB80) microspheres without BEPTF derived dithioester surface groups, b) poly(DVB80) microspheres with BEPTF derived dithioester surface expressed groups (**3**), c) comparison of wide scan signals of P atoms for poly(DVB80) microspheres with and without BEPTF derived surface

expressed dithioester groups, d) deconvoluted carbon signal for poly(DVB80) microspheres with surface expressed dithioester groups (**3**), e) deconvoluted carbon signal for poly(DVB80) microspheres functionalized with PCL (**5**), f) deconvoluted carbon signal for poly(DVB80) microspheres functionalized with PCL after thermal degradation at 160 °C for 24 h

Figure 5.1 (c) showing the wide scan of the P signal displays a signal for P atoms in microspheres (**3**), while no signal corresponding to P atoms was observed in the microspheres without RAFT surface groups.

Figure 5.3 (a) shows the comparison of ATR-IR spectra of microspheres with (**3**) and without RAFT surface groups. From the ATR-IR spectra of the pure RAFT agent (**1**) (benzyl (diethoxyphosphoryl)dithioformate, ATR spectra not shown), signals at 1 160 and 1 250 cm^{-1} can be assigned to the diethoxyphosphoryl and thiocarbonyl functions, respectively. Inspection of **Figure 5.3** (a) indicates that the microspheres (**3**) display signals at 1 160 and 1 250 cm^{-1} (confirming the presence of RAFT expressed surface groups), while no such peaks can be observed in microspheres without RAFT end groups.

The subsequent conjugation reaction between microspheres with RAFT surface groups (**3**) and 2,4-hexadienoyl terminated PCL (**4**) *via* hetero Diels-Alder (HDA) cycloaddition was performed at 50 °C in chloroform and in the presence of $ZnCl_2$ (see reaction (c) in **Scheme 5.1**) for 24 h. The $ZnCl_2$ functions as a catalyst in this particular HDA cycloaddition as it enhances the electron withdrawing nature of the RAFT Z-group. The microspheres with RAFT surface groups (**3**) are coupled to 2,4-hexadienoyl terminated PCL (**4**) through the formation of a 3,6-dihydro-*2H*-thiopyran ring, the stability of which has been previously investigated and found to be withstanding relatively harsh conditions of pH (between 0 and 14 at ambient temperature) and heat (up to 120 °C).[249] One of the most immediate signs of grafting success is the color change of the microspheres from purple to white (or off-white) during the reaction with 2,4-hexadienoyl terminated PCL (**4**) (see the optical image shown in **Figure 5.2**). The color change is due to the loss of the dithioester function.

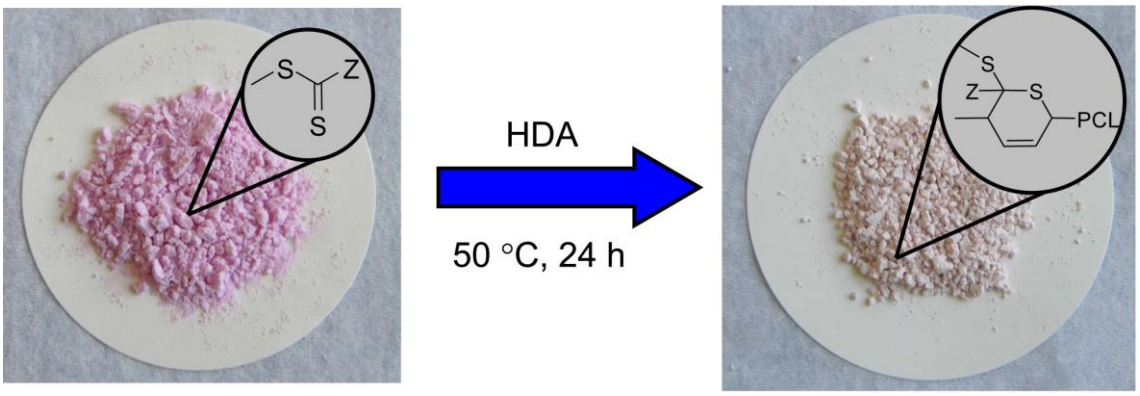

Figure 5.2 The optical images of the microspheres before and after functionalization. Before functionalization the DVB80 microspheres (**3**) are pink in color due to the presence of dithioester moieties on the surface. After functionalization the microspheres are creamish in color as dithioester moieties are converted to thiopyran ring

Further proof for the success of the grafting reaction comes from XPS analysis: **Figure 5.1**(d) and (e) show deconvoluted XPS spectra of the carbon signals for microspheres with RAFT surface groups and microspheres functionalized with PCL (**5**), respectively. The microspheres with RAFT surface groups show two peaks at 286 eV and 287 eV, which correspond to C-C and C-O bonds, respectively. The C-O peak is due to diethoxy group present in the RAFT group. The deconvoluted XPS spectra for microspheres functionalized with PCL display three signals for carbon at 286, 287, 289 eV corresponding to C-C, C-O and C=O bonds, respectively. The additional signal at 289 eV (which is due to C=O bonds), clearly confirms the presence of PCL on the poly(DVB 80) microspheres and thus the success of the grafting reaction. The PCL functionalized microspheres were also subjected to thermal treatment at 160 °C in toluene for 24 h – conditions under which the 3,6-dihydro-*2H*-thiopyran ring has previously been shown to cleave.[147] Inspection of **Figure 5.1**(f) demonstrates that the C=O function (shoulder on the right hand side of the main peak) completely disappears after the thermal treatment, indicating the reversibility of the PCL grafting process.

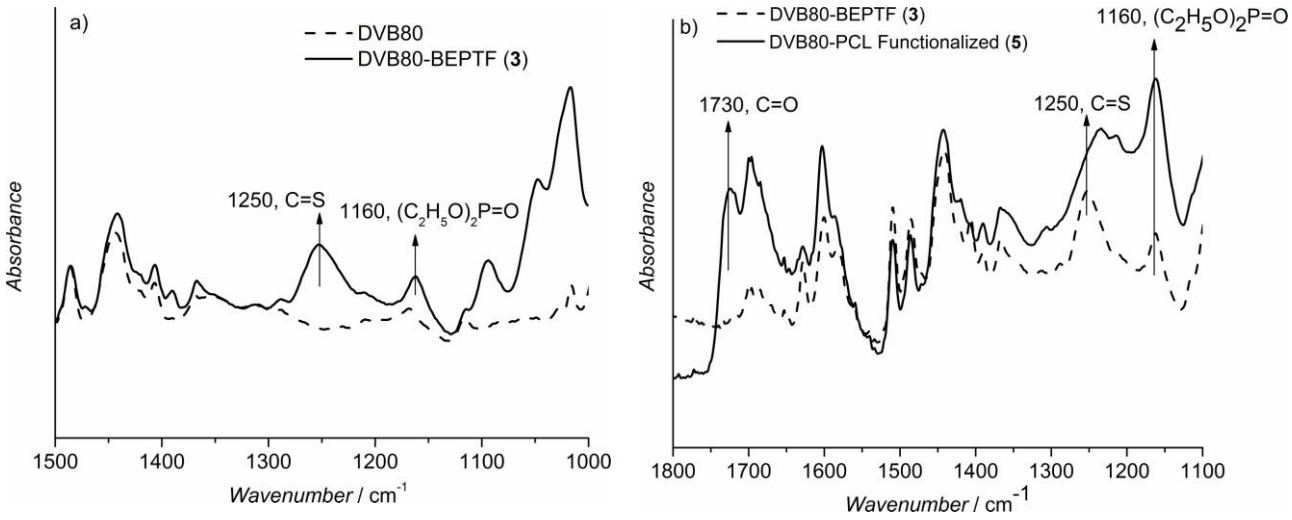

Figure 5.3 ATR-IR spectra a) comparison of signals for poly(DVB80) microspheres with (**3**) and without BEPTF derived surface expressed dithioester groups, b) comparison of signals for poly(DVB80) microspheres with surface expressed dithioester groups (**3**) and poly(DVB80) microspheres functionalized with PCL (**5**)

As in the case of the initial RAFT microspheres, the grafted material can also be analysed *via* ATR-IR spectroscopy. **Figure 5.3** (b) shows the comparison of ATR-IR spectra for microspheres (**3**) and microspheres functionalized with PCL (**5**). The microspheres functionalized with PCL (**5**) clearly display a peak at 1 730 cm^{-1} corresponding to the carbonyl functional group present in PCL, which is not present in the spectrum of microspheres (**3**). In addition, the peak at 1 160 cm^{-1} (due to presence of diethoxyphosphoryl group) is present in both microspheres with RAFT surface groups as well as microspheres functionalized with PCL (**5**). Further, there is a distinctive peak at 1 250 cm^{-1} for the microspheres with RAFT surface groups which corresponds to thiocarbonyl functions, while no such distinctive peak can be seen for microspheres functionalized with PCL, confirming that the thiocarbonyl functions have quantitatively reacted with the diene groups of the PCL.

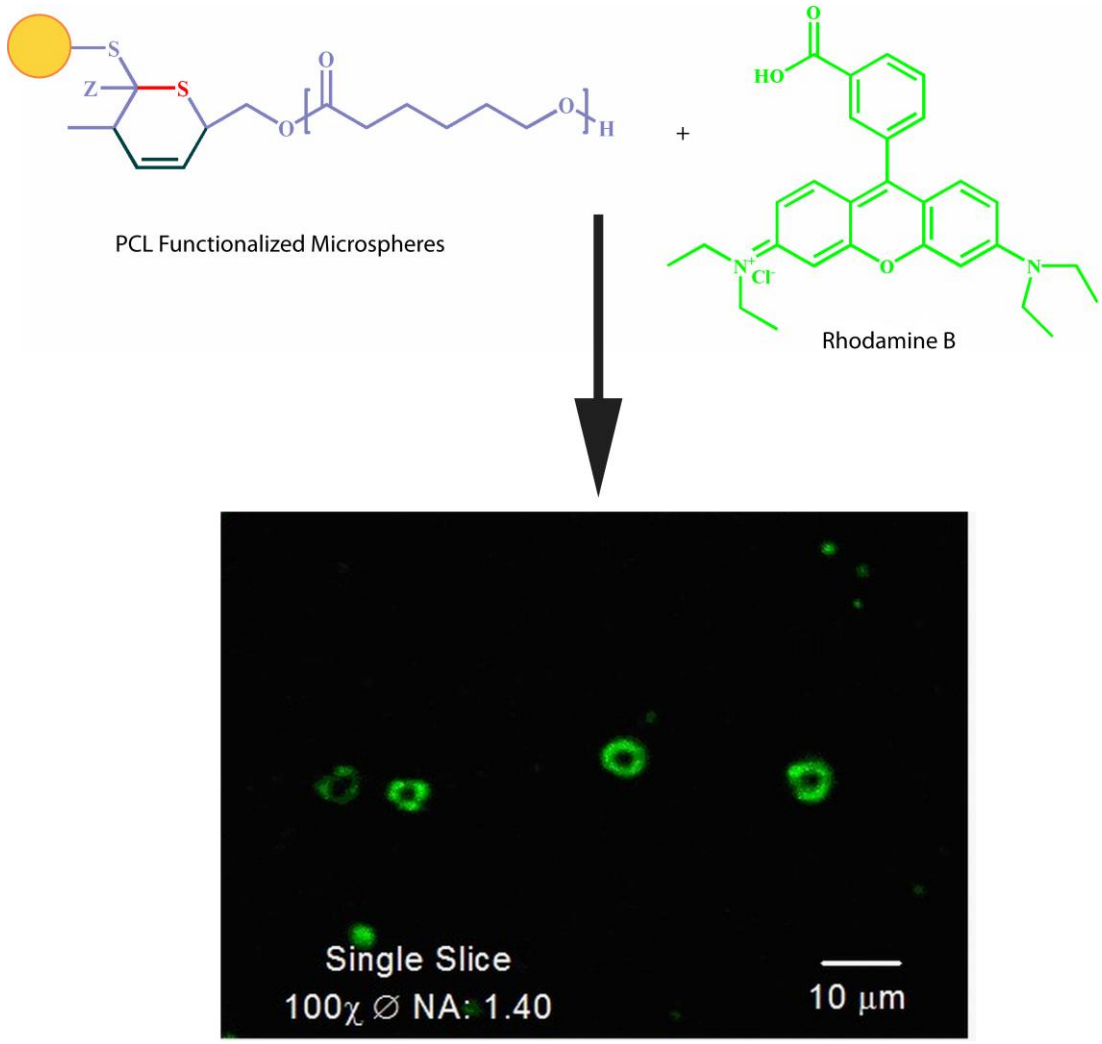

Figure 5.4 Confocal microscopy image of poly(DVB80)-BEPTF microspheres (**3**) functionalized with PCL (**5**) and reacted with a rhodamine B fluorescent tag

As the microspheres functionalized with PCL have functional -OH group at their chain ends, it is possible to label these groups with a fluoroscent dye and provide further proof for the success of the grafting reaction. Rhodamine B was selected as a fluoroscent tag as this dye has a functional carboxyl group which can react with hydroxyl functional end groups of (**5**). The coupling reaction between hydroxyl functional groups of (**5**) and carboxyl functional groups in rhodamine B was carried out *via* DCC coupling. After the reaction of PCL functional microspheres with rhodamine B, each PCL chain end was functionalized with the rhodamine B tag. These rhodamine B tagged microspheres were studied *via* confocal microscopy. As can be seen from **Figure 5.4**,

the microspheres show fluorescence only on their surface (rhodamine B has shows red fluorescence but in the image the color has been changed to green). With confocal microscopy, it is possible to select the Z-dimension (three dimensional function) which provides image depth and enables the fabrication of cross-sectional slices of the images. The image shown in **Figure 5.4** was taken selecting the Z-function and thus represents a cross-sectional slice. The fluorescence in the outer shell clearly confirms that the microspheres were functionalized with PCL. The control experiment with DVB microspheres (**3**) (not functionalized with PCL) under identical DCC conditions with rhodamine B shows no fluorescence.

In **Chapter 6**, the RAFT-HDA microsphere grafting concept is extended to variable polymer chains and to the use of highly electron deficient RAFT agent for the functionalization of microspheres. The quantification of number of grafted chains per unit surface area of the microspheres is also discussed in **Chapter 6**.

5.4 Conclusions

In the present chapter, the grafting of polymer chains *via* a combination of RAFT and HDA chemistry on the surface of DVB microspheres with surface expressed RAFT groups in a facile and efficient fashion under mild reaction conditions is discussed. The surface modification of DVB microspheres by grafting PCL chains has generated functional microspheres. The characterization of the resulting core-shell microspheres at various stages of reaction sequence *via* optical inspection, XPS, ATR-IR, and confocal microscopy techniques confirms the successful grafting of the diene functionalized PCL onto their surface. The presented RAFT-HDA grafting technique provides facile access to a host of functional grafted microspheres with applications in fields ranging from diagnostic kits, drug delivery applications and intelligent chromatographic columns.

5.5 Supporting Information

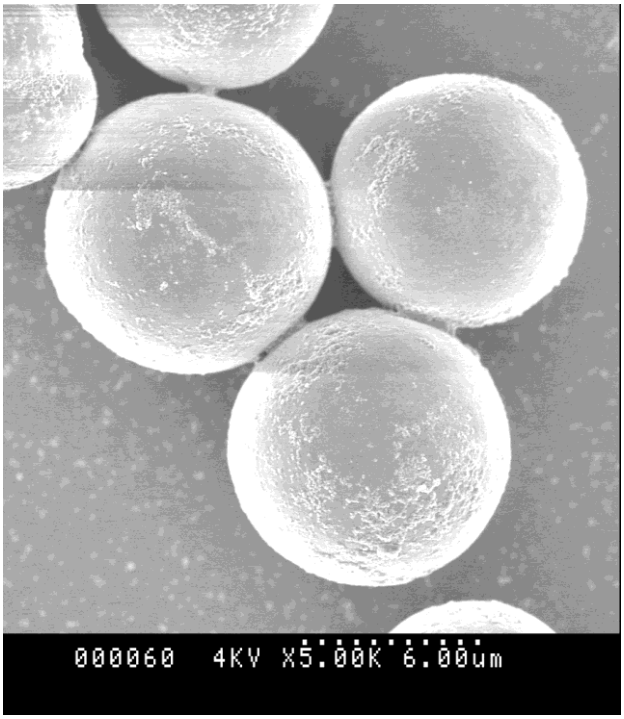

Figure S.5.1 Typical scanning electron micrograph of poly(divinylbenzene 80) microspheres (**3**) synthesized *via* precipitation polymerization

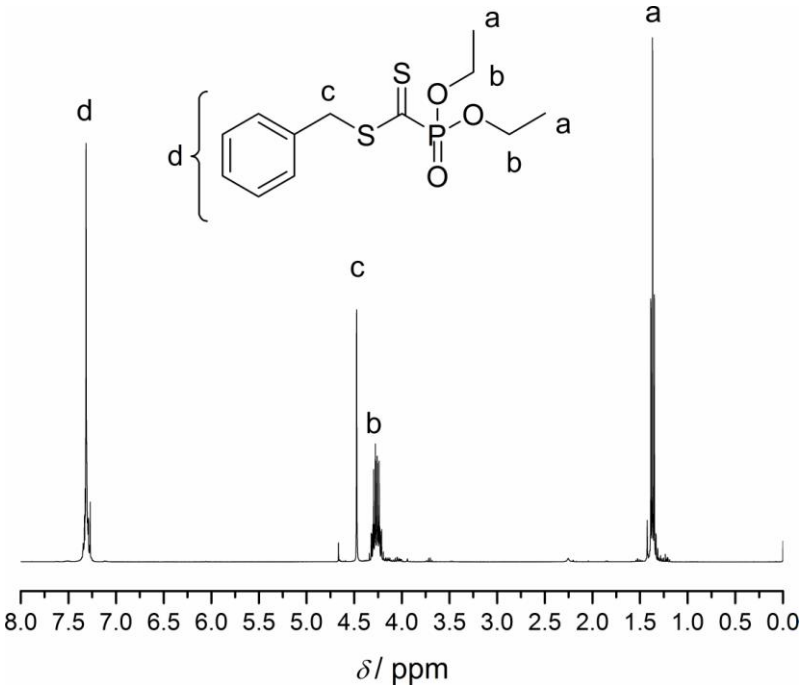

Figure S.5.2 ^{1}H NMR spectrum of benzyl (diethoxyphosphoryl)dithioformate (BEPTF) (**1**)

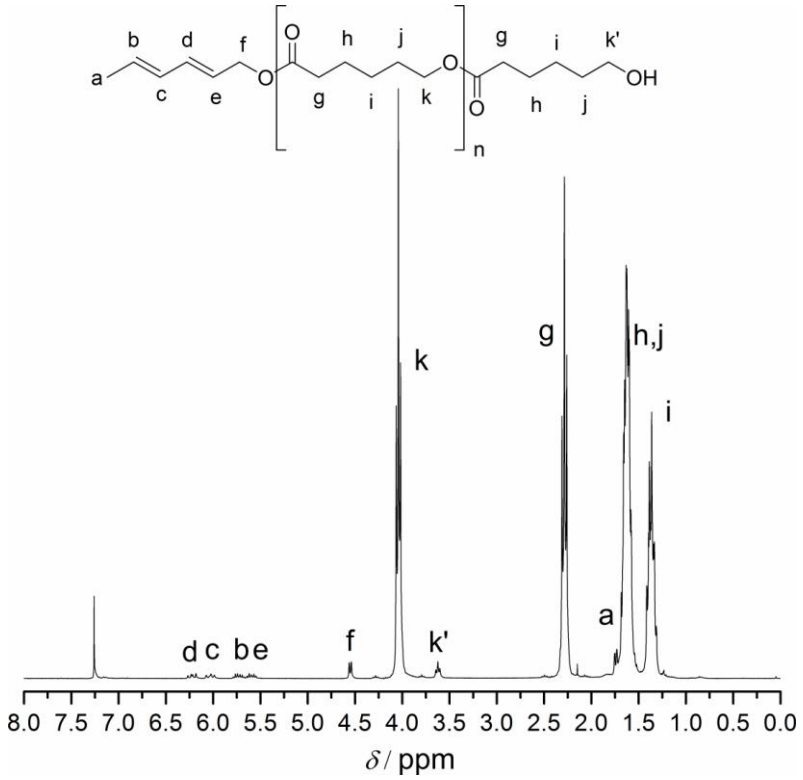

Figure S.5.3 ^{1}H NMR spectrum of 2,4-hexadienoyl terminated poly(ε-caprolactone) (**4**)

Chapter 6 Quantification of Grafting Densities *via* Modular *Grafting-to* Approaches onto Divinylbenzene Microspheres

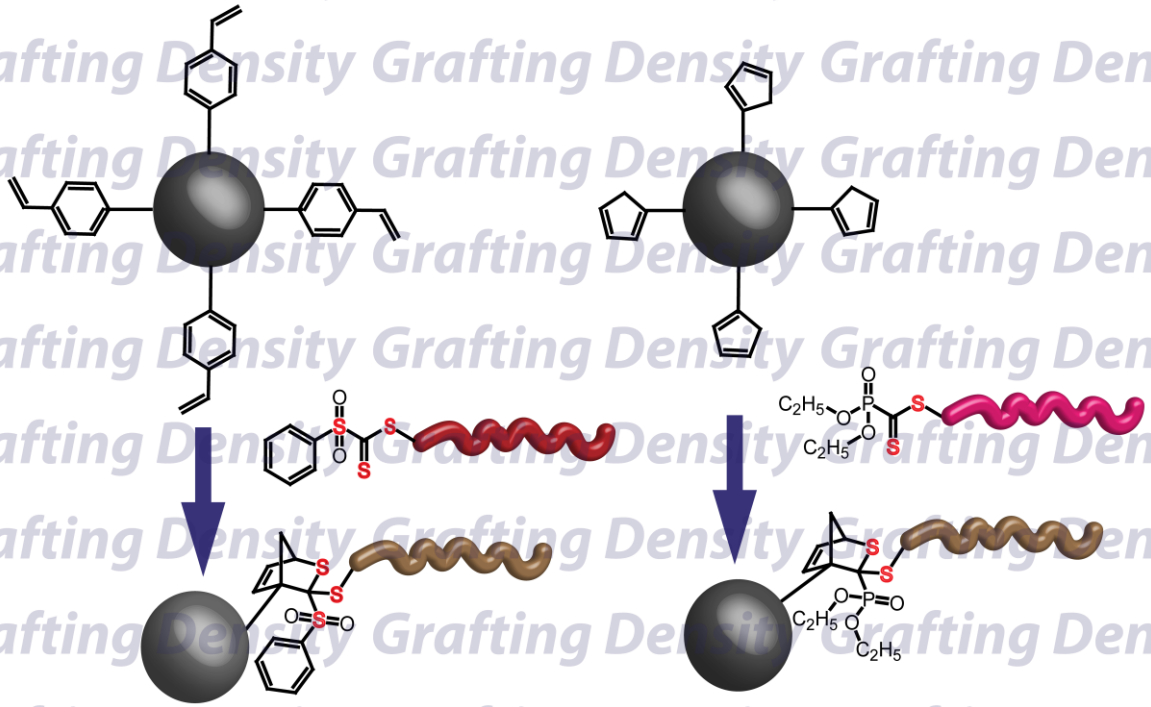

6.1 Introduction

In **Chapter 5**, the surface modification of divinylbenzene microspheres *via* RAFT-HDA chemistry based on first generation RAFT agents was discussed. In this study, the microspheres synthesized with surface expressed dithioester groups were reacted with diene capped polymer strands with the functionalization able to be achieved at 50 °C within 12 h. The motivation of the current work from a synthetic point of view is to provide functionalization protocols that efficiently functionalize microspheres under ambient conditions within short time frames and without the use of any catalyst using a *grafting-to* approach based on (ultra-rapid) RAFT-HDA *click* chemistry with the aim of quantifying the achievable grafting density or loading capacity per gram of microspheres is discussed for the first time. The availability of *click* functionalization protocols that circumvent potentially toxic transition metal catalysts is important for the application of the obtained microspheres in biological contexts. In addition, we reverse the concept of microsphere functionalization, so that they can serve as the diene component (as compared to dienophile (as discussed in **Chapter 5**)) in the HDA conjugation. Divinylbenzene based microspheres, serving as the diene component, were synthesized *via* a series of chemical transformations on the microsphere surface, which features pendant vinyl functionalities.

Quantitative data on grafting densities or loading capacities are scarce, especially when using *grafting-to* approaches, while qualitative data abounds. However, for the design of functional particles that are to be employed in specific applications (*e.g.*, in the case of microspheres as intelligent chromatographic packaging materials or in diagnostic kit applications) quantitative loading data is essential. In addition, a through understanding of *grafting-to* processes is only possible if quantitative grafting density/loading capacity data are available. This current study is designed to demonstrate that such data can indeed be obtained and all grafting studies on microspheres should contain such quantitative data. The choice of polymers that are grafted in the presented chapter is not primarily driven by the material properties that are imparted onto the microspheres, but rather serve as example materials to study the grafting behavior.

The calculation of the grafting density in the current study is based on the nominal surface area of a single microsphere, which does not take into account that the microsphere has a porous surface and the available surface area is most likely larger than that nominally calculated. However, it is very difficult to obtain a suitable value for the accessible surface area, as this area is dependent on the type of molecule that is grafted: A polymer chain will have less available surface area than a small gas molecule such as N_2. Thus, the grafting densities reported in here as per nm^2 are to be understood as nominal grafting densities (see below for details). The alternative values reported in the current study for the grafting densities as chains per gram of microsphere and the loading capacities, *i.e.* mmol of polymer chains per gram of microsphere, are surface area independent and should preferentially be employed. As all three values describe the same process and are linearly correlated. Thus, the term 'grafting density' is employed throughout the remainder of the chapter to denote all three values, which are later on provided.

In the first approach, microspheres carrying cyclopentadiene moieties as the diene were synthesized, as shown in **Scheme 6.1**. In this case, benzyl (diethoxyphosphoryl)dithioformate (BEPTF)[162] was selected as the RAFT agent to obtain polymer chains functionalized with thiocarbonyl thio end groups, which serve as the dienophilic component. The RAFT agent BEPTF falls under the category of electron deficient RAFT agents, which have been shown to be an excellent dienophiles for [4+2] cycloaddition reaction in the context of efficient block copolymer formation.[146]

In the second approach, benzyl phenylsulfonyldithioformate[26] (PSDTF) was employed as a the RAFT agent (PSDTF efficiency as RAFT agent is discussed in detail in **Chapter 4**) to synthesize phenylsulfonyldithioformate end-functionalized poly(isobornyl acrylate). The diene counterpart in this case are the double bonds intrinsically available on the surface of the DVB based microspheres as depicted in **Scheme 6.2**.[27,172] PSDTF is a so-called second generation RAFT-HDA agent, with greatly increased dienophilicity over BEPTF. As a result, it – or a polymer chain capped with it – reacts readily with styrene monomer units in [2+4] cycloadditions.[26] As a consequence, only extremely bulky monomers can be polymerized in controlled fashion using PSDTF.

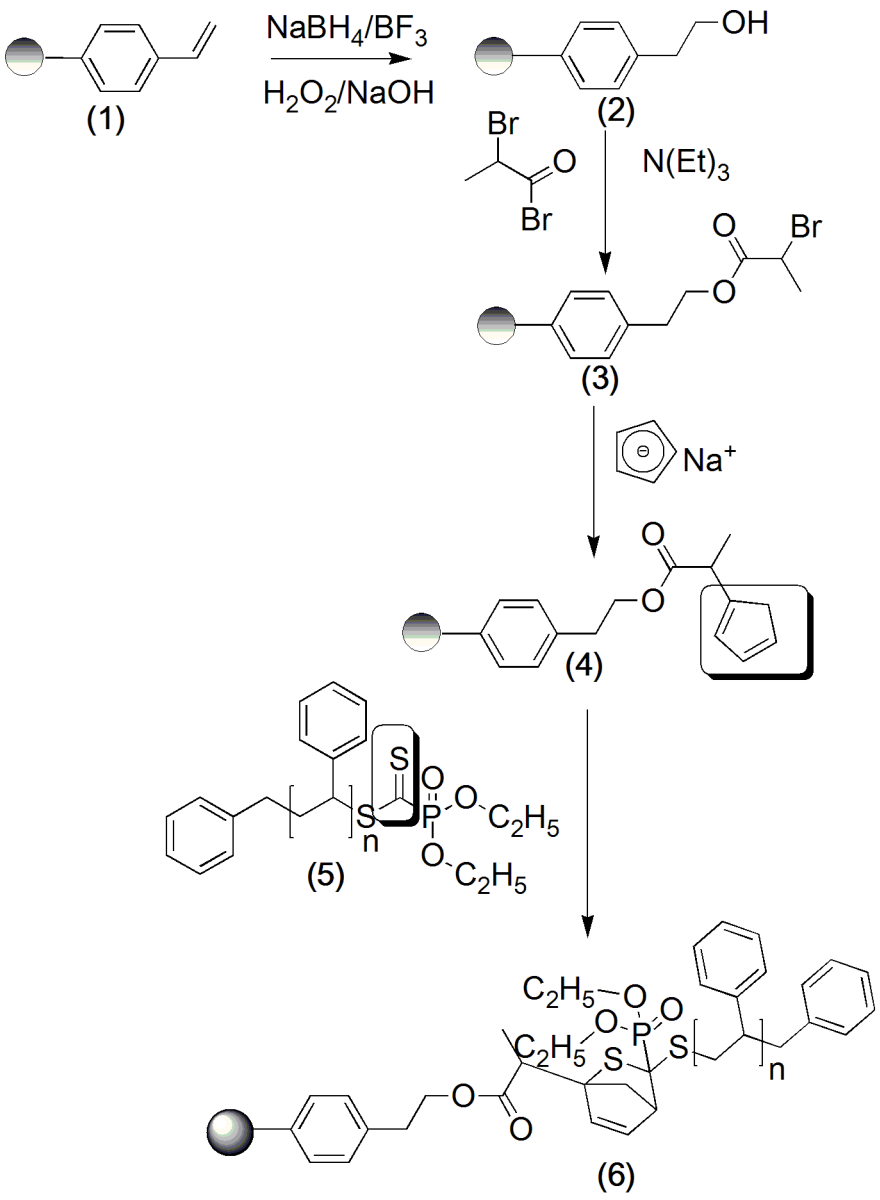

Scheme 6.1 Synthesis of hydroxy functionalized divinylbenzene 80[1] (DVB80) microspheres (DVB80-OH) (**2**) *via* the reaction of vinyl functionalized DVB80 microspheres (**1**) with $NaBH_4/BF_3$ and H_2O_2. Bromide functionalized DVB80 microspheres (DVB80-Br) (**3**) obtained *via* reaction of (**2**) with 2-bromoisoproipnylbromide. Cyclopentadienyl functionalized DVB80 microspheres

[1] The chemical composition of divinylbenzene 80 (DVB80) can be found in the **Chapter 3**

(DVB80-Cp) (**4**) obtained *via* reaction of (**3**) with sodium cyclopentadienide solution. Subsequently, DVB80 microspheres functionalized with polystyrene chains (DVB80-PS) (**6**) are obtained *via* RAFT-HDA conjugation between (**4**) and polystyrene chains functionalized with RAFT end groups (**5**) within 2 h at ambient temperature. The diene and dienophile functionalities are framed by boxes

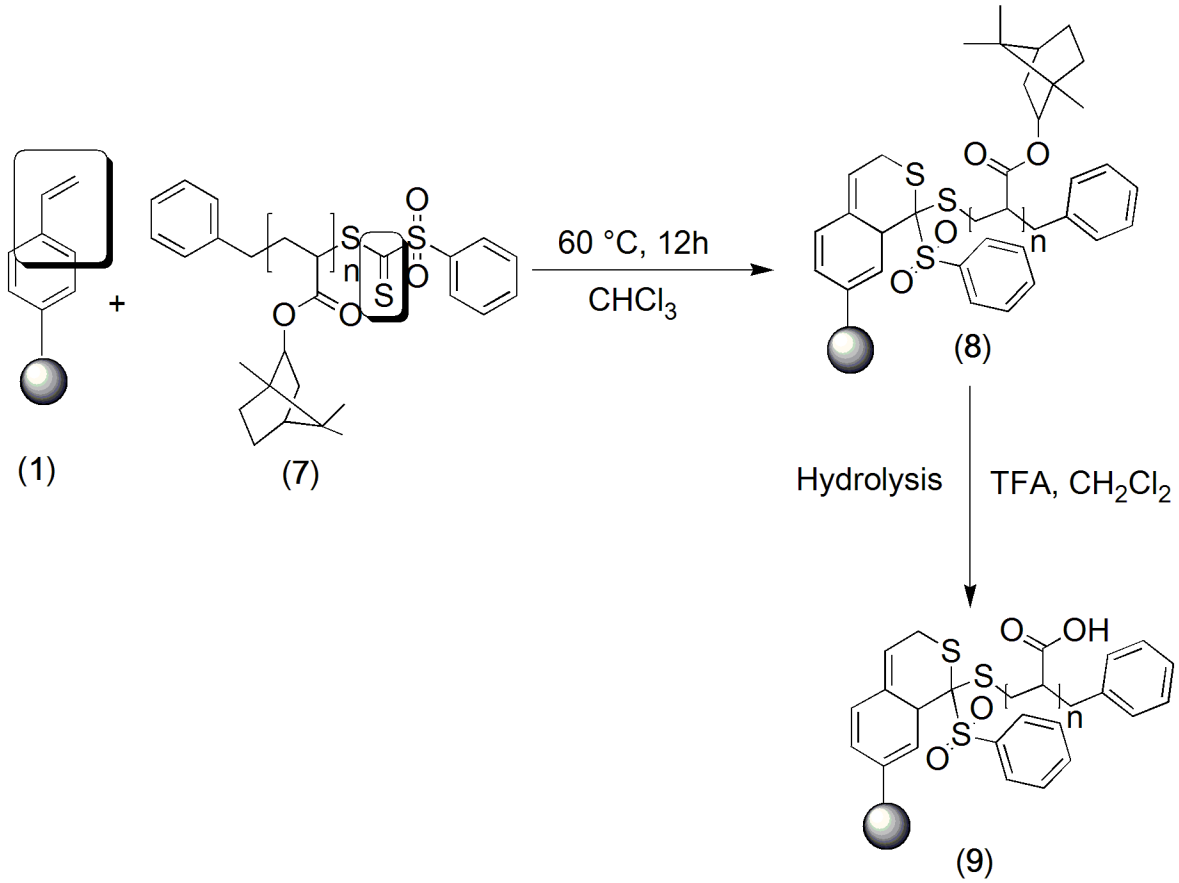

Scheme 6.2 Synthesis of DVB80 microspheres conjugated to poly(isobornyl acrylate) chains (DVB80-PiBA) (**8**) obtained *via* the reaction of DVB80 microspheres (**1**) and poly(isobornyl acrylate) functionalized with sulfonyl end groups (**7**). Subsequent hydrolysis of DVB80 microspheres conjugated to poly(isobornyl acrylate) chains (**8**) results in DVB80 microspheres conjugated to poly(acrylic acid) chains (**9**). The diene and dienophile functionalities are framed by boxes

Thus, the reactivity of two types of functional groups available on the surface of DVB80 microspheres towards their reactivity in HDA reactions based on two electron

deficient dithioesters are compared in the present chapter. It should be noted that BEPTF capped chains cannot undergo a [2+4] cycloaddition with styryl units. Therefore, in the first example, there is an extremely reactive diene, *i.e.* cyclopentadiene, available on the surface of DVB80 microspheres which is reacted with a less reactive dienophile, *i.e.* benzyl(diethoxyphosphoryl)dithioformate end-functionalized polystyrene. In the second there is a system which is based on a less reactive diene, *i.e.* styrene, which is reacted with a highly reactive dienophile, *i.e.* benzyl phenylsulfonyldithioformate functionalized poly(isobornyl acrylate).

In the current thesis, elemental analysis was employed to quantify for the first time the grafting densities on microspheres modified *via* the *grafting-to* approach using RAFT-HDA chemistry. The quantification of the grafting density opens the possibility to investigate the influence of the molecular weight of the grafted chains on the grafting density and therefore to improve the engineering of functional microspheres.

6.2 Experimental

6.2.1 Synthesis of Divinylbenzene 80 Microspheres (1)

DVB80 microspheres (**1**) were synthesized *via* distillation-precipitation polymerization. AIBN (0.092 g, 0.56 mmol, 2 wt.-% relative to the total monomer) and DVB80 (5 mL, 4.6 g, 35.35 mmol, 2.5 vol.-% relative to the reaction medium) was dissolved in 200 mL of acetonitirile in a 500 mL round bottom flask and attached to a distillation assembly. The reaction mixture was heated from ambient temperature to boiling by ramping the temperature gradually until the solvent started distilling. As the solvent starts distilling, the initially homogenous reaction mixture turns milky white. The reaction was stopped after half of the initial acetonitrile used in the reaction mixture was collected in a receiving flask. After the polymerization is completed, the resulting DVB80 microspheres were separated by filtration through a 0.45 µm membrane, washed and re-suspended several times in toluene, THF, acetone and diethylether. These washing cycles with various solvents are important to remove residual monomer. The microspheres were dried in a vacuum oven at 40 °C before characterization. 1.36 g of polymeric microspheres was obtained in 30% yield.

6.2.2 Synthesis of Hydroxy Functionalized Divinylbenzene 80 Microspheres (2)

DVB80 microspheres (**1**) (1.0 g) were suspended in dry THF (10 mL) in a 100 mL round-bottomed flask for 2 h at ambient temperature and sodium borohydride (0.1 g, 2.6 mmol) was added to the suspension after 2 h. The suspension was subsequently cooled in a cold-water bath, and boron trifluoride diethyl etherate (0.376 g, 2.6 mmol) dissolved in 1 mL of THF was added dropwise to the suspension of the microspheres. The temperature of the reaction suspension was maintained at 20 °C during the addition of BF_3 for a further 3 h. At the end of this period, the flask was immersed in an ice bath, and 5 mL of cold water was slowly added to remove any residual $NaBH_4$. Subsequently, hydrogen peroxide (0.8 mL, 36 mmol, 30% in water) was slowly added to the reaction mixture. During the addition, the pH of the solution was maintained near 8 by adding 3M sodium hydroxide as required. The final solution was filtered through a 0.45 µm membrane filter, washed with water (pH = 8), then methanol and finally toluene. The resulting microspheres were dried under vacuum at 40 °C before characterization.

6.2.3 Synthesis of Bromide Functionalized Divinylbenzene 80 Microspheres (3)

Hydroxy functionalized microspheres, DVB80-OH (**2**) (0.5 g), were suspended in 5 mL of anhydrous THF containing triethylamine (0.1 g, 1.0 mmol) in a 25 mL round bottomed flask cooled in an ice-water bath for 2 h, followed by the drop-wise addition of 2-bromoisopropionyl bromide (0.2 g, 0.92 mmol) to the suspension. After the addition of 2-bromoisopropionyl bromide the mixture was stirred at ambient temperature overnight. The bromine functionalized microspheres were filtered through a 0.45 µm membrane filter and washed thoroughly with THF and methanol. The resulting microspheres were dried in a vacuum oven at 40 °C before characterization.

6.2.4 Synthesis of Cyclopentadienyl Functionalized Divinylbenzene 80 Microspheres (4)

DVB80 (100 mg) microspheres functionalized with bromine (**3**) were suspended in 5 mL of dry THF. The resulting suspension was cooled in an ice-salt bath and 400 µL of sodium cyclopentadienide solution was added dropwise. The reaction mixture was stirred overnight at ambient temperature. The microspheres were filtered through a 0.45 µm membrane filter and washed thoroughly with dichloromethane, water and

methanol. The resulting microspheres were dried in a vacuum oven at ambient temperature before characterization.

6.2.5 Synthesis of Polystyrene (5) using Benzyl (diethoxyphosphoryl)dithioformate as RAFT Agent

A solution of styrene (8.0 mL, 7.27 g, 0.07 mol), benzyl (diethoxyphosphoryl)dithioformate (0.049g, 0.162 mmol) and AIBN (0.0043 g, 0.027·mmol) was prepared and placed in a 25 mL round bottomed flask. The flask was subsequently purged with nitrogen to remove any residual oxygen. The polymerization reaction was performed at 60 °C for 6 h. The reaction was ceased by exposing the reactants to oxygen and chilling in an ice bath. The polymers were isolated by a two-fold precipitation in cold methanol (3 g, 41% yield). M_n (SEC) = 4 200 g·mol^{-1}, PDI = 1.12. The molecular weight distribution and ^{1}H-NMR spectrum of polystyrene are depicted in **Figure S.6.1** and **S.6.2**, respectively.

6.2.6 RAFT-HDA Conjugation between Polystyrene Functionalized with Diethoxyphosphoryl End Group (5) and Cyclopentadienyl Functionalized Divinylbenzene 80 Microspheres (4)

The HDA cycloaddition between cyclopentadienyl functionalized DVB80 microspheres (**4**) and dithioester terminated polystyrene (**5**) was performed by adding phosphoryl functionalized polystyrene (150 mg) (**5**) to 1 mL of chloroform. Subsequently, cyclopentadienyl functionalized DVB80 microspheres (30 mg) were suspended in the solution. The resulting mixture was stirred at ambient temperature for 2 h, and then centrifuged at 4000 rpm. The resulting polystyryl-functional microspheres were washed thoroughly with chloroform and dried in a vacuum oven at ambient temperature prior to characterization.

6.2.7 Synthesis of Poly(isobornyl acrylate) (7) Using Benzyl phenylsulfonyldithioformate RAFT Agent

A solution of isobornyl acrylate (9.07 g, 43.55 mmol), benzyl phenylsulfonyldithioformate (PSDTF) (0.0771 g, 0.15 mmol) and AIBN (0.0082 g,

0.05 mmol) was prepared and placed in a 25 mL round bottom flask. The reaction mixture was subsequently purged with nitrogen for 15 min to remove any residual oxygen. The polymerization was carried out at 60 °C for 15 and 24 h, respectively. The reaction was stopped by exposing the reactants to oxygen and chilling in an ice bath. The polymers were isolated by two-fold precipitation in cold methanol (2 g, 22% yield, 3.75 g, 41% yield for 15 and 24 h respectively). M_n (SEC) = 6 000 g·mol^{-1}, PDI = 1.25, and M_n (SEC) = 26 000 g·mol^{-1}, PDI = 1.26. The molecular weight distribution and ^{1}H-NMR spectrum of poly(isobornyl acrylate) (M_n = 26 000 g·mol^{-1}) are provided in **Figure S.6.3** and **S.6.4** (supporting information section), respectively.

6.2.8 RAFT-HDA Conjugation Between Poly(isobornyl acrylate) Functionalized with Sulfonyldithioformate End Groups (7) and Styrene Groups on the Surface of DVB80 Based Microspheres (1)

DVB80 microspheres (**1**) (30 mg) were suspended in a solution of poly(isobornyl acrylate) (**7**) (150 mg) in chloroform (1 mL) and heated at 60 °C in a pressure tube for 12 h. After completion of the reaction, the microspheres were extensively washed with chloroform several times to remove any excess of polymer not conjugated onto the DVB80 surface. The resulting microspheres were dried in a vacuum oven at room temperature before characterization.

6.2.9 Hydrolysis of Poly(Isobornyl Acrylate) Conjugated to DVB80 Microspheres (8) to Poly(Acrylic Acid) (9)

DVB80 microspheres conjugated with poly(isobornyl acrylate) (**8**) were suspended in dichloromethane (3.5 mL) and trifluoroacetic acid (0.855 g) was added to the suspension. The resulting mixture was stirred overnight at ambient temperature. After the completion of the reaction, the microspheres were extensively washed with dichloromethane. The resulting microspheres were dried in a vacuum oven at ambient temperature before characterization.

6.2.10 Labelling of Poly(acrylic acid) Functionalized DVB80 Microspheres (9) with Fluoresceinamine (FA)

Dicyclohexylcarbodiimide (0.05 g) was dissolved in DMF (2 mL) and 10 mg of DVB80 microspheres with poly(acrylic acid) functionalities on the surface were incubated for a period of 2 h at ambient temperature. Subsequently, a freshly prepared solution of fluoresceinamine (FA, 0.04 g) in DMF (2 mL) was added. The mixture was stirred at ambient temperature for a period of 12 h. The FA-labelled microspheres were washed thoroughly with DMF, dried in a vacuum oven and were observed using a confocal microscope (LSM 510 meta, Zeiss, discussed in **Chapter 3**).

6.3 Results and Discussion

6.3.1 Cyclopentadienyl Functional Microspheres

The core microspheres were synthesized *via* a distillation-precipitation polymerization technique which results in highly monodisperse particles. Prior to the surface modification of the microspheres, their morphology, size and distribution were studied *via* SEM (typical SEM micrograph shown in **Figure S.6.1**). The number average, D_n, and weight average, D_w, diameter of the microspheres with vinyl functionality on the surface were 1.31 and 1.32 µm respectively, featuring a *PDI* of 1.00. The modification of the surface of the core microspheres was monitored *via* ATR-IR. Before grafting the polymer chains to the surface of the microspheres, the vinyl functional microspheres were modified to introduce reactive diene functionality onto their surface which can efficiently react with a polymer having a dienophilic moiety as shown in **Scheme 6.1**. Initially, the highly cross-linked DVB80 microspheres (**1**) have residual vinyl groups on the surface (discussed in detail in **Chapter 2**). A hydroboration/oxidation reaction was employed to hydroxylate the vinyl groups in the β-position. In the hydroboration/oxidation reaction the reactants are $(BH_3)_2$ formed by the *in-situ* reaction of $NaBH_4$ and BF_3 in the first step and reaction with H_2O_2 in the second step. The addition of BH_3 to the vinyl double bond is a concerted reaction, with multiple bond formation and breaking occurring simultaneously. The hydroborane adds to the double bond so that the boron always ends up on the lesser substituted carbon. In the transition state, the more substituted carbon bears a partial positive charge (a partial

carbocation). In the second hydroboration–oxidation step, the nucleophilic hydroperoxide anion attacks the boron atom. Alkyl migration to oxygen gives the alkyl borane with retention of stereochemistry.

Figure 6.1(a) and (b) show the comparison of ATR-IR spectra of DVB80 microspheres with surface expressed vinyl groups and DVB80 microspheres with surface expressed hydroxy groups (DVB80-OH) (**2**). The change from surface attached vinyl groups to hydroxy groups leads to a very significant reduction of the sharp vinyl band at 992 cm^{-1}, while due to the presence of hydroxy end groups a characteristic band at 3 454 cm^{-1} is observed, which is not present in the vinyl functionalized microspheres. The reaction of the hydroxy functionalized microspheres (**2**) with 2-bromoisopropionyl bromide leads to the functionalization of microspheres with bromine end groups (**3**). **Figure 6.1**(c) and (d) show the comparison of the ATR-IR spectra of the hydroxy functionalized microspheres and bromide functionalized microspheres. The bromide functionalized microspheres clearly display a band at 1 725 cm^{-1} due to the presence of the carbonyl functionality as well as a band at 1 265 cm^{-1} due to the C-Br stretching vibration in the bromide functionalized microspheres. No such band was observed in hydroxy functionalized microspheres. In addition, the band at 3 454 cm^{-1} (peak maximum), which is associated with the hydroxy groups, significantly decreases in the case of the bromide functionalized microspheres.

These bromide functionalized microspheres (**3**) are suitable for introducing very reactive diene moieties on their surface. The bromide end functionalized microspheres were treated with a solution of sodium cyclopentadienide in THF to achieve a substitution of the bromide end group with a cyclopentadienyl group. **Figure 6.1**(e) shows a decrease in the intensity of the C-Br band after the reaction of the bromide functionalized microspheres with sodium cyclopentadienyl and therefore clearly evidences the substitution of most of the bromide functionality by cyclopentadienyl moieties. However, as the signal for C-Br band has not completely disappeared this suggests that not all the bromides groups are being substituted by cyclopentadiene moieties. As dienophilic counterpart for the RAFT-HDA conjugation on the DVB80 microspheres, benzyl (diethoxyphosphoryl)dithioformate was used to synthesize polystyrene.

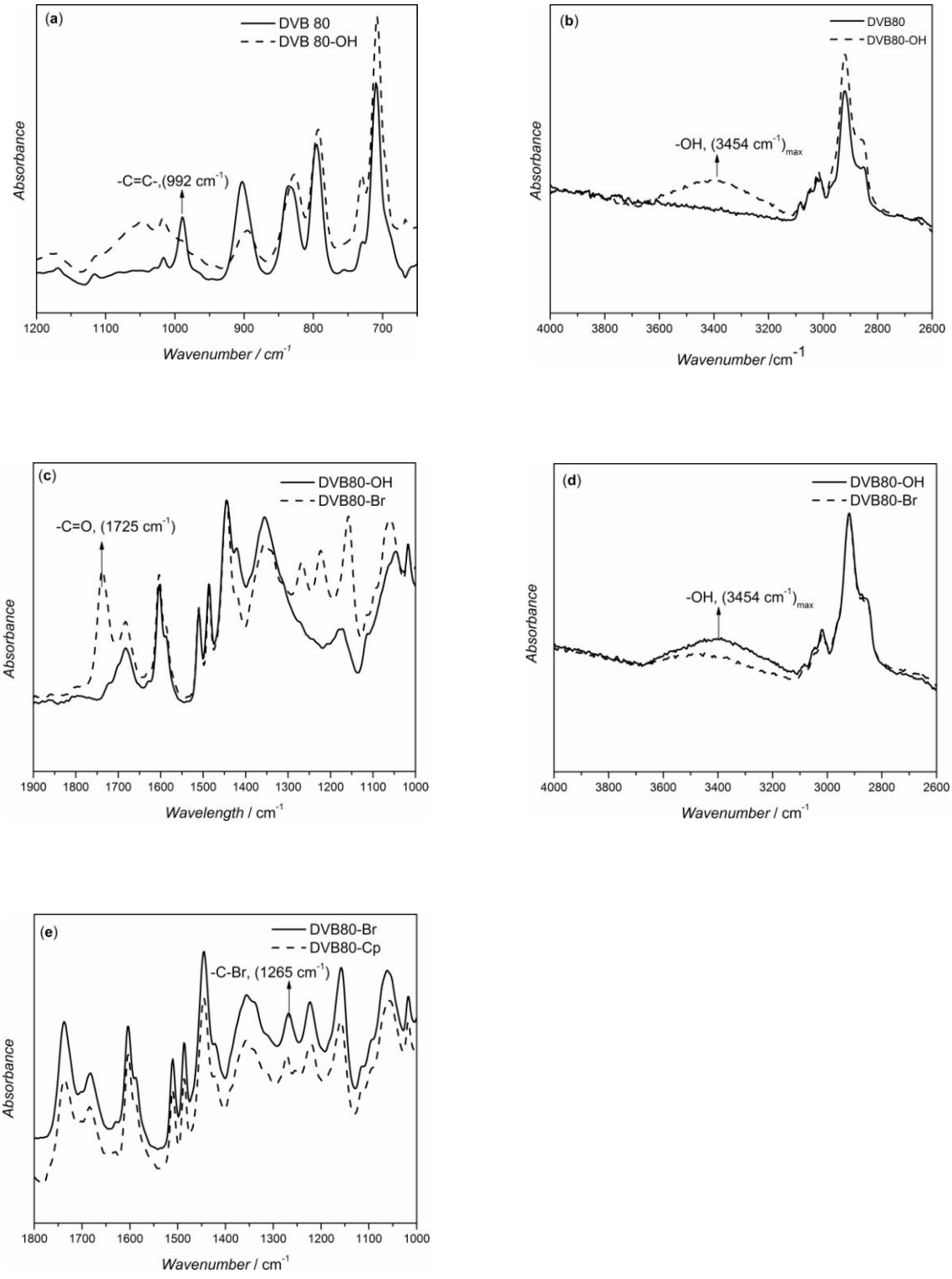

Figure 6.1 ATR-IR spectra: (a) Comparison of the signal of the initial DVB80 (**1**) microspheres and DVB80 microspheres carrying hydroxyl end groups (DVB80-OH) (**2**)

with respect to the vinyl signal; (b) comparison of the signal of DVB80 (**1**) microspheres and DVB80-OH microspheres (**2**) with respect to the hydroxy signal; (c) comparison of the signal of DVB80-OH (**2**) and DVB80 microspheres with bromide end groups (DVB80-Br) (**3**) with respect to carbonyl signal; (d) comparison of the signal of DVB80-OH microspheres (**2**) and DVB80-Br microspheres (**3**) with respect to the hydroxy signal; (e) comparison of the signal of DVB80-Br microspheres (**3**) with DVB80 microspheres featuring cyclopentadiene end groups (DVB80-Cp) (**4**)

The *click* conjugation or grafting of RAFT functionalized polystyrene was carried out on cyclopentadienyl functionalized DVB80 microspheres in chloroform at ambient temperature within 2 h in the absence of a catalyst. The microspheres with cyclopentadiene surface groups are coupled to RAFT functionalized polystyrene through the formation of a 3,6-dihydro-2*H*-thiopyran ring. The stability of the 3,6-dihydro-2*H*-thiopyran ring has previously been found to be able to withstand relatively harsh conditions of pH (between 0 and 14 at ambient temperature) and temperatures (up to 120 °C).[249] The success of the grafting of polystyrene onto cyclopentadienyl functionalized microspheres was confirmed by elemental analysis of DVB80-Cp functional microspheres and of the microspheres after conjugation with RAFT functionalized polystyrene. Elemental analysis was also employed for the calculation of the grafting density/loading capacity of the cyclopentadienyl functionalized DVB80 microspheres. **Table 6.1** collates the elemental analysis results for the microspheres starting from DVB80 to DVB80 microspheres functionalized with polystyrene (DVB80-PS).

Inspection of **Table 6.1** indicates that sulphur is only detected in the microspheres after conjugation with polystyrene, as the polystyrene used for the functionalization of microspheres carries dithioester end groups. Thus, the microspheres can only contain sulphur after successful grafting.

Table 6.1 Elemental analysis of the series of microspheres: DVB80 microspheres (**1**), DVB80-OH microspheres (**2**), DVB80-Br microspheres (**3**), DVB80-Cp microspheres (**4**), and DVB80-PS microspheres (**6**). The structural images corresponding to the individual samples can be found in **Scheme 6.1**

Sample	N	C	H	S	O
	[wt.-%]	[wt.-%]	[wt.-%]	[wt.-%]	[wt.-%]
(**1**)	0.04	87.82	7.72	0.00	1.36[a]
(**2**)	0.09	81.66	7.48	0.00	4.81
(**3**)	0.16	78.43	7.14	0.00	5.68
(**4**)	0.07	79.31	7.20	0.00	6.02
(**6**)	0.00	77.85	6.97	1.28	5.18

[a] The oxygen detected in the neat DVB80 microspheres (**1**) is most likely oxygen trapped in the porous surface topology of the microspheres. Nitrogen can be introduced into the microspheres by the initiator (AIBN) and by nitrogen trapped in the porous surface topology of the microspheres. The wt.-% of the residual oxygen and nitrogen both have only very marginal effects on the calculation of the loading capacity, *i.e.* the number of chains per g of microspheres, and the grafting density and therefore induce only a very small error.

Using the weight percentage of sulphur, the grafting density of polystyrene on the surface of the DVB80-PS microspheres is calculated. The number average particle diameter of the grafted particles (determined by SEM) is 1.31 µm. The particle surface area and volume are therefore $5.47 \cdot 10^6$ nm^2 and 1.2 µm^3 after grafting, respectively. The surface grafting density can be estimated based on the sulphur content of the grafted microspheres, determined by elemental analysis. The sulphur content of the polystyrene-grafted microspheres (determined by elemental analysis, see **Table 6.1**) is 1.28 wt.-%. This means that 1 g of grafted microspheres contains 0.0128 g sulphur. Each polymer chain contains two sulphur atoms (see **Scheme 6.1**). Therefore, the loading capacity per g of microspheres (LC) can be calculated [equation (6.1)]:

$$LC = (W(\mathrm{S}) \cdot 1000) / (\mathrm{n(S)} \cdot MW(\mathrm{S})) \qquad (6.1)$$

where *LC* is the loading capacity in mmol / g microspheres (MS), *W*(S) is the weight of the sulphur per gram of microspheres obtained *via* elemental analysis, n(S) is the number of sulphur atoms per polymer chain and *MW*(S) is the molecular weight of sulphur. The loading capacity of the microspheres after conjugation with RAFT functionalized polystyrene (**5**) is 0.2 mmol per g of microspheres. The loading capacity can be easily transformed into the number of chains per g of microspheres by multiplying the loading capacity (in mol per g of microspheres) by Avogadro's number, N_A. Therefore 1 g of polystyrene-grafted microspheres (**5**) contain $1.2 \cdot 10^{20}$ chains.

The volume of one microsphere is 1.2 μm^3 and the density of the core microspheres is 1.18 $g \cdot cm^{-3}$.[175] Therefore, one microsphere weighs $1.42 \cdot 10^{-12}$ g, which corresponds to $0.70 \cdot 10^{12}$ core microspheres per gram of material. One microsphere has a particle surface area (*SA*) of $5.47 \cdot 10^6$ nm^2. The SA per gram of microspheres is therefore $3.85 \cdot 10^{18}$ $nm^2 \cdot g^{-1}$. The grafting density can consequently be calculated by dividing the number of chains per gram of microspheres ($1.2 \cdot 10^{20}$ $chains \cdot g^{-1}$) by the surface area per gram of microspheres ($3.85 \cdot 10^{18}$ $nm^2 \cdot g^{-1}$). Therefore, the grafting density on the microspheres can be calculated using the following formula [equation (6.2)]:

$$GD = (W(S) \cdot N_A \cdot d \cdot V) / (n(S) \cdot MW(S) \cdot 4 \cdot \pi \cdot r^2) \quad (6.2)$$

GD is the grafting density obtained on the surface in chains per nm^2, *W*(S) is the weight of the sulphur per gram of microspheres obtained *via* elemental analysis, n(S) is the number of sulphur atoms per polymer chain and *MW*(S) is the molecular weight of sulphur. N_A is the Avogadro's number, *d* is the density of the microsphere in $g \cdot cm^{-3}$, *V* is the volume of microsphere in μm^3, and *r* is the radius of the microsphere in µm. The nominal grafting density calculated *via* this method is 31.1 $chains \cdot nm^{-2}$. As noted in the introduction, the reported grafting density value per unit of area is a nominal value. However, even if the accessible surface area is a factor of 10 larger, a grafting density of close to 3 chains per nm^{-2} is a value that provides strong evidence for the efficacy of the employed *grafting-to* functionalization protocol. Based on the number of polymer

chains that were available for grafting (150 mg polymer corresponds to $2.15 \cdot 10^{19}$ chains), 16.7% of these chains have actually functionalized the microspheres' surface.

6.3.2 Microspheres Functionalized with Poly(isobornyl acrylate)

In the second approach to functionalize DVB80 microspheres, the vinyl groups intrinsically available on their surface were utilized for conjugation. DVB80 microspheres have styrene moieties available on the surface and therefore styrene can function as a diene when reacted with a highly reactive dienophile.[27] The dienophile used for the conjugation to the styrene groups on the surface of DVB80 microspheres is poly(isobornyl acrylate) carrying PSDTF end groups. A detailed evaluation of the efficacy of PSDTF as a conjugation agent has previously been shown.[26] The coupling reaction between the styrene surface groups of the DVB80 microspheres and PiBA-PSDTF was performed at 60 °C in chloroform solution over 12 h. A similar reaction condition was previously employed for the functionalization of Si surfaces.[27] The conjugation between styryl groups on the surface of microspheres and thiocarbonyl group on polymer chain leads to the formation of a 3,6-dihydro-2*H*-thiopyran ring. The functionalization for DVB80 microspheres with PiBA was monitored by ATR-IR spectroscopy. As observed in **Figure 6.2**, the DVB80 microspheres after functionalization with PiBA (DVB80-PiBA) show the C=O vibration at 1 720 cm^{-1}, which is only possible when styryl groups are conjugated to the poly(isobornyl acrylate) chains.

The poly(isobornyl acrylate) chains grafted onto the surface of the DVB80 microspheres can be hydrolyzed to yield poly(acrylic acid) chains on the surface of the microspheres. The hydrolysis was carried out in dichloromethane using trifluoroacetic acid. The efficacy of the hydrolysis of poly(isobornyl acrylate) to poly(acrylic acid) was proven by labelling the freed carboxyl groups with a fluorescent dye. Fluoresceinamine was selected as a fluorescent tag as this dye has a functional amine group which can react with the carboxyl functional end groups of (**9**). The coupling reaction between the carboxyl functional groups of (**9**) and the amine functional groups in the fluoresceinamine was carried out *via* DCC coupling as shown in **Scheme 6.3**.

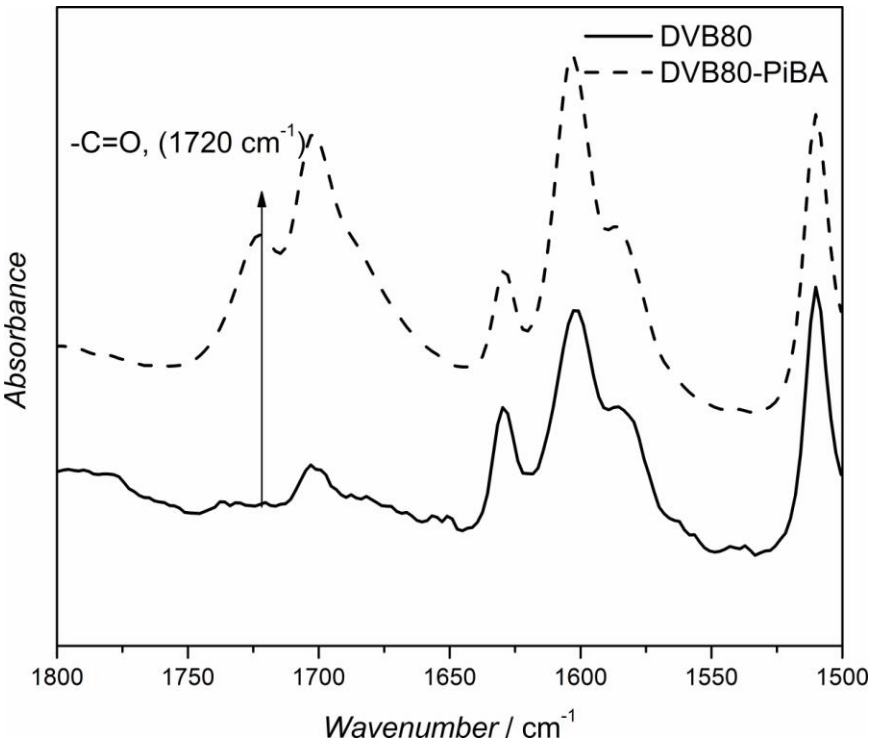

Figure 6.2 ATR-IR spectra for the comparison of signals of DVB80 microspheres (**1**) with DVB80 microspheres conjugate to poly(isobornyl acrylate) (DVB80-PiBA) (**8**) obtained *via* reaction of (**1**) with poly(isobornyl acrylate) (**7**)

After the reaction of poly(acrylic acid) functionalized microspheres (**9**) with fluoresceinamine, each poly(acrylic acid) chain end should be functionalized with the fluoresceinamine tag. These fluoresceinamine tagged microspheres were studied *via* confocal microscopy. As can be seen from **Figure 6.3**, the microspheres show fluorescence only on the surface. By employing confocal microscopy it is possible to select the Z-dimension (three dimensional function) which provides image depth and enables the fabrication of cross-sectional slices of the images. The image shown in **Figure 6.3** was taken selecting the Z-function and thus represents a cross-sectional slice. The fluorescence in the outer shell clearly confirms that the microspheres were functionalized with poly(acrylic acid). The blind-control esterification experiment with DVB80 microspheres grafted with poly(isobornyl acrylate) chains (**8**) under identical DCC conditions with fluoresceinamine shows no fluorescence.

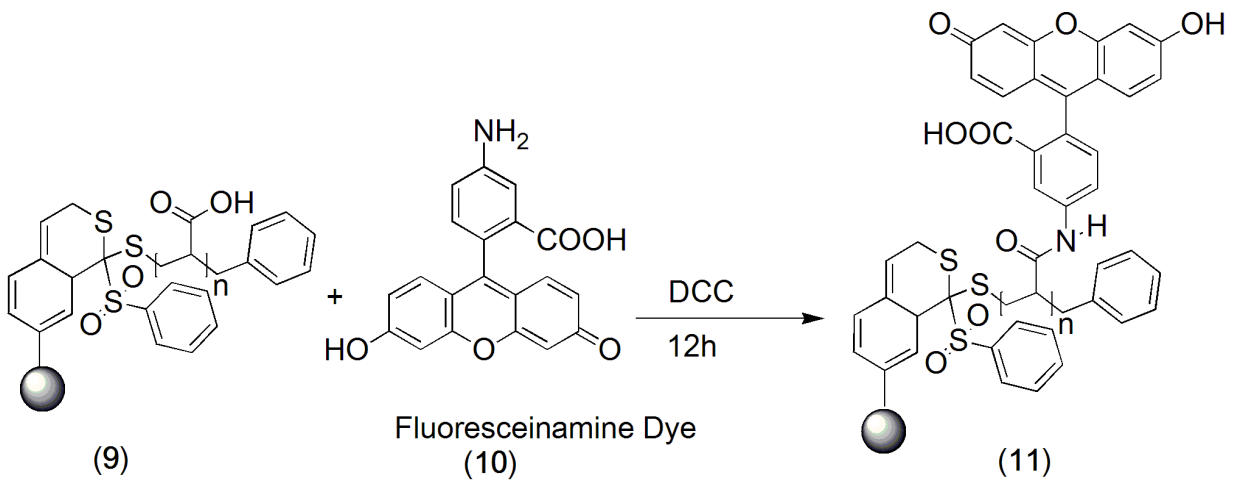

Scheme 6.3 Labelling of DVB80 microspheres conjugated to poly(acrylic acid) (**9**) with fluoresceinamine dye (**10**) using DCC coupling

In addition to ATR-IR spectroscopy and confocal microscopy, elemental analysis was utilized to confirm the functionalization of DVB80 microspheres with poly(isobornyl acrylate) as well as for the calculation of the grafting density of poly(isobornyl acrylate) to the surface of DVB80 microspheres. **Table 6.2** shows the elemental analysis results for the microspheres starting from DVB80 to DVB80-PiBA microspheres using poly(isobornyl acrylate) of two molecular weights, *i.e.* 6 000 g·mol^{-1} and 26 000 g·mol^{-1}. Polymer of two molecular weights were employed to assess how the grafting density is influenced by the molecular weight. As can be seen from the **Table 6.2**, the sulphur is present in the microspheres only after grafting. The poly(isobornyl acrylate) employed for the functionalization of the microspheres carries a dithioester end group and thus the microspheres can contain sulphur only after they are modified or functionalized with poly(isobornyl acrylate). Using the weight percentage of sulphur, the grafting density of poly(isobornyl acrylate) on the surface of DVB80-PiBA microspheres was calculated.

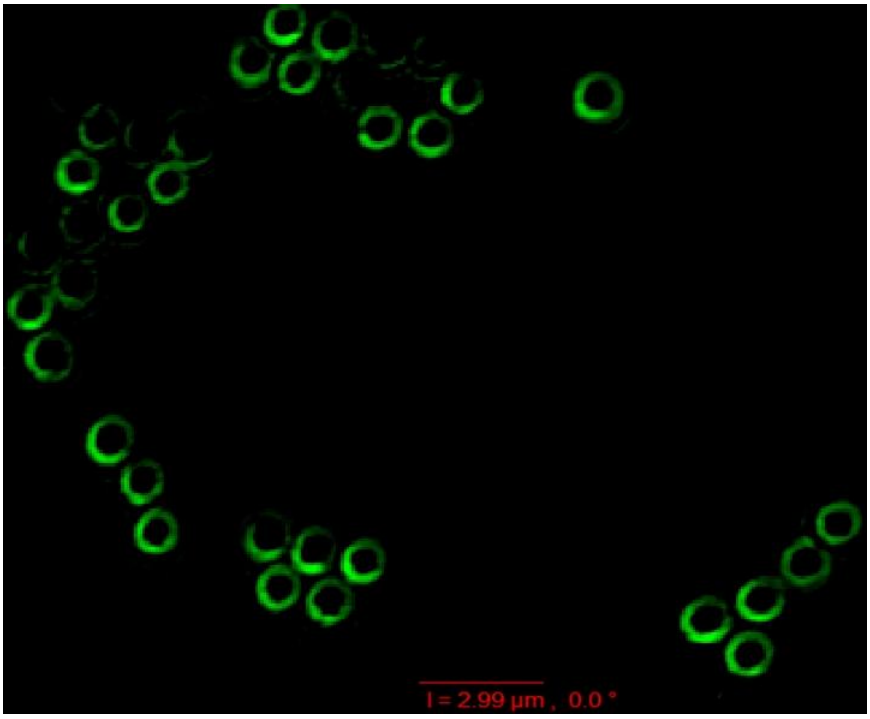

Figure 6.3 Confocal microscopy image of DVB80 microspheres conjugated to poly(acrylic acid) chains (**9**) after labelling with fluoresceinamine *via* DCC coupling. The poly(acrylic acid) is obtained on the surface of microspheres *via* hydrolysis of poly(isobornyl acrylate) chains which are conjugated to the surface of microspheres *via* the RAFT-HDA approach

As in the case of the calculation of the grafting densities when polystyrene is grafted to the surface, a detailed calculation can be made to arrive at quantitative numbers. Employing the two sulphur contents found in the microspheres for both molecular weights, *i.e.* 0.45 wt.% for 6000 g·mol^{-1} and 0.22 wt.% for 26000 g·mol^{-1} (see **Table 6.2**), one arrives at nominal grafting densities of 7.3 and 3.6 chains·nm^{-2} or – alternatively – of 2.82·10^{19} and 1.38·10^{19} chains·g^{-1}. In addition, one can also calculate – as in the case of the styrene grafting – the percentage of chains that have reacted on the surface. In the case of the 6000 Da PiBA, 12.0% of the chains in the reaction solution have been tethered to the microspheres' surface, while 6.7 % have been attached in the case of employing 26 000 Da PiBA. The results of all quantification experiments are collated in **Table 6.3**.

Table 6.2 Elemental analysis of DVB80 microspheres (**1**) and DVB80-PiBA microspheres (**8**)

Sample	N [wt.-%]	C [wt.-%]	H [wt.-%]	S [wt.-%]	O [wt.-%]
(**1**)	0.04	87.82	7.72	0.00	1.36[a]
(**8**) [M_n=6000 g·mol^{-1}]	0.67	84.61	7.30	0.45	3.42
(**8**) [M_n=26000 g·mol^{-1}]	0.00	85.17	7.40	0.22	3.36

[a] The oxygen detected in the neat DVB80 microspheres (**1**) is most likely oxygen trapped in the porous surface topology of the microspheres. Nitrogen can be introduced into the microspheres by the initiator (AIBN) and by nitrogen trapped in the porous surface topology of the microspheres. The wt.-% of residual oxygen and nitrogen both have only very marginal effects on the calculation of the loading capacity, the number of chains per g of microspheres, and the grafting density and therefore induce only a very small error.

Table 6.3 Comparison of the grafting densities obtained on DVB80 microspheres as number of chains per surface area as well as the number of chains per gram of the microspheres. Note that the grafting density reported in chains·nm^{-2} is based on the nominal surface area of a perfectly spherical microsphere

Sample	*LC* (mmol·g^{-1})	*GD* (chains·nm^{-2})	*GD* (chains·g^{-1})
(**6**) [M_n=4200 g·mol^{-1}, PS]	0.2	31.1	$1.2 \cdot 10^{20}$
(**8**) [M_n=6000 g·mol^{-1}, PiBA]	0.047	7.3	$2.82 \cdot 10^{19}$
(**8**) [M_n=26000 g·mol^{-1}, PiBA]	0.023	3.6	$1.38 \cdot 10^{19}$

It is worthwhile to consider which errors could potentially affect the obtained loading capacities, *i.e.* the primary weight percentages of the elemental analysis, particular with regard to sulphur. Could the analysis be affected by incomplete burning of the microspheres? Inspection of the primary data reveals that the mass balances, *i.e.* the weighed in sample vs. the mass of the pyrolysis products, is close to 100% in each case. Thus, the microspheres burn completely and the analysis is reliable. A factor that

cannot be 100% excluded is the potential trapping of polymer chains inside the microsphere during the *grafting-to* process, which even repeated and excessive washing may not be able remove. As the grafted microspheres were washed extensively with chloroform, which is an excellent solvent for both polystyrene as well as poly(isobornyl acrylate), the amount of such trapped chains is bound to be relatively low. Nevertheless, this potential factor needs to be kept in mind.

Before discussing the obtained grafting densities, it is worth noting that in general one would expect the *grafting-from* approach should lead to higher grafting densities compared to *grafting-to* approach. The discrepancy is thought to be caused by the fact that in the *grafting-to* approach, the polymer bearing an appropriate functional group reacts with the groups available on the surface to form covalently attached chains.[253] However, due to the steric hindrance imposed by the already grafted chains, it becomes increasingly difficult for the incoming polymer chains to diffuse to the surface, which intrinsically lowers the grafting densities. In the *grafting-from* approach, the initiators are initially anchored on the surface and are subsequently used to initiate the polymerization of the monomer from the surface. Because the diffusion of the monomer is not strongly hindered by the existing grafted chains, a *grafting-from* approach may in principle lead to higher grafting densities. However, as is demonstrated in the current contribution, *grafting-to* approaches, when coupled with efficient modular chemistry, can in certain circumstances lead to grafting densities exceeding those obtained *via grafting-from* approaches.

The comparison of the direct influence of molecular weight on the grafting densities in the sterically hindered poly(isobornyl acrylate) system was then evaluated. Upon inspection of **Table 6.3** it can be readily noted that when DVB80 microspheres are grafted with poly(isobornyl acrylate) of two molecular weights, the grafting density strongly varies: With 6 000 $g \cdot mol^{-1}$, $2.82 \cdot 10^{19}$ polymeric chains per gram are attached, while the grafting density achieved with 26 000 $g \cdot mol^{-1}$ polymeric chains is $1.38 \cdot 10^{19}$ $chains \cdot g^{-1}$. Thus, when the molecular weight of the grafted chains is reduced by a factor of approximately 4, the grafting density increases by a factor of 2, indicating that grafting density and molecular weight are not scaling by the same factor. Such an observation indicates that a grafted chain covers less surface space/area than would be anticipated

from its molecular weight. While longer chains occupy more space on the surface, the grafting penalty is more severe than the decrease in molecular weight suggests.

In contrast to the poly(isobornyl acrylate) system, significantly higher grafting densities were achieved when polystyrene of approximately similar weight as that employed in the low molecular weight case of PiBA system was attached. It is more challenging to compare the grafting densities which are obtained using the two different approaches described in the present contribution, as differences in the nature of the chemical groups which are used to achieve grafting on the surfaces *via* a *grafting-to* approach may also have influence on the achieved grafting densities. If one takes into consideration the influence of the difference in reactivities and compares the grafting densities achieved one can see that the approach in which cyclopentadienyl functionalized microspheres were used, the obtained *GD* are significantly higher than those achieved in the system where styrene functionalized microspheres are employed. Recall that when Cp functional microspheres are employed, the reaction takes place at ambient temperature within 2 h, while the reaction with the significantly less reactive styryl-diene on the surface of the microspheres requires heating to 60 °C and 12 h reaction time. The grafting density achieved on cyclopentadienyl functionalized microspheres after grafting with polystyrene chains of 4 200 g·mol^{-1} is 31 chains·nm^{-2} or 1.2·10^{20} chains·g^{-1}. It is immediately clear that the change in polymer (steric bulk) and reactivity of the system, has reduced the grafting densities by a factor of close to 4 (going from 1.2·10^{20} to 2.82·10^{19} chains·g^{-1}) at approximately the same molecular weight of the grafted polymer. This significant difference could be due to the fact that the cyclopentadienyl functionalized microspheres represent an extremely reactive surface which will undergo functionalization with polymeric chains faster without the aid of any external catalyst while the reactivity of intrinsically available styrene groups on the surface of microspheres is less compared to the cyclopentadiene moieties. Thus, the substantial difference in grafting densities could possibly be due to the highly disparate rates of the two ligation reactions. In addition to the influence of chemical reactivities of functionalities taken into consideration in the present discussion, the nature of the polymeric chain can also have an influence on the grafting densities achieved. For instance, polystyrene chains can be considered more flexible as

compared to that of poly(isobornyl acrylate) chains due to the bulkiness imposed by the pendant isobornyl groups; thus, steric reasons may also play a significant role in influencing the achieved grafting densities. The immediate question is raised is what the grafting density of such a system would be, where a polystyrene capped with PSDTF RAFT group is reacted with a Cp covered microsphere. While the results of such an experiment would certainly be instructive, it can not be carried out. For this purpose, the polymerization of styrene would have to be mediated with PSDTF to generate a PSDTF capped polystyrene analog to (**7**) and enable its subsequent reaction with the microspheres (**1**). However, PSDTF is such a strong dienophile, that it would immediately react with the monomeric styrene units in solution in a [2+4] cycloaddition, preventing the RAFT process to occur.[26] In addition, it is obvious from the results of the present study, where PSDTF capped PiBA is reacted with (**1**).

It is important to compare the grafting densities achieved in the current study, with those determined by others previously. The first comparison that should be made is with the quantitative *grafting-from* results obtained by Joso *et al*.[175] These authors obtained grafting densities between 1 and 2 chains·nm^{-2} by elemental and change in weight, employing *grafting-from* techniques to tether poly(ethylene oxide) (PEO) onto the surface *via* anionic polymerization. The molecular weight of the grafted PEO was close to 14 000 g·mol^{-1} and thus lies between the molecular weights employed for the PiBA in the current study. A comparison between the data obtained in the current study and the data of Joso *et al*. is feasible, as both grafting densities are based on the nominal surface area of a single microsphere. It is immediately clear that the both RAFT-HDA approaches employed in the current contribution exceed the approach taken by Joso *et al*. in placing polymeric chains onto the surface of the microspheres. It appears that the accessibility of the vinylic double bonds on the microspheres' surface *via* anionic *grafting-from* is not as high as if the same double bonds are accessed *via* direct conjugation. Compared to numbers obtained *via grafting-from* on silicon wafers *via* living radical polymerization techniques (*i.e.* RAFT) of close to 0.7 chains·nm^{-2} [184,185] the numbers obtained in the current study seem to far exceed these values. However, a direct comparison is fraught with danger, as in the present study only nominal surface areas are employed. Thus, it may well be that the grafting densities for both approaches

are comparable in magnitude. A further highly useful comparison comes from microspheres (identical to those employed in the current study) that were also modified *via* a *grafting-to* approach, yet with a different polymer. Irgum and colleagues[254] provide loading capacities of microspheres grafted with sulfur containing telomers *via* a ring opening reaction on the surface of the microspheres. The resulting core-shell microspheres were analyzed by these authors *via* elemental analysis using sulfur as a chemical sensor to determine the grafting densities. They find a loading capacity of 0.2 $mmol \cdot g^{-1}$ (derived from a sulfur weight content of 0.6 wt.-% caused by the presence of one sulfur atom per grafted chain, quoting an error of ±0.03 wt.-%). It is pleasing to note that our values are in good agreement with those of Irgum and colleagues.

6.4 Conclusions

The grafting of polymer chains to DVB80 microspheres *via* RAFT-HDA chemistry is carried out under mild, catalyst-free and ambient temperature reaction conditions for surfaces functionalized with highly reactive cyclopentadiene moieties and at 60 °C for microspheres carrying a less reactive diene, *i.e.* styrene. The characterization of the microspheres at various stages of modification *via* ATR-IR spectroscopy, confocal microscopy and elemental analysis techniques confirms the successful grafting of RAFT functionalized polymers to the surface of microspheres. The elemental analysis provides access to the quantification of the grafting densities – expressed both in chains per nominal nm^2 as well as chain per gram of microspheres – achieved using the RAFT-HDA *grafting-to* approach. Variable grafting densities were obtained using different approaches for the functionalization of microspheres and using different molecular weight of grafted polymer chains. The DVB80 microspheres functionalized with the highly reactive cyclopentadiene moiety and further grafted with polystyrene chains of molecular weight of 4 200 $g \cdot mol^{-1}$ features the highest grafting density of $1.2 \cdot 10^{20}$ $chains \cdot g^{-1}$ corresponding to approximately 16.7% of chains in the experiment that have been grafted to the surface. The grafting densities achieved employing a second approach in which intrinsically available styrene groups on the surface of the microsphere were used for functionalization with poly(isobornyl acrylate) chains of different molecular weight *i.e.* 6 000 $g \cdot mol^{-1}$ and 26 000 $g \cdot mol^{-1}$, displays a dependence

of the grafting density on the molecular weight of polymeric chains to be grafted. The grafting densities achieved in this case were $2.82 \cdot 10^{19}$ chains·g^{-1} for 6 000 g·mol^{-1} and $1.38 \cdot 10^{19}$ chains·g^{-1} for 26 000 g·mol^{-1}, corresponding to a total of 12.0 and 6.7% of grafted chains, respectively. The current study has demonstrated that the grafting densities available on the surface of microspheres by *grafting-to* approaches are significant and are comparable in magnitude – and even exceed – those obtainable *via grafting-from* approaches. The design of functional microspheres for applications ranging from chromatographic packing materials to diagnostic kit applications should thus – also based on the catalyst free nature of our in-here proposed ligation chemistry – preferably proceed *via* the presented modular approach.

6.5 Supporting Information

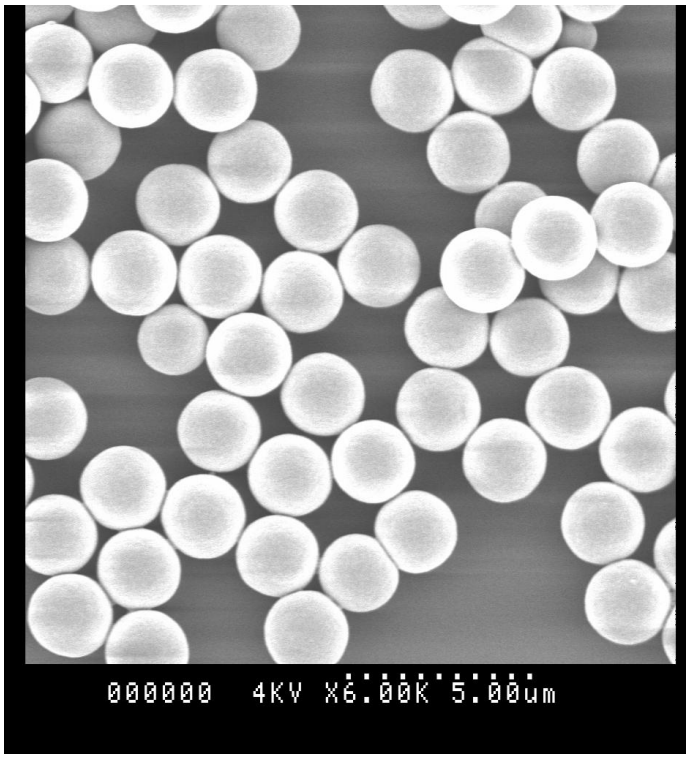

Figure S.6.1 Typical scanning electron micrograph of poly(divinylbenzene 80) microspheres synthesized *via* distillation precipitation polymerization

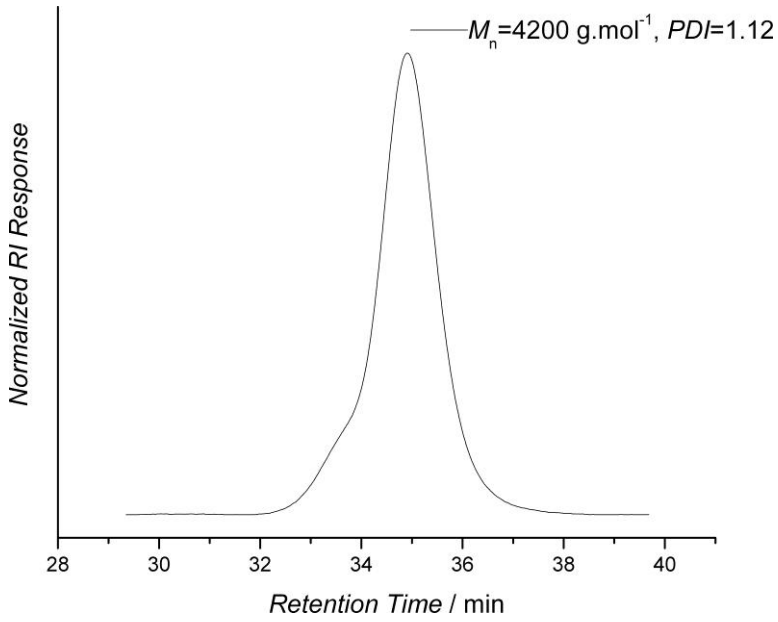

Figure S.6.2 Molecular weight distribution of polystyrene (**5**) synthesized *via* RAFT polymerization using benzyl (diethoxyphosphoryl)dithioformate as RAFT agent (0.162 mmol) and AIBN (0.0043 g, 0.027 mmol) at 60 °C for 6 h

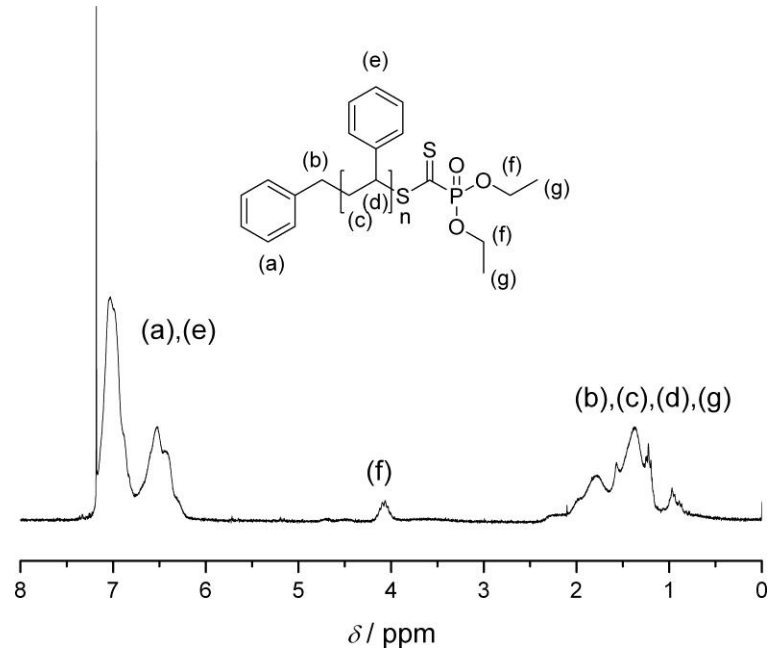

Figure S.6.3 ^{1}H-NMR spectrum of polystyrene (**5**) synthesized *via* RAFT polymerization using benzyl (diethoxyphosphoryl)dithioformate as RAFT agent (0.162 mmol) and AIBN (0.0043 g, 0.027 mmol) at 60 °C for 6 h

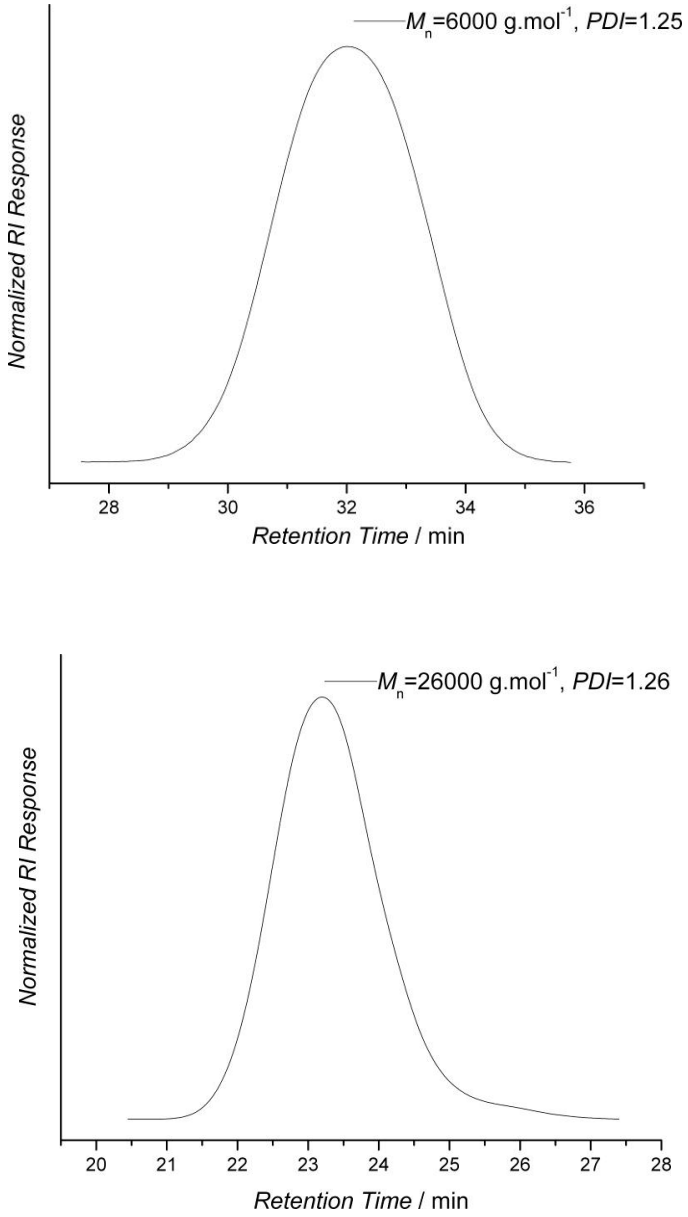

Figure S.6.4 Molecular weight distributions of poly(isobornyl acrylate) (**7**) synthesized *via* RAFT polymerization utilizing benzyl phenylsulfonyldithioformate (PSDTF) (0.0771 g, 0.15 mmol) as RAFT agent and AIBN (0.0082 g, 0.05 mmol) at 60 °C for 15 and 24 h, respectively

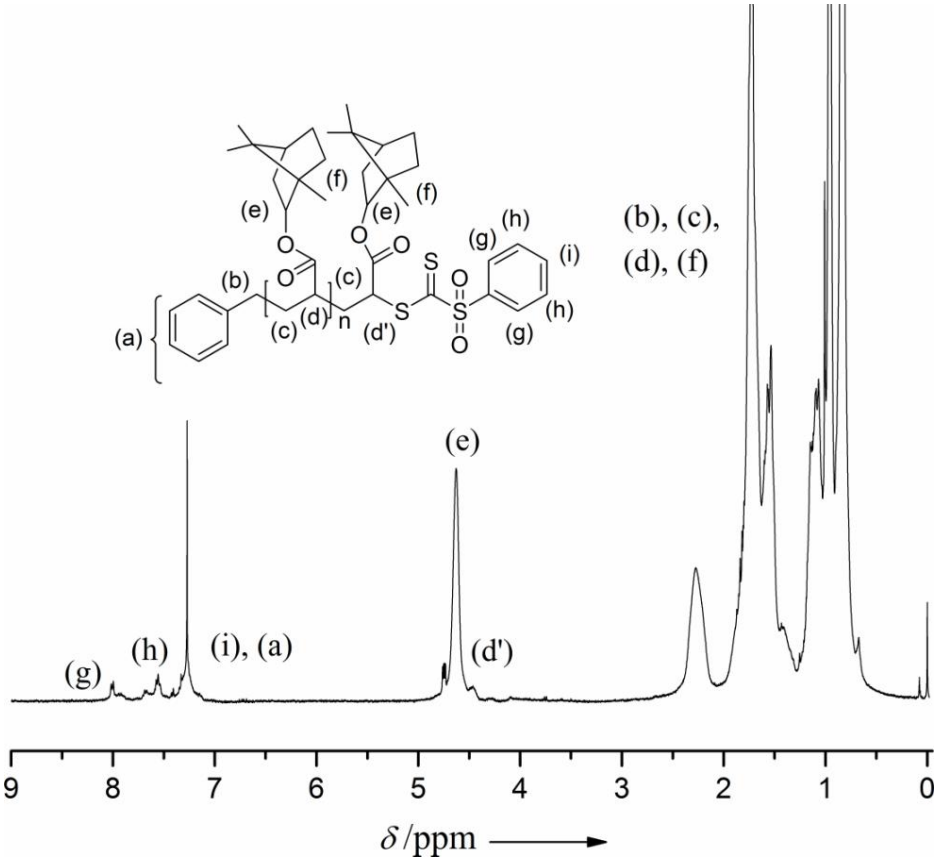

Figure S.6.5 ^{1}H-NMR spectrum of poly(isobornyl acrylate) (**7**) synthesized *via* RAFT polymerization using benzyl phenylsulfonyldithioformate (PSDTF) (0.0771 g, 0.15 mmol) as RAFT agent and AIBN (0.0082 g, 0.05 mmol) at 60 °C for 24 h

Chapter 7 Efficient and Mild Modification of Si Surfaces *via* Orthogonal Hetero Diels-Alder Reaction

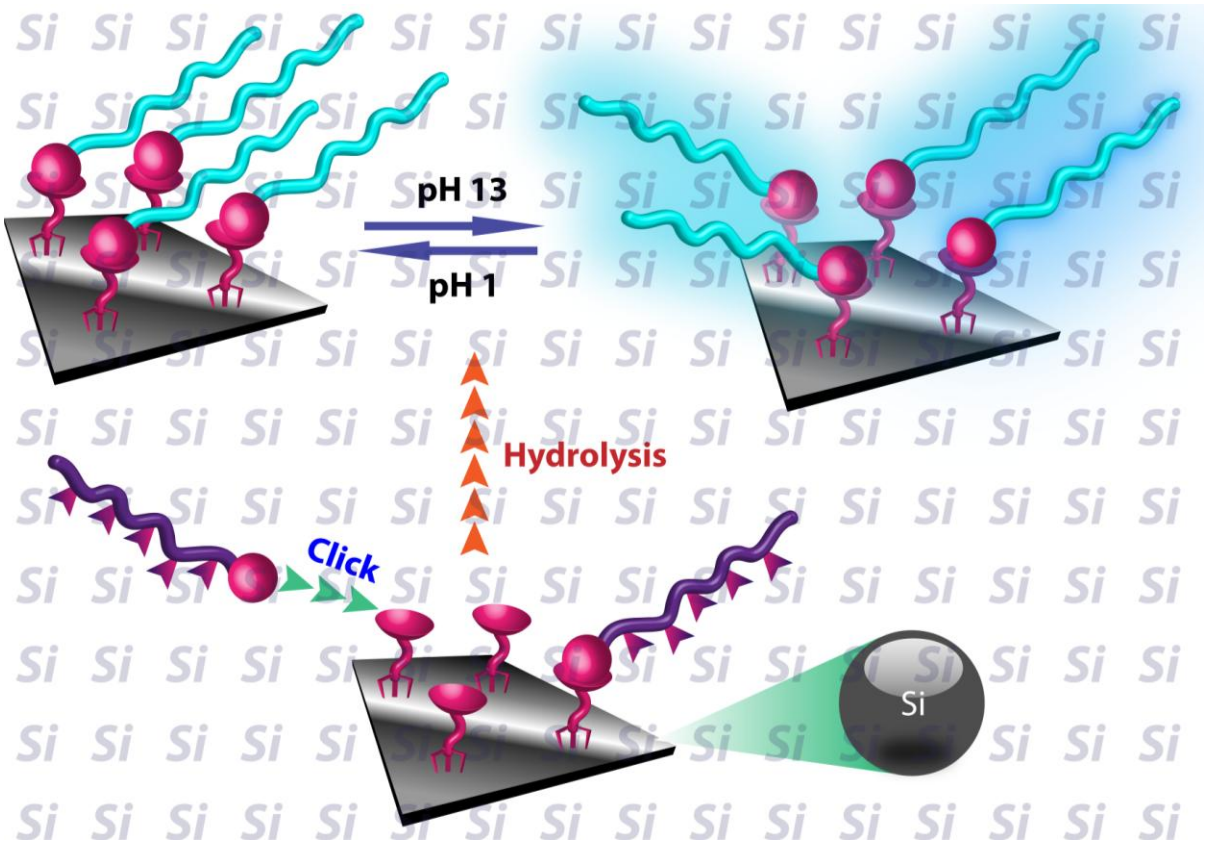

7.1 Introduction

In the present chapter, a facile chemical strategy to modify Si surfaces *via* orthogonal hetero Diels-Alder conjugation (shown in **Scheme 7.1**) is discussed. In **Chapter 5** and **6**, RAFT-HDA chemistry was utilized to modify divinylbenzene microspheres. To illustrate the feasibility of the present approach towards planar surfaces, a silicon wafer was modified with a stimuli responsive polymer. Stimuli responsive surfaces have long been a focus of contemporary material science[255] and it thus seems apt to demonstrate the applicability of RAFT-HDA chemistry in this area.[256-258] Conjugation of polymers onto a solid substrate is an effective method for modifying its surface properties. Considerable attention has been paid to the manipulation and control of the physiochemical properties of silicon surfaces by immobilizing dense polymer brushes because of their potential importance to the modern microelectronics industry as well as in sensors and photovoltaics applications.[259] The present approach is based on the use of dithioesters that display an extremely high HDA activity. The RAFT agent employed herein, phenylsulfonyl dithioformate (PSDTF) (discussed in detail in **Chapter 4**) is one in which the dithioester is made highly electron deficient *via* attaching a strongly electron withdrawing sulfonyl substituent as the Z group. The electron deficiency of the C=S bond facilitates the HDA cycloaddition with less reactive dienes, *i.e.* PSDTF based HDA conjugations can be performed under milder conditions, in shorter reaction times and without the use of catalysts than other RAFT agents.

7.2 Experimental

7.2.1 Pre-treatment of Si Wafers

The Si wafers were cleaned successively three times by ultrasonification for 10 min in chloroform, acetone and ethanol and dried in a stream of argon in between. This was followed by treatment with piranha solution (3:1 mixture of sulfuric acid and 30% hydrogen peroxide) for 30 min at 90 °C. Finally, the wafers were washed several times with water and dried in a stream of argon.

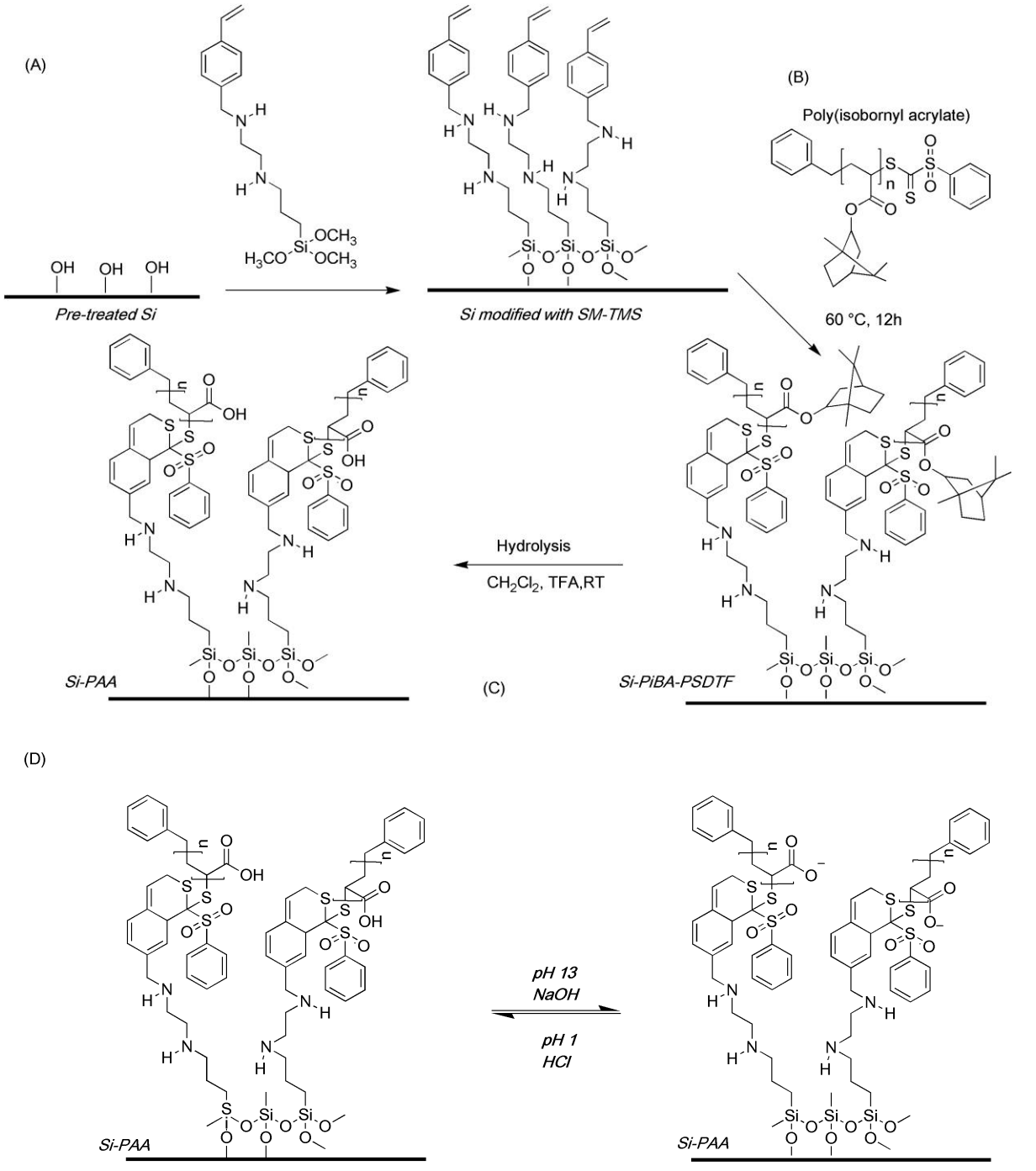

Scheme 7.1 (A) Generation of a modified Si surface (Si-SM-TMS) from a pre-treated Si wafer, (B) Conjugation of poly(isobornyl acrylate) (PiBA-PSDTF) to the Si-SM-TMS surface serving as diene in the RAFT-HDA approach, (C) Hydrolysis of PiBA grafted Si surfaces (Si-PiBA-PSDTF) to Si-poly(acrylic acid) (Si-PAA-PSDTF), (D) Stimuli responsive behaviour of Si-PAA under variable pH.

7.2.2 Silanization of Pre-treated Si Wafers

The silanization of the Si wafers was performed using 2% v/v anhydrous acetone solution of 3-(*N*-Styryl methyl-2-aminoethylamino)-propyl trimethoxy silane (SM-TMS) to generate Si wafers modified with SM-TMS. The Si wafers were immersed in the silane solution for 3 min with water and acetone washing in between. The wafers were then finally dried in a stream of argon.

7.2.3 RAFT Polymerization of Isobornyl Acrylate

A solution of isobornyl acrylate (9.071 g, 43.55 mmol), benzyl phenylsulfonyldithioformate (PSDTF) (0.0771 g, 0.15 mmol) and AIBN (0.0082 g, 0.05 mmol) was prepared and placed in a 25 mL round bottomed flask. The reaction mixture was subsequently purged with nitrogen for 15 minutes to remove residual oxygen. The polymerization was performed at 60 °C for 24 h. The reaction was stopped by exposing the reactants to oxygen and chilling in an ice bath. The polymers were isolated by two-fold precipitation in cold methanol (3.75 g, 41% yield). The molecular weight distribution and ^{1}H-NMR spectrum of poly(isobornyl acrylate) is shown in **Figure S.7.1** and **S.7.2**, respectively.

7.2.4 Conjugation of Poly(isobornyl acrylate) to SM-TMS Modified Si Wafers

Si wafers modified with SM-TMS were suspended in a solution of poly(isobornyl acrylate) (300 mg) in chloroform (1 mL) in a pressure tube at 60 °C for 12 h. After the completion of the reaction, the Si wafer was extensively washed with chloroform several times so as to remove any excess of polymer not conjugated onto the Si surface. Finally, the Si wafer was dried in a stream of argon.

7.2.5 Hydrolysis of Poly(isobornyl acrylate) Conjugated to Si Wafer to Poly(acrylic acid)

Si wafers conjugated poly(isobornyl acrylate) were suspended in dichloromethane (3.5 mL) and 0.855 g of trifluoroacetic acid was added to the suspension. The resulting mixture was stirred overnight at ambient temperature. After the completion of the reaction, the Si wafer was extensively washed with dichloromethane and subsequently dried in a stream of argon.

7.3 Results and Discussion

The modification of Si wafers[260] was achieved by the silanization of pre-treated Si surfaces using 3-(*N*-Strylmethyl-2-aminoethylamino)-propyl trimethoxy silane (SM-TMS) (**Scheme 7.1**(A)). By the use of this silanizing agent it is possible to generate styrene functionalized Si surfaces. As the reactivity of the C=S moiety in PSDTF is high, styrene functions as a diene in Diels-Alder chemistry. The dienophile for the conjugation to the styrene functionalized Si surface is PiBA carrying PSDTF end groups. The RAFT-HDA reaction between the PSDTF functionalized PiBA and the styryl functionalized Si surface proceeds in the absence of catalysts at 60 °C (**Scheme 7.1**(B)). A detailed performance evaluation of PSDTF as a conjugation agent is provided in ref.[26] The coupling reaction between Si surfaces modified with a styrene linker and PiBA-PSDTF was performed at 60 °C in chloroform solution within 12 h. The conjugation leads to the formation of a 3,6-dihydro-2*H*-thiopyran ring, the stability of which has been investigated and found to be withstanding relatively harsh conditions of pH (between 0 and 14 at ambient temperature) and heat (up to 120 °C).[249]

The conjugation of polymer chains to the Si surface is achieved *via* a *grafting-to* approach. Generally, a *grafting-to* approach will somewhat limit the achievable grafting densities as compared to those achieved *via* a *grafting-from* approach (as discussed in detail in **Chapter 2**). However, the *grafting-to* approach offers the advantage of using well-defined pre-made polymer strands compared to an immersion polymerization process.[261] *Grafting-to* thus allows for a covalent dip-coat type procedure. The successful conjugation of the PiBA onto the silicon surface can be evidenced *via* ATR-IR spectroscopy. No characteristic absorption (**Figure 7.1**) is observed for pre-treated Si wafers as well as Si wafers modified with SM-TMS, while the Si wafers conjugated with PiBA clearly shows the characteristic absorptions of the polymer. The absorption at 1732 cm^{-1} is due to the carbonyl (C=O) stretching vibration, while the absorptions at 2858 and 2926 cm^{-1} are associated with C-H stretching vibrations. As a control, pre-treated Si wafers (which were not modified with SM-TMS) were subjected to identical reaction conditions. In this case no characteristic absorption corresponding to the polymer can be observed. Thus, PiBA can be conjugated onto Si surfaces modified with a styrene linker molecule.

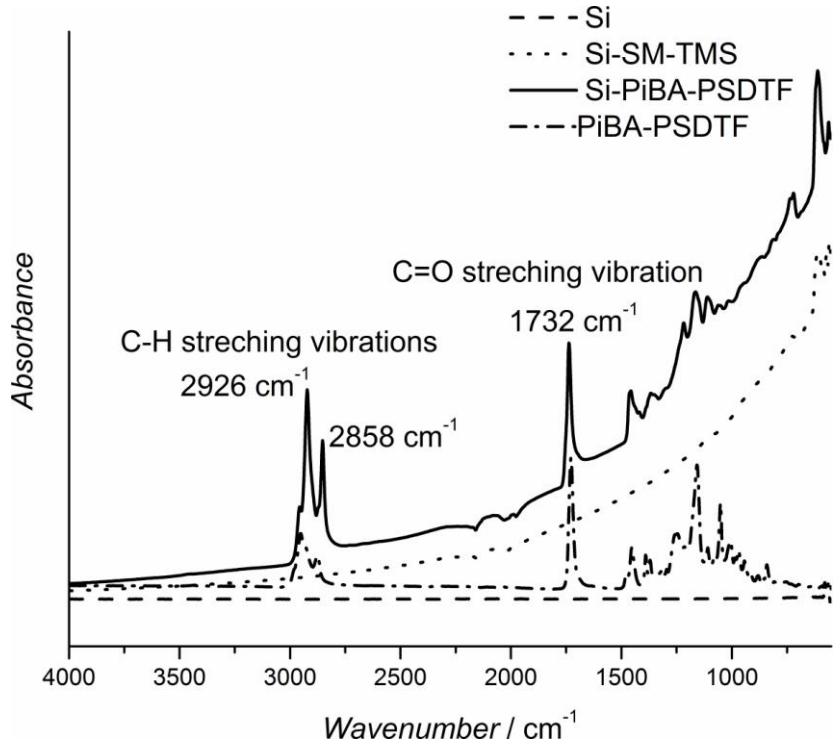

Figure 7.1 ATR-IR spectra of pre-treated Si surface, Si surface modified with styrene (Si-SM-TMS), Si surface conjugated with poly(isobornyl acrylate) (Si-PiBA-PSDTF) and the initial poly(isobornyl acrylate) (PiBA-PSDTF)

In addition, the homogeneity of the PiBA grafting was probed *via* IR microscopy. The absorption intensity of the Si wafer modified with PiBA was measured at a particular wavelength, in this case at 1732 cm^{-1}, corresponding to the C=O stretching vibration associated with the ester side chain of the PiBA. The intensity of absorption at this wavenumber is obtained *via* scanning the Si surfaces in a 32 by 32 micron area, resolved into 4096 individual FT-IR spectra. As inspection of **Figure 7.2** demonstrates, the surface of the Si wafer grafted with PiBA displays a rather uniform grafting within the studied area. The functionalization density varies by approximately 20%.

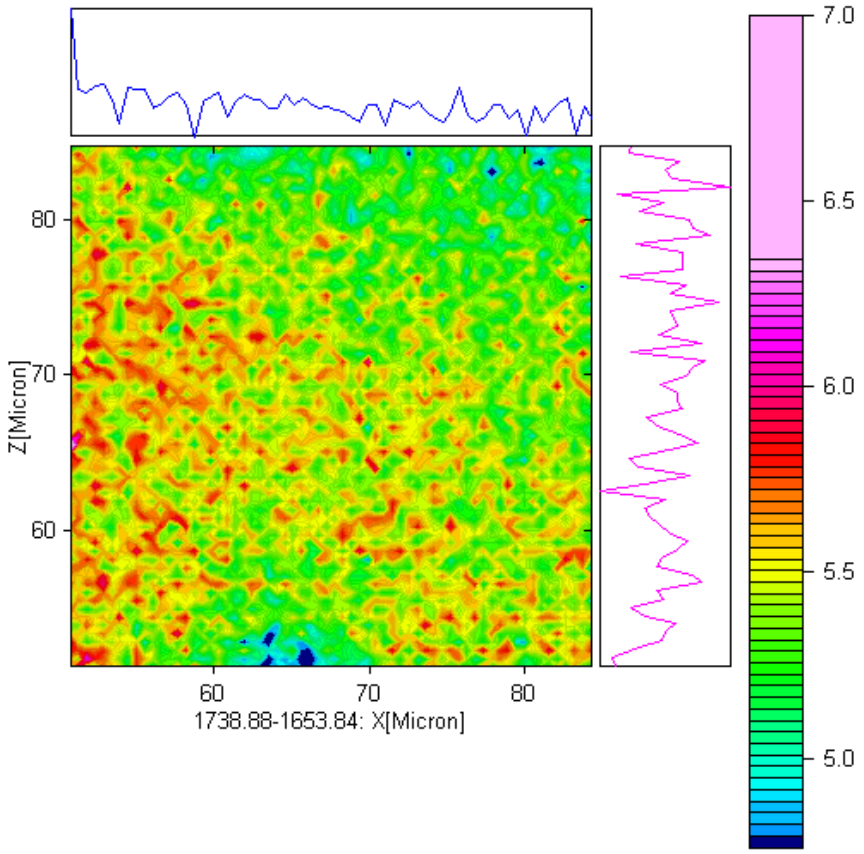

Figure 7.2 IR microscope image of Si wafer conjugated with poly(isobornyl acrylate) probed in a 32 by 32 µm area at the wavelength of 1732 cm^{-1}

The changes in topography of the Si surface after modification with SM-TMS and further conjugation with PiBA were investigated *via* Atomic Force Microscopy (AFM). **Figure 7.3** shows AFM images of the (a) pre-treated Si wafer, (b) the Si wafer modified with SM-TMS, and (c) the Si wafer conjugated PiBA-PSDTF. The pre-treated Si surface is rather smooth, with a root-mean-square surface (RMS) roughness close to 0.139 nm. After the modification of the pre-treated Si surface with SM-TMS, the RMS value increases to approximately 0.584 nm. The increased surface roughness of the Si wafers modified with SM-TMS provides evidence that the method which has been selected for the silanization of the pre-treated Si wafer does not produces a monolayer assembly of SM-TMS on the Si surface; rather, a multilayer of SM-TMS is obtained on the surface. The $-OCH_3$ groups interact with OH groups on the oxidized surface, forming Si-O-

bonds on the surface. In addition, Si-O-Si bonds are formed between adjacent head groups, creating a cross-linked network.[262] In addition to AFM, the Si wafers were characterized by ellipsometry. After the modification of the Si wafers with a styrene layer (SM-TMS) the thickness of the Si wafer increased by 1.1 nm. The increased surface thickness of the Si wafer modified with SM-TMS can be explained by the same cross-linked network formation which is discussed above as an explanation for the increased roughness obtained by AFM measurements. After the conjugation of the polymer onto the SM-TMS modified Si surfaces, the roughness of the surface again increases (RMS 1.35 nm) indicating, conjugation of PiBA onto the surface.

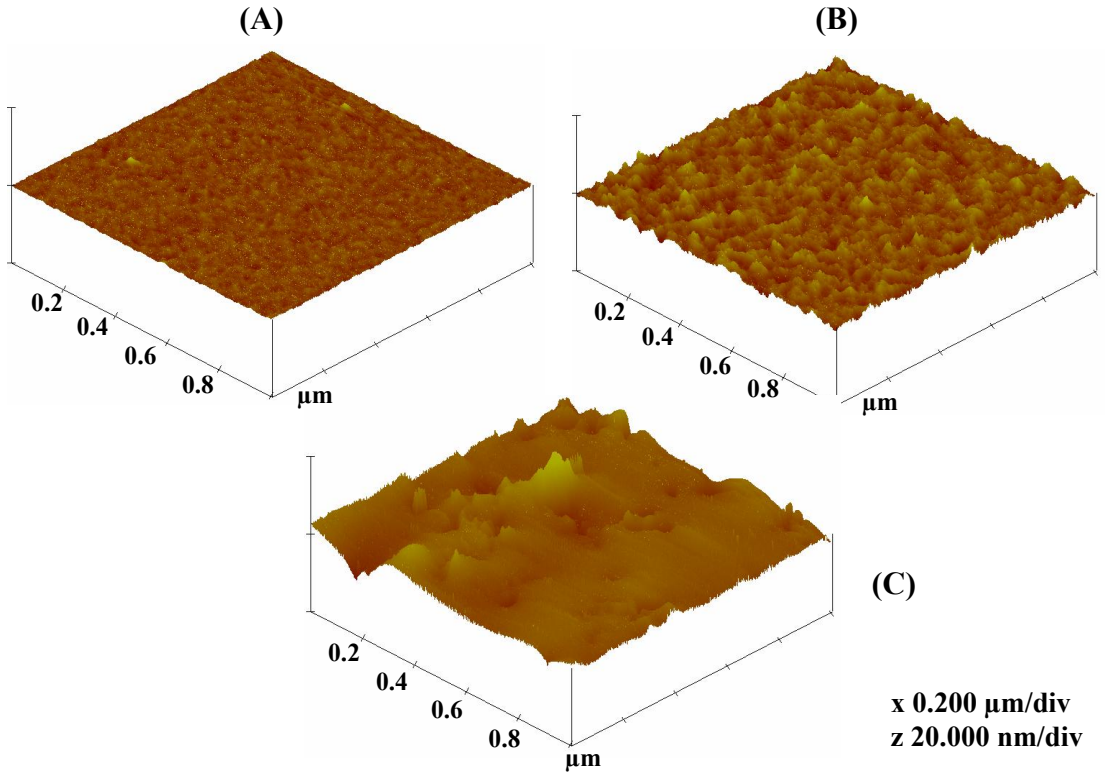

Figure 7.3 AFM images of (A) the pre-treated Si surface, (B) Si surface modified with styrene (Si-SM-TMS) (C) Si surface conjugated to poly(isobornyl acrylate) (Si-PiBA-PSDTF). The corresponding 2D phase and height images can be found in the supplementary information section (**Figure S.7.3**)

After the conjugation of PiBA onto the surface, the PiBA was hydrolyzed to poly(acrylic acid) (PAA). The hydrolysis was carried out in dichloromethane in the presence of trifluoroacetic acid (TFA). Evidence for the successful hydrolysis is provided by ATR-IR and contact angle (CA) measurements. The ATR-IR spectra of PiBA conjugated to the Si surface before and after hydrolysis are depicted in **Figure 7.3**. Before hydrolysis the C=O absorption is at 1732 cm^{-1} while after hydrolysis the C=O shifts to lower wavenumber that is 1701 cm^{-1}.[263]

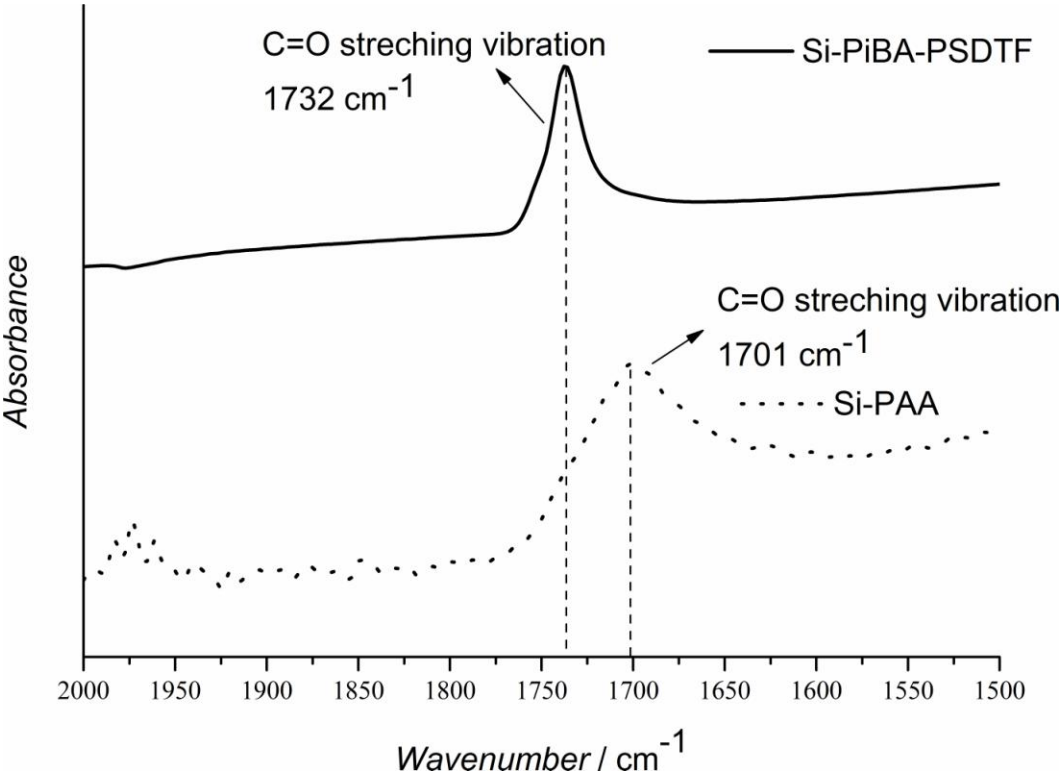

Figure 7.4 Comparison of ATR-IR spectra of Si surfaces conjugated with PiBA before and after hydrolysis to PAA

The surface modification was also confirmed by measuring the thickness – *via* ellipsometry – of the Si wafers after hydrolysis. The thickness of the Si wafers modified with the SM-TMS layer was 1.1 nm while the thickness of Si wafer conjugated to PiBA after hydrolysis is – at the maximum – 13 nm. It should be noted that the thickness increase of the layer was measured at multiple points on the surface, with values obtained between 8 and 13 nm at different points. The increased thickness of the Si

wafer after hydrolysis provides further proof that the polymer conjugation has occurred in an efficient fashion.

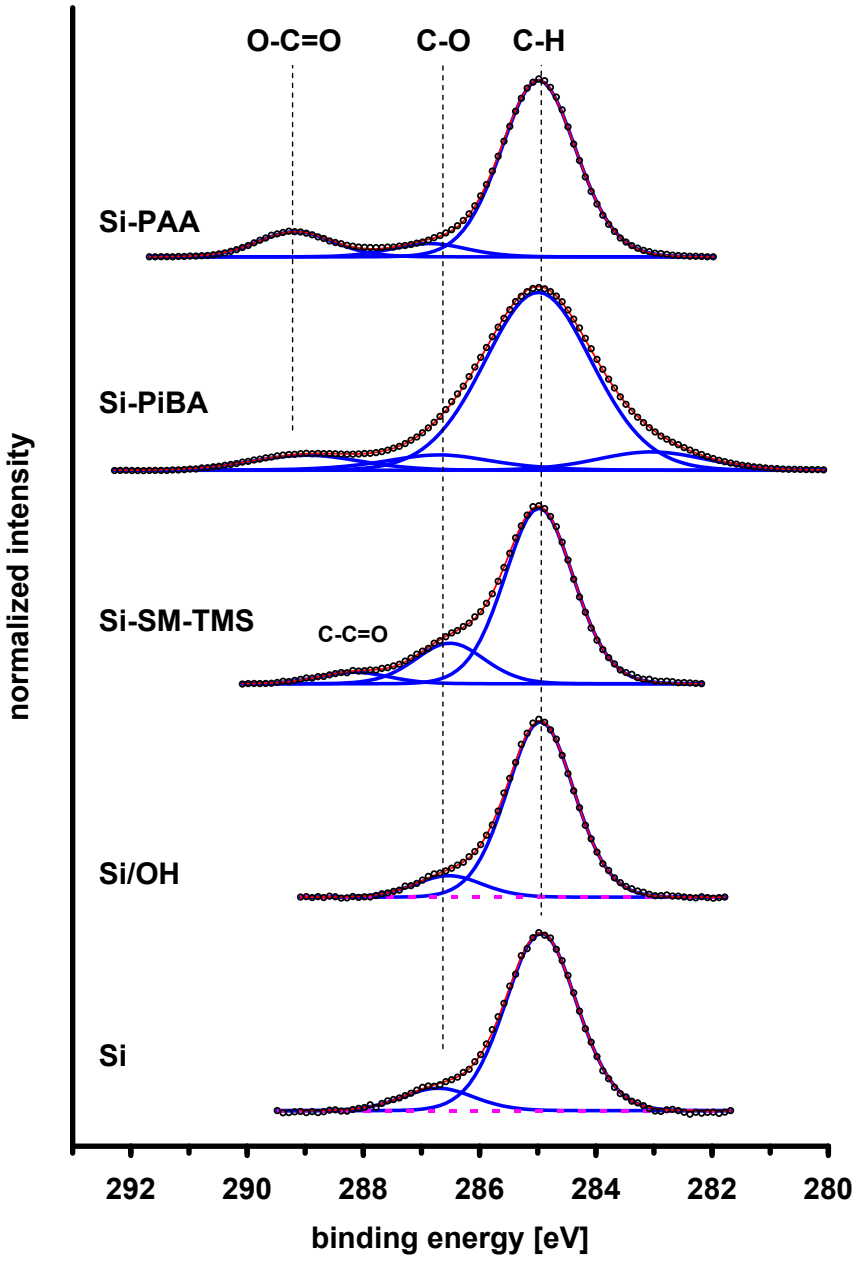

Figure 7.5 C 1s XPS spectra of the Si wafer, the pre-treated Si wafer (Si-OH), the Si wafer modified with styrene (Si-SM-TMS), the Si wafer modified with poly(isobornyl acrylate) (Si-PiBA-PSDTF), the Si wafer modified with poly(acrylic acid) (Si-PAA-PSDTF). All spectra are normalized to maximum intensity

Spectroscopic evidence for the presence of acrylate and acrylic acid on Si wafer was additionally obtained by XPS of the Si wafer, the pre-treated Si wafer, the Si wafer modified with the styrene layer (Si-SM-TMS), the Si wafer modified with poly(isobornyl acrylate) (Si-PiBA-PSDTF) as well as after the hydrolysis of poly(isobornyl acrylate) to poly(acrylic acid) (Si-PAA-PSDTF). As shown in **Figure 7.5**, the O-C=O group on the Si wafer modified with poly(isobornyl acrylate) (Si-PiBA-PSDTF) and the Si wafer modified with poly(acrylic acid) (Si-PAA-PSDTF) is validated by the C 1s component at 289.0 eV after referencing the spectrum to the main carbon component C 1s at 285.0 eV and the corresponding O 1s component at 534.0 eV.[264,265] Moreover, in the case of the Si-PAA-PSDTF sample the weak S 2p peaks at 163.9 eV and 167.7 eV prove the presence of the –C-S-C- and $–SO_2-$ groups.[266] In the Si-SM-TMS and Si-PAA-PSDTF samples the N 1s at 400.8 eV can be attributed to –NH[267] functionalities present in the monolayer. In the Si-PiBA-PSDTF sample N and S cannot be found due to the detection limits inherent to XPS.

The surface modification was further confirmed *via* contact angle measurements (CA) (**Figure 7.6**). The CA of the pre-treated Si wafer is very low as the surface is hydrophilic due the presence of -OH groups. The CA after the modification with SM-TMS increases from 10° to 74° as the hydrophobicity of the surface is enhanced after silanization. No significant change in the wetting behaviour of the surface after conjugation with PiBA can be observed. However, after the hydrolysis of PiBA to PAA, the CA changes from 74° to 49°. This decrease in contact angle provides further confirmation for the change in the chemical functionality present on Si surface.

To provide evidence of our synthetic aim of establishing a facile RAFT-based conjugation approach, the responsive behaviour of PAA grafted Si surfaces obtained after hydrolysis of PiBA was investigated. After immersion of the wafer in solutions of variable pH, the wafers were rapidly dried under argon and CA measurements were carried out immediately. The measurement of the contact angle after the hydrolysis of the PiBA to PAA provides a clear result. The Si wafers become pH responsive. The CA of the Si wafer grafted with PAA when switching repeatedly from a protonated to a non-protonated state is shown in **Figure 7.6**.

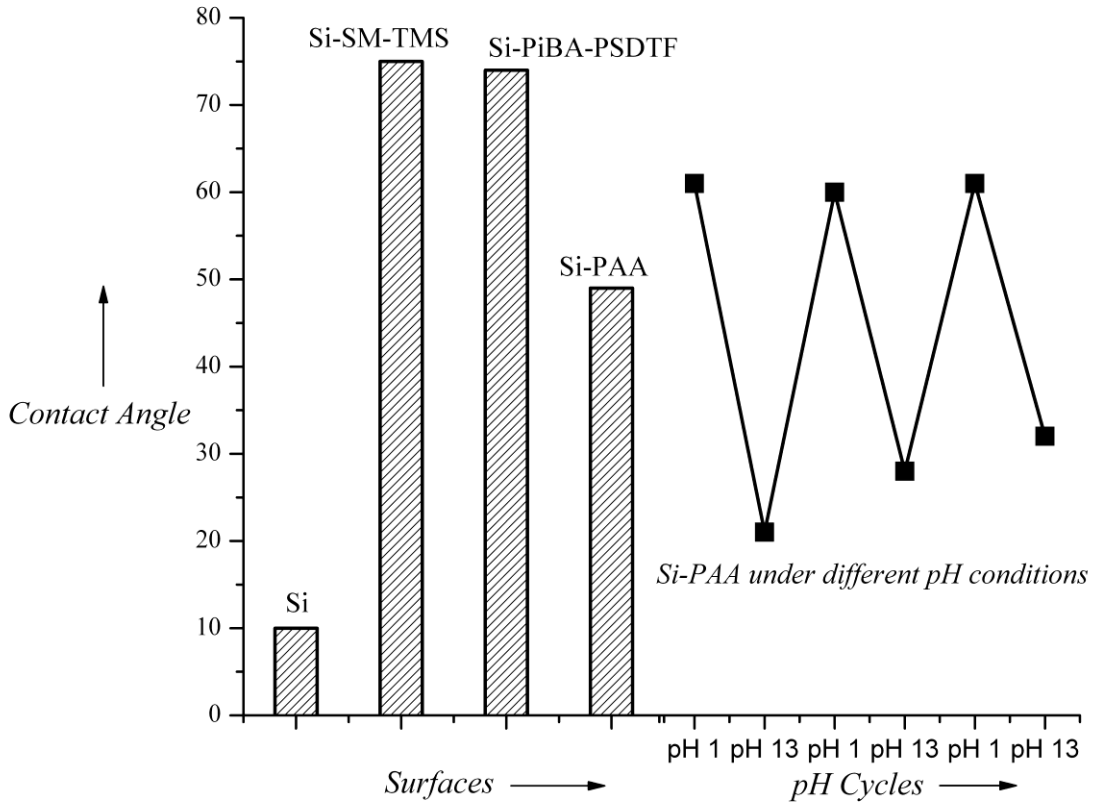

Figure 7.6 Contact angle measurement with different surfaces and reversible pH-responsive behaviour under acidic (pH 1) and basic (pH 13) conditions for Si surfaces conjugated to PAA

The lowest water CA was obtained after treatment with basic solution (pH 13). This can be explained by surface –COOH groups being converted to $–COO^-$, or even hydrated ions. The electrostatic repulsion overcomes the hydrophobic interactions between the alkyl chains. As result, the PAA chains are uncoiled and in turn making the surface very hydrophilic. When exposed to acidic solution (pH 1), the water CA switches to higher values. In this case, the hydrophobic interactions among alkyl chains become the predominant factor, causing the chains to collapse. As shown in **Figure 7.6**, the surface wettability can be reversibly switched between a relatively hydrophobic state and a relatively hydrophilic one.

7.4 Conclusions

The chemical approach for achieving *grafting-to* conjugation discussed in the current chapter cannot only be employed in scenarios where the sulfonyldithioformate is employed to mediate a RAFT polymerization – which is preferentially possible for monomers exhibiting a significant degree of steric bulk[26] – but may also be employed in cases where sulfonyldithioformate moieties are attached to a surface or the end of a polymer chain to achieve rapid grafting with suitable dienes. The present example features a relatively low reactivity diene (*i.e.* styrene) and with higher reactivity dienes tethered to a surface (such as cyclopentadiene) reaction times of a few minutes at ambient temperature should be feasible (as discussed in **Chapter 6**).

7.5 Supporting Information

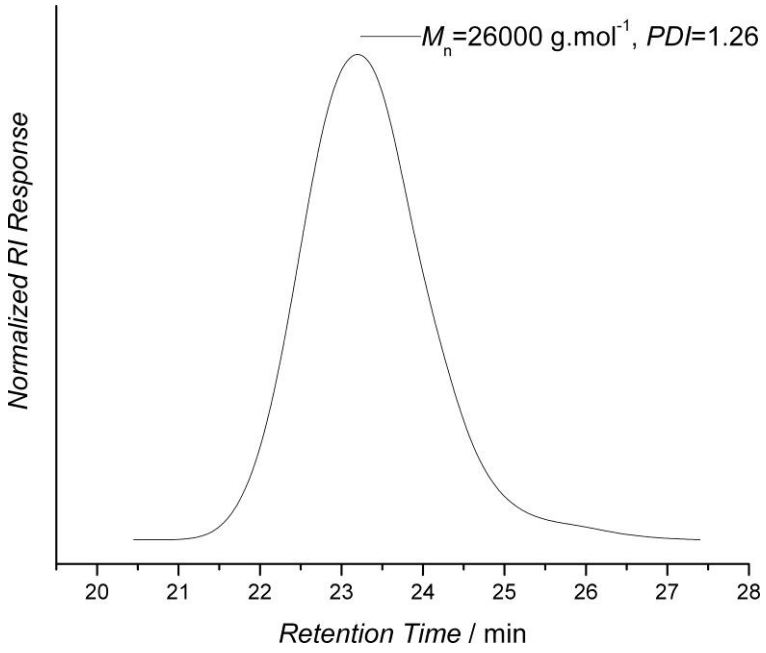

Figure S.7.1 Molecular weight distributions of poly(isobornyl acrylate) (**7**) synthesized *via* RAFT polymerization utilizing benzyl phenylsulfonyldithioformate (PSDTF) (0.0771 g, 0.15 mmol) as RAFT agent and AIBN (0.0082 g, 0.05 mmol) at 60 °C for 24 h

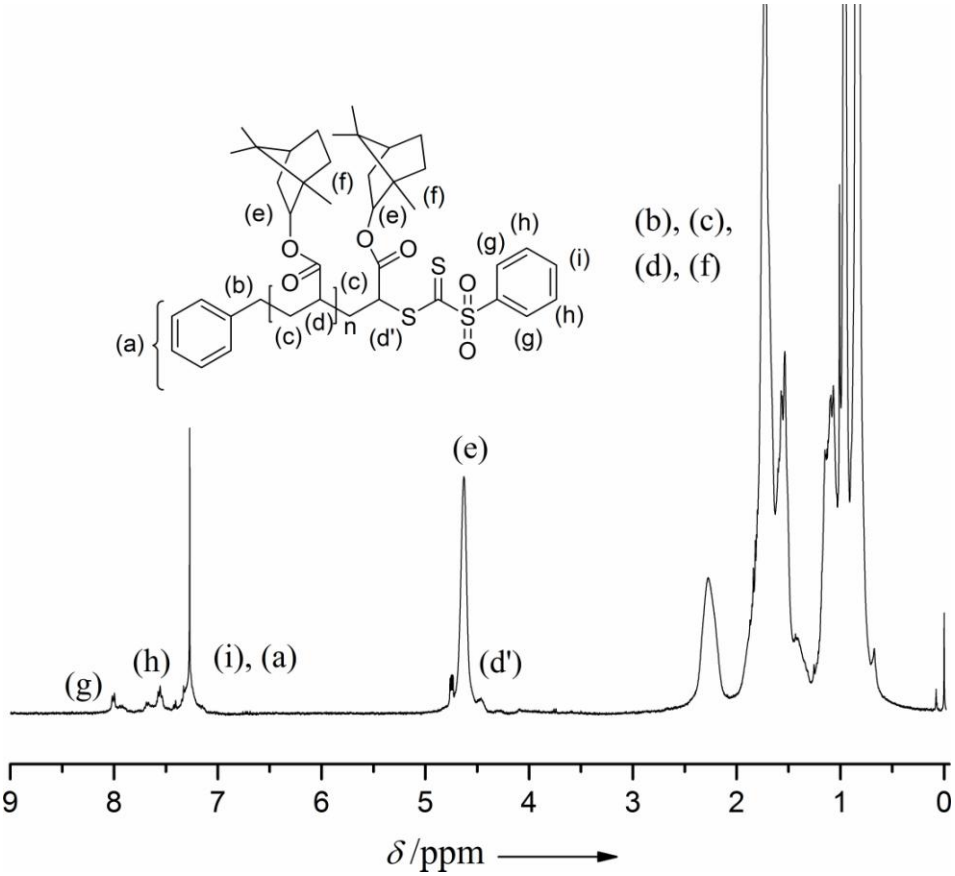

Figure S.7.2 ^{1}H-NMR spectrum of poly(isobornyl acrylate) (**7**) synthesized *via* RAFT polymerization using benzyl phenylsulfonyldithioformate (PSDTF) (0.0771 g, 0.15 mmol) as RAFT agent and AIBN (0.0082 g, 0.05 mmol) at 60 °C

(A1)

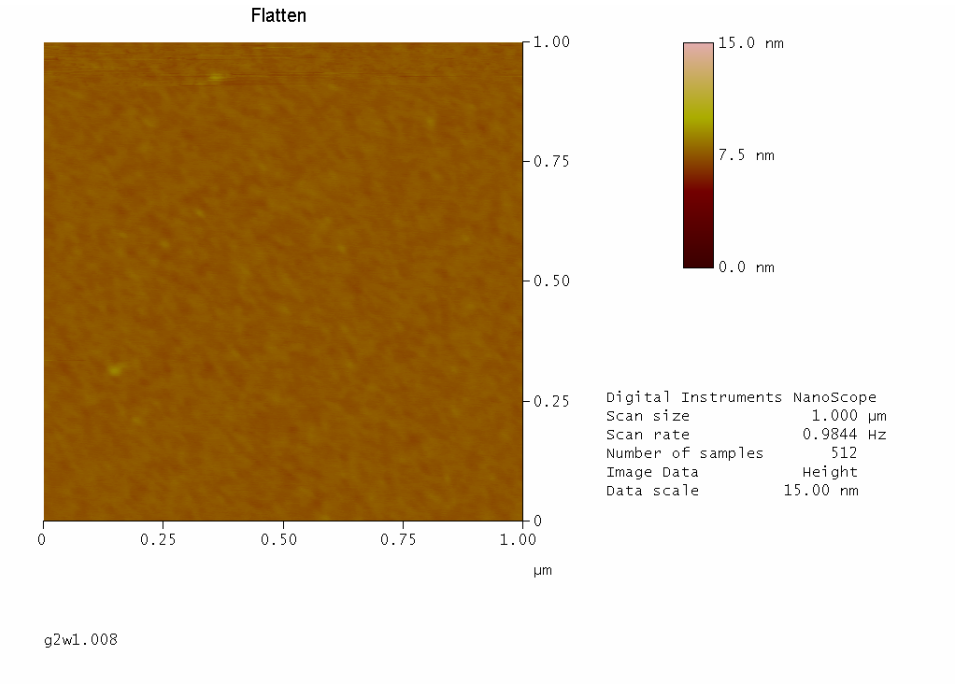
Flatten
1.00
0.75
0.50
0.25
0
0
0.25
0.50
0.75
1.00
µm
15.0 nm
7.5 nm
0.0 nm
Digital Instruments NanoScope
Scan size 1.000 µm
Scan rate 0.9844 Hz
Number of samples 512
Image Data Height
Data scale 15.00 nm
g2w1.008

(A2)

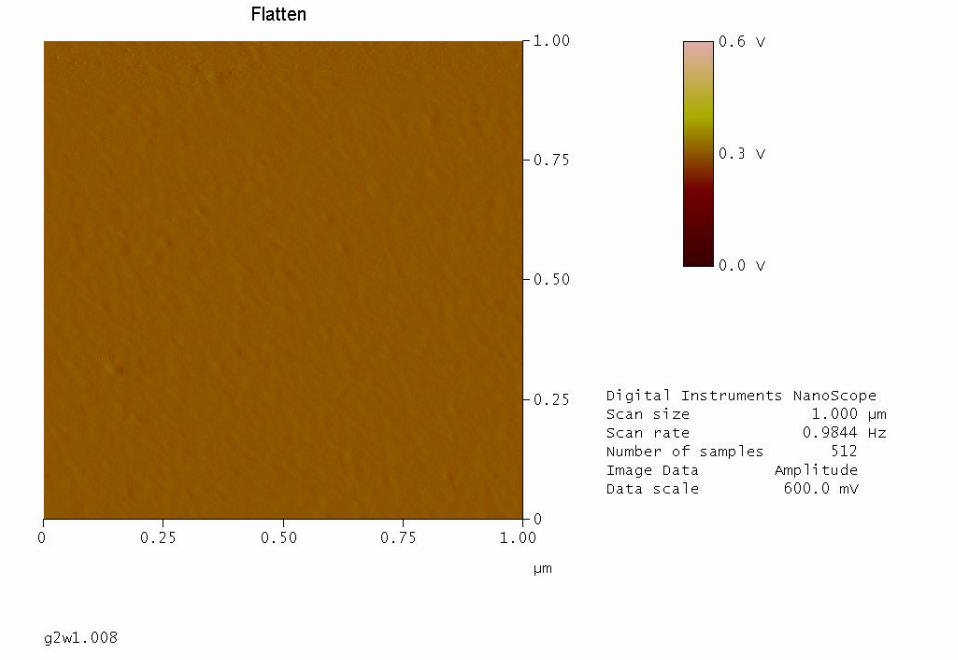
Flatten
1.00
0.75
0.50
0.25
0
0
0.25
0.50
0.75
1.00
µm
0.6 V
0.3 V
0.0 V
Digital Instruments NanoScope
Scan size 1.000 µm
Scan rate 0.9844 Hz
Number of samples 512
Image Data Amplitude
Data scale 600.0 mV
g2w1.008

(B1)

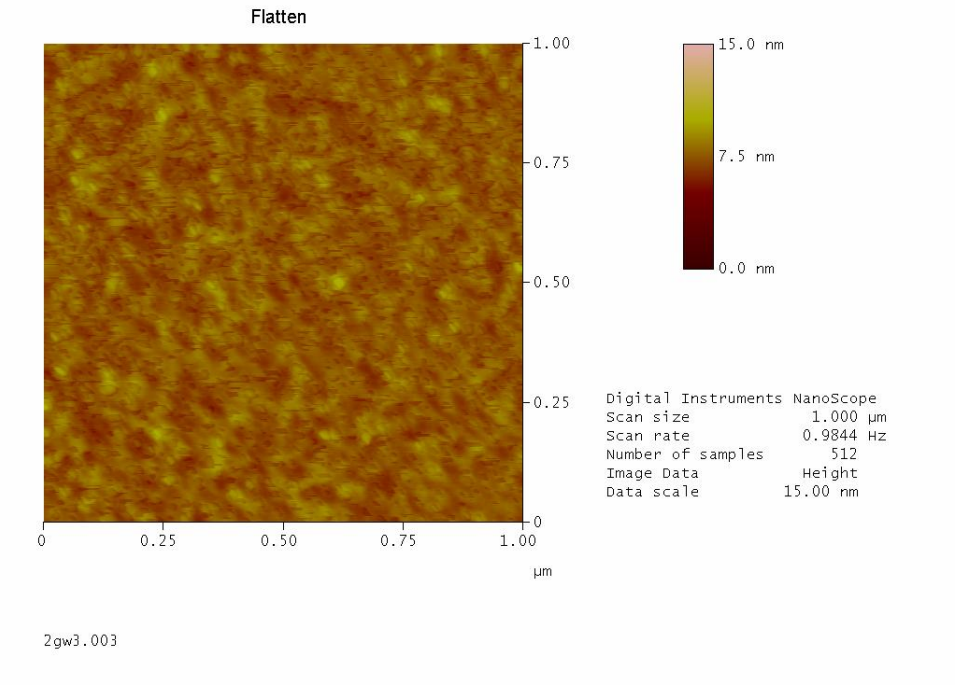
Flatten
1.00
0.75
0.50
0.25
0
0
0.25
0.50
0.75
1.00
µm
15.0 nm
7.5 nm
0.0 nm
Digital Instruments NanoScope
Scan size 1.000 µm
Scan rate 0.9844 Hz
Number of samples 512
Image Data Height
Data scale 15.00 nm
2gw3.003

(B2)

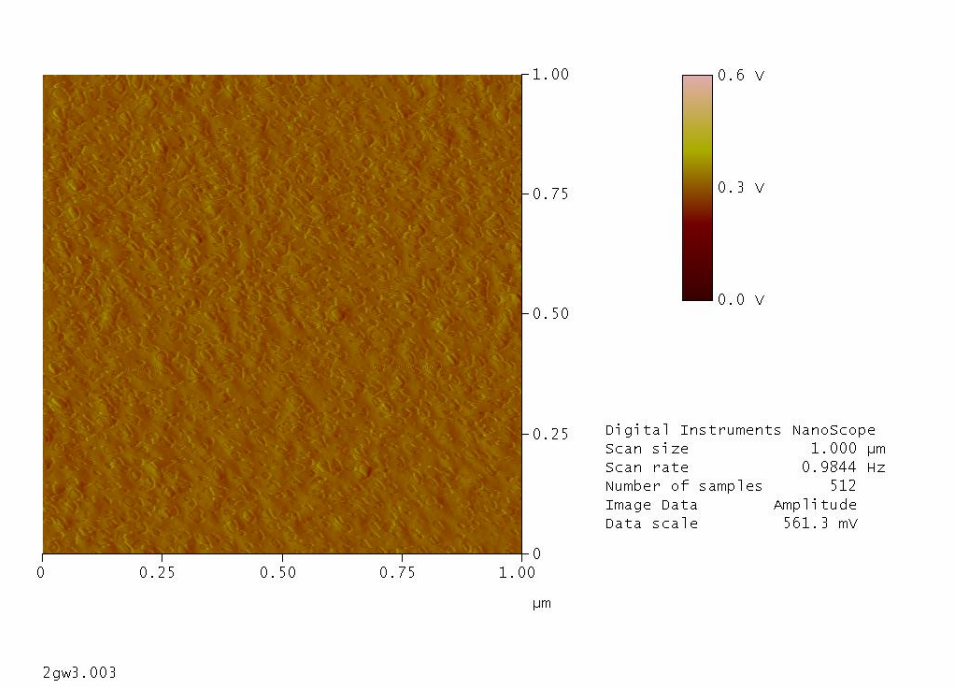
1.00
0.75
0.50
0.25
0
0
0.25
0.50
0.75
1.00
µm
0.6 V
0.3 V
0.0 V
Digital Instruments NanoScope
Scan size 1.000 µm
Scan rate 0.9844 Hz
Number of samples 512
Image Data Amplitude
Data scale 561.3 mV
2gw3.003

(C1)

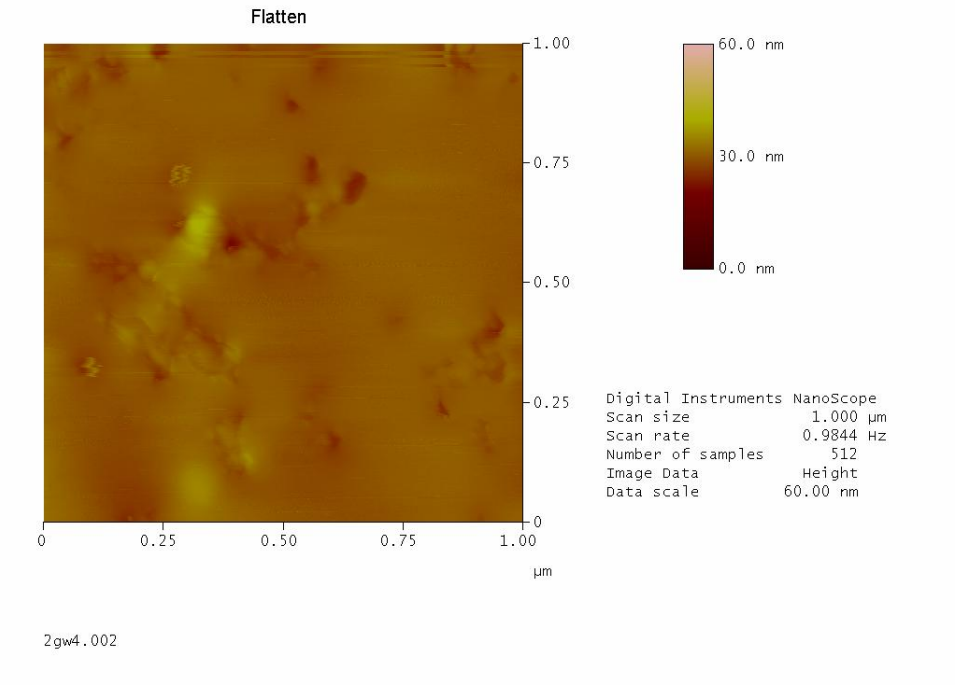

(C2)

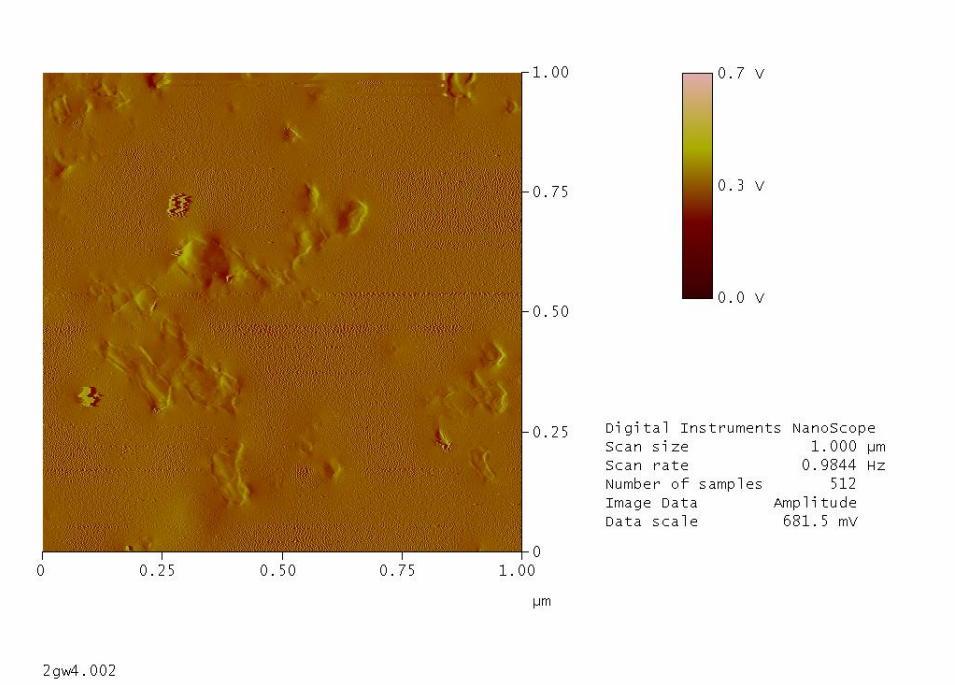

Figure S.7.3 2D height and phase images of: pre-treated Si wafer (A1 and A2), Si wafer modified with styrene [Si-SM-TMS (B1 and B2)] and Si wafer conjugated with PiBA-PSDTF (C1 and C2)

Chapter 8 Accessing Quantitative Degrees of Functionalization on Solid Substrates *via* Solid-State NMR Spectroscopy

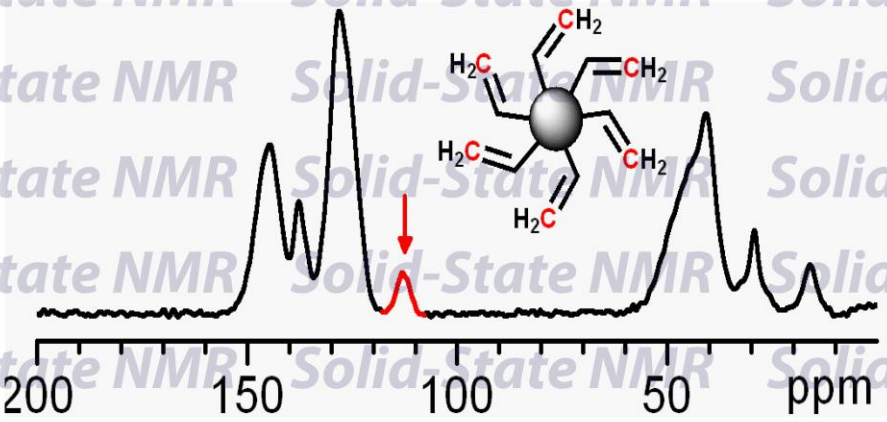

8.1 Introduction

In the **Chapters 5** and **6**, the functionalization of divinylbenzene microspheres using dithioester end groups expressed on the surface or using vinyl groups available on the surface *via* the RAFT-HDA approach was discussed. The residual vinyl groups available on the surface of the microspheres offer the possibility to graft a polymeric shell from or to an existing particle thus constituting an ideal synthetic handle for the preparation of core-shell microspheres and add further chemical functionalities to the particles. So far, a wide variety of techniques have been used to functionalize these microspheres, as discussed in detail in **Chapter 2**. However, in order to exploit the full potential of these functional microspheres, it is extremely valuable to have information about the amount of accessible active sites (*e.g.* vinyl groups) on the surface of the particles.[149] Being highly crosslinked, these systems are insoluble and must be characterized in the gel state or the solid-state.

Solid-state NMR spectroscopy is a versatile technique for the characterization of local structure and dynamics in polymers.[268-273] ^{13}C solid-state NMR spectroscopy under magic-angle spinning (MAS) exhibits significantly higher resolution than ^{1}H solid-state NMR spectroscopy but lower sensitivity, because only 1% of the carbon nuclei are NMR-sensitive ^{13}C nuclei. The sensitivity issue of the common ^{13}C single-pulse excitation (SPE) NMR spectroscopy can be overcome by the use of cross-polarization (CP), which consists of the transferring of magnetization from ^{1}H to ^{13}C nuclei before recording ^{13}C signals. CP takes advantage of the higher natural abundance and faster relaxation of ^{1}H spins compared to those of ^{13}C.[274,275] It generally yields higher intensities, but is usually not quantitative because of different cross-polarization efficiencies and relaxation properties of the observed groups. Alternative pulse schemes have recently been proposed to record quantitative CP-MAS spectra.[276-279] Although these allow for more uniform CP dynamics, the measurements still suffer from adverse effects of the short relaxation properties or heterogeneous local mobility[277] or need extensive complementary measurements to correct the experimental CP intensity.[279] Lowering the temperature of the measurements may help in reducing the local dynamic heterogeneity, but is experimentally more challenging.[280] Here in, solid-state NMR spectroscopy was applied to polymer systems exhibiting homogeneous local mobility

and homogeneous ^{1}H density, in which all sample parts contribute to the NMR signal without bias. The investigated microspheres are formed by distillation-precipitation polymerization, a process during which the polymer chains gradually precipitate onto the particles as they are polymerized; no stabilizer or further additives are used. Furthermore, their surface is (highly) porous, and they are best described as porous particles than as bulk particles limited by a sharp surface. We thus expect these pure poly(divinyl benzene) particles with homogenous chain topology to exhibit homogeneous local mobility and ^{1}H density across the whole sample in the solid state.

In the current chapter, the development of a solid-state nuclear magnetic resonance (NMR) method is presented allowing - for the first time – the quantification of active sites (*i.e.* residual vinyl groups) accessible for chemical functionalization on the surface of poly(divinyl benzene) (PDVB) microspheres. The study has been carried out in close collaboration with the solid-state NMR group of Prof. Hans W. Spiess with Dr Marianne Gaborieau and Dr Robert Graf of the Max Planck Institute of Polymer Research, Mainz.

8.2 Experimental

8.2.1 Synthesis of PDVB80 and PDVB55 Microspheres *via* Distillation-Precipitation Polymerization

PDVB80 and PDVB55 microspheres were synthesized by distillation-precipitation polymerization. 2,2'-azoisobutyronitrile (AIBN) (0.092 g, 0.56 mmol, 2 wt.-% relative to the total monomer) and DVB80 or DVB55 (5 mL, 4.6 g, 35.35 mmol, 2.5 vol.-% relative to the reaction medium) was dissolved in 200 mL of acetonitrile in a 500 mL round-bottom flask, attached to a distillation assembly. The reaction mixture was heated from ambient temperature to boiling state by ramping the temperature gradually, until the solvent started distilling. As the solvent started distilling the initially homogenous reaction mixture turned milky white. The reaction was stopped after half of the initial acetonitrile used in the reaction mixture was collected in the receiving flask. After the polymerization was finished, the resulting PDVB80 or PDVB55 microspheres were separated by filtration through a 0.45 µm membrane, washed with and re-suspended several times in toluene, THF, acetone and diethylether. The washing of the

microspheres with toluene is very critical in this case as through washing with toluene it is possible to remove the residual monomer. The microspheres were dried in a vacuum oven at 40 °C before characterization. 1.36 g of PDVB80 and 1.5 g of PDVB55 were obtained in 30% and 33% yields respectively.

8.2.2 Synthesis of Hydroxy Functionalized PDVB80 and PDVB55 Microspheres

PDVB80 or PDVB55 microspheres (1.0 g) were suspended in dry THF (10 mL) in a dry 100 mL round-bottom flask for 2 h, and sodium borohydride (0.1 g, 2.6 mmol) was added. The suspension was cooled in a cold-water bath, and boron trifluoride diethyl etherate (0.376 g, 2.6 mmol) dissolved in 1 mL of THF was added dropwise to the suspension of microspheres. The temperature of the reaction suspension was maintained at 20 °C during the addition of BF_3 and for a further 3 h. At the end of this period, the flask was immersed in an ice bath, and 5 mL of cold water was slowly added to destroy any residual $NaBH_4$. Subsequently, hydrogen peroxide (0.8 mL, 36 mmol, 30% in water) was slowly added to the reaction mixture. During the addition, the pH of the solution was maintained near pH = 8 by adding 3 $mol \cdot L^{-1}$ sodium hydroxide as needed. The final solution was filtered through a 0.45 μm membrane filter and washed with water (pH = 8) followed by methanol. The resulting microspheres were dried in a vacuum oven before characterization.

8.2.3 Grafting of *n*-Butyl Acrylate from Microspheres

All RAFT polymerizations were carried out in toluene. A solution of *n*-butyl acrylate (19.45 g, 0.1518 mol), AIBN (0.0318 g, 3.7 $mmol \cdot L^{-1}$) and CPDB (0.15 g, 0.12 $mmol \cdot L^{-1}$) in toluene (35 mL) was prepared. 5 mL of the above solution was transferred into glass sample vials, each containing 300 mg of the microspheres. The sample vials were capped with rubber septa and deoxygenated by purging with nitrogen for 15 min. The samples were stirred with a magnetic bar at 80 °C. The polymerization was stopped after 3 h. The resulting grafted microspheres were isolated by filtration through a 0.45 μm membrane, washed several times with toluene and dichloromethane and dried in a vacuum oven overnight. Polymers from the solutions were collected to determine the apparent molecular weight[29] by SEC (M_n = 18 000 $g \cdot mol^{-1}$, *PDI* = 1.2 for PDVB80

and M_n = 19 000 g·mol^{-1}, *PDI* = 1.2 for PDVB55). An alternative SEC data treatment taking into account the possible influence of long chain branching was outside the scope of the present study.[281,282,283]

8.3 Results and Discussion

The highly cross-linked PDVB microspheres employed in the current work were synthesized by distillation-precipitation polymerization.[170] This technique only requires divinylbenzene (DVB) (which is also a cross-linker), a radical initiator, AIBN, and a near Θ-solvent for PDVB (acetonitrile). DVB is available in two technical grades, DVB55 and DVB80, which are composed of meta and para isomers of DVB, as well as 3- and 4-ethylvinyl benzene. 3- and 4-ethylvinyl benzene have only one functional vinyl group and can for this reason not act as a cross-linker. Core microspheres exhibit three types of structural aromatic units in the backbone of PDVB as depicted on the upper left hand side in **Scheme 8.1** (note that isomeric structures are not included). One structure is based on a DVB unit where both vinyl groups have reacted forming the cross-linked network in the other case only one of the two vinyl groups has reacted, resulting in a residual vinyl group. In addition, a further structural entity results from the incorporated 3- or 4-ethylvinyl benzene. This structural entity therefore does not include a residual vinyl group, but an ethyl group. In the subsequent modification of the microspheres only the residual vinyl groups (also termed 'active' sites) are involved in the *grafting-from* polymerization and therefore a simplified representation of the core microspheres including only these active sites is depicted on the upper right side of **Scheme 8.1**.The capital letters next to the atoms in **Scheme 8.1** are used for the complete chemical shift assignments in the ^{13}C NMR spectra (refer to **Figure 8.2a**). A detailed signal assignment[284-287] is given in the Supporting Information section (**Table S.8.1**). Signals C and D were integrated over the ranges from 134 to 118 ppm and from 118 to 107.5 ppm, respectively. The morphology and size of these microspheres was studied *via* Scanning Electron Microscopy (SEM) technique. The SEM micrographs for PDVB80 and PDVB55 are shown in **Figures S.8.1** and **S.8.2** respectively.

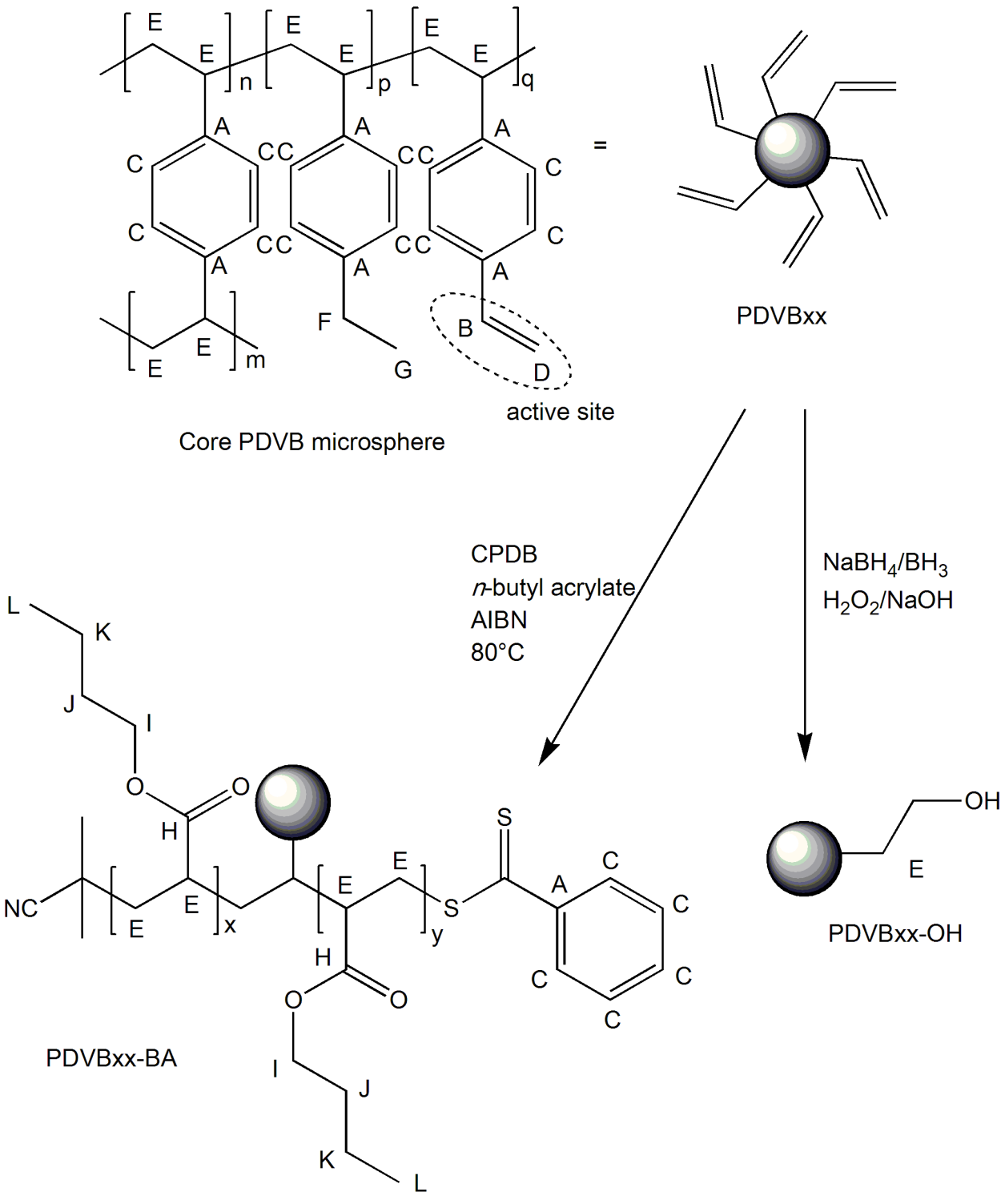

Scheme 8.1 Schematic representation of the core, hydroxylated and poly(*n*-butyl acrylate)-*graft*-poly(divinyl benzene) microspheres. Capital letters relate to the ^{13}C chemical shift assignment in **Figure 8.2**a

Residual vinyl groups, *e.g.* 'active' sites, are present within and on the surface of the particle. However, residual vinyl groups in the centre of the particle are not easily accessible for reagents (*e.g.* reagents cannot easily diffuse to the centre of the microspheres due to the highly crosslinked nature of the particles), therefore not all of the 'active' sites will be able to take part in the subsequent modification of the particles *via grafting-from* polymerization. Only a certain degree of the 'active' sites will be accessible for further functionalization. In order to estimate the number of 'accessible active' sites, the residual vinyl groups of the PDVB microspheres which are accessible for reagents were hydroxylated (see **Scheme 8.1**, lower right side).

In addition, core PDVB microspheres were functionalized by grafting *n*-butyl acrylate (BA) from the microspheres using the RAFT agent cyanopropyl dithiobenzoate (CPDB), resulting in PDVB-*g*-PBA-microspheres (see **Scheme 8.1**, lower left side). Subsequently, all synthesized microspheres were characterized *via* ^{1}H and ^{13}C NMR spectroscopy to quantitatively access the degrees of functionalization.

^{1}H solid-state NMR spectra recorded at high field under fast MAS showed insufficient resolution for selectively observing signals from vinyl groups, expected in the 6 to 7 ppm range (**Figure 8.1**). The only resolved signals are indeed a massif of aliphatic signals, centered around 1 ppm, and a massif of aromatic and unsaturated signals centered around 6 ppm. Signals may be broad because of the low mobility of the samples due to their high degree of crosslinking. No significant change in the spectrum of PDVB55 was observed upon heating up to 120 °C (**Figure 8.1**). Therefore ^{1}H solid-state NMR spectroscopy is not appropriate for observing or quantifying active sites in PDVB microspheres, because of its limited resolution. Note that weak narrow signals were originally observed at 5.2, 6.2 and 6.7 ppm for the sample PDVB80 (see Supporting Information, **Figure S.8.3**), which originate from vinyl groups. These signals disappeared upon repeated washing of the sample with toluene and were thus assigned to residual monomer units rather than active sites (residual vinyl groups on the polymer chains). Care was taken to ensure that all core PDVB microspheres used for the present work had been washed appropriately to remove any residual monomer, before functionalization or NMR measurement. Careful purification is particularly important since the signal of vinyl groups from residual monomer would overlap with those from

the polymer chains, inducing an error in the active sites quantified by ^{13}C NMR spectroscopy.

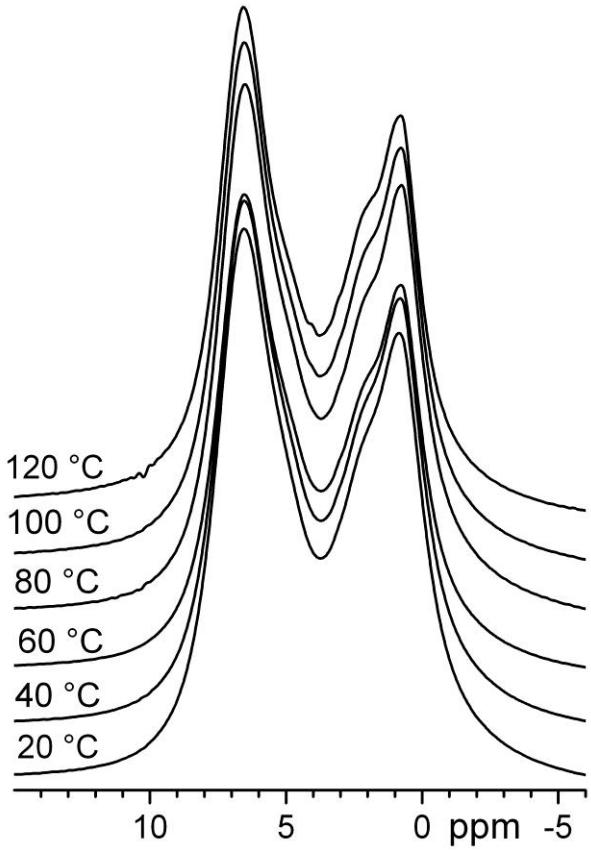

Figure 8.1 ^{1}H solid-state NMR spectra at high field and fast MAS of PDVB55 microspheres at different temperatures

Improved resolution was sought through ^{13}C solid-state NMR spectroscopy. ^{13}C SPE-MAS NMR spectroscopy allows for the observation of a resolved signal at 113 ppm for the active site. It originates in the methylene carbon of the vinyl groups pending from the polymer chain (signal D on **Figure 8.2**a for PDVB80, see **Scheme 8.1** and Supporting Information **Table S.8.1** for complete signals assignment). The signal at 128 ppm (C on **Figure 8.2**a) solely originates in the non-substituted carbons of the aromatic rings (4 per monomer unit). In terms of chemical shift and shape of signal observed in ^{13}C SPE-MAS spectra, sample PDVB80 (**Figure 8.2**a) is representative of core and hydroxylated microspheres, while sample PDVB80-BA (**Figure 8.2**c) is representative of poly(*n*-butyl acrylate)-grafted microspheres. The active sites can, in

principle, be quantified as a percentage of the monomer units by ^{13}C NMR spectroscopy *via* signals D and C for all samples. However, a broad signal underlying the aromatic region was observed with intensity comparable to that of the signals of interest. The broad underlying signal renders the quantification of the narrow C and D signals difficult.

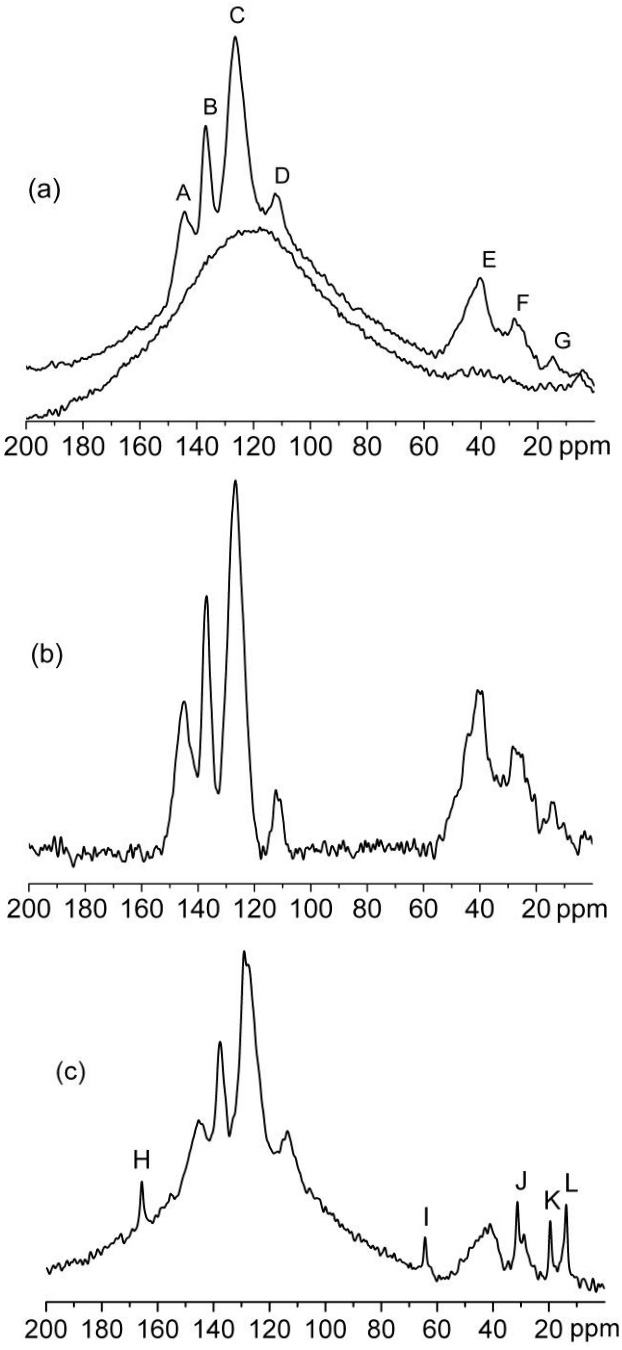

Figure 8.2 ^{13}C solid-state SPE-MAS NMR spectra of (a, top) PDVB80 microspheres, (a, bottom) background, and (c) PDVB80-BA microspheres (b) shows the subtraction of the

spectra of PDVB80 microspheres and background (a). The letters refer to **Scheme 8.1**; a complete ^{13}C chemical shift assignment is given in Supporting Information, **Table S.8.1**

Possible causes for the observation of the broad signal were subsequently examined. Signal broadening due to paramagnetic impurities was ruled out since no paramagnetic species were present in any step of the synthesis. The broad signal may originate in highly-crosslinked parts of the sample, which would be locally less mobile than the rest of the sample. If this was the case, the signal should narrow with increasing local mobility upon heating. Variable-temperature experiments showed that this was not the case (see the Supporting Information section for details, **Figure S.8.4**). Thus the broad underlying signal most probably originates from components other than the sample, namely the cap of the rotor containing the sample and various components of the probe. This was checked by comparing the ^{13}C SPE-MAS spectra of sample PDVB80 in a given rotor and of the same empty rotor under the exact same conditions (**Figure 8.2**a): the broad underlying signal observed for PDVB80 exactly overlays with the background signal. Thus, the quantification of signals C and D is possible on a quantitative ^{13}C SPE-MAS spectrum after subtraction of the background signals. The acquisition of a quantitative spectrum, however, was found to require prohibitively long measuring times to be carried out on all samples.

Improved sensitivity was therefore sought through ^{13}C CP-MAS NMR spectroscopy. It overcame two problems: spectra with a resolved signal from the methylene group of the active site at 113 ppm could be recorded in shorter times without background signal (**Figure 8.3**b). ^{13}C CP-MAS spectra are not intrinsically quantitative. However, a range of contact times was identified over which the relative intensities of the signals of interest did not vary, allowing quantitative comparison between samples on the same arbitrary scale (**Figure 8.3**a). The representative ^{13}C CP-MAS spectra of PDVB55, PDVB55-OH and PDVB55-BA are shown in **Figure 8.3**b, **8.3**c and **8.3**d respectively. The additional spectra are shown for other samples in the Supporting Information in **Figure S.8.6**.

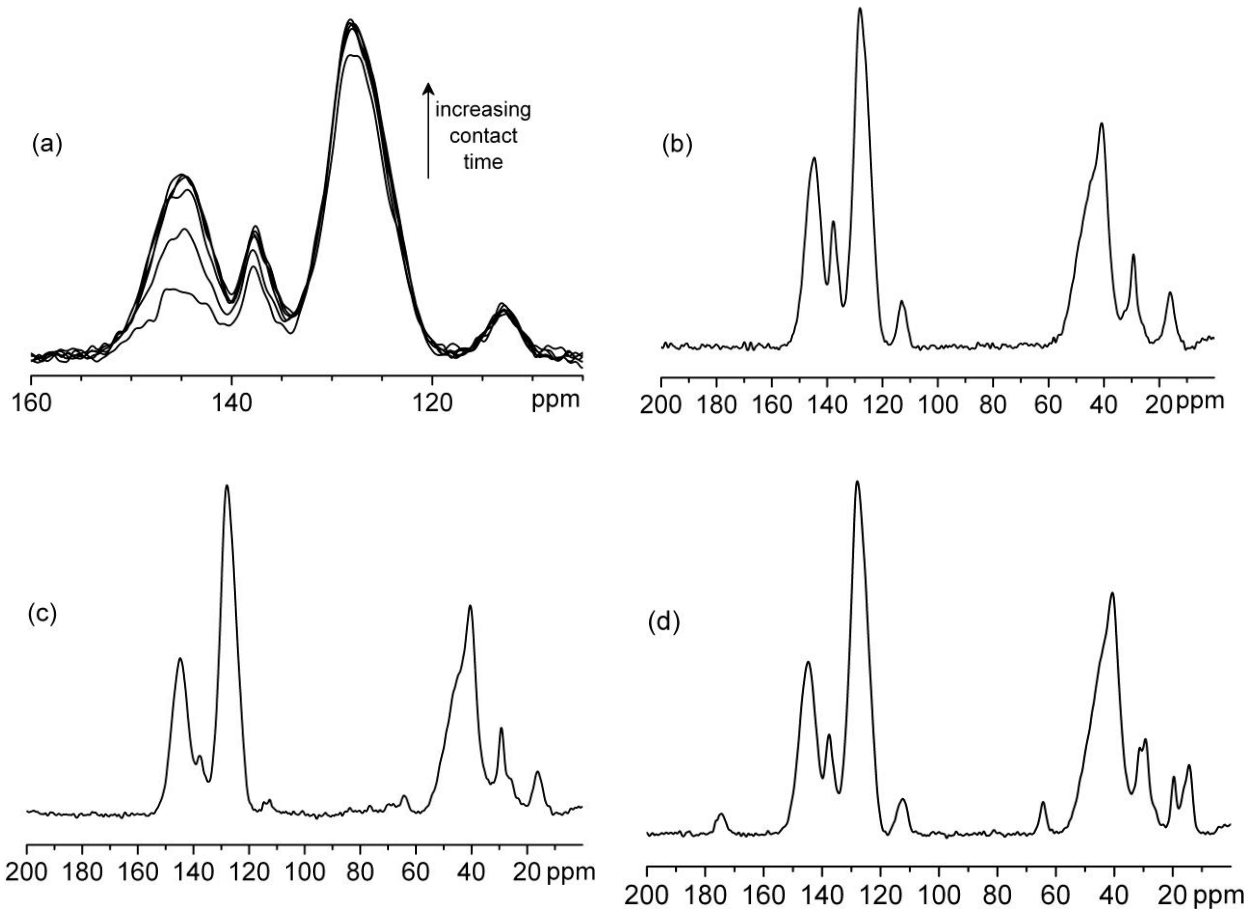

Figure 8.3 ^{13}C solid-state CP-MAS NMR spectra of (a) PDVB55 microspheres with short measuring time and variable contact time (250 µs, 500 µs, 1 ms, 2 ms, 2.5 ms, 3 ms), (b) PDVB55, (c) PDVB55-OH and (d) PDVB55-BA microspheres

The active sites *AS* (*i.e.* residual vinyl groups on the polymer chains) were quantified for all samples from ^{13}C CP-MAS spectra, on the same arbitrary scale with respect to the monomer units, using equation (8.1):

$$AS(\text{a.u.}) = \frac{100 \cdot I(\text{D}) \cdot 4}{I(\text{C})} \tag{8.1}$$

where I(D) is the area of the signal centered around 113 ppm, originating solely in one (methylene) carbon of residual vinyl groups, and I(C) is the area of the signal centered around 128 ppm, originating solely in four carbons per phenyl group of the

monomer unit (unsubstituted carbons). Active sites quantified on the same arbitrary scale are given for all samples in **Table 8.1**. The peak at 128 ppm is not fully resolved from the signals centered around 138 and 145 ppm; however, considering the similar signal areas present on both sides of the minimum at 134 ppm, the error introduced is small compared to the experimental error, and systematic for all samples. Note that for the samples grafted with poly(*n*-butyl acrylate), the signal centered around 128 ppm also contains the signal of the 5 non-substituted aromatic carbons of the dithioester group, which is assumed to be negligible compared to the experimental error made during the measurements. Such an assumption is supported by the fact that the C=S signal of the same dithioester group at approximately 225 ppm is below the detection limit for both PDVB55-BA and PDVB80-BA microspheres (see Supporting Information, **Figure S.8.6**). Solid-state NMR spectroscopy measures the whole sample volume and not only its surface; therefore the active sites are quantified throughout the sample. Actives sites inside the microspheres, however, will not be accessible for functionalization because reagents will not be able to penetrate the microspheres to react with them. Active sites accessible for functionalization (*ASAF*) may however be quantified *via* comparison of actives sites remaining after hydroxylation $AS_{\text{hydroxylated}}$ with the active sites present in the corresponding core microspheres AS_{core}, using equation (8.2):

$$ASAF\ (\%) = \frac{100 \cdot \left(AS_{\text{core}} - AS_{\text{hydroxylated}}\right)}{AS_{\text{core}}} \qquad (8.2)$$

Similarly, an absolute quantification of the active sites actually functionalized during PBA-grafting, in percent of the active sites originally present on the core microspheres, may be calculated by replacing $AS_{\text{hydroxylated}}$ by $AS_{\text{PBA-grafted}}$ in Equation (8.2). *ASAF* values are shown for all hydroxylated and PBA-grafted samples in **Table 8.1**.

Table 8.1 Overview of the quantitative degrees of functionalization for various microspheres as described in **Scheme 8.1**

Sample	*AS* (a.u.)[a]	*ASAF* (%)[b]	*AS* (%)[c]	*CL* (%)[d]	F_{mon} (%)[e]	F_{part} (groups particle^{-1})[f]	F_{surf} (groups nm^{-2})[g]	*LC* (mmol g^{-1})[h]
PDVB55-1	29		22	33				
PDVB55-OH	11	62	8		14	$1.50 \cdot 10^9$	188	1.05
PDVB55-2	35		27	28				
PDVB55-BA	24	30	19		8	$8.70 \cdot 10^8$	110	0.61
PDVB80-1	39		30	50				
PDVB80-OH	26	34	20		10	$1.53 \cdot 10^9$	213	0.77
PDVB80-2	43		33	47				
PDVB80-BA	32	26	25		9	$1.28 \cdot 10^9$	179	0.65

[a] *AS* (a.u.) are the active sites quantified with respect to the monomer units on the same arbitrary scale for all samples, *via* ^{13}C-CP MAS NMR spectroscopy.

[b] *ASAF* (%) are the active sites accessible for functionalization, quantified on an absolute scale by comparison of *AS* (a.u.) of the functionalized microspheres and of the corresponding core ones.

[c] *AS* (%) are the active sites quantified with respect to the monomer units on an absolute scale, obtained from *AS* (a.u.) *via* the same correction factor for all samples.

[d] *CL* (%) is the degree of crosslinking calculated on the corresponding core microsphere.

[e] F_{mon} (%) is the degree of functionalization quantified in percents of the monomer units.

[f] F_{part} (groups·particle^{-1}) is the number of active groups per particle.

[g] F_{surf} (groups·nm^{-1}) is the number of active groups per nm^2.

[h] *LC* (loading capacity) is the moles of active groups per gram of particle.

Residual vinyl groups are quantified with equation (8.1) on the same arbitrary scale. This scale can be calibrated with the measurement of *AS* as a percentage of the monomer unit of one sample in a quantitative way. A quantitative ^{13}C SPE-MAS spectrum can be recorded using a sufficiently long relaxation delay between scans to ensure full sample relaxation. Comparison of the spectra of PDVB80 recorded with relaxation delays ranging from 2 to 20 s indicated that a relaxation delay of 10 s is not sufficient to ensure full relaxation (see Supporting Information, **Figure S.8.7**). Therefore a very long relaxation delay of 60 s was chosen.

To increase the sensitivity, a larger sample volume was measured (filling a 4 mm rotor rather than a 2.5 mm rotor). A quantitative ^{13}C SPE-MAS spectrum of PDVB80 was recorded, using a sufficiently long relaxation delay between scans to ensure full sample relaxation (**Figure 8.2**a). A ^{13}C SPE-MAS spectrum of the empty rotor was subsequently recorded under the exact same experimental conditions to yield the background signal (**Figure 8.2**a). The subtraction of the background from the ^{13}C SPE-MAS spectrum of sample PDVB80 yields the quantitative ^{13}C SPE-MAS spectrum of sample PDVB80 (**Figure 8.2**b).

Equation (8.1) was used to determine the absolute percentages of residual vinyl groups in PDVB80: it was found that 30% of the monomer units contain residual vinyl groups. The percentage of active sites of PDVB80 on the arbitrary scale was found to be 39%. Thus, a correcting factor of 30/39=0.77 must be applied to percentages of vinyl groups determined from ^{13}C CP-MAS to convert them into actual percentages of vinyl groups, using equation (8.3):

$$AS\,(\%) = AS\,(\text{a.u.}) \cdot \frac{AS_{\text{PDVB80}}\,(\%)}{AS_{\text{PDVB80}}\,(\text{a.u.})} = AS\,(a.u.) \cdot 0.77 \qquad (8.3)$$

The corrected values are given in **Table 8.1** for all samples. Note that the active sites concentration measured by ^{13}C CP-MAS is overestimated. This observed overestimation of the signal intensity for the vinyl methylene carbons with respect to that of the non-substituted aromatic carbons is attributed to the higher number of directly bound ^{1}H nuclei (two versus one) leading to a more efficient polarization transfer, whereas the relaxation of the bound ^{1}H nuclear spins under the applied radio-frequency

field ($T_{1\rho}$) can be expected to be identical (see Supporting Information for detailed discussion).

Several conclusions can be drawn from the comparison of the samples in terms of active sites quantified with respect to the monomer units on the same arbitrary scale *via* ^{13}C-CP MAS NMR spectroscopy (**Table 8.1**, first and second columns). Firstly, PDVB80 samples have a higher degree of active sites *AS* (*e.g.* 41 a.u.) than PDVB55 ones (*e.g.* 32 a.u.). However, PDVB80 samples have proportionally less active sites accessible for functionalization *ASAF* (%) than those of PDVB55. Both findings can be rationalized as follows. PDVB80 microspheres are synthesized from a monomer mixture with a higher proportion of difunctional monomer than is the case for PDVB55, therefore they are expected to be more crosslinked, and consequently less swellable. This results in a higher number of active sites (vinyl groups) being trapped inside the microspheres, which are therefore not accessible for functionalization. Secondly, for both PDVB80 and PDVB55 systems, more active sites are accessible for functionalization (*ASAF* (%)) in the case of hydroxylation than in the case of grafting with *n*-butyl acrylate, BA. Such an observation is in agreement with the larger reagent size in the case of BA. Note that during the hydroxylation of sample PDVB80-OH, a side reaction leading to the hydrogenation of the vinyl group[288] leads to a signal increase in the pending ethyl groups observed at 16 and 30 ppm. Both hydroxylation and hydrogenation of the vinyl group lead to the disappearance of this signal, thus in both cases the active site is quantified as being functionalized.

The quantification of active sites with respect to the monomer units on an absolute scale provides additional information (**Table 8.1**, third column). First, the core PDVB55 and PDVB80 microspheres have approximately 25 and 32% residual vinyl groups per monomer unit, while the initial monomer mixture contained 55 and 80% of difunctional monomer, respectively. Thus a significant fraction of the difunctional monomers have reacted only once (assuming there is no bias towards mono- or difunctional monomer the first time its reacts). This observation is consistent with an earlier report of significant amounts of residual vinyl groups in poly(styrene-*co*-divinyl benzene) networks, as soon as more than 10% divinyl benzene was used for the synthesis.[188] The resulting microspheres are highly crosslinked. The degree of

crosslinking, defined as the proportion of monomer units which have reacted twice in the final polymer, may be calculated as follows:

$$CL\,(\%) = DM(\%) - AS(\%) \tag{8.4}$$

where *DM* (%) is the proportion of difunctional monomer in the initial monomer mixture (55% for PDVB55 and 80% for PDVB80, respectively). Note that this formula holds only for the core microspheres before functionalization, and assumes that there is no bias towards mono- or difunctional monomer the first time a monomer unit reacts. The degree of crosslinking of the microspheres is high: approximately 30% for PDVB55 and approximately 50% for PDVB80 (**Table 8.1**, fourth column), which is much higher than the usual 2 to 10% observed in the more common poly(styrene-*co*-divinyl benzene) systems (*e.g.* Merrifield resins). The higher degree of crosslinking results in a lower swellability of PDVB80 compared to PDVB55 microspheres.

The extent of the functionalization may be quantified in different ways: with respect to the monomer units, to the number of groups per particle, to the nominal particle surface area and even as the loading capacity of the particles. The number of functional groups is easily calculated in percents of the monomer units as follows:

$$F_{\text{mon}}\,(\%) = \left(AS_{\text{core}}(\%) - AS_{\text{hydroxylated}}(\%)\right) \tag{8.5}$$

Hydroxylated microspheres have a higher number of functional groups per monomer unit, F_{mon}, than PBA-grafted ones, as was expected from the smaller reagent size. Interestingly, PDVB55 and PDVB80 microspheres exhibit a slightly different number of hydroxyl groups per monomer unit, but the same number of PBA grafts per monomer unit within experimental error.

The number of functional groups per particle may be calculated according to equation 8.6:

$$F_{\text{part}} = \frac{F_{\text{mon}}(\%)\cdot n}{100} = \frac{\left(AS_{\text{core}}(\%) - AS_{\text{hydroxylated}}(\%)\right)}{100}\cdot\frac{\pi\cdot d^{3}\cdot\rho\cdot \text{N}}{6\cdot M} \tag{8.6}$$

where n is the number of monomer units per particle, d is the particle diameter, ρ is the density of the PDVB microspheres (1.82 g·cm^{-3} and 1.12 g·cm^{-3} for PDVB80 and PDVB55 microspheres respectively), N is the Avogadro's number and M is the molar mass of the divinyl benzene monomer unit (130.19 g·mol^{-1}). PDVB55 microspheres contain 8.70·10^{8} and PDVB80 microspheres contain 1.28·10^{9} active groups (*e.g.* vinyl groups) per particle that are accessible for grafting with BA.

The number of functional groups can also be expressed as a number of functional groups per nominal surface area (groups per nm^2). The calculation of the number of functional groups per surface area in the current study is based on the nominal surface area of a single microsphere, which does not take into account that the microsphere has a porous surface and the available surface area is clearly significantly larger than that nominally calculated. However, it is very difficult to obtain a suitable value for the accessible surface area, as this area is dependent on the type of molecule that is grafted as discussed earlier. The number of functional groups per nominal surface area (groups per nm^{-2}) may be calculated according to equation 8.7:

$$F_{surf} = \frac{F_{mon}(\%) \cdot n}{100 \cdot SA} = \frac{\left(AS_{core}(\%) - AS_{hydroxylated}(\%)\right)}{100} \cdot \frac{d \cdot \rho \cdot N}{6 \cdot M} \qquad (8.7)$$

where SA is the nominal surface area of one microsphere. Derived from Equation 8.7, PDVB55 microspheres contain 110 and PDVB80 microspheres contain 179 active groups (*e.g.* vinyl groups) per nominal surface area, *i.e.* nm^2, that are accessible for grafting with BA. Inspection of the ratio of the degree of crosslinking of the two types of particles (30/50 = 0.6) and comparison with the ratio of the number of functional groups per nominal surface area of the two types of particles (110/179 = 0.61) demonstrates that the number of accessible active groups is directly linked with the degree of crosslinking.

In addition, the loading capacity LC (in mmol·g^{-1}) of the microspheres may be calculated according to equation 8.8:

$$LC = \frac{6000 \cdot F_{part}}{\pi \cdot \rho \cdot N \cdot d^3} \qquad (8.8)$$

The PDVB55-BA and PDVB80-BA microspheres have a loading capacity of 0.61 and 0.65 mmol·g^{-1}, respectively. These loading capacities are not too far removed from the loading capacities found for Merrifield resins, *e.g.* Merrifield resins of mesh size 100-200 (which corresponds to a particle diameter of 74 to 149 (μm) have loading capacities from 1.5 to 4.5 mmol·g^{-1}.

8.4 Conclusions

The potential of solid-state NMR spectroscopy to characterize surface functionalization in highly crosslinked microspheres is demonstrated. For the first time, residual vinyl groups were quantified in poly(divinyl benzene) microspheres as a percentage of the monomer units through solid-state NMR spectroscopy. ^{13}C CP-MAS NMR spectroscopy allows the comparison of samples on the same arbitrary scale in a short measuring time. This scale was calibrated by one longer measurement for the absolute quantification of vinyl groups using ^{13}C SPE-MAS NMR spectroscopy. Solid-state NMR spectroscopy detects all vinyl groups present in the sample, not distinguishing if they are located inside or at the surface of the particle. A comparison of core microspheres with the corresponding hydroxylated ones yields the proportion of the vinyl groups available for chemical functionalization. The proportion of the reacted vinyl groups is quantified by comparison of poly(*n*-butyl acrylate)-grafted microspheres with the corresponding core ones. It was found that not all vinyl groups available for functionalization were actually functionalized *via* grafting of BA. The degree of cross-linking was calculated to be 30% and 50% for PDVB55 and PDVB80 microspheres, respectively. The number of active groups per nominal surface area was 110 and 179 groups per nm^{-2} for PDVB55 and PDVB80 microspheres, respectively. The loading capacities of the microspheres are not to far from those found in Merrifield resins of comparable sizes.

8.5 Supporting Information

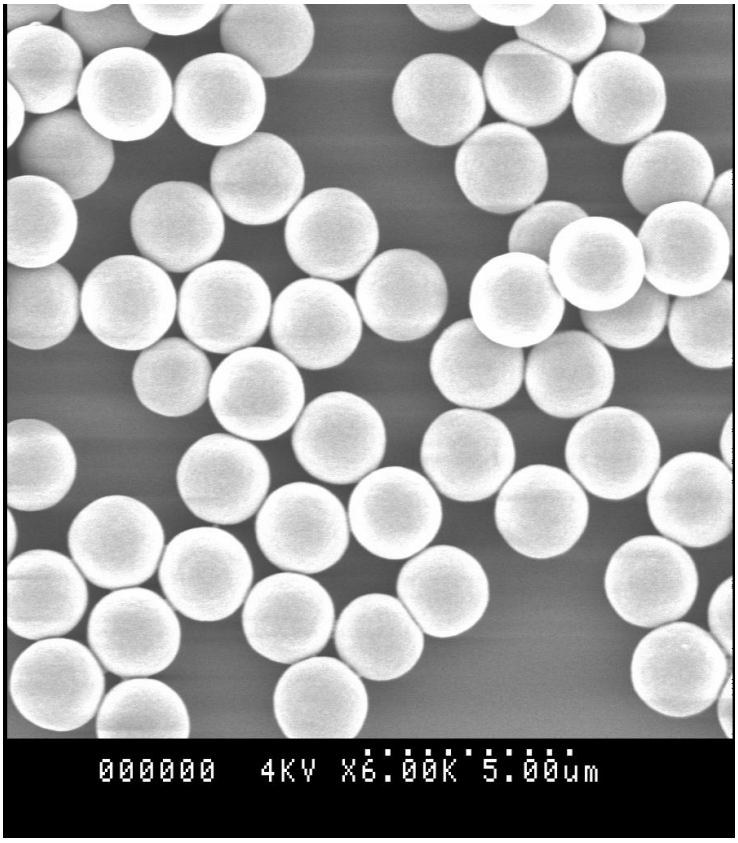

Figure S.8.1 Typical scanning electron micrograph of poly(divinylbenzene 80) microspheres synthesized *via* distillation precipitation polymerization

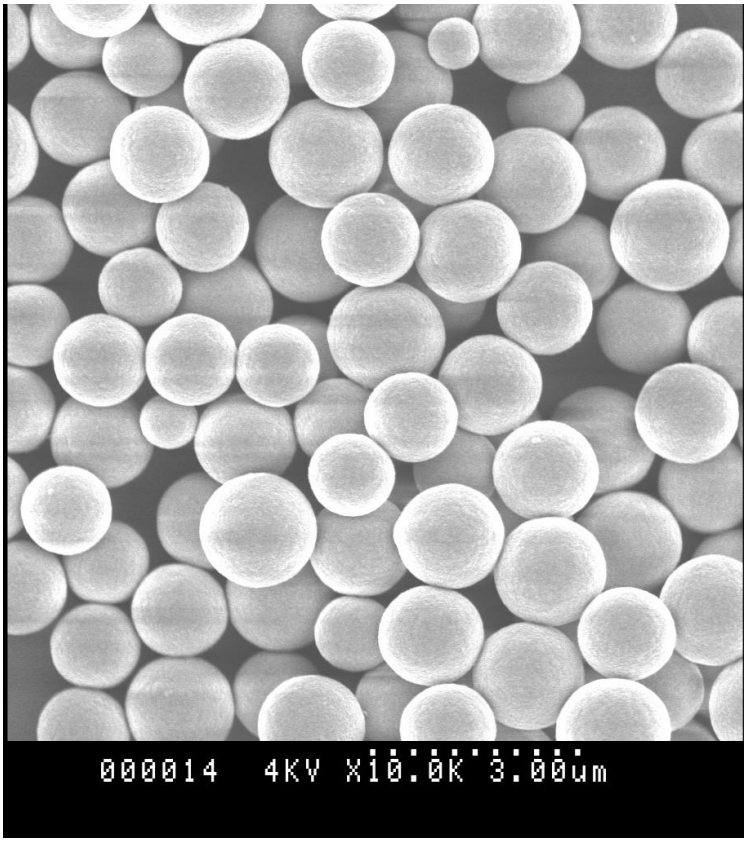

Figure S.8.2 Typical scanning electron micrograph of poly(divinylbenzene 55) microspheres synthesized *via* distillation precipitation polymerization

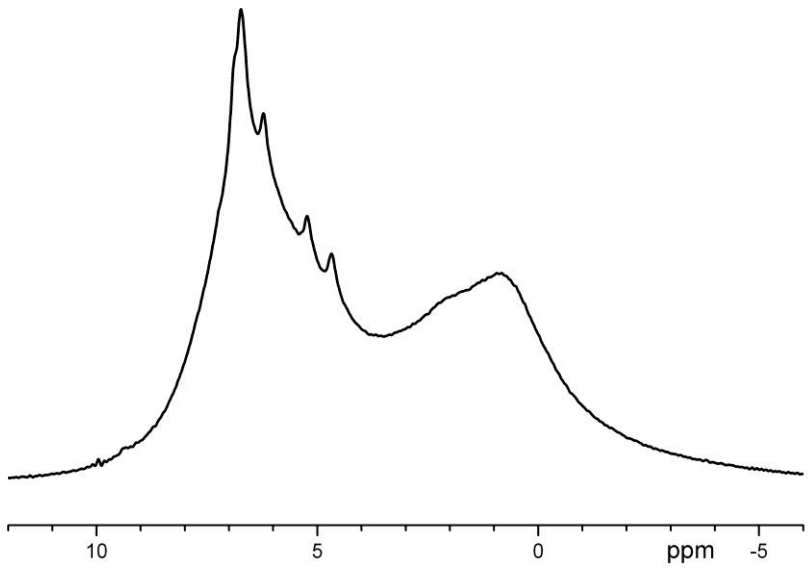

Figure S.8.3 ^{1}H MAS spectrum of sample PDVB80 with residual monomer

The weak narrow signals visible in **Figure S.8.3** originally observed at 5.2, 6.2 and 6.7 ppm for sample PDVB80 originate from vinyl groups. They disappeared upon repeated washing of the sample with toluene. They were thus assigned to residual monomers rather than active sites (residual vinyl groups on the polymer chains). Care was taken to ensure that all core PDVB microspheres used for the present work had been washed appropriately to remove any residual monomer, before functionalization or NMR measurement. This is particularly important since the signal of vinyl groups from residual monomer would overlap with those from the polymer chains, inducing an error in the active sites quantified by ^{13}C NMR.

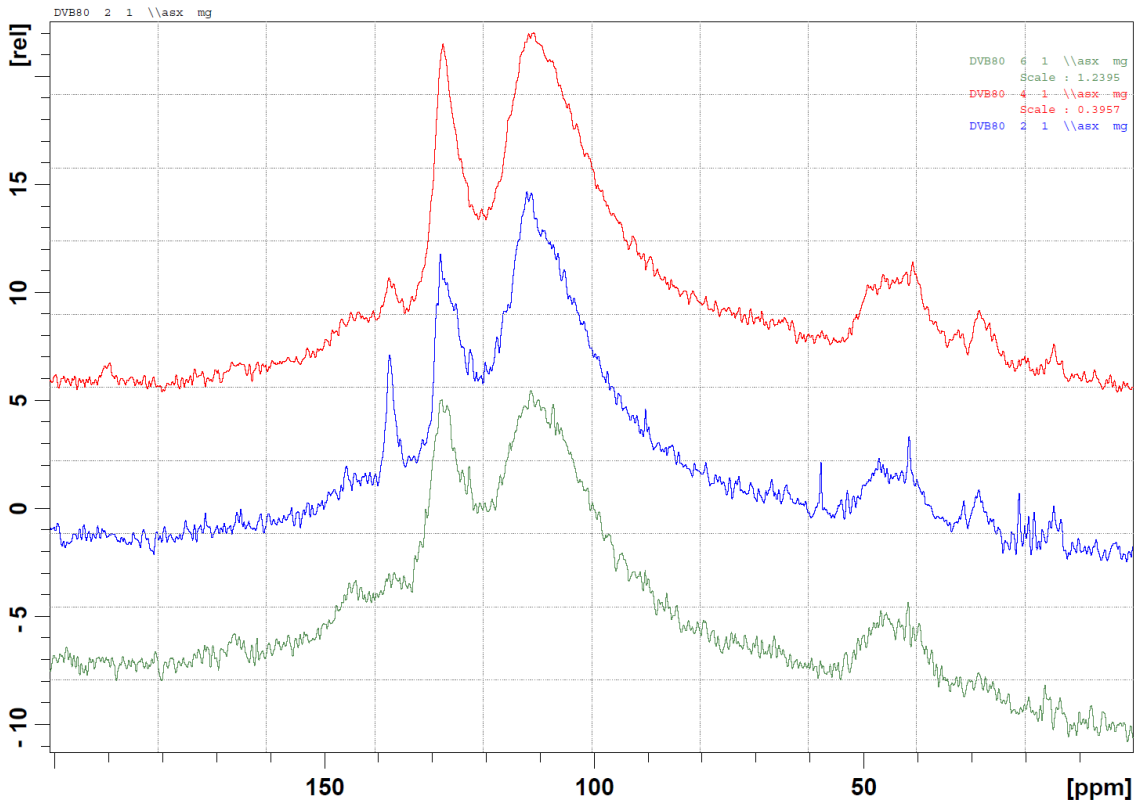

Figure S.8.4 No influence of temperature on broad underlying signal observed on the ^{13}C CP-MAS NMR spectrum of the PDVB80 microspheres. Spectra recorded at 100°C, 150 °C, and 200 °C are shown from top to bottom

Variable-temperature experiments shown in **Figure S.8.4** revealed that the broad underlying signal in the aromatic region does not originate in highly-crosslinked samples parts, but is actually a background signal from the rotor caps and the probes.

Experimental conditions: Bruker Avance 500, 4 mm MAS probe, ZrO_2 rotor with BN cap, 10 kHz MAS, ^{13}C SPE-MAS, 4 µs 90° pulse, 10 s repetition delay, no temperature calibration thus approximate temperatures; at 150 °C with NS = 1 360 in 3 h 50; at 200 °C with NS = 4 038 in 11 h 20; at 100 °C with NS = 1 024 in 2 h 50.

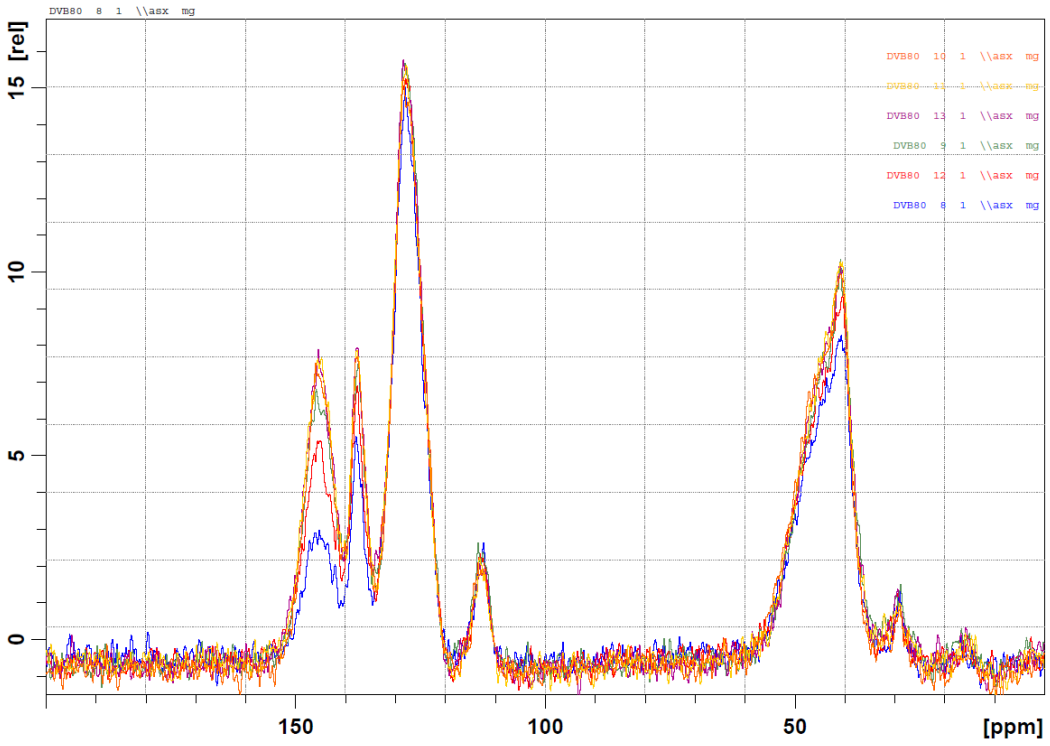
DVB80 8 1 \\asx mg
DVB80 10 1 \\asx mg
DVB80 13 1 \\asx mg
DVB80 9 1 \\asx mg
DVB80 12 1 \\asx mg
DVB80 8 1 \\asx mg
15 [rel]
10
5
0
150
100
50
[ppm]

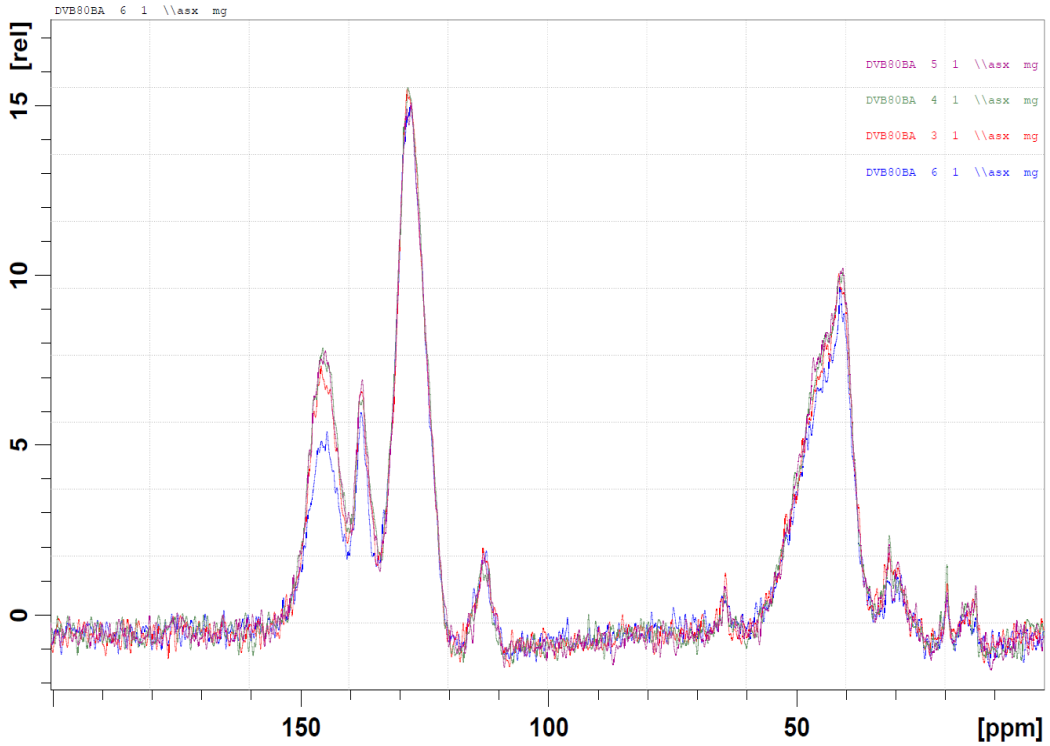
DVB80BA 6 1 \\asx mg
DVB80BA 5 1 \\asx mg
DVB80BA 4 1 \\asx mg
DVB80BA 3 1 \\asx mg
DVB80BA 6 1 \\asx mg
15 [rel]
10
5
0
150
100
50
[ppm]

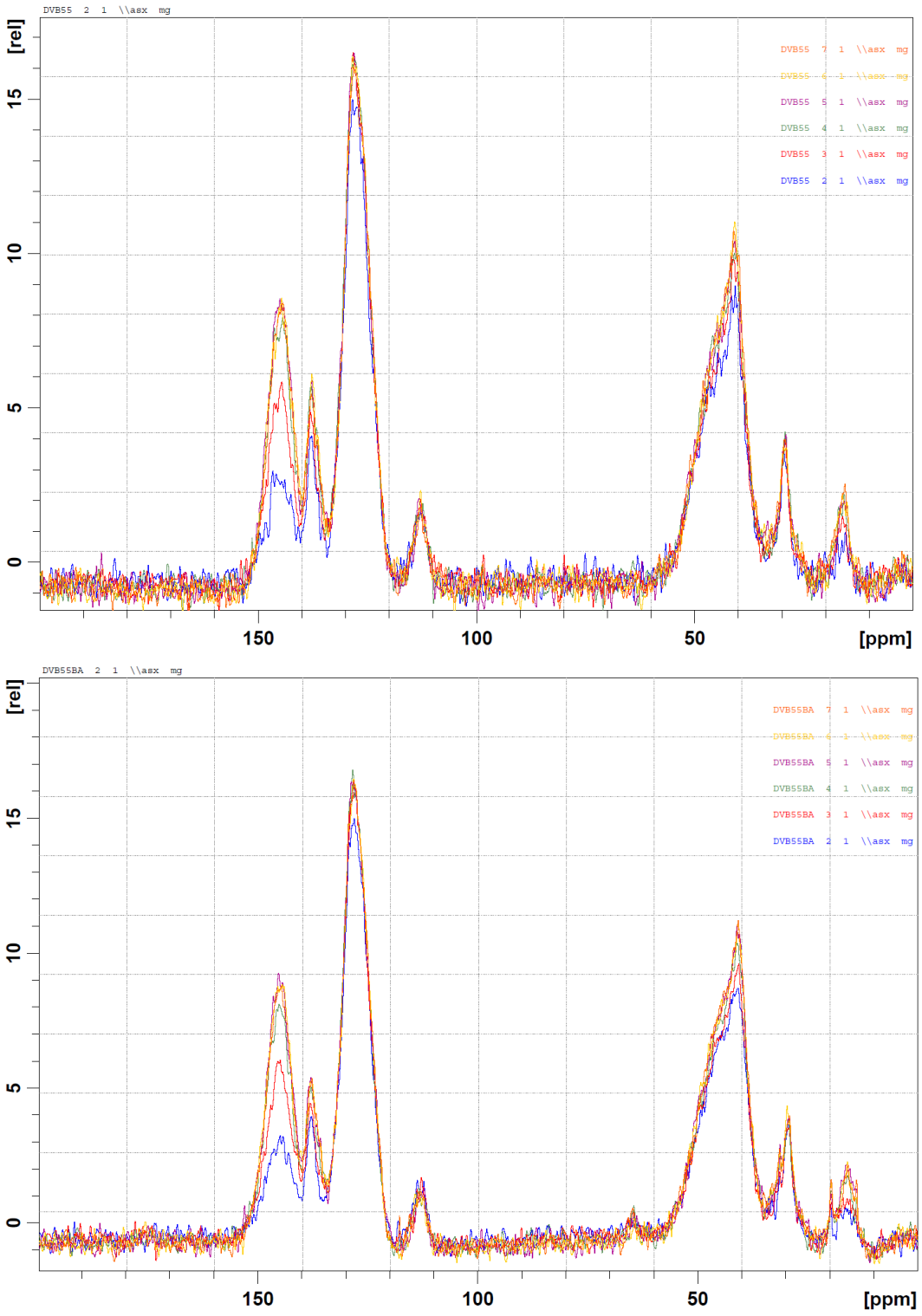

Figure S.8.5 Influence of contact time on signal intensities in ^{13}C CP-MAS spectra for samples PDVB80, PDVB80-BA, PDVB55, PDVB55-BA (from top to bottom)

Experimental conditions used to obtain spectra in **Figure S.8.5**: Bruker Avance 500, 2.5 mm MAS probe, room temperature, 18 kHz MAS, ^{13}C CP-MAS, 2.5 µs 90° pulse, 5 s repetition delay ; PDVB80 with 1 536 transients in 2 h 10 and contact times of 250 µs, 500 µs, 1 ms, 1.5 ms , 2 ms and 3 ms; PDVB80-BA with 1 256 transients in 1 h 46 and contact times of 500 µs, 1 ms, 2 ms, 3 ms; PDVB55 with 1 024 transients in 1 h 26 and contact times of 250 µs, 500 µs, 1 ms, 2 ms, 2.5 ms, 3 ms; PDVB55BA with 1 536 transients in 2 h 10 and contact times of 250 µs, 500 µs, 1 ms, 2 ms, 2.5 ms, 3 ms.

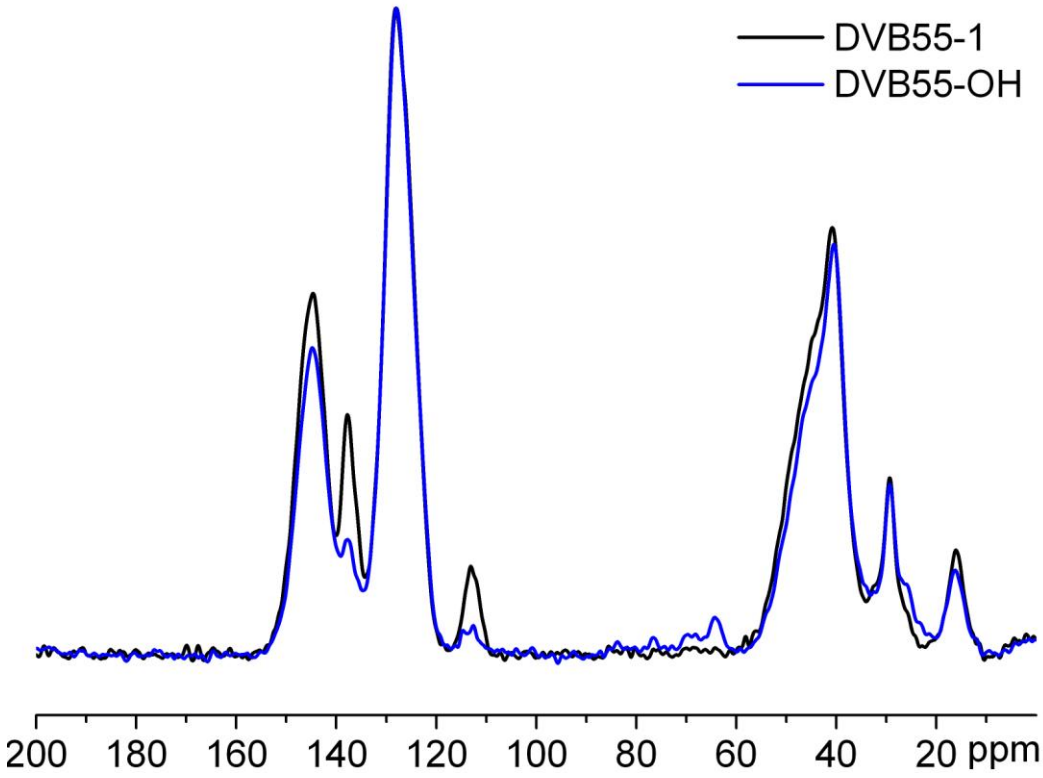
DVB55-1
DVB55-OH
200
180
160
140
120
100
80
60
40
20 ppm

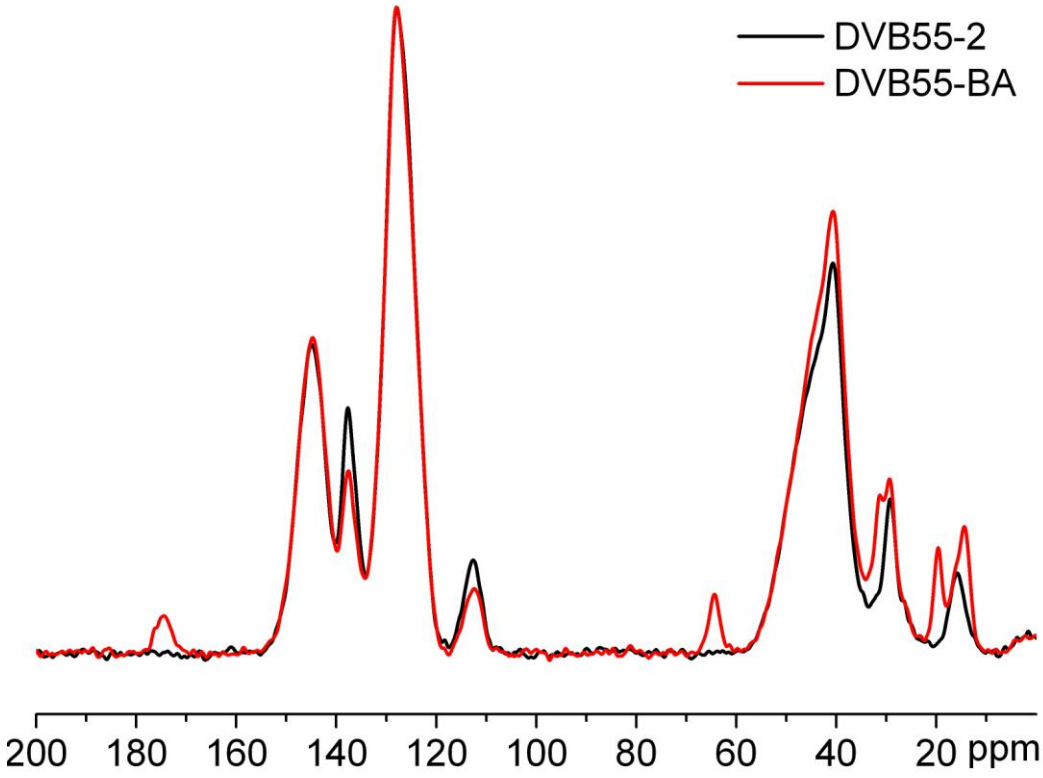
DVB55-2
DVB55-BA
200
180
160
140
120
100
80
60
40
20 ppm

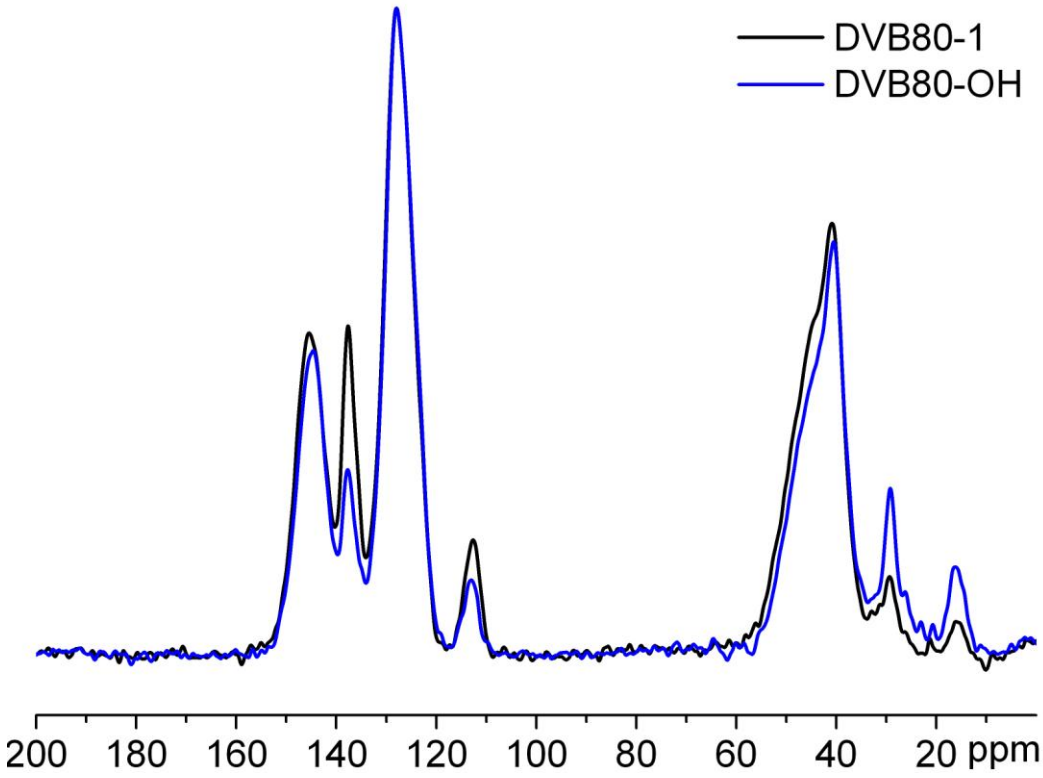
DVB80-1
DVB80-OH
200 180 160 140 120 100 80 60 40 20 ppm

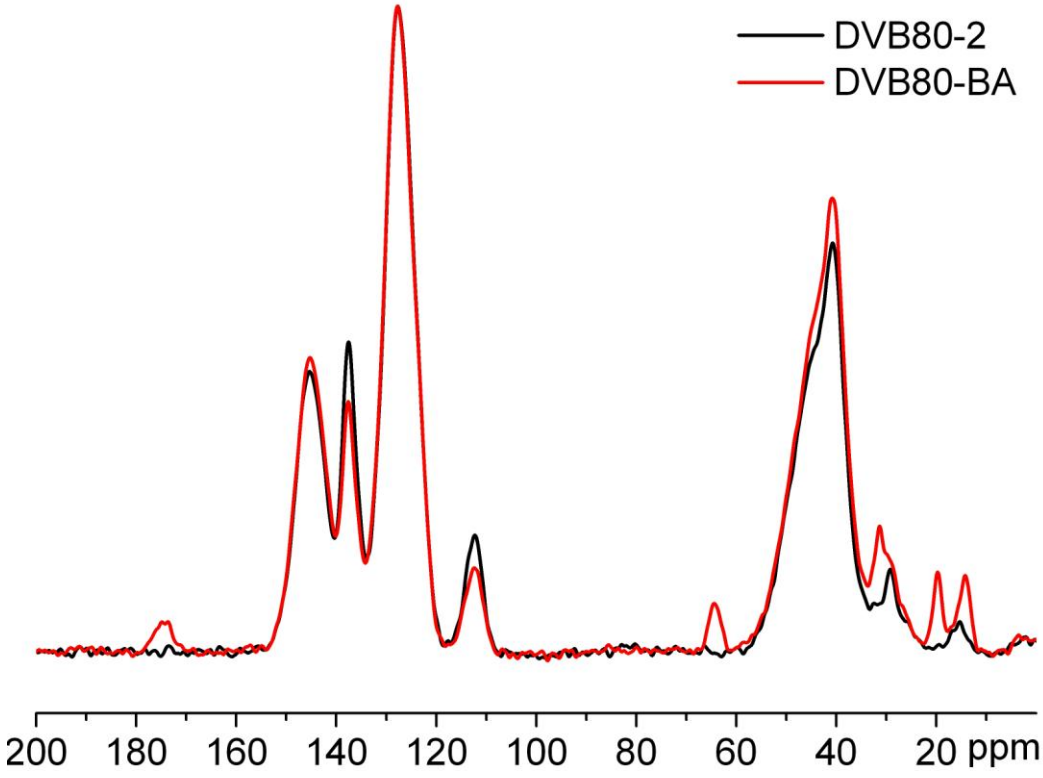
DVB80-2
DVB80-BA
200 180 160 140 120 100 80 60 40 20 ppm

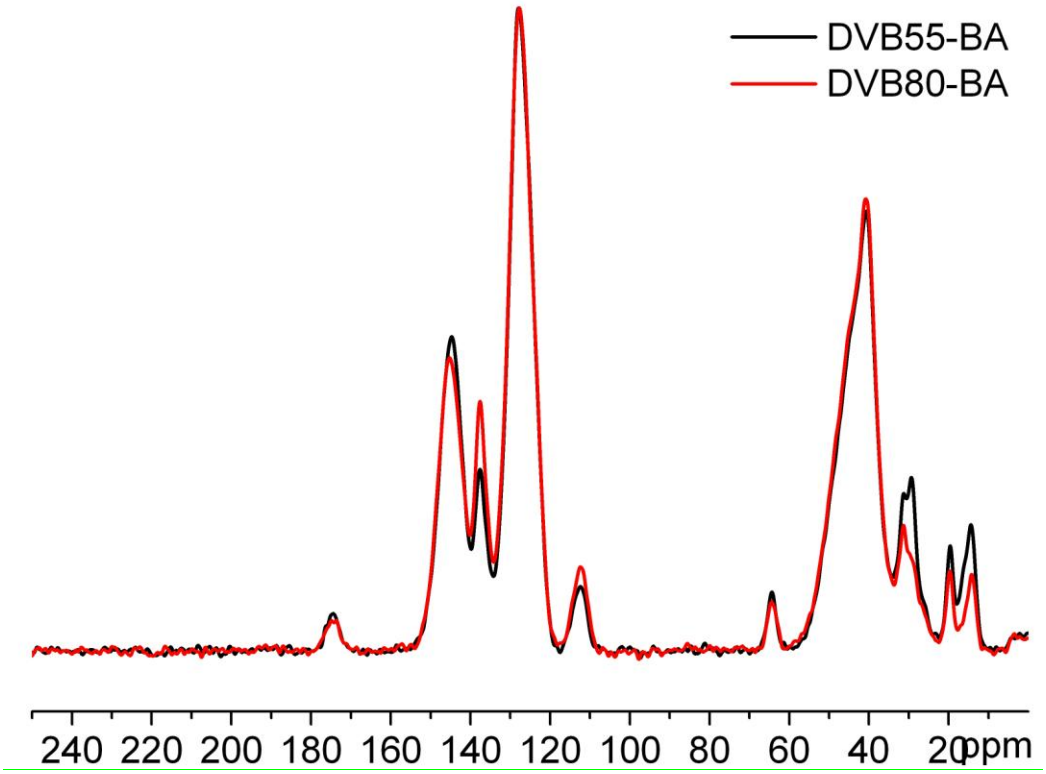

Figure S.8.6 Semi-quantitative ^{13}C CP-MAS spectra. The experimental conditions used for obtaining the spectra in **Figure S.8.6**: ^{13}C CP-MAS, semi-quantitative: Avance 500, 2.5 mm MAS probe, 18 kHz MAS, 2.5 µs 90° pulse, 5 s repetition delay, T_{cp} = 2ms, NS = 5 632, expt = 7 h 54.

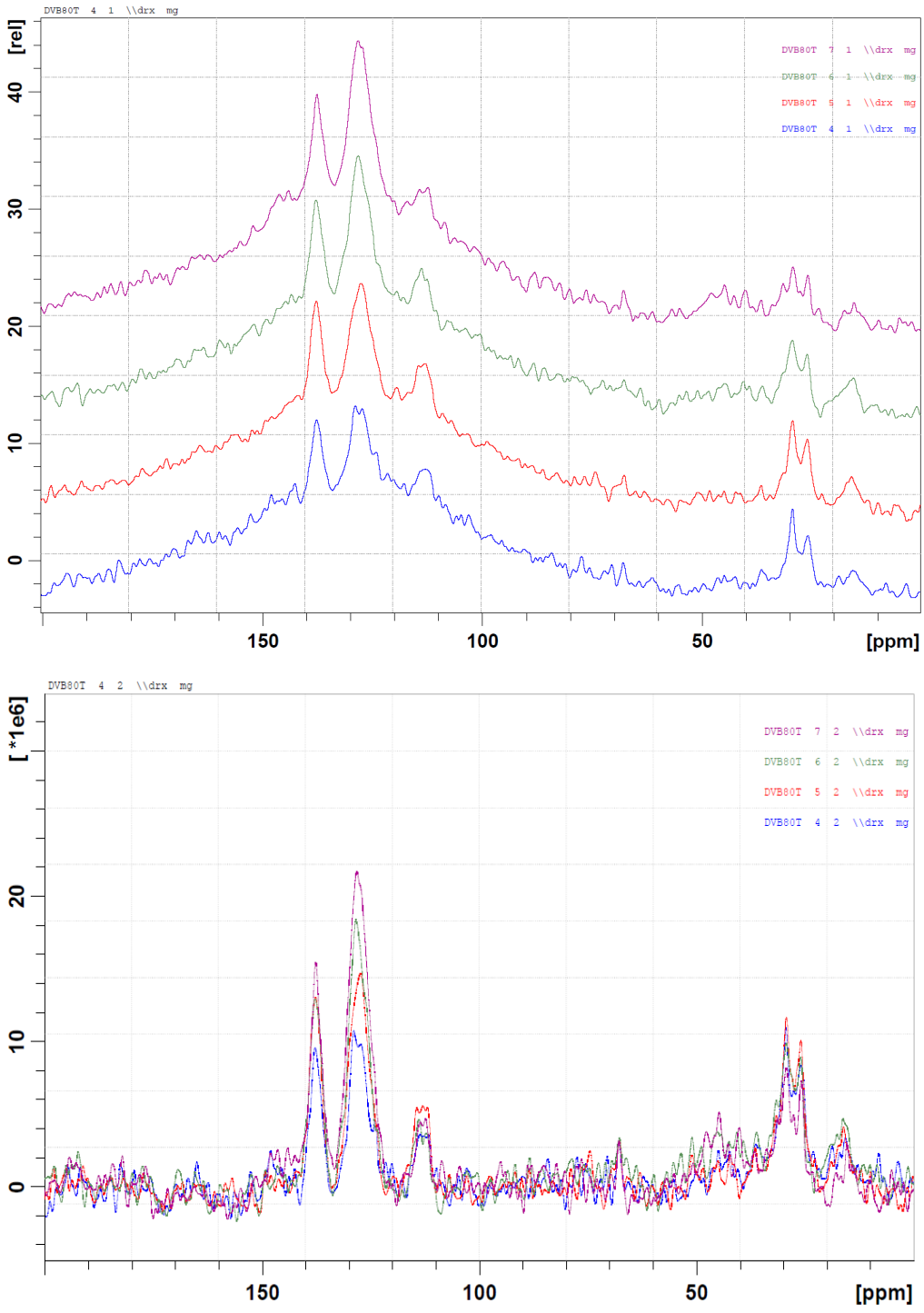

Figure S.8.7 Determining conditions for quantitative ^{13}C SPE-MAS spectra. Spectra shown in **Figure S.8.7** were recorded with relaxation delays ranging from 2 to 20 s. Due to limited sensitivity, no significant difference between spectra recorded with 10 and 20 s. However, after the background signal was recorded on another day, the background subtraction was done, yielding the spectra below

It is now obvious that there is a big difference in the signal C at ca 128 ppm between 10 and 20 s. Thus 10 s relaxation delay is not sufficient to record a quantitative ^{13}C SPE-MAS spectrum of PDVB80. As it would be too time-consuming to test various longer relaxation delays, it was decided to directly use a very long relaxation delay (60 s) and record the ^{13}C SPE-MAS spectra of PDVB80 and the background.

Table S.8.1 Full ^{13}C chemical shifts assignment

Complete ^{13}C chemical shifts assignment for ^{13}C NMR spectra of core, hydroxylated and PBA-grafted poly(divinyl benzene) microspheres. Chemical formulae are given in **Scheme 8.1**, letters refer to **Scheme 8.1**

Groups	Chemical shift / ppm	Assignment
L	13	CH_3 of side chain of PBA
G	16	CH_3 of ethyl on aromatic ring
K	20	CH_2 of side chain of PBA in α of CH_3
J	29-31	CH_2 of side chain of PBA adjacent to O-CH_2-
F	30	CH_2 from ethyl on aromatic ring
E	41-50	CH backbone PDVB and PBA CH_2 backbone PDVB and PBA CH_2 of ethyl-OH in α of aromatic ring (if OH in β of ring)
I	64	O-CH_2 of side chain of PBA
D	113	C=C (C not adjacent to aromatic ring)
C	128	benzene ring (not substituted) of PDVB or RAFT group
B	138	C=C (C adjacent to aromatic ring) aromatic ring (adjacent to C=C, or to ethyl-OH if OH in α of ring)
A	146	aromatic ring (adjacent to ethyl or backbone, or to ethyl-OH if OH in α of ring, or to C=S in RAFT group)
H	166	C=O of PBA

It was checked that the presence of 2 substituents in meta or para on the aromatic ring did not change the chemical shift of aromatic C to the point that they would come out in another massif observed by solid-state NMR. Note: the following signals were below the detection limit:

CH_3 of ethyl-OH (if OH in α of ring), expected at ca. 25 ppm

CH_2 of ethyl-OH in α of aromatic ring (if OH in β of ring), expected at ca. 63 ppm

CH from ethyl-OH (if OH in α of ring), expected at ca .70 ppm

C=S of RAFT group, expected at ca. 225 ppm

Discussion of the overestimation of AS by ^{13}C CP-MAS measurements

The active sites concentration measured by ^{13}C CP-MAS is overestimated, meaning that the signal intensity for the vinyl methylene carbons is overestimated with respect to that of the non-substituted aromatic carbons.

The ^{13}C CP-MAS experiment is divided in three parts: first the flip of the hydrogen magnetization to the xy-plane, then the transfer of the magnetization between ^{1}H and ^{13}C nuclei in the xy-plane *via* cross-polarization during a time T_{CP}, followed by the recording of the FID. During T_{CP}, polarization transfer is possible *via* heteronuclear dipole-dipole interactions since the ^{1}H spins are locked with an rf field $B_1{}^{1H}$, while the ^{13}C spins are irradiated with a different magnetic field $B_1{}^{13C} = 4 \cdot B_1{}^{1H}$, so that they finally have the same precession frequency $\omega^C = \gamma_C \cdot B_1{}^C = \gamma_H \cdot B_1{}^H = \omega^H$ in the locking fields (so-called Hartmann-Hahn conditions). During T_{CP}, both ^{1}H and ^{13}C loose magnetization (in the xy-plane) through $T_{1\rho}$ relaxation phenomena (corresponding to the relaxation under an applied radio-frequency field). Efficient magnetization transfer is possible only if the relaxation time constants $T_{1\rho}$ are higher than the time constant T_{CH} of the magnetization transfer. As the cross-polarization and the $T_{1\rho}$ relaxation of the ^{1}H nuclei are the fastest phenomena, the intensity $M_C(t)$ of the ^{13}C nuclei magnetization over time approximately follows the equation:

$$M_C(t) = M_0 \cdot e^{-t/T_{1\rho}} \cdot (1 - e^{-t/T_{CH}})$$

where M_0 is the initial ^1H magnetization, $T_{1\rho}$ the longitudinal relaxation time of ^1H nuclei under Hartmann-Hahn conditions, and $1/T_{CH}$ the magnetization transfer rate from ^1H to ^{13}C nuclei under Hartmann-Hahn conditions.[289]The intensity of the magnetization of a ^{13}C nucleus as a function of the contact time T_{CP} is sketched on the figure below (typical time constants are indicated):

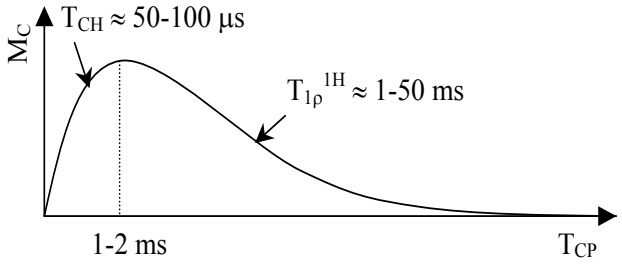

From these two time constants, T_{CH} and $T_{1\rho}$, we expect T_{CH} to contribute predominantly to the observed overestimation of the signal intensity for the vinyl methylene carbons with respect to that of the non-substituted aromatic carbons. First, $T_{1\rho}$ can be expected to be very similar for the vinyl proton sites and the aromatic protons, since the vinyl group is directly bound to the aromatic ring leading to a conjugation of the vinyl double bond and the aromatic ring, which excludes molecular motions with correlation times differing on a logarithmic scale needed to cause different $T_{1\rho}$ relaxation times. The shorter T_{CH} of the vinyl group can be attributed to the fact that the vinyl methylene carbons are bound to two ^1H nuclei each, while the non-substituted aromatic ones are bound to only one each. Moreover the shorter T_{CH} of the vinyl methylene group is supported by the experimental finding that the CP-MAS signal of this group build up fastest with short CP contact times, as shown in **Figure 8.3**, whereas all other signals need longer CP contact times to achieve contact time independent relative intensities.

Chapter 9 Facile and Direct Functionalization of Fullerenes with Polymeric Building Blocks *via* Diels-Alder Chemistry

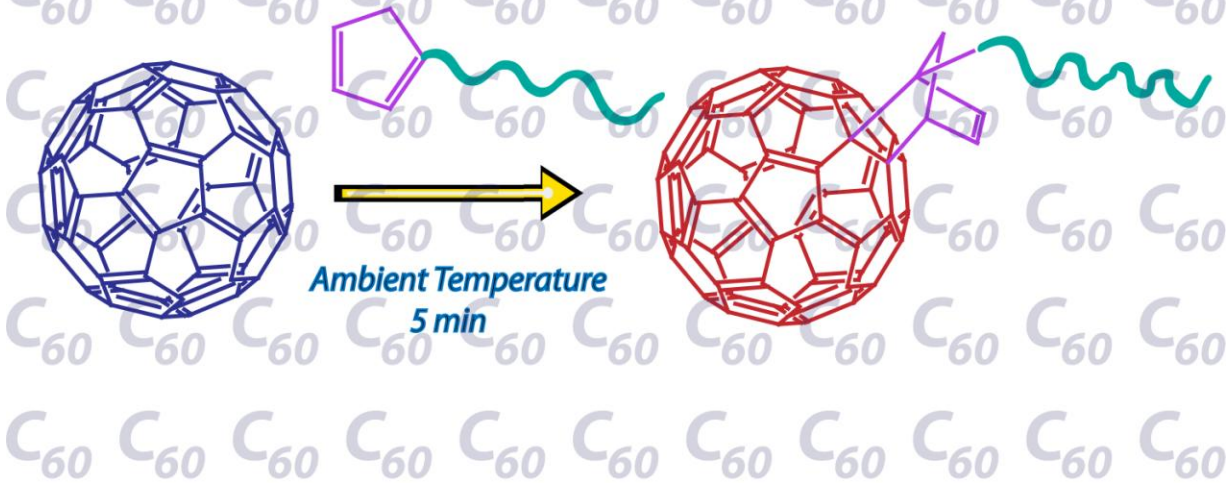

9.1 Introduction

In the previously discussed chapters, RAFT-HDA chemistry was utilized to functionalize a variety of surfaces, such as microspheres[14,28] and Si wafers.[27] In the current chapter, the functionalization of fullerenes *via* Diels-Alder chemistry is described. Fullerenes can undergo such reactions due to their electron deficient nature. The double bonds on the surface of the fullerenes functions as the 2π electron electrophile which readily undergo [4+2] cycloadditions with a variety of reactive dienes, including anthracene and cyclopentadiene.[210,211] To date, such cycloadditions have only being investigated using small ring systems while polymeric chains with akin end groups being overlooked completely. Recently, the synthesis of various cyclopentadienyl functionalized polymers *via* an ambient temperature methodology was reported.[168] In the present thesis, the facile (as well as in one case rapid and ambient temperature) functionalization of fullerenes with cyclopentadienyl and anthracenyl functionalized poly(ethylene glycol) using Diels-Alder cycloadditions is reported. The evidence for the successful modification of fullerenes is provided *via* a variety of techniques including size exclusion chromatography (SEC) coupled to electrospray ionization mass spectrometry (ESI-MS), UV-Vis spectroscopy and thermogravimetric analysis (TGA). SEC-ESI-MS is selected due to its ability to slice-by-slice analyze the product polymers, allowing for an elimination of ion suppression effects and access to higher charge states.

9.2 Experimental

9.2.1 Synthesis of Tosylated Poly(ethylene glycol) monomethylether (2)

NaOH (1.4 g) was dissolved in water (7.5 mL), solution of poly(ethylene glycol) monomethylether (5.0 g, 2.5 mmol) in 6.2 mL THF was subsequently added. The resulting mixture was cooled in an ice bath. A solution of *p*-toluenesulfonyl chloride (4.3 g, 2.2 mmol) in 6.2 mL THF was added. The mixture was stirred overnight at ambient temperature. The mixture was extracted with CH_2Cl_2 and the CH_2Cl_2 phase was washed three times with water. The CH_2Cl_2 phase was dried over $MgSO_4$, filtered and concentrated. The concentrated solution was precipitated in cold diethyl ether (4.5 g,

81% yield). M_n (NMR) = 2200 g·mol^{-1}. ^{1}H-NMR (400 MHz, $CDCl_3$, δ / ppm) (as shown in **Figure S.9.1** in the supporting information section): 2.45 (s, CH_3^a), 3.38 (s, CH_3^e), 3.63 (m, CH_2^d), 4.15 (t, $CH_2^{d'}$), 7.36 (m, $C_6H_5^b$), 7.81 (m., $C_6H_5^c$).

9.2.2 Synthesis of Cyclopentadienyl Functionalized Poly(ethylene glycol) monomethylether (3)

Tosylated poly(ethylene glycol) monomethylether (1.0 g, 0.45 mmol) was dissolved in anhydrous THF (5 mL) and cooled to 0 °C in an ice-salt bath. To this solution 3 equivalents sodium cyclopentadienide solution (2.0 M in THF) (0.7 mL, 1.36 mmol) were slowly added. The reaction solution was subsequently stirred overnight at ambient temperature, filtered through a pad of silica gel and washed with THF. The filterate was concentrated *in vacuo* and the polymer was precipitated in cold diethyl ether (0.7 g, 73% yield). The polymer was analyzed *via* SEC-ESI-MS (see **Figure 9.1** and **Figure S.9.2**).

9.2.3 Synthesis of C_{60} Functionalized Poly(ethylene glycol) monomethylether (4)

C_{60} (10 mg, 0.014 mmol) was dissolved in anhydrous toluene. To this solution was slowly added cyclopentadienyl functionalized poly(ethylene glycol) monomethylether (31 mg, 0.014 mmol) under a nitrogen atmosphere. As soon as the solution of cyclopentadienyl functionalized poly(ethylene glycol) monomethylether was added, the purple solution of C_{60} turned to reddish brown. The resulting mixture was stirred at ambient temperature for 5 min. After 5 min the solvent was removed *in vacuo* and the mixture was dissolved in THF to remove C_{60} which had not conjugated to polymer chains *via* centrifugation. The supernatant solution obtained after centrifugation was concentrated *in vacuo* and analyzed *via* SEC-ESI-MS (see **Figure 9.1** and **Figure S.9.3**).

9.2.4 Synthesis of Anthracenyl Functionalized Poly(ethylene glycol) monomethylether (6)

9-Chloromethylanthracene (**5**) (1.2 g, 5.34 mmol) of in 2 mL THF was added to a suspension of sodium hydride (0.5 g, 12.2 mmol) in 30 mL THF. After the addition of

poly(ethylene glycol) monomethylether (**1**) (5.3 g, 2.7 mmol) under nitrogen counter flow, the mixture was stirred overnight at ambient temperature. The mixture was washed with 20 mL aqueous ammonium chloride solution (1M) and the aqueous phase was extracted twice with chloroform. The polymer (**6**) was isolated from the organic phases by precipitation into cold diethylether (5 g, 84% yield). The resulting polymer was analyzed *via* SEC-ESI-MS (see **Figure 9.1** and **Figure S.9.4**).

9.2.5 Synthesis of C_{60} Functionalized Poly(ethylene glycol) monomethyl ether (7)

C_{60} (30 mg, 0.042 mmol) was dissolved in anhydrous toluene. To this solution was slowly added anthracenyl functionalized poly(ethylene glycol) monomethylether (**6**) (31 mg, 0.014 mmol) under a nitrogen atmosphere. The resulting mixture was stirred at 80 °C for 1.5 h. After 1.5 h the solvent was removed *in vacuo* and the mixture was dissolved in tetrahydrofuran to remove C_{60} which had not conjugated to polymer chains *via* centrifugation. The supernatant solution obtained after centrifugation was concentrated *in vacuo* and analyzed *via* SEC-ESI-MS (see **Figure 9.1** and **Figure S.9.5**).

9.3 Results and Discussion

In the following, the modification of fullerenes *via* PEGs featuring different diene end groups, which can react with the double bonds on the fullerene surface in [4+2] cycloadditions is described in detail. The polymers which have been used in the present study are cyclopentadienyl functionalized poly(ethylene glycol) (**3**) and anthracenyl functionalized poly(ethylene glycol) (**6**). These two types of diene (*i.e.* cyclopentadienyl and anthracenyl) functionalized polymers have been synthesized due their difference in reactivity when they function as dienes in a Diels-Alder reaction.[167]

Cyclopentadiene is a very reactive diene towards fullerenes in Diels-Alder reactions and usually the reactions of cyclopentadiene with suitable dienophiles progress rapidly and without the need of an external catalyst. Anthracene on the other hand is a less reactive diene and is only able to react with the dienophiles at elevated temperatures (however still in the absence of a catalyst).

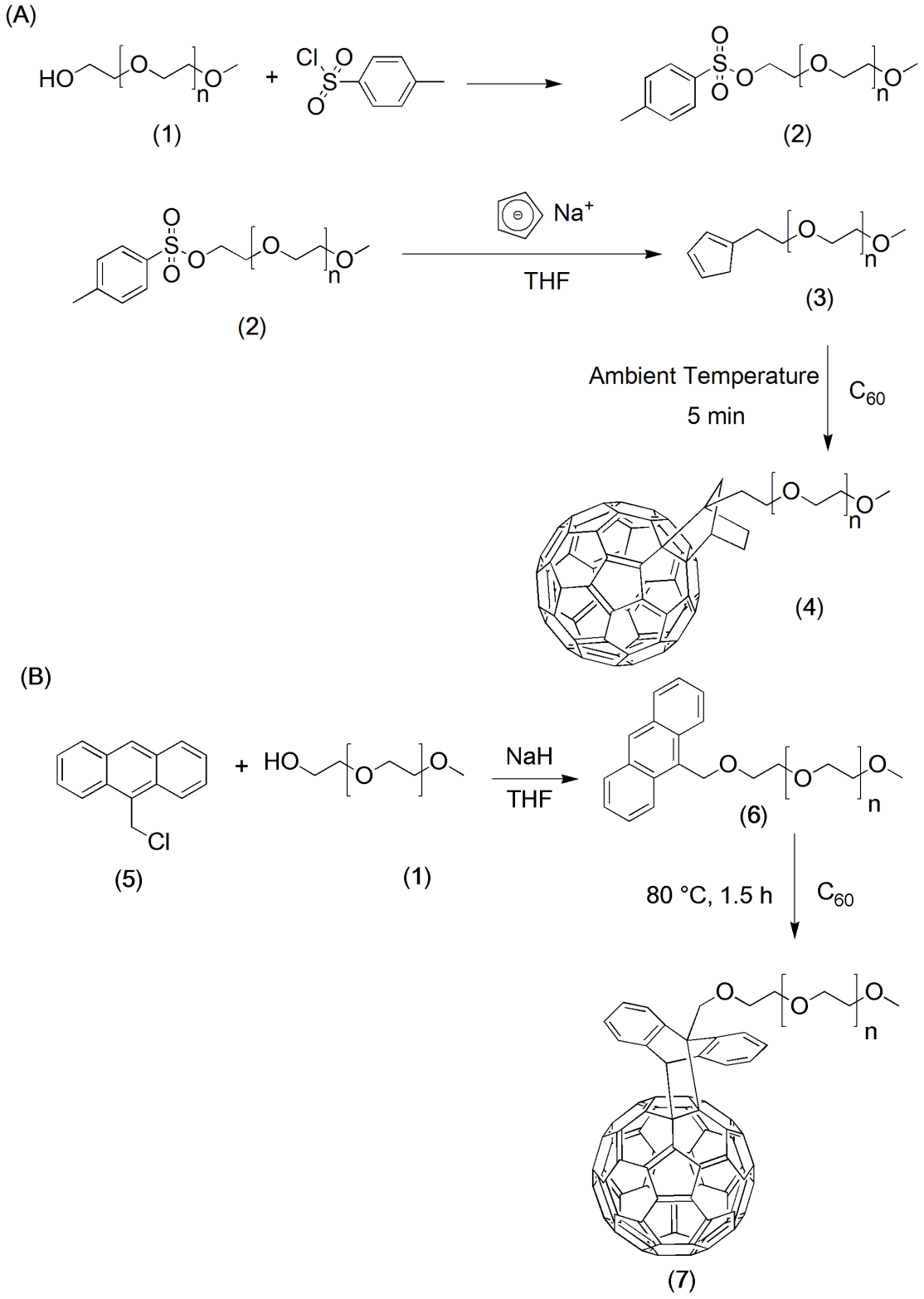

Scheme 9.1 Functionalization of fullerenes *via* two approaches: (A) cyclopentadienyl functionalized PEG (**3**) synthesized from tosylated PEG (**2**), which in turn is obtained *via*

reaction of PEG (**1**) with *p*-toluenesulfonyl chloride. (B) Anthracenyl functionalized PEG (**6**) synthesized *via* reaction of 9-chloromethylanthracene (**5**) and PEG (**1**)

Scheme 9.1 depicts the functionalization of C_{60} using the cyclopentadienyl functionalized poly(ethylene glycol) monomethylether (**3**), which is synthesized in a two step procedure. The first step involves tosylation of poly(ethylene glycol) monomethylether (**1**) to form the tosylated poly(ethylene glycol) monomethylether (**2**) followed by a nucleophilic substitution of the tosyl group with cyclopentadiene, resulting in the formation of cyclopentadienyl functionalized poly(ethylene glycol) monomethylether (**3**). The cyclopentadienyl functionalized poly(ethylene glycol) monomethylether (**3**) was subsequently used for the functionalization of fullerenes at ambient temperature within 5 min in the absence of a catalyst. In a similar fashion, fullerenes were reacted with anthracenyl functionalized PEG (**6**), which is obtained *via* the reaction of 9-chloromethylanthracene (**5**) with PEG (**1**). However, due to the difference in reactivity of the anthracenyl functionalized polymer compared to the cyclopentadienyl functionalized building block, the reaction with (**6**) was carried out at 80 °C for 1.5 h.

Evidence of the successful functionalization of fullerenes with (**3**) and (**6**) was obtained *via* several methods. An immediate indication of the success of the reaction can already be obtained by visual inspection of the reaction mixture. As observed previously by others, the unfunctionalized fullerenes exhibits a purple color in toluene, yet when fullerenes are functionalized the purple color changes to dark or reddish brown.[290] In our case too when fullerenes are reacted with the diene functionalized PEGs (**3**) or (**6**), the purple color of fullerenes changes to reddish brown. However, notable differences in the efficiency of the PEG functionalization of fullerenes with (**3**) and with (**6**) were found, which will be discussed below. For an in-depth assessment of the functionalization of fullerenes with the diene functional macromolecular building blocks, several characterization techniques such as, ESI-MS, UV-Visible spectroscopy and thermogravimetric analysis were utilized.

Figure 9.1 depicts the ESI-MS spectra of the reaction products resulting from the fullerene-polymer ligation reactions as described in **Scheme 9.1**, as well as the initial diene functional PEG polymeric building blocks. Inspection of **Figure 9.1** indicates that

the two starting PEG dienes (ESI-MS data sets (**A**) and (**C**)), almost entirely pure, with only very minor traces of side products visible. The full SEC-ESI-MS spectra of the starting materials (representing the entire elution volume) can be found in the supporting information section (**Figure S.9.2** (**3**) and **S.9.4** (**6**), respectively). In the reaction of the diene functionalized polymers (**3**) and (**6**) with fullerenes (ESI-MS data sets (**B**) and (**D**)), the main product peak – generated *via* the reaction of one double bond on the fullerene with the diene end group on the polymer – can be unambiguously assigned to the fullerene-PEG hybrids. The full product spectra (see **Figure S.9.3** (**4**) and **S.9.5** (**7**) in the supporting information section) show the individual double and triple charged distributions of the polymer conjugates, of which the double charged one is depicted in **Figure 9.1**. Inspection of spectra set (**B**) in conjugation with **Figure S.9.3** indicates a close to quantitative functionalization of the fullerenes with one Cp-PEG unit each (species (**4**)) as the peaks from the starting reactant Cp-PEG has almost completely disappeared.

Spectra set (**D**) corresponds to the product sub-distribution of the anthracenyl-PEG-C_{60} hybrids (**7**) in the overall SEC-ESI-MS spectrum depicted in **Figure S.9.5**. While there is no doubt that the fullerene mono-PEG adduct has been formed, the conversion rate remains significantly under that found in the PEG-Cp system, with unconverted amounts of (**6**) dominating the spectrum. Extended reaction times (up to 12 h) and variable reaction temperature (60 to 80 °C) did not increase the yields. Conducting the anthracenyl-PEG and C_{60} ligation reaction at ambient temperatures results in extremely low conversions (only trace amounts of conjugation product are visible in the SEC-ESI-MS spectra). Such an observation is consistent with earlier reports on non-polymeric anthracene reactions with C_{60}.[291] In the same context it is also noteworthy that at elevated temperatures significant retro Diels-Alder reactions may occur in the anthracene systems,[291] potentially lowering the functionalization yields. Thus, a reaction temperature of 80 °C with a reaction time of 1.5 h may constitute a compromise between the retro- and forward-DA reactions in the anthracene system.

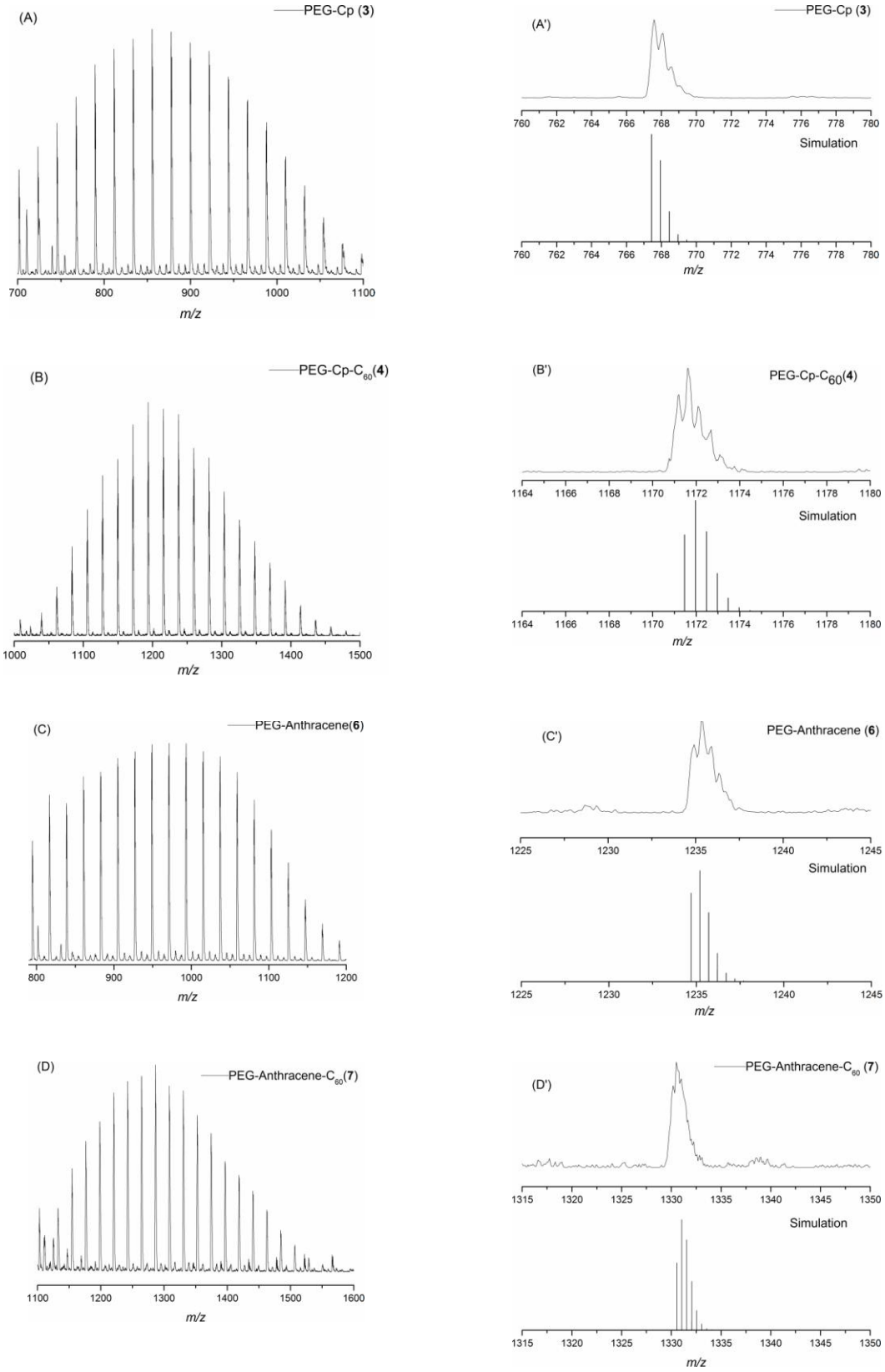

Figure 9.1 Experimental and theoretical ESI-MS spectra evidencing the ligation reaction. In the case of (D) the product region of the SEC-ESI-MS spectrum is depicted.

The full spectra can be viewed in the supporting information section. Note in addition that for reasons of consistency the double charged (z = 2) distributions are provided. For species (**3**) and (**6**) single charged distributions also exist (see **Figures S.9.2** and **S.9.4** as well as **Table 9.1**, respectively). (A) Cyclopentadienyl functionalized PEG (**3**); (A') expanded region for cyclopentadienyl functionalized PEG (**3**) and comparison with the associated simulated peak pattern; (B) C_{60} functionalized PEG (**4**); (B') expanded region for the C_{60} functionalized PEG (**4**) and comparison with simulated peak pattern; (C) anthracenyl functionalized PEG (**6**); (C') expanded region for the anthracenyl functionalized PEG (**6**) and comparison with the simulated peak pattern; (D) C_{60} functionalized PEG (**7**); (D') expanded region of the C_{60} functionalized PEG (**7**) and comparison with simulated peak pattern

The spectra provided in **Figure 9.1** have been further expanded in specific regions for the detailed assignment of the peaks. The individual peak assignments of the spectra are collated in **Table 9.1**, indicating excellent agreement between the experimental and theoretically expected values. In addition, the simulated isotopic peak patterns of all species (*i.e.* the macromolecular PEG building blocks as well as the C_{60}-PEG hybrids) are in excellent agreement with the experimentally observed isotopic peak patterns. Thus, the ESI-MS data unambiguously support the notion that conjugation – in the case of (**3**) to (**4**) in a quantitative fashion – of the PEGs with the fullerenes has occurred.

Further confirmation for the functionalization of C_{60} is achieved *via* UV-Vis spectroscopy. **Figure 9.2** shows the UV-Vis spectra of PEG-Cp (**3**) and anthracene-PEG (**6**) before and after ligation with C_{60}. The UV-Vis absorption spectra (see **Figure 9.2**) for the chloroform solution of hybrid PEG-Cp-C_{60} (**4**) as well as the building block PEG-Cp (**3**) differ in the presence of a band at 325 nm, which is a characteristic absorption for C_{60}.[292] For the anthracenyl-PEG, the anthracenyl-PEG before functionalization with C_{60} shows a characteristic five-finger absorbance from 300 to 400 nm as shown in **Figure 9.2**.[293] This characteristic absorbance for anthracene is not observed after the anthracenyl-PEG (**6**) has reacted with C_{60} while presence of new band at 320 nm (characteristic for the absorption for C_{60}) indicates that Diels-Alder reaction has

occurred. It appears that even non-quantitative conversion of (**6**) to (**7**) can suppress the characteristic anthracene UV-Vis absorptivity.

Table 9.1 Theoretical and experimental *m/z* values for the first peak in the isotopic pattern distribution of (**3**), (**4**), (**6**) and (**7**) of the peaks depicted in **Figure 9.1**. Note that some of the peaks provided are doubly charged species ($z = 2$) and that the agreement between the theoretical and experimental *m/z* values is of the same quality throughout the entire mass range. The table also provides selected theoretical and experimental *m/z* values for the single charged species of (**3**) and (**6**) to evidence the structural assignments

$m/z_{exp.}$	Ion Assignment	Molecular Formula	$m/z_{theo.}$	$\Delta m/z$
767.6	(**3**) (n=30)+2Na$^+$	$[C_{70}H_{136}O_{32}Na_2]^{++}$	767.4	0.2
1732.1	(**3**) (n=35)+Na$^+$	$[C_{80}H_{156}O_{37}Na]^+$	1732.0	0.1
1171.7	(**4**) (n=32)+2Na$^+$	$[C_{134}H_{144}O_{34}Na_2]^{++}$	1171.4	0.3
1234.8	(**6**) (n=49)+2Na$^+$	$[C_{116}H_{214}O_{51}Na_2]^{++}$	1234.7	0.1
1742.1	(**6**) (n=33)+Na$^+$	$[C_{84}H_{150}O_{35}Na]^+$	1742.0	0.1
1330.6	(**7**) (n=37)+2Na$^+$	$[C_{152}H_{166}O_{39}Na_2]^{++}$	1330.8	0.2

In addition, thermogravimetric analysis[294] (TGA) was employed for the analysis of the fully functional (see **Figure S.9.3** in supporting information section) C_{60}-PEG-Cp system (**4**) to confirm the quantitative functionalization of C_{60} with PEG-Cp. **Figure 9.3** depicts the results from TGA of PEG-Cp before and after reaction with C_{60}.

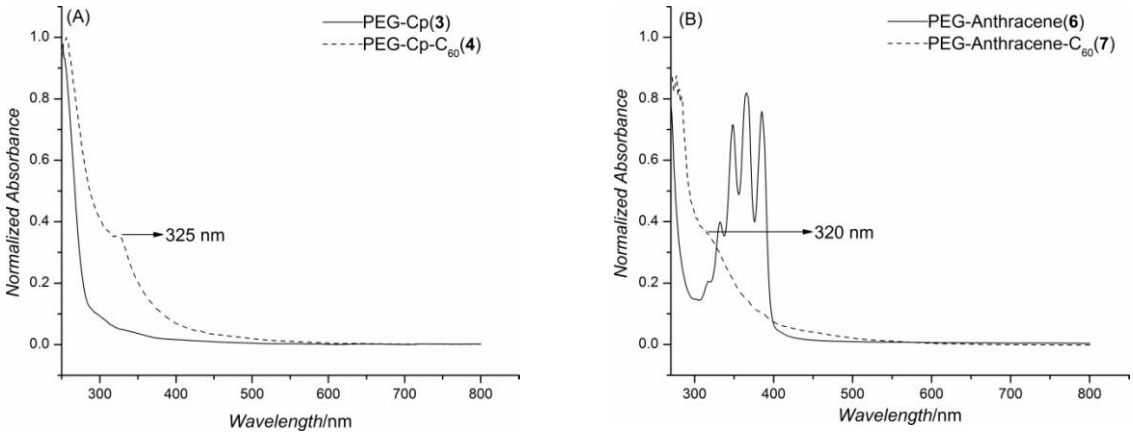

Figure 9.2 Comparison of UV-Vis absorption spectra for: (A) PEG-Cp (**3**) and PEG-Cp-C_{60} (**4**); (B) for anthracene-PEG (**6**) and anthracene-PEG-C_{60} (**7**)

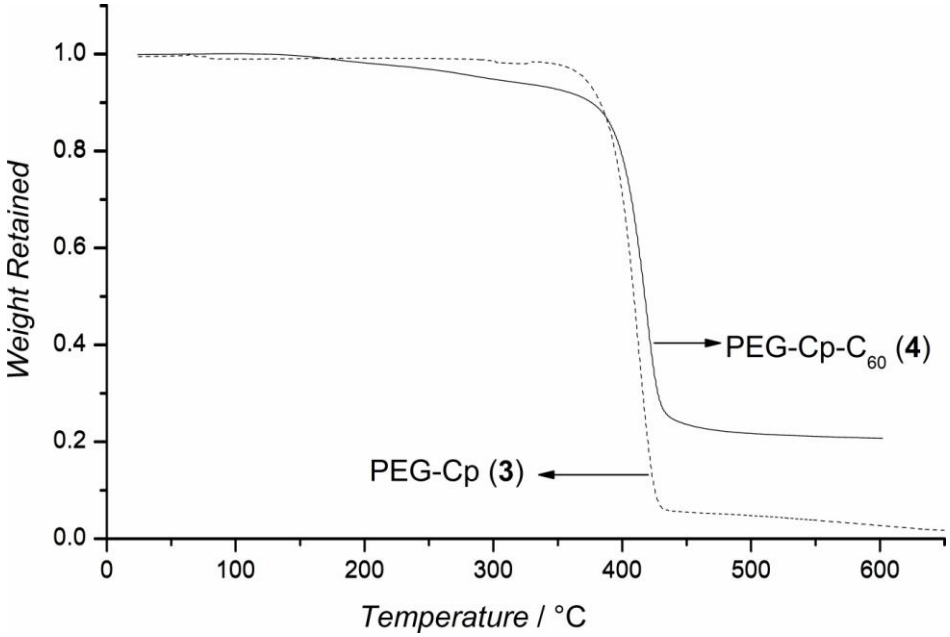

Figure 9.3 Thermogravimetric analysis of PEG-Cp (**3**) and PEG-Cp-C_{60} (**4**)

The TGA indicates the decomposition of the poly(ethylene glycol) component of (**4**) between 350 °C and 450 °C, which is confirmed by direct comparison with the TGA of the starting PEG-Cp (**3**) material. It is clear that the thermally stable material remaining beyond 450 °C corresponds to C_{60}, which undergoes minor weight loss up to 600 °C. The experimentally determined relative weight percents of each part (70±5% PEG and 30±5% C_{60}) are very close to the theoretical expected ones (68% PEG and 32% C_{60})

further confirming that each chain of PEG has selectively reacted *via* mono-addition of C_{60} as indicated by the SEC-ESI-MS experiments.

9.4 Conclusions

A direct and – in the case of Cp-PEG – quantitative, ambient temperature and extremely rapid synthesis of C_{60}-PEG hybrid materials has been presented. The structure of the obtained fullerene-PEG hybrids was unambiguously established *via* an ESI-MS analysis and underpinned by thermogravimetry as well as UV-Vis spectroscopy. This approach can potentially be expanded to a wide variety of Cp-capped polymers, which are easily accessible *via* our recently introduced ambient temperature route to Cp-functional polymers,[168] in which all polymers prepared *via* ATRP can be transformed into Cp-capped macromolecules. The fullerene functionalization can also be readily carried out *via* the use of anthracene capped PEGs, albeit at an increased reaction temperature (80 °C), prolonged reaction times (1.5 h) and reduced efficiency, however still in the absence of a catalyst. The fidelity (one PEG chain per fullerene) of the C_{60} functionalization for both the cyclopentadiene as well as anthracene approach is comparable and high.

9.5 Supporting Information

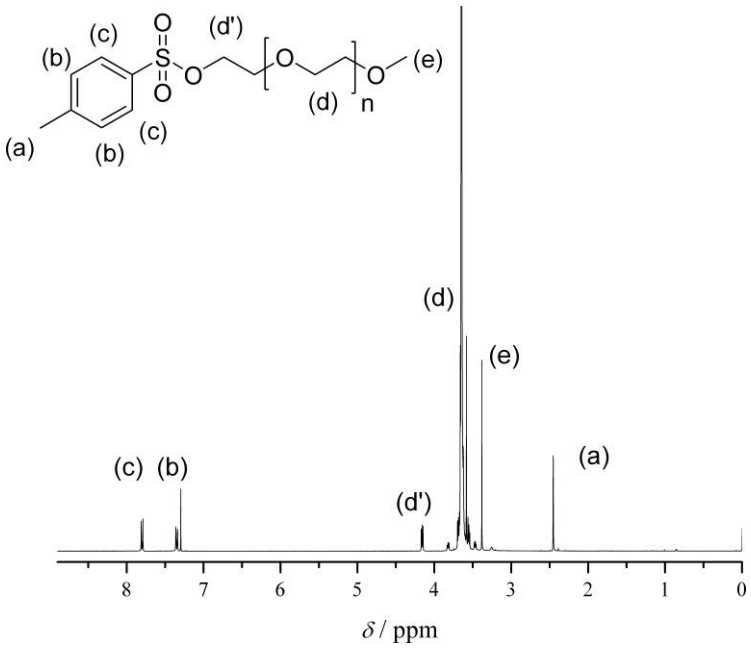

Figure S.9.1 ^{1}H NMR spectrum of tosylated poly(ethylene glycol) monomethylether (**2**) obtained by reaction of poly(ethylene glycol) monomethylether (**1**) and *p*-toluene sulfonyl chloride

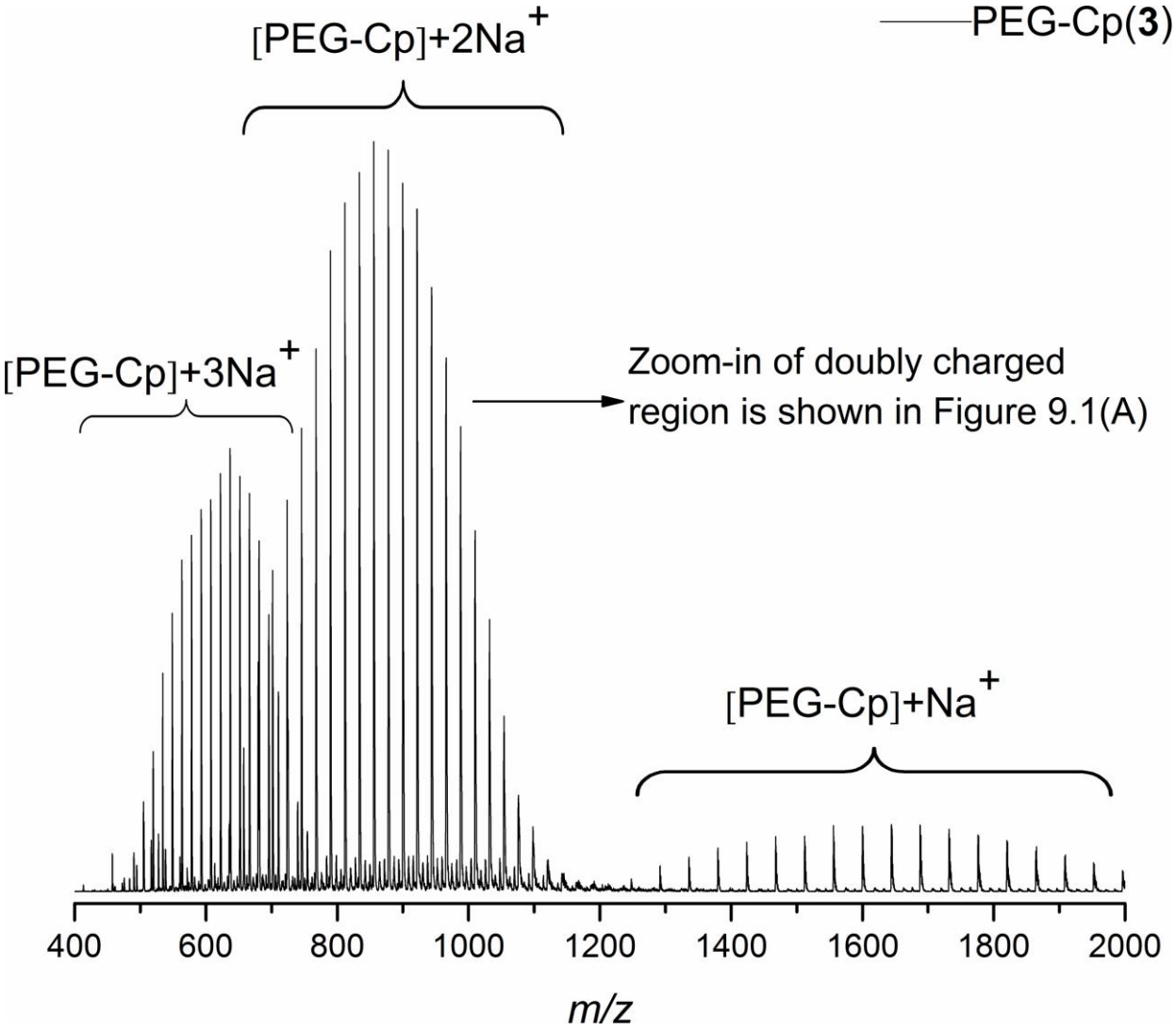

Figure S.9.2 Full SEC-ESI-MS (entire elution volume) spectra of cyclopentadienyl functionalized poly(ethylene glycol) (**3**)

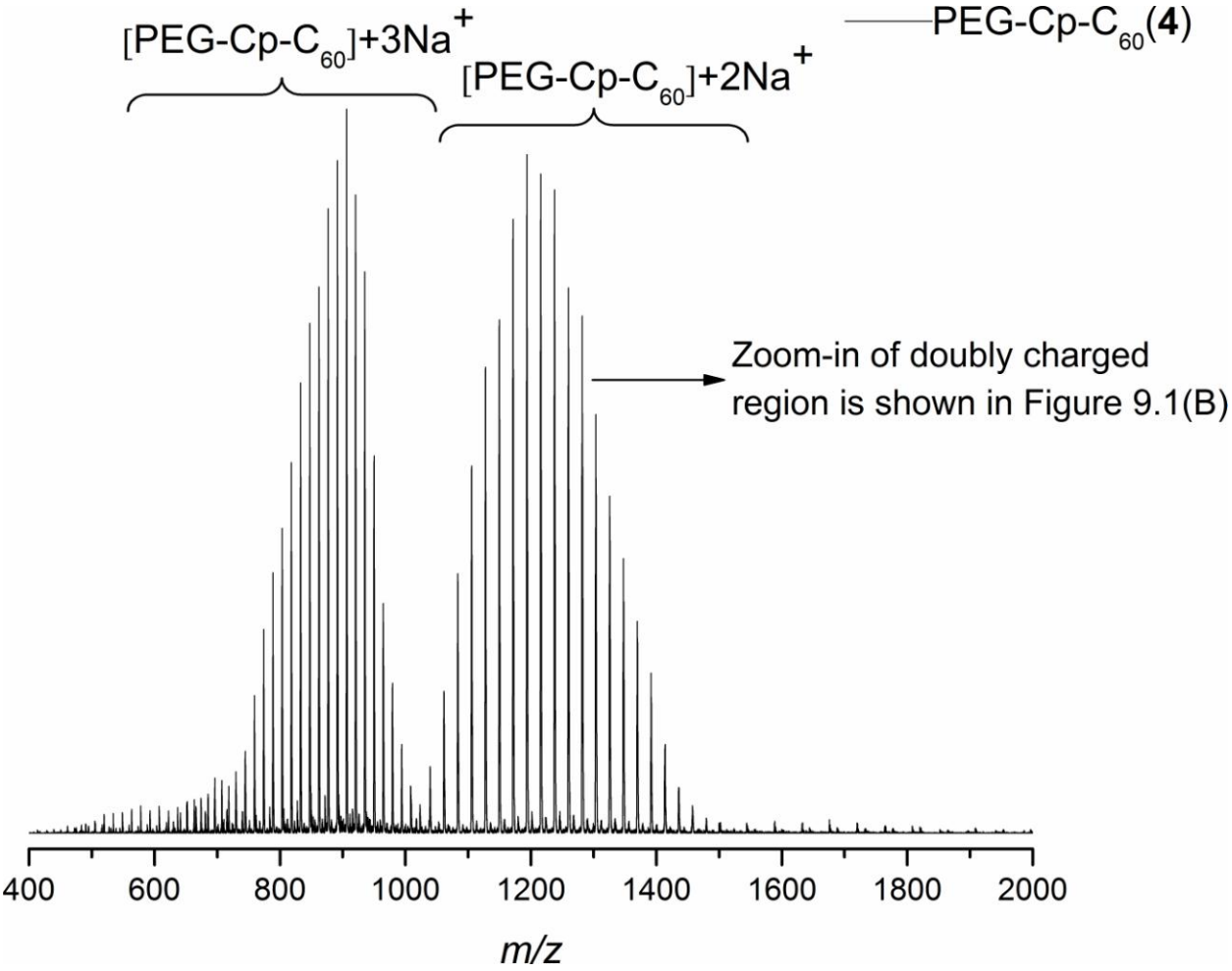

Figure S.9.3 Full SEC-ESI-MS (entire elution volume) spectra of C_{60} functionalized poly(ethylene glycol) (**4**)

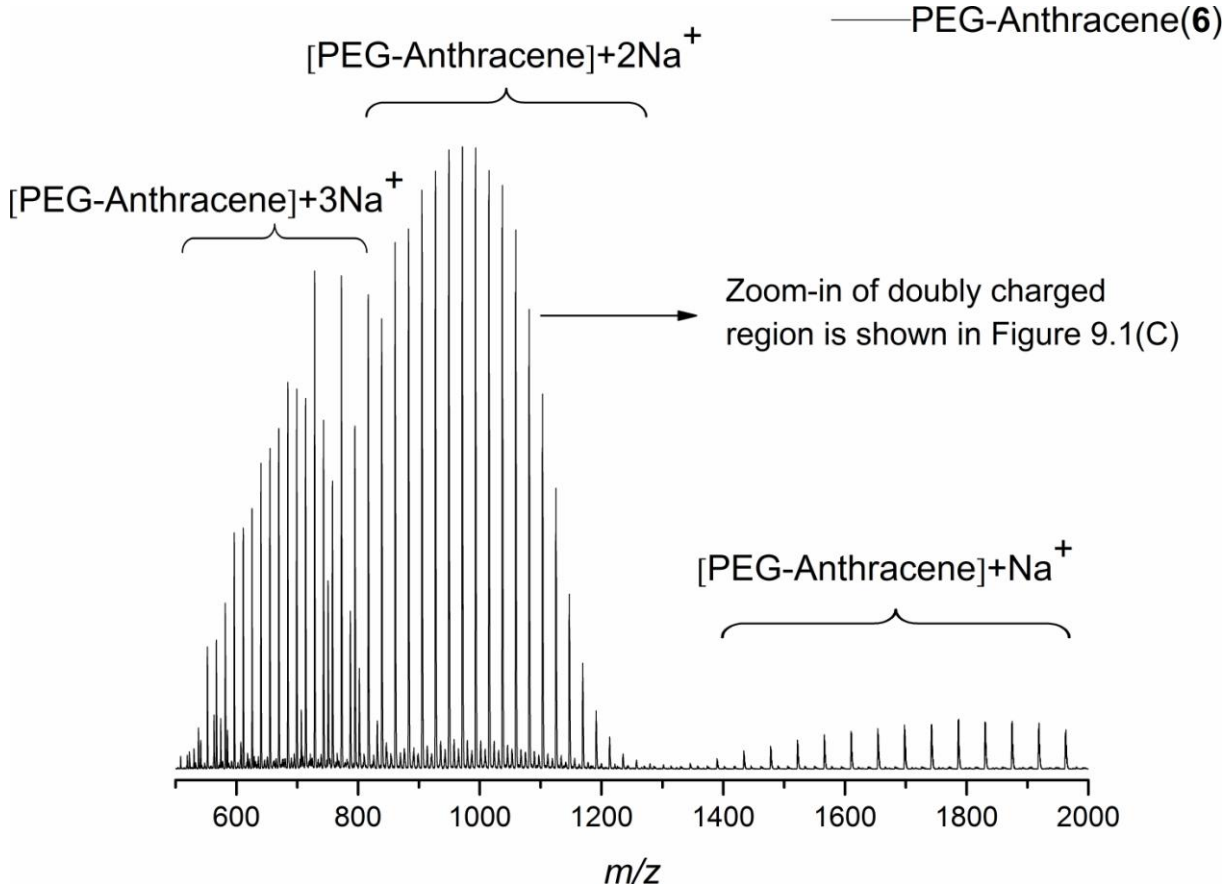

Figure S.9.4 Full SEC-ESI-MS (entire elution volume) spectra of anthracenyl functionalized poly(ethylene glycol) (**6**)

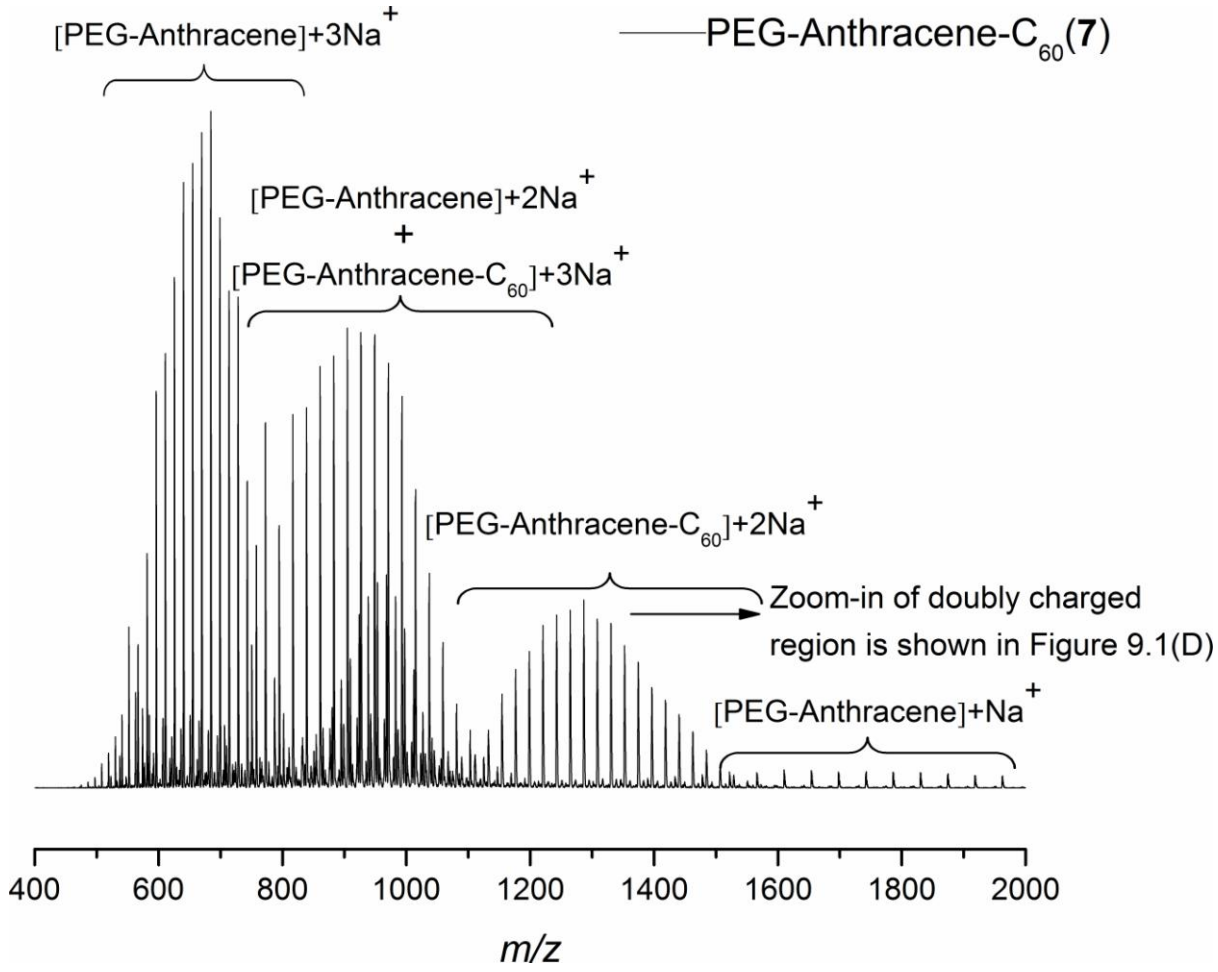

Figure S.9.5 Full SEC-ESI-MS (entire elution volume) spectra of C_{60} functionalized poly(ethylene glycol) (**7**)

Chapter 10 Rapid Bonding/Debonding on Demand: Reversibly Cross-Linked Functional Polymers *via* Hetero Diels-Alder Chemistry

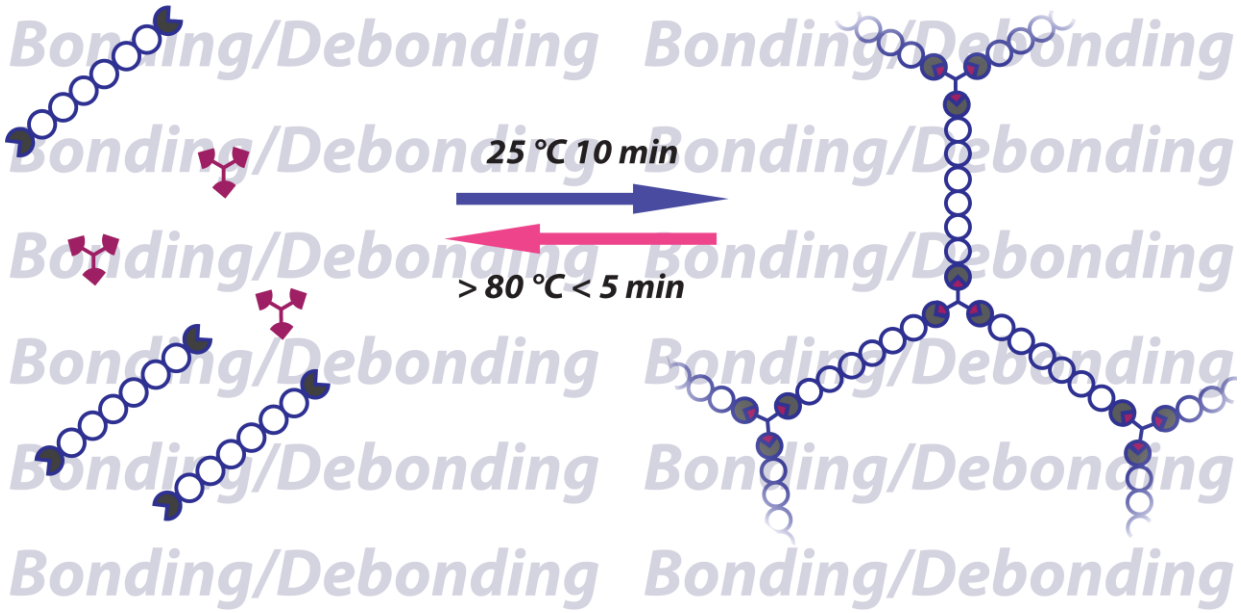

Note: The work presented in **Chapter 10** was carried out in collaboration with Andrew Inglis and will appear in the same format in his Ph.D thesis. The project was kindly supported by Evonik Industries.

10.1 Introduction

The design of reversibly linked and cross-linked polymeric materials that are able to change their physical characteristics rapidly, within a well-defined temperature interval and in a cyclic fashion, continues to be a highly investigated area in materials research.[295,296] What lies at the core of such research is the exploitation of reversible covalent bonds within a polymer network. To date, there has been a wealth of chemistries that have been investigated within this context, such as thiol-driven sulphide coupling,[297] photo-reversible olefin cycloadditions,[298] carbene dimerization,[299] nucleophilic addition of isocyanates with imidazoles and thermally cleavable alkoxyamines.[300] However, the most widely investigated technique by far has been Diels-Alder (DA) chemistry.[301-307] The use of DA cycloadditions (most specifically those between various maleimide and furan derivatives) in such technology has greatly been facilitated by both the commercial availability and chemical accessibility of such functional groups. To illustrate two very recent examples, low molecular weight star-shaped molecules were prepared by Aumsuwan and Urban[308] in which a maleimide-furan cycloadduct formed the linkage between the arms of the star and its core. From a variable-temperature ^{1}H NMR and ATR-IR spectroscopic analysis, the forward star-forming DA reaction was determined to proceed at 40 °C. The stars could subsequently be un-made through a 90 °C retro-DA reaction. In the other example, Syrett *et al.* synthesized maleimide- and furan-capped polymers *via* atom transfer radical polymerization (ATRP) which could be linked (60 °C, 24 h) and un-linked (110 °C, 24 h).[309]

A particularly rapid version of hetero-DA chemistry where a highly electron-deficient dithioester undergoes a [4+2] cycloaddition with cyclopentadiene (Cp) derivatives quantitatively within a few minutes under ambient conditions have recently reported.[310] The rapidity of the reaction has since been employed in the facile modular construction of block copolymers and in surface modifications.[14,27,146] Although the quantitative reversion of such chemistry by thermal treatment is already been explored,[310] it is with a recent report that its reversibility within the context of color switching in polymeric materials is investigated.[311]

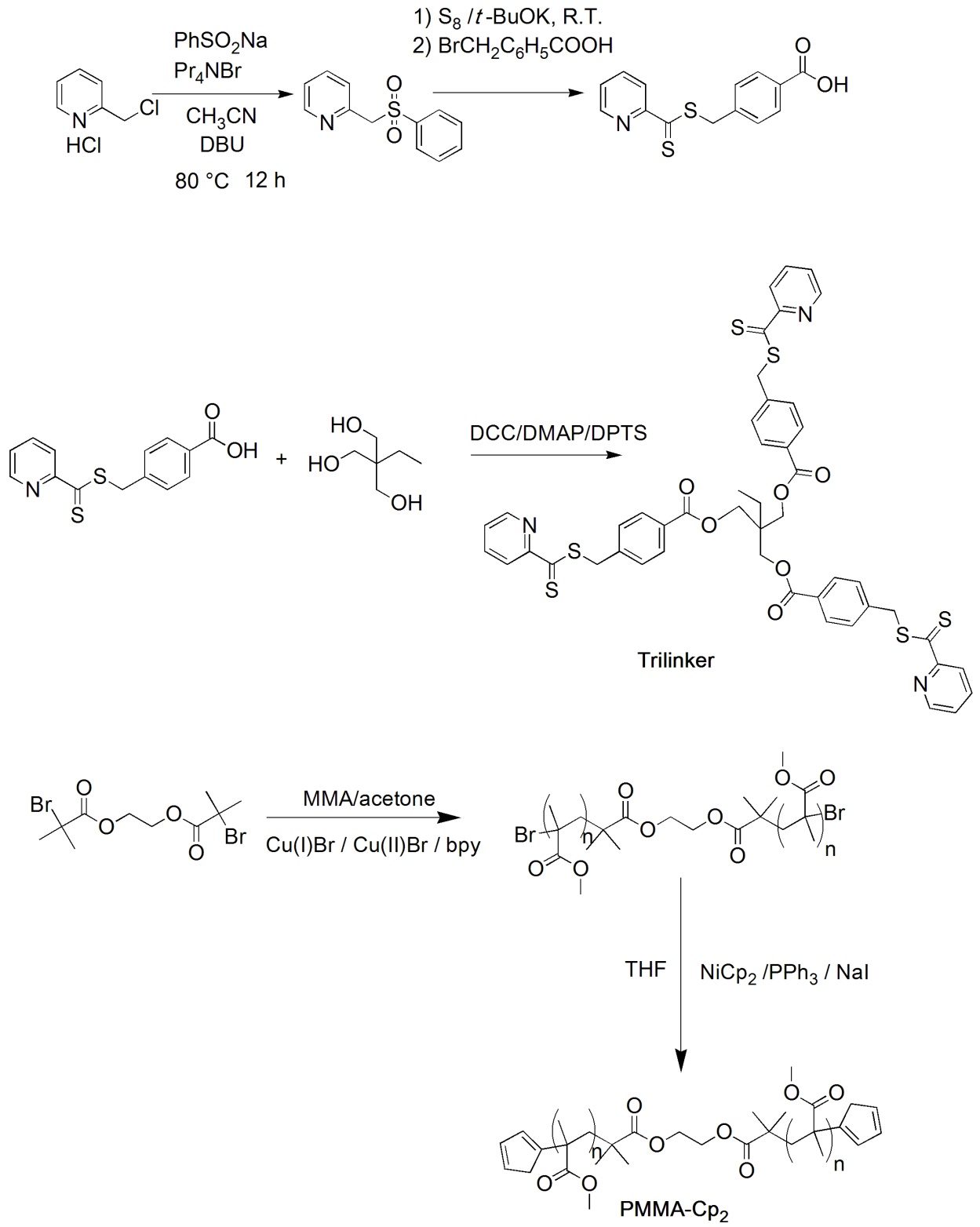

Scheme 10.1 Synthetic pathway to the Tri-linker (top) and α,ω-functional PMMA-Cp_2 (bottom), which are the two principal components in the bonding/debonding on demand

system. The α,ω-functionalization of the PMMA proceeds *via* recently reported nickelocene procedure

While the forward reaction is swift, the resulting cycloadducts are temperature stable up to a relatively moderate temperature range (60-90 °C), depending on the dithioester-Cp combination utilized. Beyond this temperature, an effective retro-DA reaction sets in, leading to a quantitative reformation of the starting materials. A characteristic of DA chemistry that renders it highly attractive in such technologies is the wide variety of diene-dienophile pairs that can potentially be utilized, which allows one to fine-tune the temperature profile in which bonding and debonding take place. To date, particularly ultra-rapid hetero-DA chemistry has not been reported in the preparation of reversible cross-linked polymeric structures. Thus, herein the synthesis of a novel poly(methyl methacrylate) (PMMA) chain bearing Cp functionality at both chain ends and a tri-functional pyridinyldithioformate linker molecule (see **Scheme 10.1**), which are able to rapidly and reversibly cross-link on demand within a highly accessible temperature range is reported.

10.2 Experimental

10.2.1 Synthesis of Bis(cyclopentadienyl) Poly(methyl methacrylate) (PMMA-Cp_2)

Methyl methacrylate (MMA), 1,2-bis(bromoisobutyryloxy)ethane (Initiator), copper (I) bromide (Cu(I)Br), copper (II) bromide (Cu(II)Br) and 2,2'-bipyridyl (bpy) were added to a round bottom flask in the ratio 50/1/0.105/0.0125/0.25. Acetone was subsequently added such that the resulting mixture was 50 vol.% acetone. Nitrogen was then bubbled through the mixture for 40 min to remove residual oxygen. The mixture was subsequently sealed under nitrogen and placed in a thermostated oil bath set to 50 °C. After 2 h, the polymerization was stopped by cooling the mixture in an ice-bath and exposure to oxygen. The mixture was then passed through a short column of neutral alumina to remove the copper catalyst. α,ω-functional poly(methyl methacrylate) (PMMA-Br_2) was isolated by two-fold precipitation in cold *n*-hexane. SEC (THF): M_n = 3500 g·mol^{-1}, *PDI* = 1.2.

According to our previously reported nickelocene Cp-functionalization procedure,[168] α,ω-functional PMMA-Br_2, sodium iodide, triphenylphosphine and nickelocene in the ratio 1/12/4/8 were dissolved, under nitrogen, in anhydrous THF such that the solution was 0.1 M with respect to the polymer. The ambient temperature reaction was allowed to proceed for at least 12 h at ambient temperature before the reaction mixture was passed through a short column of basic alumina. PMMA-Cp_2 was the isolated by a two-fold precipitation in cold *n*-hexane.

10.2.2 Synthesis of 4-((pyridine-2-carbonothioylthio)methyl) benzoic acid

STEP I: A mixture of 2-(chloromethyl)pyridine hydrochloride (1.64 g, 10 mmol), sodium phenylsulfinate (2.46 g, 15 mmol), and catalytic amount of tetrapropyl ammonium bromide (0.53 g, 2 mmol), DBU (1.52 g, 10 mmol) in CH_3CN (10 mL), was refluxed for 12 h. The solvent was subsequently removed under vacuum and the residue was dissolved in CH_2Cl_2, washed with brine, dried over $MgSO_4$ and the solvent removed. The crude product was obtained in quantitative yield, as a white solid and was used without purification in the next step.

STEP II: A mixture of sulfone (1.9 g, 8.51 mmol) (from Step I) and elemental sulfur (0.78 g, 24.3 mmol) was placed into THF (10 mL) under magnetic stirring. After addition of *t*-BuOK (2.72 g, 24.3 mmol), the color of the solution changed to dark brown. The reaction was stirred at ambient temperature for 12 h. Subsequently, 4-methylbenzoic acid (2.6 g, 12.15 mmol) in THF (10 mL) was added dropwise to the solution and stirring was continued for 5 h at ambient temperature. The color changed to reddish-pink. The product was washed with aqueous HCl (2N) and extracted in CH_2Cl_2. The crude product was finally purified by extraction with acetone.

^{1}H-NMR (DMSO-d_6, 400 MHz): δ / ppm = 4.63 (s, 2H, CH_2^d), 7.51-7.54 (m, 2H, $C_6H_5^c$), 7.67-7.71 (m, 1H, $C_5H_5N^f$), 7.87-7.91 (m, 2H, $C_5H_5N^e$), 7.95-8.26 (m, 2H, $C_6H_5^b$), 8.62-8.64 (m, 1H, $C_5H_5N^g$), 13.0 (s, 1H, -$COOH^a$). ^{13}C-NMR (DMSO-d_6, 100 MHz): δ / ppm = 40.1 (1C, CH_2^f), 121.89 (2C, $C_5H_5N^i$), 127.87 (2C, $C_6H_5^d$), 129.42 (2C, $C_6H_5^c$), 129.5 (1C, $C_6H_5^b$), 137.78 (1C, $C_5H_5N^j$), 140.67 (1C, $C_6H_5^e$), 148.34 (1C, $C_5H_5N^k$), 155.37 (1C, $C_5H_5N^h$), 166.94 (1C, C=O^a), 226.09 (1C, C=S^g). The ^{1}H and ^{13}C NMR spectra can be found in the supporting information section (**Figures S.10.1** and **S.10.2**).

10.2.3 Synthesis of the Trifunctional Linker

1,1,1-Tris(hydroxymethyl)propane (TMP) (0.072 g, 0.536 mmol), 4-(Dimethylamino)-pyridinium-4-toluene sulfonate (DPTS) (0.118 g, 0.402 mmol) and (dimethylamino)pyridine (DMAP) (0.025 g, 0.201 mmol) were dissolved in 10 mL of CH_2Cl_2. 4-((pyridine-2-carbonothioylthio)methyl) benzoic acid (0.581 g, 2.01 mmol) were dissolved in 3 mL of DMF and then added to the solution. After 10 min, dicyclohexylcarbodiimide (DCC) (0.622 g, 3.01 mmol) in 2 mL of dichloromethane was added to this solution. The reaction mixture was stirred overnight at ambient temperature. It was subsequently filtered, evaporated and the remaining product was purified by column chromatography over silica gel eluting with hexane/ethyl acetate (6:4) to obtain pure red solid tri-linker, yielding 0.301 g (59 %). ^{1}H NMR ($CDCl_3$, 250 MHz): δ / ppm = 8.61-8.59 (d, 3H, $C_5H_5N^a$), 8.32-8.29 (d, 3H, $C_5H_5N^d$), 7.94-7.91 (d, 6H, $C_6H_5{}^g$), 7.83-7.76 (m, 3H, $C_6H_5{}^b$), 7.50-7.47 (m, 3H, $C_6H_5{}^c$), 7.44-7.41 (d, 6H, $C_6H_5{}^f$), 4.57 (s, 6H, $CH_2{}^e$), 4.47 (s, 6H, $CH_2{}^h$), 1.79-1.70 (q, 2H, $CH_2{}^i$), 1.07-1.00 (t, 3H, $CH_3{}^j$). ^{13}C-NMR ($CDCl_3$, 100 MHz): δ / ppm = 6.6 (1C, $CH_3{}^a$), 22.76 (1C, $CH_2{}^b$), 24.59 (1C, C^c), 39.71 (3C, $CH_2{}^d$), 64.06 (3C, $CH_2{}^k$), 121.30 (6C, $C_5H_5N^n$), 125.89 (6C, $C_6H_5{}^h$), 128.47 (6C, $C_6H_5{}^g$), 128.86 (3C, $C_6H_5{}^f$), 135.99 (3C, $C_5H_5N^o$), 140.02 (3C, $C_6H_5{}^i$), 146.39 (3C, $C_5H_5N^p$), 155.14 (3C, $C_5H_5N^m$), 164.44 (3C, $C{=}O^e$), 226.09 (3C, $C{=}S^l$). ESI-MS+Na (*m*/*z*): theo. 970.12; exp. 970.08. The ^{1}H-NMR and MS spectra of the trilinker are depicted in **Figure 10.2**. The ^{13}C NMR spectrum can be found in the Supporting Information section (please refer to **Figure S.10.3**, which also contains the peak assignments).

10.2.4 Cross-linking (bonding) between PMMA-Cp_2 and Trifunctional Linker

PMMA-Cp_2 and trifunctional linker were mixed in 1:1 ratio with respect to functional groups in chloroform such that the concentration of polymer was 0.05 M. 1.5 equivalents of trifluoroacetic acid (TFA) was added and the resulting mixture shaken at ambient temperature for 10 min. The solvent was removed and the residue directly analysed by SEC prior to gelation.

10.2.5 De-cross-linking (Debonding) between PMMA-Cp_2 and Trifunctional Linker

The resulting cross-linked polymer was placed in toluene and heated to above 80 °C for 5 min. During this time, the colourless toluene turned pink in colour, indicative of the release of the trifunctional linker *via* a retro Diels-Alder cycloaddition and the polymer dissolved.

10.2.6 Re-Cross-Linking (Re-bonding) between PMMA-Cp_2 and Trifunctional Linker

The non-cross-linked polymer was dissolved in chloroform as described above and additional TFA added (1.5 equivalents). The solvent was removed within the space of 1 minute and the residue directly analysed by SEC prior to gelation.

10.2.7 Solid State Cross-linking

PMMA-Cp_2 and trifunctional linker were mixed in 1:1 ratio with respect to functional groups. Upon the addition of 1.5 equivalents of TFA, the mixture was thoroughly mixed with a mortar and pestle. Fully cross-linked (*i.e.* completely insoluble) material resulted within the space of seconds.

10.3 Results and Discussion

In the current study, reversibly cross-linked polymeric structures were generated utilizing rapid hetero Diels-Alder (HDA) chemistry. Unlike the majority of reports, in which maleimide and furan DA chemistry is used as the reversible linking mechanism, the present use of the highly reactive Cp moiety and pyridinyldithioformate allows for facile ambient temperature conjugations to be performed within the space of several minutes at ambient temperatures rather than several hours at elevated temperatures. Herein, α,ω-Cp-functional PMMA is reversibly and rapidly cross-linked by reaction with a tri-pyridinyldithioformate functional linker molecule.

Bis(cyclopentadienyl) poly(methyl methacrylate) (PMMA-Cp_2) was synthesized from the corresponding dibromo precursor. Dibromo poly(methyl methacrylate) (PMMA-Br_2) was obtained *via* ATRP of methyl methacrylate using the difunctional initiator 1,2-bis(bromoisobutryloxy)ethane. Subsequently, the PMMA-Br_2 was transformed into the targeted PMMA-Cp_2 *via* nucleophilic substitution of the bromide moieties with

cyclopentadienyl moieties *via* facile and recently reported nickelocene pathway.[168] The quantitative conversion of PMMA-Br_2 into PMMA-Cp_2 was monitored *via* ESI-MS, which is a very convenient technique in determining low molecular weight polymer end-group functionalization. **Figure 10.1** depicts the comparison of the ESI-MS spectra of the starting PMMA-Br_2 and PMMA-Cp_2.

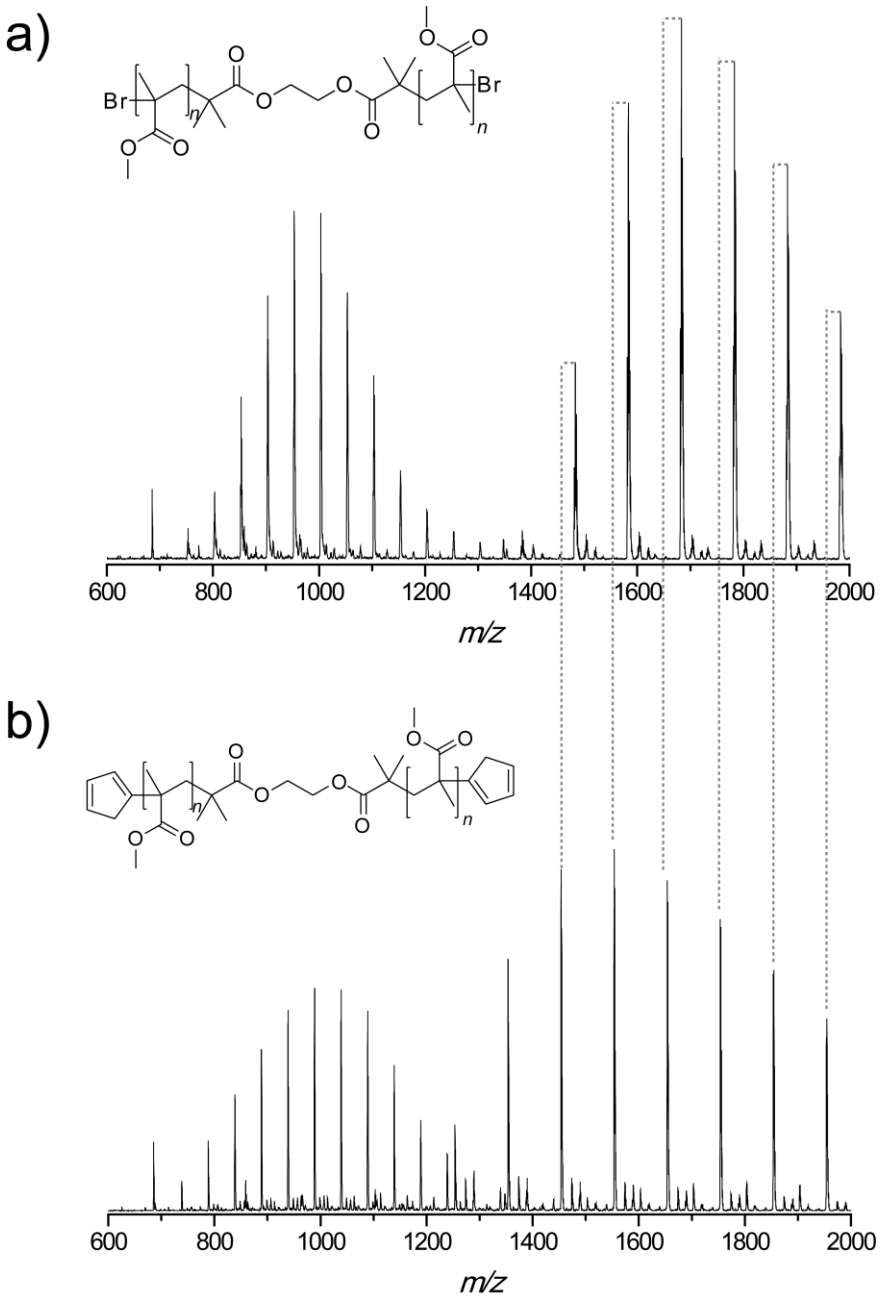

Figure 10.1 ESI-MS spectra of the starting α,ω-functional PMMA-Br_2 (a) and the corresponding α,ω-functional PMMA-Cp_2 (b). Note that both a single and double

charged distribution of the polymeric materials are visible. Minor impurities due to side products formed in the ATRP process (bimolecular termination and elimination) are visible

As can be observed, a shift of the dominant series of signals to lower *m/z* values is complete and consistent with the targeted transformation. All minor species, which are associated with various minor by-products of the ATRP process such as bimolecular coupling and elimination species, are carried through the substitution process. A comparison of the experimentally observed and the theoretically calculated *m/z* values for the dominant series is presented in **Table S.10.1** in the Supporting Information.

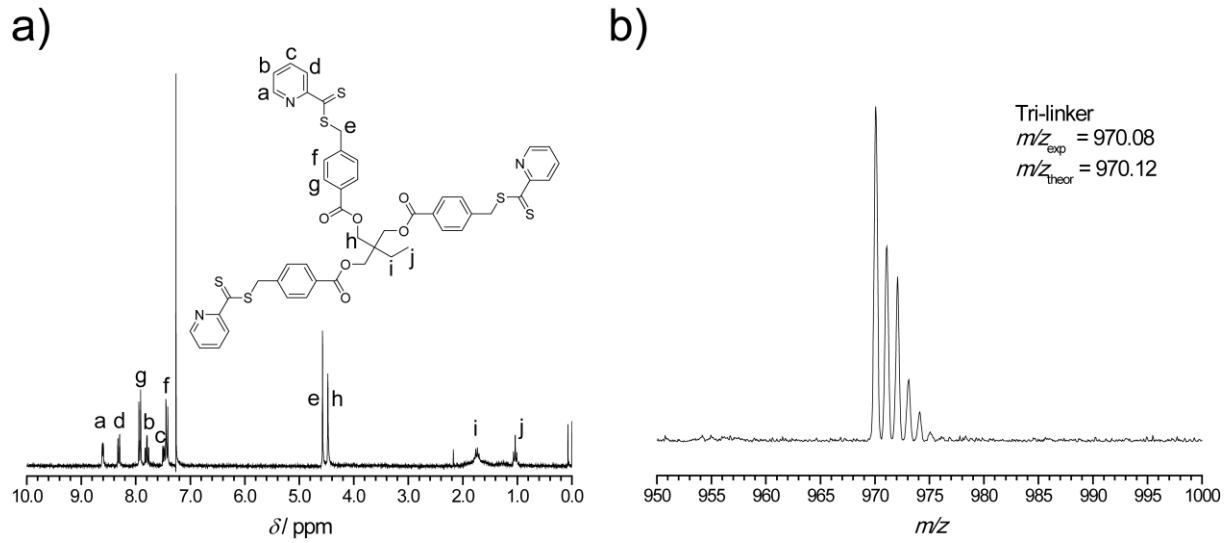

Figure 10.2 ^{1}H NMR spectrum (a) and ESI-MS spectrum (b) of the Tri-linker. The ^{13}C NMR spectrum of the Tri-linker can be found in the supporting information section (see **Figure S.10.3**)

The dienophilic tri-functional linker is based upon the dithioester molecule 4-((pyridine-2-carbonothioylthio)methyl) benzoic acid, the synthesis of which has been appropriated from a two step procedure reported in the literature.[312] In the first step, commercially available 2-(chloromethyl)pyridine hydrochloride is transformed into the corresponding sulfone by reaction with sodium phenylsulfinate in the presence of DBU and tetrapropyl ammonium bromide. The targeted sulfone was isolated in quantitative

yields and used without further purification for the next step. The second step was carried out by reacting the above sulfone with sulfur (S_8) in the presence of potassium *tert*-butoxide and subsequent alkylation with 4-methylbenzoic acid yielded the desired 4-((pyridine-2-carbonothioylthio)methyl) benzoic acid. The ^{1}H and ^{13}C NMR of 4-((pyridine-2-carbonothioylthio)methyl) benzoic acid are shown in **Figure S.10.1** and **S.10.2** in the supporting information section. The tri-functional linker was obtained *via* esterification of 1,1,1-tris(hydroxymethyl)propane with 4-((pyridine-2-carbonothioylthio)methyl)) benzoic acid in the presence of DCC, 4-(dimethylamino)-pyridinium-4-toluene sulfonate (DPTS) and DMAP. The tri-functional linker was purified *via* column chromatography and the purity was determined by ^{1}H NMR spectroscopy and ESI-MS (**Figure 10.2**).

In order to generate cross-linked structures under ambient conditions, the tri-linker core was reacted with PMMA-Cp_2 in a 1:1 ratio with respect to functional groups using chloroform as the solvent and TFA as a catalyst. Within a maximum time frame of 30 min at ambient temperatures completely cross-linked structures were synthesized, as indicated by their lack of solubility. When the cross-linking reaction was performed in the solid state, fully cross-linked material was formed within the space of seconds. Therefore, in order to perform an SEC analysis to visualize the changes in molecular weight that occur, the crude reaction mixtures were quickly diluted with THF prior to the gel point (< 10 min) and directly analyzed. **Figure 10.3**a depicts the SEC distribution of the starting tri-functional linker and PMMA-Cp_2 having a molecular weight of 3500 $g \cdot mol^{-1}$ and 990 $g \cdot mol^{-1}$, respectively. After a reaction time of 10 min, the molecular weight of the system markedly increases to 12 700 $g \cdot mol^{-1}$. It is also noted that the polydispersity of the system increases from 1.21 to 2.57. Both of these observations are indicative of the progression of rapid cross-linking reactions. Aside from the rapid nature of the above cycloadditions, another advantage of the use of the reactive Cp moiety is the reduction in temperature at which the retro-HDA reaction occurs. In previous investigations, open-chain dienes were utilized, the HDA adducts of which underwent reversion at temperatures exceeding 120 °C. At such temperatures, the liberated dithioesters readily decompose which precludes such systems to be used in a continually reversible fashion. In the present study, the retro or debonding reactions

were performed at temperatures between 80 and 100 °C. Referring back to **Figure 10.3**a, it is noted that heating the highly cross-linked structure for no more than 5 min at > 80 °C results in debonding taking place. One can clearly observe not only the reduction in molecular weight of the system (M_n = 3800 g·mol^{-1}), but also an increase in the signal representing the tri-linker molecule, indicating its release into solution. The final part of **Figure 10.3**a depicts an attempt at rebonding the above debonded sample. The debonded polymer/tri-linker mixture was dissolved in fresh chloroform and a catalytic amount of TFA added. Analysis of the reaction mixture *via* SEC reveals that an increase in molecular weight (10 200 g·mol^{-1}) and polydispersity (2.14) occurred, thus confirming the ability of the system to bond, debond and rebond on demand. The system is graphically depicted in **Figure 10.3**b. Furthermore, the molecular weight data for the above study is included in **Table 10.1**.

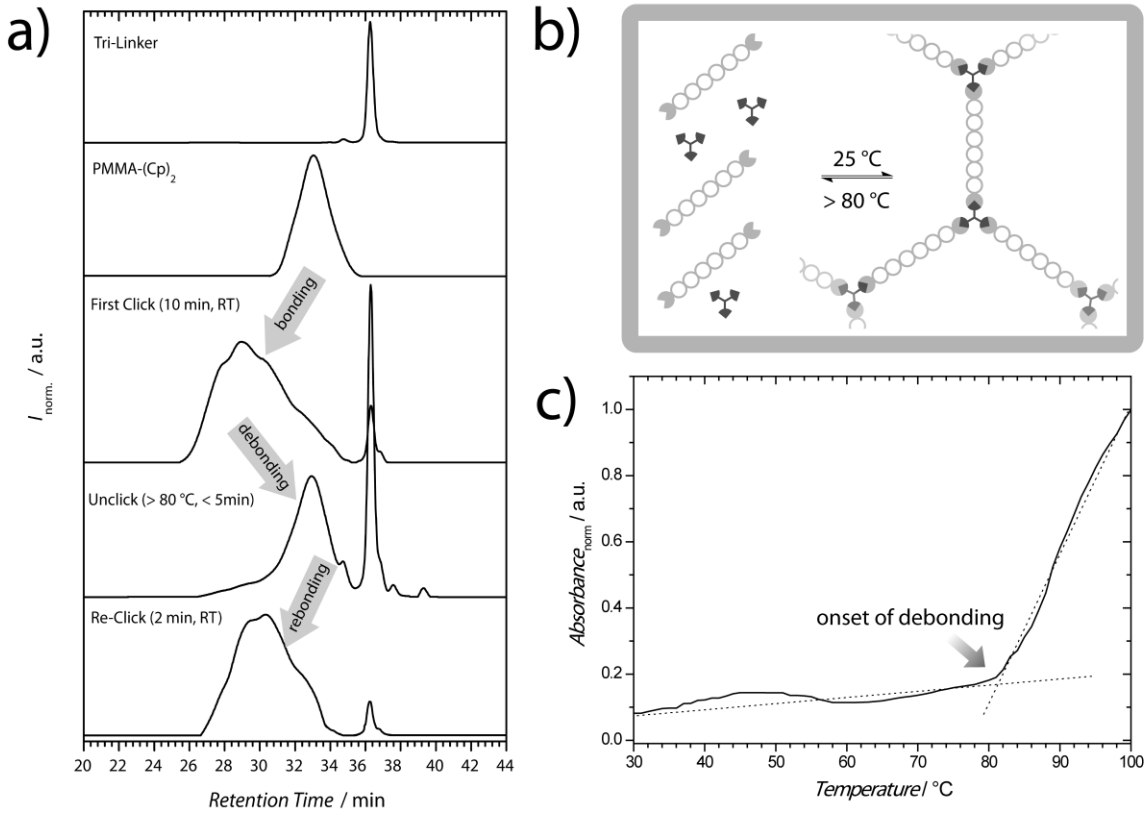

Figure 10.3 (a) Visualizing the changes in molecular weight in the cross-linking system by SEC; (b) Graphical representation of the bonding/debonding on demand, which

occurs within minutes in either direction, (c) UV-Vis monitoring of the onset of debonding (*i.e.* the reaction solution becomes colored again) at close to 80 °C, absorption was measured in toluene solution (3 mg·mL^{-1}) at a wavelength of 522 nm at temperatures ranging from 30 to 100 °C (using a 0.5 °C·min^{-1} heating rate)

Table 10.1 Characterization of the bonded and debonded polymer systems, demonstrating the switching behavior both in the observed molecular weight as well as the polydispersity index

Polymer	$M_{n,\,SEC}$/g·mol^{-1}	*PDI*
PMMA-Cp_2	3500	1.20
Bond	12700	2.57
De-Bond	3800	1.26
Bond	10200	2.14

The onset of debonding was also monitored *via* UV-Vis spectroscopy. In an initial qualitative trial, fully crosslinked material was suspended in toluene. Upon heating with a hand-held heat gun, the material gradually dissolved and the toluene solution turned pink, indicating the release of the starting tri-linker molecule. Performing the same reaction quantitatively inside a UV-Vis spectrophotometer allowed for the absorbance of the solution to be monitored as a function of temperature. **Figure 10.3**c depicts the results of such an analysis and it is observed that a sharp increase in the absorbance of the system occurs at around 80 °C (the solution returns the color of the dithioester), corresponding to the rapid onset of debonding.

10.4 Conclusions

The reversibility of rapid HDA reactions has been exploited for the generation of a highly reversibly stimuli-responsive cross-linked polymeric network. The ambient

temperature cross-linking of PMMA (bonding) could be reversed upon thermal treatment (debonding) and subsequently reformed (rebonding) again at ambient temperature. The provision and continued development of such systems will ultimately lead to significant advances in such fields as coatings, adhesives and self-healing polymeric materials.

10.5 Supporting Information

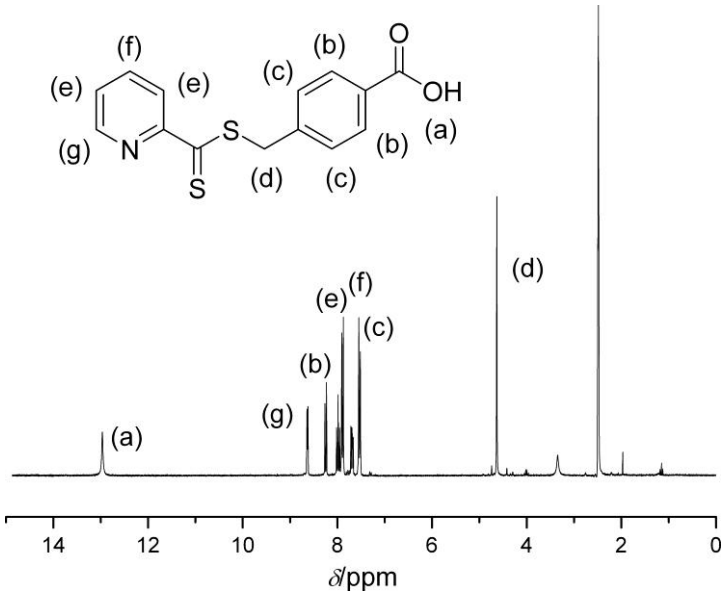

Figure S.10.1 ^{1}H NMR spectrum of 4-((pyridine-2-carbonothioylthio)methyl) benzoic acid (in DMSO-d_6 as NMR solvent). Note that the peak at 2.54 is associated with the DMSO solvent and the minor (broad) absorbance at 3.33 is caused by water

Table S.10.1 Experimental and theoretical values for a representative peak in the ESI-MS spectra of α,ω-functional PMMA-Br_2 and α,ω -functional PMMA-Cp_2 (refer to **Figure 10.1**)

$m/z^{exp.}$	Ion assignment	Formula	$m/z^{theo.}$	$\Delta m/z$
1481.2	PMMA-Br_2 [n = 11] + Na^+	$[C_{65}H_{104}Br_2O_{26}Na]^+$	1481.5	0.3
1453.6	PMMA-Cp_2 [n = 11] + Na^+	$[C_{75}H_{114}O_{26}Na]^+$	1453.7	0.1

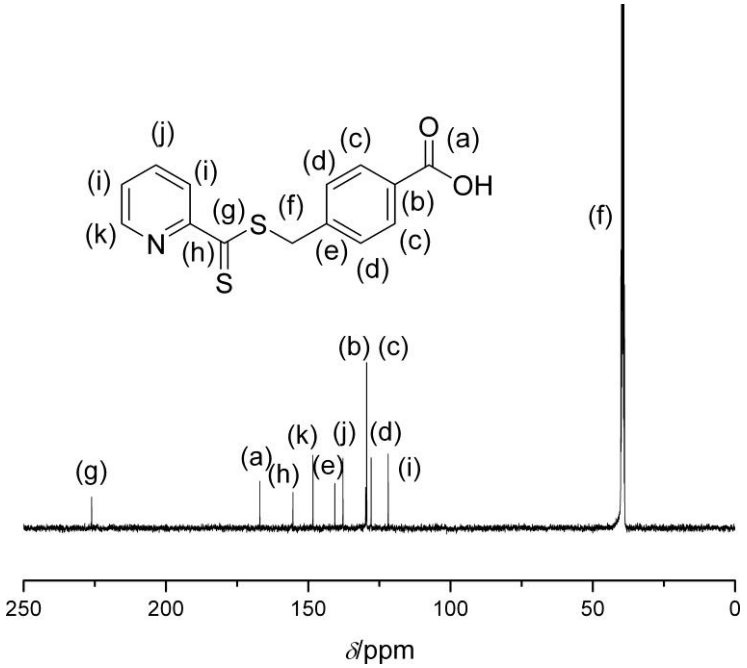

Figure S.10.2 ^{13}C NMR spectrum of 4-((pyridine-2-carbonothioylthio)methyl) benzoic acid (in DMSO-d_6 as NMR solvent)

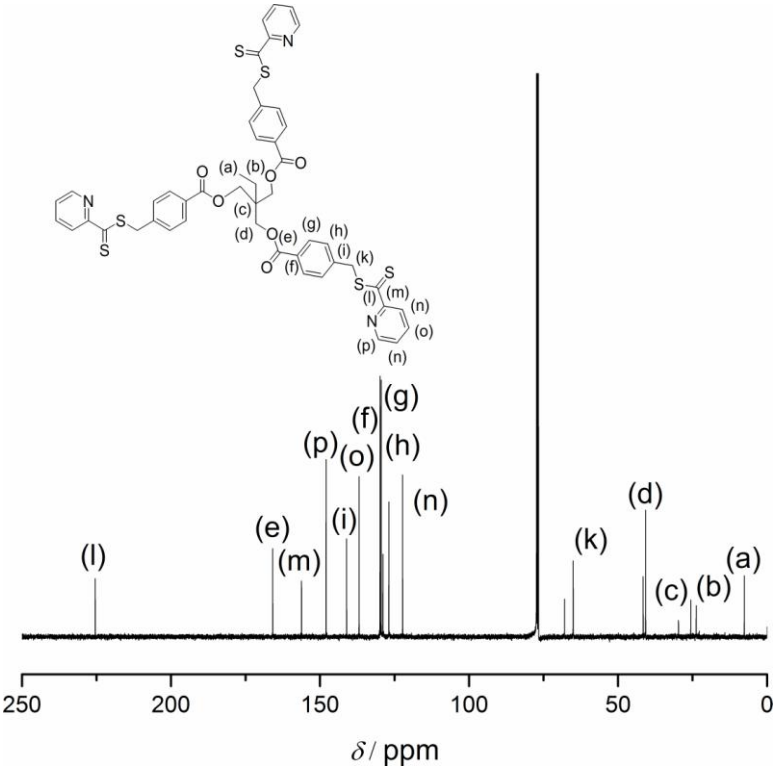

Figure S.10.3 ^{13}C NMR spectrum of the trifunctional linker recorded in $CDCl_3$

Concluding Remarks

In the present thesis, RAFT-HDA chemistry was explored as an efficient conjugation technique to modify a variety of solid substrates. It is clear that very significant progress has been made in our ability to effectively modify surfaces employing the highly orthogonal RAFT-HDA approach. Nevertheless, specific areas need further attention to bring these promising methodologies to fruition in real-life applications. It seems to be a matter of priority to enable the attachment of biomolecules as well as stimuli responsive polymers to micro- and nano-particles that can be employed as drug and gene delivery vectors using RAFT-HDA chemistry. Similarly, it would be desirable to have straight forward modification procedures based on RAFT-HDA chemistry that allow for the facile alteration of surfaces in areas such as filtration membranes (to prevent biofouling) as well as the attachment of growth factors to tissue engineering polymeric materials to enhance wound healing processes and tissue regeneration.

A further interesting field for the development of the use of RAFT-HDA chemistry for surface modification is the use of AFM tips to facilitate the reaction on a specific surface.[313] Such an approach will provide high spatial resolution as to where the RAFT-HDA reaction will takes place. Potential application fields are in nano-electronics as well as circuit design and it seems a matter of priority to further explore the potential of this technology.

Further efforts are required in the efficient functionalization of nano-sized polymeric particles *via* RAFT-HDA chemistry approaches. A particular field of interest here is the modification of self-assembled block copolymer systems (*i.e.* micellar structures), which have been stabilized *via* – for example – covalent cross-linking. Since most of these nano-structures are synthesized with the aim of providing stimuli responsive drug delivery systems, it would appear logical to employ macromolecular building blocks which carry dithioester or diene functionalities for the attachment of biomolecules which can aid in specific cell recognition (*e.g.* at cancer sites). A similarly large development potential remains to be unlocked in the field of the efficient modification of carbon nanotubes (CNTs), which are interesting materials in the

electronics field. In addition, polymer-CNT conjugates may be readily processed in polymer matrices to enhance the material's strength, while circumventing CNT bundling.

It would be fascinating to explore the design of drug loaded nano-particles which have been efficiently functionalized *via* RAFT-HDA chemistry and can release their payload by virtue of a retro-RAFT-HDA reaction. Of course, such retro-RAFT-HDA concepts are not limited to surface modifications, but can also find applications in other fields. The above select examples of further development opportunities in the field of orthogonal surface modifications have made clear that we have only started to unlock the vast potential of HDA chemistries and their application in variable fields. It is hoped that the current thesis will serve as stimulus for further research in the area.

Abbreviations

µm	Micrometer
µs	Microsecond
A	Absorbance
AFM	Atomic force microscopy
AIBN	2,2'-Azoisobutyronitrile
AS	Active sites
ASAF	Active sites accessible for functionalization
ATR	Attenuated total reflectance
ATR-IR	Attenuated total reflectance-infra red spectroscopy
ATRP	Atom transfer radical polymerization
BA	Butyl acrylate
BBOT	2,5-bis-5-tert-butyl-2-benzoxazolylthiophene
BEPTF	Benzyl (diethoxyphosphoryl)dithioformate
bpy	2,2’-bipyridyl
C	Carbon
c	Concentration of substance
C_{60}	Fullerenes
CA	Contact angle
CAE	Constant analyzer energy mode
CCD	Charged coupled device
$CDCl_3$	Deuterated chloroform
CH_2Cl_2	Dichloromethane
CH_3CN	Acetonitrile
CL	Cross-linking
cm	Centimeter
CNT	Carbon nano tube
CO	Carbon monoxide
Cp	Cyclopentadiene
CP	Cross-polarization

CPDB	Cyanopropyl dithiobenzoate
CRP	Controlled radical polymerization
CSA	Chemical-shift anisotropy
Cu(I)Br	Copper(I)bromide
Cu(II)Br	Copper(II)bromide
CuAAC	Copper catalyzed azide-alkyne coupling
DA	Diels-Alder
DBU	1,8-Diazabicycloundec-7-ene
DCC	*N*,*N*'-Dicyclohexylcarbodiimide
DEPN	*N*-tert-butyl-*N*-[1-diethylphosphono-(2,2-dimethylpropyl)] nitroxide
DIC	Differential interference contrast
DIPEA	*N*,*N*-diisopropylethylamine
DMAP	4-Dimethylaminopyridine
DMF	*N*,*N*-Dimethyl formamide
DMSO	Dimethyl sulphoxide
D_n	Number average diameter of microspheres
DNA	Deoxyribonucleic acid
DPTS	4-(Dimethylamino)-pyridinium-4-toluene sulfonate
DVB	Divinylbenzene
DVB55	Divinylbenzene 55
DVB80	Divinylbenzene 80
D_w	Weight average diameter of microspheres
E_B	Binding energy of an electron
E_k	Kinetic energy of an electron
ESI	Electrospray Ionization
ESI-MS	Electrospray ionization-mass spectrometry
f	Initiation efficiency
FA	Fluoresceinamine
FID	Free induction decay
FPA	Focal plane array
FT	Fourier transform

FT-NIR	Fourier-transform near infra red
g	Gram
GD	Grafting density
GPC	Gel permeation chromatography
H	Hydrogen
HDA	Hetero Diels-Alder
HEMA	2-Hydroxyethyl methacrylate
HOMO	Highest occupied molecular orbital
HPLC	High pressure liquid chromatography
HR	Hindered rotor
HR-MAS	High-resolution magic-angle spinning
$h\nu$	Photon energy
IR	Infra red
J	Joule
k_{ad}	Rate constant for addition/activation
k_{d}	Rate constant for decomposition
k_{da}	rate constant for deactivation
K_{eq}	Equilibrium constant
kHz	Kilohertz
k_{i}	Rate constant for initiation
kJ	Kilojoule
k_{p}	Rate constant for propagation
k_{t}	Rate constant for termination
k_{tc}	Rate constant for termination by combination
k_{td}	Rate constant for termination by disproportionation
k_{β}	Rate constant for fragmentation
l	Optical path length
L	Litre
LC	Loading capacity
LED	Light emitting diode
LRP	Living radical polymerization

LUMO	Lowest unoccupied molecular orbital
MADIX	Macromolecular architectures *via* interchange of xanthates
MAS	Magic-angle spinning
mg	Milligram
$MgSO_4$	Magnesium sulphate
MHz	Megahertz
mL	Millilitre
mm	Millimeter
MMA	Methyl methacrylate
mmol	Millimole
M_n	Number average molecular weight
mol	Mole
ms	Millisecond
MSDTF	Benzyl methylsulfonyldithioformate
N_A	Avogadro's number
NaH	Sodium hydride
NaI	Sodium iodide
nm	Nanometer
NMP	Nitroxide mediated polymerization
NMR	Nuclear magnetic resonance
O	Oxygen
P	Phosphorous
PAA	Poly(acrylic acid)
PCL	Poly(ε-caprolactone)
PDI	Poly dispersity index
PDVB	Poly(divinylbenzene)
PDVB55	Poly(divinylbenzene 55)
PDVB80	Poly(divinylbenzene 80)
PEG	Poly(ethylene glycol)
PEO	Poly(ethylene oxide)
PHEMA	Poly(2-Hydroxyethyl methacrylate)

PiBA	Poly(isobornyl acrylate)
PMDETA	*N*,*N*,*N*',*N*'',*N*''-pentamethyldiethylenetriamine
PMMA	Poly(methyl methacrylate)
PMMA-Cp_2	Bis(cyclopentadienyl) poly(methyl methacrylate)
PRE	Persistent radical effect
PS	Polystyrene
PSDTF	Benzyl phenylsulfonyldithioformate
PSi	Porous Silicon
P*t*-BA	Poly(*t*-butyl acrylate)
r	Radius of microsphere
RAFT	Reversible addition-fragmentation chain transfer
rf	Radio-frequency
RMS	Root mean square
ROP	Ring opening polymerization
R_p	Rate of polymerization
RP	Radical polymerization
S	Sulphur
s	Second
S_8	Elemental sulphur
SA	Surface area of microsphere
SAM	Self assembled monolayer
SEC	Size exclusion chromatography
SEM	Scanning electron microscopy
SFRP	Stable free radical polymerization
Si	Silicon
SM-TMS	3-(*N*-Styryl methyl-2-aminoethylamino)-propyl trimethoxy silane
SPE	Single pulse excitation
T	Transmittance
t-BuOK	Potassium tert-butoxide
TC	Temperature corrections
TCD	Thermal conductivity detection

TEMPO	2,2,6,6-Tetramethylpiperidinyoxy
TFA	Trifluoroacetic acid
TGA	Thermogravimetric analysis
THF	Tetrahydrofuran
TIPNO	*N*-tert-butyl-*N*-[1-phenyl-2-(methylpropyl)]nitroxide
TMP	1,1,1-tris(hydroxymethyl)propane
U	Polydispersity index of microspheres
UV-Vis	Ultraviolet-visible
V	Volume of microsphere
W	Work function
X-AES	X-ray induced Auger electron spectroscopy
XPS	X-Ray photoelectron spectroscopy
ZPVE	Zero-point vibrational energy
Δ	Phase difference
ε	Molar absorptivity
ρ	Density
Ψ	Amplitude ratio

Curriculum Vitae

Education

1) July'08–July'10: **Ph.D in Polymer Chemistry continuation** at the Karlsruhe Institute of Technology (KIT) under the supervision of Prof. Christopher Barner-Kowollik.
2) September'07-June'08: **Ph.D in Polymer Chemistry** at the Centre for Advanced Macromolecular Design, University of New South Wales, Sydney, Australia, under the supervision of Prof. Christopher Barner-Kowollik and Dr. Leonie Barner.
3) July'05–June'07: **Master of Technology in Polymer Science and Technology** from the Indian Institute of Technology Delhi, India with a cumulative GPA of **9.8** on a 10 point scale. Master thesis carried out at the Technical University Dresden as a part of DAAD scholarship.
4) 2001-2003: **Master of Science in Chemistry (Specialization: Organic Chemistry)** from the Department of Chemistry, University of Rajasthan, Jaipur, India with **79.4%**.
5) 1998-2001: **Bachelor of Science in Chemistry (Honours)** (Subsidiary subject Industrial Microbiology) from Maharani's College, University of Rajasthan, Jaipur, India with **75.8%**.

Achievements

1) Scholarship from the **DAAD** (Deutscher Akademischer Austausch Dienst) to attend the *American Chemical Society 239th National Meeting and Exposition* (March 2010), San Francisco, USA.
2) **Postgraduate scholarship** from the Faculty of Engineering, University of New South Wales, Sydney, Australia which included annual stipend and remission of tuition fees.
3) **DAAD** (German Academic Exchange) scholarship for completing a Master of Technology final year project at the Technical University Dresden, Germany.
4) **First position** in Master of Technology, Indian Institute of Technology Delhi, India.

5) All India rank of **64th** in Graduate Aptitude Test in Engineering (**GATE**) with percentile of 98.13.

6) Qualified **Junior Research Fellowship** examination conducted jointly by CSIR-UGC (Council of Scientific and Industrial Research-University Grants Commission).

7) **Second** position in Master of Sciences, University of Rajasthan, India.

8) **Seventh** position in Bachelor of Sciences (Honours), University of Rajasthan, India.

9) **Third** position in Industrial Microbiology examination, University of Rajasthan, India.

Scientific Collaborations

1) Dr. Leonie Barner (*Fraunhofer Institute for Chemical Technology*, Pfinztal).

2) Dr. Marianne Gaborieau (formerly MPI, Mainz, currently *University of Western Sydney,* Sydney), Dr. Robert Graf and Prof. Dr. Hans W. Spiess (*Max Planck Institute of Polymer Research*, Mainz).

3) A/Prof. Michelle Coote (*Australian National University*, Canberra).

4) A/Prof. Dr. Martina Stenzel (*Centre for Advanced Macromolecular Design*, Sydney).

5) Industrial collaboration with *Evonik Industries*, Germany.

6) March'08-June'08: Scientific coworker in the group of Dr. Suzanne Smith, Australian Nuclear Science and Technology Organization (ANSTO), Australia.

7) Sept'06-May'07: Scientific coworker in the group of Prof. Dr. Hans-Jürgen P. Adler and Prof. Dr. Dirk Kuckling, Technical University Dresden, Germany for the completion of Master's thesis.

8) May'06-Aug'06: Scientific coworker in the group of Dr. Josemon Jacob, Indian Institute of Technology Delhi, India.

Referred Journals Publication List and Conference Presentations

Patents

Two patents submitted.

Publication List

1) Rapid Bonding/Debonding on Demand: Reversibly Cross-Linked Functional Polymers via Diels-Alder Chemistry, A. J. Inglis, L. Nebhani, O. Altintas, F.-G. Schmidt C. Barner-Kowollik, *Macromolecules* **2010**, *43*, 5515.

2) Functionalization of Fullerenes with Cyclopentadienyl and Anthracenyl Capped Polymeric Building Blocks via Diels-Alder Chemistry, L. Nebhani, C. Barner-Kowollik, *Macromol. Rapid Commun.* **2010**, *31*, 1298.

3) Quantification of Grafting Density Achieved *via* Modular *'Grafting-to'* Approaches on Divinylbenzene Microspheres, L. Nebhani, D. Schmiedl, L. Barner, C. Barner-Kowollik, *Adv. Funct. Mat.* **2010**, *20*, 2010.

4) Accessing Quantitative Degrees of Functionalization on Solid Substrates via Solid State NMR Spectroscopy, M. Gaborieau, L. Nebhani, R. Graf, L. Barner, C. Barner-Kowollik, *Macromolecules* **2010**, *43*, 3868.

5) Strongly Electron Withdrawing Sulfonyldithioformate Based RAFT Agents for Hetero Diels-Alder Conjugation, L. Nebhani, S. Sinnwell, C. Y. Lin, M. Coote, M. H. Stenzel, C. Barner-Kowollik, *Polymer Preprints* **2010**, *51*, 324.

6) Efficient and Mild Modification of Si Surfaces via Orthogonal Hetero Diels-Alder Chemistry, L. Nebhani, P. Gerstel, P. Atanasova, C. Barner-Kowollik, *J. Polym. Sci. Part A: Polym. Chem.* **2009**, *47*, 7090.

7) Efficient Access to Macromolecules via Living/Controlled Radical Polymerization: Control, Coupling and Characterization, C. Barner-Kowollik, S. Sinnwell, T. Junkers, M. H. Stenzel, E. H. H. Wong, S. P. S. Koo, L. Nebhani, *Macromolecular Bioscience*, **2009**, *9*, F100.

8) Strongly Electron Deficient Sulfonyldithioformate Based RAFT agents for Hetero-Diels Alder (HDA) Conjugation: Computational Design and Experimental Evaluation, L. Nebhani, S. Sinnwell, C. Y. Lin, M. L. Coote, M. H. Stenzel, C. Barner-Kowollik, *J. Polym. Sci. Part A: Polym. Chem.* **2009**, *47*, 6053.

9) Surface Modification of Poly(divinyl benzene) Microspheres via Thiol-ene Chemistry and Alkyne-Azide Click Reactions, A. S. Goldmann, A. Walther, L. Nebhani, R. Joso, D. Ernst, K. Loos, C. Barner-Kowollik, L. Barner, A. H. E. Mueller, *Macromolecules* **2009**, *42*, 3707.

10) Orthogonal Transformations on Solid Substrates: Efficient Avenues to Surface Modification, L. Nebhani, C. Barner-Kowollik, *Adv. Mater.* **2009**, *21*, 3442.

11) Efficient Surface Modification of Divinylbenzene Microspheres via a Combination of RAFT and Hetero Diels-Alder chemistry, L. Nebhani, S. Sinnwell, A. J. Inglis, M. H. Stenzel, C. Barner-Kowollik, L. Barner, *Macromol. Rapid Commun.* **2008**, *29*, 1431.

Conference Presentations

1) Strongly Electron Deficient Sulfonyldithioformate Based RAFT Agents for Hetero Diels-Alder Conjugation (Oral Presentation), L. Nebhani, S. Sinnwell, C. Y. Lin, M. L. Coote, M. H. Stenzel, C. Barner-Kowollik, **Spring 2010**, *American Chemical Society 239th National Meeting and Exposition,* San Francisco, USA.

2) Accessing Quantitative Degrees of Functionalization on Solid Substrates *via* solid state NMR spectroscopy (Poster Presentation), M. Gaborieau, L. Nebhani, R.

Graf, L. Barner, C. Barner-Kowollik, **2009**, *11th Pacific Polymer Conference*, Cairns, Australia.

3) Surface Characterization of Poly(divinyl benzene) Microspheres by Solid-State NMR (Poster Presentation) M. Gaborieau, L. Nebhani, C. Barner-Kowollik, L. Barner, R. Graf, GDCh **2009**, *31st Discussion Meeting: Magnetic Resonance in Chemistry and Materials Research*, Dresden, Germany.

4) Orthogonal Modification of Solid Substrates *via* RAFT-HDA Chemistry (Oral Presentation), L. Nebhani, C. Barner-Kowollik, **2009**, *Controlled/living Radical Polymerizations: Latest Trends in Synthesis, Characterization and Industrial Applications*, Houffalize, Belgium.

5) Efficient Modification of Variable Surfaces (Poster presentation), L. Nebhani, S. Sinnwell, P. Gerstel, L. Barner, C. Barner-Kowollik, **2009**, *Frontiers In Polymer Science*, Mainz, Germany.

6) Effiziente Zugänge zu Komplexen Makromolekülen Mittels Lebender/Kontrollierter Radikalischer Polymerisation. Kontrolle, Kopplung und Charakterisierung (Invited Talk), C. Barner-Kowollik, S. Sinnwell, T. Junkers, M. H. Stenzel, E. H. H. Wong, S. P. S. Koo, L. Nebhani, **2009**, *Makromolekulares Kolloquium*, Freiburg, Germany.

7) New Avenues to Complex Polymers: Synthesis and Characterization (Invited Talk), C. Barner-Kowollik, S. Sinnwell, T. Junkers, M. H. Stenzel, E. H. H. Wong, S. P. S. Koo, L. Nebhani, **2009**, *Polymer Chemistry Conference*, Cancun, Mexico.

8) Exploring New Avenues for the Synthesis and Characterization of Well-Defined Polymeric Materials (Invited Talk), C. Barner-Kowollik, S. Sinnwell, M. H. Stenzel, T. Junkers, A. J. Inglis, L. Nebhani, L. Barner, G. Hart-Smith, H. Chaffey-Millar, S. P. S.

Koo, T. Gruendling, M. Guilhaus, C. Synatschke, E. H. H. Wong, **2008**, *30th Australasian Polymer Symposium*, Melbourne, Australia.

9) Smart Hydrogels Based on *N*-[2-(Dimethylamino)ethyl]acrylamide Possessing Metal Ion Sensitivity (Poster presentation) L. Nebhani, D. Kuckling, H. J.-P. Adler, V. Choudhary, M. Guenther, M., **2007**, *3rd International Symposium on Reactive Polymers in Inhomogeneous Systems, in Melts and at Interfaces*, Dresden, Germany.

Acknowledgements

There are a range of people whom I would like to thank and who are directly or indirectly related to the successful completion of the current Ph.D. thesis. The first person whom I would like to gratefully acknowledge is my Ph.D advisor, Prof. Dr. Christopher Barner-Kowollik, for giving me the opportunity to work on the challenging topics included in the present work in his group. I am thankful to him for his constant encouragement and motivation during this work.

I am thankful to Dr. Leonie Barner (Fraunhofer Institute for Chemical Technology, Pfinztal) for her supervision during the beginning of my Ph.D, for continued scientific discussions and good advice. I would also like to thank Prof. T. P. Davis (UNSW, Sydney) for assisting me in organizing a scholarship at UNSW, Australia.

Furthermore, I would like to thank the people with whom the collaborative projects were carried out, *i.e.* A/Prof. M. L. Coote (ANU, Canberra), A/Prof. M. Stenzel (UNSW, Sydney), Dr. M. Gaborieau (UWS, Sydney), Dr. R. Graf (Max Planck Institute of Polymer Research, Mainz) and Dr. F.-G. Schmidt (Evonik Industries). In addition, I would also like to thank Prof. Dr. J. Podlech (KIT) for helpful discussions related to sulfonyl RAFT agents. Further, I would like to thank Prof. Dr. M. Wilhelm (KIT) and his group members for providing any help whenever needed.

For the help with the characterization techniques, I would like to thank Dr. M. Bruns (KIT) for the XPS measurements, Dr. D. Schmiedl (Fraunhofer Institute for Chemical Technology, Pfinztal) for the elemental analyses, Dr. P. Atanasova (Max Planck Institute of Metals Research, Stuttgart) for the AFM analyses, Mr. H. Weickenmeier (KIT) for the TGA measurements, Dr. B. Reznik (KIT) for the SEM analyses and Ms. M. Langhauser (KIT) for the confocal microscopy measurements. Further, I would like to thank Dr. J. Hook (UNSW, Sydney) for the fruitful discussions related to the solid-state NMR studies presented herein and reminding me of very famous quote that '*God helps those who help themselves*'.

I am thankful to Dr. S. Sinnwell and Andrew for helping me with RAFT-HDA chemistry at the beginning of this work and several scientific discussions. In addition, I would like to thank Ozcan for the good discussions related to organic reaction mechanisms and also for introducing me to delicious Turkish cuisine.

Many thanks go to Dr. J. Blinco and Andrew for proof-reading this thesis and helpful suggestions. I would also like to thank Peter for his help during the Si wafer project and the good scientific discussions. Thanks to Thomas for assisting me in the fullerene project.

Special thanks to Maribel for introducing me to everything at CAMD and UNSW, for scientific help as well any help whenever needed. I would like to thank Sandy for being such a good friend, for her help at any moment and making me more knowledgeable about different foods, shopping etc.

I would like to thank my colleagues in Karlsruhe, *i.e.* Prof. Dr. T. Junkers (formerly KIT, now Universiteit Hasselt), Dr. T. Gruendling, Dr. F. Bennet, Dr. A. Kaiser, Christina, Mathias Dietrich, Dominik, Mathias Glassner, Anna, Nicholas, David, Michael, Lin and my friends at CAMD Ling, Eunhee, Simon, Hien, Edgar for their readiness to help whenever needed.

I would also like to thank Frau Schneider and Dr. Anja Goldmann for the excellent lab organization. Thanks to Frau Herrmann for the office organization and for all the beautiful souvenirs.

Last but not the least; I would like to thank Ashish for making me perfect in playing chess, for several philosophical as well as spiritual discussions, for sparking my ambitions and heaps of other things.

Finally, I would like to thank my family for their love and support and my Bhagwanji for endless blessings and making me LEENA.

References

[1] L. Nebhani, C. Barner-Kowollik, *Adv. Mater.* **2009**, *21*, 3442.

[2] K. K. Iu, X. S. Liu, K. J. Thomas, *J. Photochem. Photobiol. A: Chem.* **1994**, *79*, 103.

[3] H. R. Brown, C. -Y. Hui, E. Raphael, *Macromolecules* **1994**, *27*, 608.

[4] H. R. Brown, *Macromolecules* **1993**, *26*, 1666.

[5] C. Creton, H. R. Brown, K. Shull, *Macromolecules* **1994**, *27*, 3174.

[6] W. F. Reichert, H. R. Brown, *Polymer* **1994**, *34*, 2289.

[7] M. Deruelle, M. Tirrell, Y. Marciano, H. Hervet, L. Leger, *Faraday Discuss.* **1994**, *98*, 55.

[8] M. Deruelle, L. Leger, M. Tirrell, *Macromolecules* **1995**, *28*, 7419.

[9] a) C. D. Bain, G. M. Whitesides, *Angew. Chem., Int. Ed.* **1989**, *101*, 522; b) G. M. Whitesides, P. E. Laibinis, *Langmuir* **1990**, *6*, 87.

[10] P. E. Laibnis, G. M. Whitesides, D. L. Allara, Y. -T. Tao, A. N. Parikh, R. G. Nuzzo, *J. Am. Chem. Soc.* **1991**, *113*, 7152.

[11] W. Senaratne, L. Andruzzi, C. K. Ober, *Biomacromolecules* **2005**, *6*, 2427.

[12] J.-F. Lutz, *Angew. Chem., Int. Ed.* **2007**, *46*, 1018.

[13] N. K. Devaraj, J. P. Collman, *QSAR Comb. Sci.* **2007**, *26*, 1253.

[14] L. Nebhani, S. Sinnwell, A. J. Inglis, M. H. Stenzel, C. Barner-Kowollik, *Macromol. Rapid Commun.* **2008**, *29*, 1431.

[15] S. Ciampi, T. Böcking, K. A. Kilian, M. Janes, J. B. Harper, J. J. Gooding, *Langmuir* **2007**, *23*, 9320.

[16] J. P. Collaman, N. K. Devaraj, C. E. D. Chidsey, *Langmuir* **2004**, *20*, 1051.

[17] A. G. Marrani, E. A. Dalchiele, R. Zanoni, F. Decker, F. Cattaruzza, D. Bonifazi, M. Prato, *Electrochim. Acta* **2008**, *53*, 3903.

[18] H. C. Kolb, M. J. Finn, K. B. Sharpless, *Angew. Chem., Int. Ed.* **2001**, *40*, 2004.

[19] V. V. Rostovtsev, G. Green, V. V. Fokin, K. B. Sharpless, *Angew. Chem. Int. Ed.* **2002**, *41*, 2596.

[20] H. Durmaz, B. Colakoglu, U. Tunca, G. Hizal, *J. Polym. Sci. Part A: Polym. Chem.* **2006**, *44*, 1667.

[21] A. Dag, H. Durmaz, G. Hizal, U. Tunca, *J. Polym. Sci. Part A: Polym. Chem.* **2008**, *46*, 302.

[22] B. Le Droumaguet, K. Velonia, *Macromol. Rapid Commun.* **2008**, *29*, 1073.

[23] G. A. Lemieux, C. L. de Graffenried, C. R. Bertozzi, *J. Am. Chem. Soc.* **2003**, *125*, 4708.

[24] N. J. Agard, J. A. Prescher, C. R. Bertozzi, *J. Am. Chem. Soc.* **2004**, *126*, 15046.

[25] S. Bräse, C. Gil, K. Knepper, V. Zimmermann, *Angew. Chem., Int. Ed.* **2005**, *44*, 5188.

[26] L. Nebhani, S. Sinnwell, C. Y. Lin, M. L. Coote, M. H. Stenzel, C. Barner-Kowollik, *J. Polym. Sci. Part A: Polym. Chem.* **2009**, *47*, 6053.

[27] L. Nebhani, P.Gerstel, P. Atanasova, C. Barner-Kowollik, *J. Polym. Sci. Part A: Polym. Chem.* **2009**, *47*, 7090.

[28] L. Nebhani, D. Schmiedl, L. Barner, C. Barner-Kowollik, *Adv. Funct. Mat.* **2010**, *DOI: 10.1002/adfm.200902330*.

[29] M. Gaborieau, L. Nebhani, R. Graf, L. Barner, C. Barner-Kowollik, *Macromolecules* **2010**, *43*, 3868.

[30] L. Nebhani, C. Barner-Kowollik, *Macromol. Rapid Commun.* **2010**, *DOI: 10.1002/marc201000142*.

[31] A. Inglis, L. Nebhani, O. Altintas, F.-G. Schmidt, C. Barner-Kowollik, *Macromolecules*, **2010**, submitted

[32] G. Moad, D. H. Solomon, *The Chemistry of Free Radical Polymerization*, Pergamon, Oxford, **1995**.

[33] C. H. Bamford, *Encyclopedia of Polymer Science and Engineering*, 2nd edn, Ed. J. I. Kroschwitz, Wiley Interscience, New York, **1988**, *13*, 708.

[34] T. Junkers, D. Voll, C. Barner-Kowollik, *e-polymers* **2009**, 076

[35] B. Dervaux, T. Junkers, M. Schneider-Baumann, F. E. Du Prez, C. Barner-Kowollik, *J. Polym. Sci.Part A: Polym. Chem.* **2009**, *47*, 6641.

[36] R. G. W. Norrish, R. R. Smith, *Nature* **1942**, *150*, 336.

[37] C. Barner-Kowollik, G. T. Russell, *Prog. Polym. Sci.* **2009**, *34*, 1211.

[38] K. Matyjaszewski, P. Kubisa, S. Penczek, *J. Polym. Sci., Polym. Chem. Ed.* **1974**, *12*, 1333.

[39] K. Matyjaszewski, P. Sigwalt, *Polym. Int.* **1994**, *35*, 1.

[40] N. Hadjichristidis, M. Pitsikalis, S. Pispas, H. Iatrou, *Chem. Rev.* **2001**, *101*, 3747.

[41] D. Greszta, D, Mardare, K. Matyjaszewski, *Macromolecules* **1994**, *27*, 638.

[42] A. Goto, T. Fukuda, *Prog. Polym. Sci.* **2004**, *29*, 329.

[43] H. Fischer, *Chem. Rev.* **2001**, *101*, 3587

[44] M. K. Georges, R. P. N. Veregin, P. M, Kazmaier, G. K. Hamer, *Macromolecules* **1993**, *26*, 2987.

[45] C. J. Hawker, A. W. Bosman, E. Harth, *Chem. Rev.* **2001**, *101*, 3661.

[46] B. B. Wayland, G. Poszmik, S. L. Mukerjee, M. Fryd, *J. Am. Chem. Soc.* **1994**, *116*, 7943.

[47] P. Vana, T. P. Davis, C. Barner-Kowollik, *Macromol. Rapid Commun.* **2002**, *23*, 952.

[48] G. T. Russell, R. G. Gilbert, D. H. Napper, *Macromolecules* **1992**, *25*, 2459.

[49] M. K. Georges, R. P. N. Veregin, P. M. Kazmaier, G. K. Hamer, *Macromolecules* **1993**, *26*, 2987.

[50] C. J. Hawker, *In Handbook of Radical Polymerization*; K. Matyjaszewski, Ed.; Wiley: London, **2002**.

[51] D. Benoit, S. Grimaldi, S. Robin, J. -P. Finet, P. Tordo, Y. Gnanou, *J. Am. Chem. Soc.* **2000**, *122*, 5929.

[52] D. Benoit, V. Chaplinski, R. Braslau, C. J. Hawker, *J. Am. Chem. Soc.* **1999**, *121*, 3904.

[53] K. Matyjaszewski, *Macromol. Symp.* **1998**, *134*, 105.

[54] K. Matyjaszewski, *Macromolecules* **1998**, *31*, 4710.

[55] W. A. Braunecker, T. Pintauer, N. V. Tsarevsky, G. Kickelbick, K. Matyjaszewski, *J. Organomet. Chem.* **2005**, *690*, 916.

[56] W. Braunnecker, N. V. Tsarevsky, T. Pintauer, R. R. Gil, K. Matyjaszewski, *Macromolecules* **2005**, *38*, 4081.

[57] N. V. Tsarevsky, T. Pintauer, K. Matyjaszewski, *Macromolecules* **2004**, *37*, 9768.

[58] K. Matyjaszewski, K. Davis, T. E. Patten, M. Wei, *Tetrahedron* **1997**, *53*, 15321.

[59] J. -F. Lutz, K. Matyjaszewski, *Macromol. Chem. Phys.* **2002**, *203*, 1385.

[60] J. -F. Lutz, K. Matyjaszewski, *J. Polym. Sci., Part A: Polym. Chem.* **2005**, *43*, 897.

[61] J. Chiefari, Y. K. Chong, F. Ercole, J. Krstina, J. Jeffery, T. P. T. Le, R. T. A. Mayadunne, G. F. Meijs, C. L. Moad, G. Moad, E. Rizzardo, S. H. Thang, *Macromolecules* **1998**, *31*, 5559.

[62] P. Copart, D. Charmot, T. Biadatti, S, Z. Zard, D. Michelet, WO 9858974 **1998**.

[63] P. Delduc, C. Tailhan, S. Z. Zard, *J. Chem. Soc., Chem. Commun.* **1988**, 308.

[64] J. Chiefari, R. T. A. Mayadunne, C. L. Moad, G. Moad, E. Rizzardo, A. Postma, M. A. Skidmore, S. H. Thang, *Macromolecules* **2003**, *36*, 2273.

[65] Y. K. Chong, J. Krstina, T. P. T. Le, G. Moad, A. Postma, E. Rizzardo, S. H. Thang, *Macromolecules* **2003**, *36*, 2256.

[66] C. Barner-Kowollik, M. Buback, B. Charleux, M. L. Coote, M. Drache, T. Fukuda, A. Goto, B. Klumperman, A. B. Lowe, J. B. Mcleary, G. Moad, M. J. Monteiro, R. D. Sanderson, M. P. Tonge, P. Vana, *J. Polym. Sci., Part A: Polym. Chem.* **2006**, *44*, 5809.

[67] C. Barner-Kowollik, J. F. Quinn, D. R. Morsley, T. P. Davis, *J. Polym. Sci., Part A: Polym. Chem.* **2001**, *39*, 1353.

[68] M. J. Monteiro, H. de Brouwer, *Macromolecules* **2001**, *34*, 349.

[69] D. Konkolewicz, B. S. Hawkett, A. Gray-Weale, Sébastien Perrier, *Macromolecules* **2008**, *41*, 6400.

[70] K. Matyjaszewski , Y. Gnanou, L. Leibler, *Macromolecular Engineering, Volume 1: Synthetic Techniques*, **2007**, Wiley-VCH.

[71] C. Barner-Kowollik, *Handbook of RAFT Polymerization*, **2008**, Wiley-VCH.

[72] K. Matyjaszewski, P. Miller, J. Pyun, J. Kickelbick, S. Diamanti, *Macromolecules* **1999**, *32*, 6526.

[73] S. Angot, K. S. Murthy, D. Taton, Y. Gnanou, *Macromolecules* **1998**, *31*, 7218.

[74] X. Hao, C. Nilsson, M. Jesberger, M. Stenzel, E. Malmström, T. Davis, *J. Polym. Sci., Part A: Polym. Chem.* **2004**, *42*, 5877.

[75] M. Stenzel-Rosenbaum, T. P. Davis, V. Chen, A. G. Fane, *J. Polym. Sci., Part A: Polym. Chem.* **2001**, *39*, 2777.

[76] H. Gao, K. Matyjaszewski, *Macromolecules* **2006**, *39*, 4960.

[77] H. T. Lord, J. F. Quinn, S. D. Angus, M. R. Whittaker, M. H. Stenzel, T. P. Davis, *J. Mater. Chem.* **2003**, *13*, 2819.

[78] A. Bosman, R. Vestberg, A. Heumann, J. Fréchet, C. Hawker, *J. Am. Chem. Soc.* **2003**, *125*, 715.

[79] X. Zhang, J. Xia, K. Matyjaszewski, *Macromolecules* **2000**, *33*, 2340.

[80] U. Stehling, E. Malmstrom, R. Waymouth, C. Hawker, *Macromolecules* **1998**, *31*, 4396.

[81] K. Beers, S. Gaynor, K. Matyjaszewski, *Macromolecules* **1998**, *31*, 9413.

[82] S. Qin, K. Matyjaszewski, *Macromolecules* **2003**, 36, 605.

[83] H. Paik, S. Gaynor, K. Matyjaszewski, *Macromol. Rapid Commun.* **1998**, *19*, 47.

[84] J. Vosloo, M. P. Tonge, C. M. Fellows, F. D'Agosto, R. D. Sanderson, R. G. Gilbert, *Macromolecules* **2004**, *37*, 2371.

[85] B. S. Sumerlin, N. V. Tsarevsky, G. Louche, R. Y. Lee, K. Matyjaszewski, *Macromolecules*, **2005**, *38*, 5774.

[86] S. J. Lord, S. S. Sheiko, I. LaRue, H. –I. Lee, K. Matyjaszewski, *Macromolecules* **2004**, *37*, 4235.

[87] Y. G. Li, P. J. Shi, Y. Zhou, C. –Y. Pan, *Polym. Int.* **2004**, *53*, 349.

[88] H. Shinoda, K. Matyjaszewski, *Macromol. Rapid Commun.* **2001**, *2*, 1176.

[89] H. Mori, A. H. E. Mueller, *Prog. Polym. Sci.* **2003**, *28*, 1403.

[90] C. J. Hawker, J. M. J. Fréchet, R. B. Grubbs, J. Dao, *J. Am Chem. Soc.* **1995**, *117*, 10763.

[91] K. Matyjaszewski, S. G. Gaynor, *Macromolecules* **1997**, *30*, 7042.

[92] B. Lepoittevin, R. Matmour, R. Francis, D. Taton, Y. Gnanou, *Macromolecules* **2005**, *38*, 3120.

[93] J. Du, Y. Chen, *J. Polym. Sci.,Part A: Polym. Chem.* **2004**, *42*, 2263.

[94] N. V. Tsarevsky, B. S. Sumerlin, K. Matyjaszewski, *Macromolecules* **2005**, *38*, 3558.

[95] V. Cossens, T. Pintauer, K. Matyjaszewski, *Prog. Polym.Sci.* **2001**, *26*, 337.

[96] S. Voccia, C. Jerome, C. Detrembleur, P. Leclere, R. Gouttebaron, M. Hecq, B. Gilbert, R. Lazzaroni, R. Jerome, *Chem. Mat.* **2003**, *15*, 923.

[97] J. B. Hutchison, P. F. Stark, C. J. Hawker, K. S. Anseth, Kristi S., *Chem. Mat.* **2005**, *17*, 4789.

[98] J. Parvole, J.-P. Montfort, G. Reiter, O. Borisov, L. Billon, *Polymer* **2006**, *47*, 972.

[99] F. G. Garcia, M. R. Pinto, B. G Soares, *Euro. Polym. J.* **2002**, *38*, 759.

[100] A. V.Vivek, R. Dhamodharan, *J. Polym. Sci., Part A: Polym. Chem.* **2007**, *45*, 3818.

[101] Y. Inoue, T. Matsugi, N. Kashiwa, K. Matyjaszewski, *Macromolecules* **2004**, *37*, 3651.

[102] Y. Li, L. S. Schadler, B. C. Benicewicz, "Surface and Particle Modification *via* the RAFT Process: Approach and Properties", in: *Handbook of RAFT Polymerization*, C. Barner-Kowollik, Ed., Wiley-VCH, Weinheim **2008**, 423.

[103] J. Quinn, T. P. Davis, L. Barner, C. Barner-Kowollik, *Polymer* **2007**, *48*, 6467.

[104] S. Perrier, P. Takolpuckdee, *J. Polym. Sci., Part A: Polym. Chem.* **2005**, *43*, 5347.

[105] W. A. Braunecker, K. Matyjaszewski, *Prog. Polym. Sci.* **2007**, *32*, 93.

[106] L. Barner, C. Barner-Kowollik, T. P. Davis, M. H. Stenzel, *Aust. J. Chem.* **2004**, *57*, 19.

[107] L. Barner, T. P. Davis, M. H. Stenzel, C. Barner-Kowollik, *Macromol. Rapid Commun.* **2007**, *28*, 539.

[108] L. Barner, C. Li, X. Hao, M. H. Stenzel, C. Barner-Kowollik, T. P. Davis, *J. Polym Sci., Part A: Polym. Chem.* **2004**, *42*, 5067.

[109] R. Joso, M. H. Stenzel, T. P. Davis, C. Barner-Kowollik, L. Barner, *Aust. J. Chem.* **2005**, *58*, 468.

[110] L. Barner, *Aust. J. Chem.* **2003**, *56*, 1091.

[111] S. Huang, R. Joso, A. Fuchs, L. Barner, S. V. Smith, *Chem. Mat.* **2008**, *20*, 5375.

[112] H. C. Kolb, M. G. Finn, K. B. Sharpless, *Angew. Chem. Int. Ed.* **2001**, *40*, 2004.

[113] C. W. Torne, C. Christensen, M. Medal, *J. Org. Chem.* **2002**, *67*, 3057.

[114] C. Barner-Kowollik, A. J. Inglis, *Macromol. Rapid Commun.* **2009**, *210*, 987.

[115] R. Huisgen, *Angew. Chem.* **1963**, *75*, 604.

[116] R. Huisgen, *Angew. Chem.* **1963**, *75*, 742.

[117] V. V. Rostovtsev, L. G. Green, V. V. Fokin, K. B. Sharpless, *Angew. Chem., Int. Ed.* **2002**, *41*, 2596.

[118] H. C. Kolb, K. B. Sharpless, *Drug Discovery Today* **2003**, *8*, 1128.

[119] W. H. Binder, R. Sachsenhofer, *Macromol. Rapid Commun.* **2007**, *28*, 15.

[120] V. D. Bock, H. Hiemstra, J. H. Van Maarseveen, *Eur. J. Org. Chem.* **2006**, *1*, 51.

[121] J.-F. Lutz, Z. Zarafshani, *Advanced Drug Delivery Review* **2008**, *60*, 958.

[122] C. J. Hawker, K. L. Wooley, *Science* **2005**, *309*, 1200.

[123] W. H. Binder, C. Kluger, *Curr. Org. Chem.* **2006**, *10*, 1791.

[124] L. F. Tietze, G. Kettschau, *Top. Curr. Chem.* **1997**, *189*, 1.

[125] H. Walsmann, *Synthesis* **1994**, 535.

[126] S. Kagabu, C. Kaiser, R. Keller, P. G. Becker, K. H. Mueller, L. Knothe, G. Rihs, H. Prinzbach, *Chem. Ber.* **1988**, *121*, 741.

[127] T. Suami, S. Ogawa, H. Uchino Y. Funaki, *J. Org. Chem.* **1975**, *40*, 456.

[128] E. Vogel, F. Kuebart, J. A. Marco, R. Andree, *J. Am. Chem. Soc.* **1983**, *105*, 6982.

[129] S. G. Im, K. W. Bong, B. -S. Kim, S. H. Baxamusa, P. T. Hammond, P. S. Doyle, K. K. Gleason, *J. Am. Chem. Soc.* **2008**, *130*, 14424.

[130] H. Adolfsson, A. Converso, K, B. Sharpless, *Tetrahedron Lett.* **1992**, *40*, 3991.

[131] T. Katsuki, V. S. Martin, *Org. React.* **1996**, *48*, 1.

[132] T. Katsuki, *J. Mol. Catal. A* **1996**, *113*, 87.

[133] H. C. Kolb, M. Van Nieuwenhze, K. B. Sharpless, *Chem. Rev.* **1994**, *94*, 2483.

[134] U. Jeong, B. Tao, I. Sagasser, H. Henniges, K. B. Sharpless, *J. Am. Chem. Soc.* **1998**, *120*, 6844.

[135] D. A. Evans, M. M. Faul, M. T. Bilodeau, *J. Org. Chem.* **1991**, *56*, 6744.

[136] R. R. Schmidt, *Acc. Chem. Res.***1986**, *19*, 250.

[137] P. Buonora, J.-C. Olsen, T. Oh, *Tetrahedron* **2001**, *57*, 6099.

[138] K. C. Nicolaou, S. A. Snyder, T. Montagnon, G. Vassilikogiannakis, *Angew. Chem. Int. Ed.* **2002**, *41*, 1668.

[139] E. M. Stocking, R. M. Williams, *Angew. Chem. Int. Ed.* **2003**, *42*, 3078.

[140] H. Oikawa, T. Tokiwano, *Nat. Prod. Rep.* **2004**, *21*, 321.

[141] G. Stork, E. E. Van Tamalen, L. J. Friedman, A. W. Burgstahler, *J. Am. Chem. Soc.* **1951**, *73*, 4501.

[142] G. Stork, E. E. Van Tamalen, L. J. Friedman, A. W. Burgstahler, *J. Am. Chem. Soc.* **1953**, *75*, 384.

[143] M. Gates, G. Tschudi, *J. Am. Chem. Soc.* **1952**, *74*, 1109.

[144] M. Gates, G. Tschudi, *J. Am. Chem. Soc.* **1956**, *78*, 1380.

[145] M. Gates, *J. Am. Chem. Soc.* **1950**, *72*, 228.

[146] S. Sinnwell, A. J. Inglis, T. P. Davis, M. H. Stenzel, C. Barner-Kowollik, *Chem. Commun.* **2008**, 2052.

[147] a) A. J. Inglis, S. Sinnwell, T. P. Davis, C. Barner-Kowollik, M. H. Stenzel, *Macromolecules* **2008**, *41*, 4120; b) A. J. Inglis, S. Sinnwell, M. H. Stenzel, C. Barner-Kowollik, *Angew. Chem. Int. Ed.* **2009**, *48*, 2411.

[148] S. Sinnwell, A. J. Inglis, M. H. Stenzel, C. Barner-Kowollik, *Macromol. Rapid Commun.* **2008**, *29*, 1090.

[149] L. Barner, *Adv. Mater.* **2009**, *21*, 2547.

[150] a) V. Pozsgay, N. E. Vieira, A. Yergey, *Org. Lett.* **2002**, *4*, 3191; b) A. Kumar, *Chem. Rev.* **2001**, *101*, 1; c) R. Breslow, D. C. Rideout, *J. Am. Chem. Soc.* **1980**, *102*, 7816.

[151] a) H. Durmaz, A. Dag, D. Gursoy, A. Levent Demirel, G. Hizal, U. Tunca *J. Polym. Sci., Part A: Polym. Chem.* **2010**, *48*, 1557; b) H. Durmaz, A. Dag, A. Hizal, G. Hizal, U. Tunca, *J. Polym. Sci., Part A: Polym. Chem.* **2008**, *46*, 7091.

[152] P. Beslin, P. Metzner, *Tetrahedron Lett.* **1980**, *21*, 4657.

[153] G. B. Kirby, *Phosphorous, Sulfur, Silicon* **1993**, *1-4*, 17.

[154] P. Metzner, *Organosulfur Chemistry I, Topics in Current Chemistry* (Springer-Verlag, Heidelberg, Germany) **1999**, *204*, 128.

[155] P. Herczegh, M. Zsély, R. Bognár, *Tetrahedron Lett.* **1986**, *27*, 1509.

[156] A. A. Freer, N. W. Isaacs, G. B. Kirby, A. Littejohn, M. S. Rhaman, *J. Chem. Soc., Perkin Trans.* **1992**, *1*, 1261.

[157] E. Vehejs, R. J. Galante, P. G. Gokjian, *J. Am. Chem. Soc.* **1998**, *120*, 3613.

[158] (a) D. M. Vyas, G. W. Hay, *Can. J. Chem.* **1971**, *49*, 3755; (b) D. M. Vyas, G. W. Hay, *J. Chem. Soc., Perkin Trans.* **1975**, *1*, 180.

[159] (a) E. Vedejs, J. Eustache, *J. Org. Chem.* **1980**, *45*, 2601; (b) G. W. Kirby, A. W. Lochead, S. Willamson, *J. Chem. Soc., Perkin Trans.* **1996**, *1*, 977.

[160] C. Portella, Y. G. Shermolovich, O. Tschenn, *Bull. Soc. Chim. Fr.* **1997**, *134*, 697.

[161] J. A. Boerma, N. H. Nilsson, A. Senning, *Tetrahedron* **1974**, *30*, 2735.

[162] M. Laus, R. Papa, K. Sparnacci, A. Alberti, M. Benaglia, D. Macciantelli, *Macromolecules* **2001**, *34*, 7269.

[163] A. Alberti, M. Benaglia, M. Guerra, M. Gulea, P. Hapiot, M. Laus, D. Macciantelli, S. Masson, A. Postma, K. Sparnacci, *Macromolecules* **2005**, *38*, 7610.

[164] B. Heuze, R. Gasparova, M. Heras, S. Masson, *Tetrahedron Letters* **2000**, *41*, 7327.

[165] R. Bastin, H. Albadri, A. C. Gaumont, M. Gulea, M. *Organic Letters* **2006**, *8*, 1033-1036.

[166] M. Gulea, S. Masson, In *New Aspects in Phosphorus Chemistry III* **2003**, *229*, 161.

[167] J. Sauer, D. Lang, A. Mielert, *Angew. Chem., Int. Ed.* **1962**, *1*, 268.

[168] A. J. Inglis, T. Paulöhrl, C. Barner-Kowollik, *Macromolecules* **2010**, *43*, 33.

[169] K. Li, H. D. H. Stöver, *J. Polym. Sci. Part A: Polym. Chem.* **1993**, *31*, 3257.

[170] F. Bai, X.Yang, W. Huang, *Macromolecules* **2004**, *37*, 9746.

[171] H. D. H. Stöver, K. Li, W. H. Li, US 5,599, 889, **1994**.

[172] J. S. Downey, R. S. Frank, W.-H. Li, H. D. H. Stöver, *Macromolecules* **1999**, *32*, 2838.

[173] H. Kawaguchi, *Prog. Polym. Sci.* **2000**, *25*, 1171.

[174] L. Barner, C. Li, X. J. Hao, M. H. Stenzel, C. Barner-Kowollik, T. P. Davis, *J. Polym. Sci., Part A: Polym. Chem.* **2004**, *42*, 5067.

[175] R. Joso, S. Reinicke, A. Walther, H. Schmalz, A. H. E. Müller, L. Barner, *Macromol. Rapid Commun.* **2009**, *30*, 1009.

[176] F. Lime, K. Irgum, *J. Polym. Sci., Part A: Polym. Chem.* **2009**, *47*, 1259.

[177] A. S. Goldmann, A. Walther, L. Nebhani, R. Joso, D. Ernst, K. Loos, C. Barner-Kowollik, L. Barner, A. H. E. Müller, *Macromolecules* **2009**, *42*, 3707.

[178] B. Zhao, W. J. Brittain, *J. Prog. Polym. Sci.* **2000**, *25*, 677.

[179] J. Pyun, Y. Kowalewski, K. Matyjazewski, *Macromol. Rapid Commun.* **2003**, *24*, 1043.

[180] S. Edmonsdon, V. L. Osborne, W. T. S. Huck, *Chem. Soc. Rev.* **2004**, *33*, 14.

[181] G. Zheng, H. D. H. Stöver, *Macromolecules* **2002**, *35*, 6828.

[182] D. Bontempo, N. Tirelli, G. Masci, V. Crescenzi, J. A. Hubell, *Macromol. Rapid Commun.* **2002**, *23*, 417.

[183] (a) L. Barner, N. Zwaneveld, S. Perera, Y. Pham, T. P. Davis, *J. Polym. Sci., Part A: Polym. Chem.* **2002**, *40*, 4180; (b) L. Barner, S. Pereira, S. Sandanayake, T. P. Davis, *J. Polym. Sci., Part A: Polym. Chem.* **2006**, *44*, 857.

[184] Y. Tsujii, M. Ejaz, K. Sato, A. Goto, T. Fukuda, *Macromolecules* **2001**, *34*, 8872.

[185] C. Yoshikawa, A. Goto, Y. Tsujii, T. Fukuda, K. Yamamoto, A. Kishida, *Macromolecules* **2005**, *38*, 4604.

[186] H. D. H. Stoever, J. M. J. Fréchet, *Macromolecules* **1989**, *22*, 1574.

[187] H. D. H. Stoever, J. M. J. Fréchet, *Macromolecules* **1991**, *24*, 883.

[188] M. Periyasamy, W. T. Ford, F. J. McEnroe, *J. Polym. Sci., Part A: Polym. Chem.* **1989**, *27*, 2357.

[189] W. T. Ford, M. Periyasamy, S. Mohanraj, F. J. McEnroe, *J. Polym. Sci., Part A: Polym. Chem.* **1989**, *27*, 2345.

[190] W. T. Ford, S. Mohanraj, H. Hall, D. J. O'Donnell, *J. Magn. Res.* **1985**, *65*, 156.

[191] a) S. T. Milner, *Science* **1991**, *251*, 905.; b) X. X. Kong, T. Kawai, J. Abe, T. Iyoda, *Macromolecules* **2001**, *34*, 1837; c) H. N. Waltenburg, J. T. Yates, *Chem. Rev.* **1995**, *95*, 1589.

[192] C. Haensch, M. Chiper, C. Ulbricht, A. Winter, S. Hoeppener, U. S. Schubert, *Langmuir* **2008**, *24*, 12981.

[193] S. Ciampi, T. Böcking, K. A. Kilian, J. B. Harper, J. J. Gooding, *Langmuir* **2008**, *24*, 5888.

[194] A. G. Cullis, L. T. Canham, P. D. J. Calcott, *J. Appl. Phys.* **1997**, *82*, 909.

[195] R. -V. Ostaci, D. Damiron, S. Capponi, G. Vignaud, L. Lager, Y. Grohens, E. Drockenmuller, *Langmuir* **2008**, *24*, 2732.

[196] F. Giacalone, N. Martin, *Chem. Rev.* **2006**, *106*, 5136.

[197] K. E. Geckeler, S. Samal, *Polym. Int.* **1999**, *48*, 743.

[198] L. Dai, A. W. H. Mau, *Adv. Mater.* **2001**, *13*, 899.

[199] C. Wang, Z.-X. Guo, S. Fu, W. Wu, D. Zhu, *Prog. Polym. Sci.* **2004**, *29*, 1079.

[200] W. T. Ford, T. D. Graham, T. H. Mourey, *Macromolecules* **1997**, *30*, 6422.

[201] H. Okamura, T. Terauchi, M. Minoda, T. Fukuda, K. Komatsu, *Macromolecules* **1997**, *30*, 5279.

[202] P. Zhou, G. Q. Chen, H. Hong, F. S. Du, Z. C. Li, F. M. Li, *Macromolecules* **2000**, *33*, 1948.

[203] N. Tsubokawa, *Polym. J.* **2005**, *37*, 637.

[204] K. Hinokuma, M. Ata, *Chem. Phys. Lett.* **2001**, *341*, 442.

[205] D. E. Bergbreiter, H. N. Gray, *J. Chem. Soc., Chem. Commun.* **1993**, 645.

[206] (a) A. Trabolsi, M. Elhabiri, M. Urbani, J. L.D. de laCruz, F. Ajamaa, N. Solladie, A. M. Albrecht-Gary and J. F. Nierengarten, *Chem. Commun.* **2005**, 5736; (b) J. Iehl, R. P.

De Freitas, B. Delavaux-Nicot and J. F. Nierengarten, *Chem. Commun.* **2008**, 2450; (c) J. Iehl, R. P. De Freitas and J. F. Nierengarten, *Tetrahedron Lett.* **2008**, *49*, 4063.

[207] W. B. Zhang, Y. Tu, R. Ranjan, R. M. Van Horn, S. Leng, J. Wang, M. J. Polce, C. Wesdemiotis, R. P. Quirk, G. R. Newkome and S. Z. D. Cheng, *Macromolecules* **2008**, *41*, 515.

[208] A. Hirsch, *Top. Curr. Chem.* **1999**, *199*, 1.

[209] (a) Y. Rubin, S. Khan, D. I. Freerdberg, C. Yeretzian, *J. Am. Chem. Soc.* **1993**, *115*, 344; (b) M. Iyoda, F. Sultana, S. Sasaki, M. Yoshida, *J. Chem. Soc., Chem. Commun.* **1994**, 1929; (c) M. Sander, T. Jarrosson, S. -C. Chuang, S. I. Khan, Y. Rubin *J. Org. Chem.* **2007**, *72*, 2724.

[210] K. I. Guhr, M. D. Greaves, V. M. Rotelllo, *J. Am. Chem. Soc.* **1994**, *116*, 5997.

[211] F. Ilhan, V. M. Rotello, *J. Org. Chem.* **1999**, *64*, 1455.

[212] S. Perrier, C. Barner-Kowollik, J. F. Quinn, P. Vana, T. P. Davis, *Macromolecules* **2002**, *35*, 8300.

[213] S. Karanam, H. Goossens, B. Klumperman, P. Lemstra, *Macromolecules* **2003**, *36*, 8304.

[214] P. C. Braga, D. Ricci, *Atomic Force Microscope: Biomedical Methods and Applications*, **2004**, Humana Press.

[215] G. Binning, C. F: Quate, Ch. Gerber, *Phys. Rev. Lett.* **1986**, *56*, 930.

[216] M. Minsky, *Scanning* **1988**, *10*, 128.

[217] J. F. Watts, *An Introduction to Surface Analysis by XPS and AES*, **2005**, Wiley.

[218] K. L. Parry, A. G. Shard, R. D. Short, R. G. White, A. Wright, *Surf. Interface Anal.* **2006**, *38*, 1497.

[219] J. H. Scofield, *J. Electron Spectrosc. and Relat. Phenom.* **1976**, *8*, 129.

[220] P. A. Mirau, *A Practical Guide to Understanding the NMR of Polymers*, **2005**, Wiley.

[221] D. D. Laws, H. -M. Bitter, A. Jerschow, *Angew. Chem. Int. Ed.* **2002**, *41*, 3096.

[222] M. Gaborieau, Ph.D thesis, *Solid-state NMR investigations of spatial and dynamic heterogeneity in acrylic pressure sensitive adhesives (PSAs) compared to model poly(n-alkyl acrylates) and poly(n-alkyl methacrylates)*, **2005**.

[223] C. Strazielle, H. O. Benoit, O. Vogl, *Eur. Polym. J.* **1978**, *14*, 331.

[224] S. Beuermann, D. A. Paquet, J. H. McMinn, R. A. Hutchinson, *Macromolecules* **1996,** *29*, 4206.

[225] A. Rudin, H. L. W. Hoegy, *J. Polym. Sci., Part A: Polym. Chem.* **1972,** *10*, 217.

[226] A. Schindler, Y. M. Hibionada, C. G. Pitt, *J. Polym. Sci., Polym. Chem. Ed.* **1982**, *20*, 319.

[227] B. Dervaux, T. Junkers, M. Schneider-Baumann, F. E. Du Prez, C. Barner-Kowollik, *J. Polym. Sci., Part A: Polym. Chem.* **2009**, *47*, 6641.

[228] J. B. Fenn, M. Mann, C. K. Meng, S. F. Wong, C. M. Whitehouse, *Science* **1989**, *246*, 64.

[229] K. Markides, A. Gräslund, *Advanced information on Nobel prize in Chemistry* **2002**.

[230] T. Gruendling, M. Guilhaus, C. Barner-Kowollik, *Anal. Chem.* **2008,** *80*, 6915.

[231] T. Gruendling, M. Guilhaus, C. Barner-Kowollik, *Macromol. Rapid Commun.* **2009,** *30*, 589.

[232] (a) N. Houbenov, S. Minko, M. Stamm, *Macromolecules* **2003**, *36*, 5897-5901, b) K. Swaminatha Iyer, B. Zdyrko, H. Malz, J. Pionteck, I. Luzinov, *Macromolecules* **2003**, *36*, 6519)

[233] I. El-Sayed, O. M. Ali, A. Fischer, A. Senning, *Heteroatom Chemistry* **2003**, *14*, 170.

[234] M. J. Frisch, G. W. Trucks, H. B. Schlegel, G. E. Scuseria, M. A. Robb, J. R. Cheeseman, J. A. Montgomery Jr., T. Vreven, K. N: Kudin, J. C. Burant, J. M. Millam, S. S. Iyengar, J. Tomasi, V. Barone, B. Mennucci, M. Cossi, G. Scalmani, N. Rega, G. A. Petersson, H. Nakatsuji, M. Hada, M. Ehara, K. Toyota, R. Fukuda, J. Hasegawa, M. Ishida, T. Nakajima, Y. Honda, O. Kitao, H. Nakai, M. Klene, X. Li, J. E. Knox, H. P. Hratchian, J. B. Cross, C. Adamo, J. Jaramillo, R.. Gomperts, R. E. Stratmann, O. Yazyev, A. J. Austin, R. Cammi, C. Pomelli, J. W. Ochterski, P. Y. Ayala, K. Morokuma, G. A. Voth, P. Salvador, J. J. Dannenberg, V. G. Zakrzewski, S. Dapprich, A. D. Daniels, M. C. Strain, O. Farkas, D. K. Malick, A. D. Rabuck, K. Raghavachari, J. B. Foresman, J. V. Ortiz, Q. Cui, A. G. Baboul, S. Clifford, J. Cioslowski, B. B. Stefanov, G. Liu, A. Liashenko, P. Piskorz, I. Komaromi, R. L: Martin, D. J. Fox, T. Keith, M. A. Al-Laham, C. Y. Peng, A. Nanayakkara, M. Challacombe, P. M. W. Gill, B. Johnson, W. Chen, M. W. Wong, C. Gonzalez, J. A. Pople, *Gaussian 03, Revision B.03. Gaussian, Inc.*, Pittsburgh PA, **2003**.

[235] H.-J. Werner, P. J. Knowles, R. Lindh, F. R. Manby, M. Schütz, P. Celani, T. Korona, G. Rauhut, R. D. Amos, A. Bernhardsson, A. Berning, D. L. Cooper, M. J. O. Deegan, A. J. Dobbyn, F. Eckert, C. Hampel, G. Hetzer, A. W. Lloyd, S. J. McNicholas, W. Meyer, M. E. Mura, A. Nicklass, P. Palmieri, R. Pitzer, U. Schumann, H. Stoll, A. J. Stone, R. Tarroni, T. Thorsteinsson, see *http://www.molpro.net*.

[236] A. Ah Toy, H. Chaffey-Millar, T. P. Davis, M. H. Stenzel, E. I. Izgorodina, M. L. Coote, C. Barner-Kowollik, *Chem. Commun.* **2006**, 835.

[237] (a) E. I. Izgorodina, M. L. Coote, *J. Phys. Chem. A* **2006,** *110*, 2486; (b) E. I. Izgorodina, D. R. B. Brittain, J. L. Hodgson, E. H. Krenske, C. Y. Lin, M. Namazian, M. L. Coote, *J. Phys. Chem. A* **2007**, *111*, 10754; (c) C. Y. Lin, J. L. Hodgson, M. Namazian, M. L. Coote, *J. Phys. Chem. A* **2009**, *113*, 3690.

[238] C. Y. Lin, E. I. Izgorodina, M. L. Coote, *J. Phys. Chem. A* **2008,** *112*, 1956.

[239] M. L. Coote, E. H. Krenske, E. I. Izgorodina, *Macromol. Rapid Commun.* **2006,** *27*, 473.

[240] I. El-Sayed, O. M. Ali, A. Fischer, A. Senning, *Heteroatom Chemistry* **2003**, *14*, 170.

[241] E. H. Krenske, E. I. Izgorodina, M. L. Coote, In: *Controlled/Living Radical Polymerization: From Synthesis to Materials*; K. Matyjaszewski, Ed. ACS Symp. Ser. 944 American Chemical Society **2006,** 406.

[242] M. L. Coote, D. J. Henry, *Macromolecules* **2005,** *38*, 1415.

[243] G. Moad, E. Rizzardo, S. H. Thang, *Aust. J. Chem.* **2005,** *58*, 379.

[244] A. Theis, M. H. Stenzel, T. P. Davis, M. L. Coote, C. Barner-Kowollik, *Aust. J. Chem.* **2005**, *58*, 437.

[245] I. El-Sayed, M. F. Abdel-Megeed, S. M. Yassin, A. Senning, *Phosphorous, Sulfur and Silicon* **1994**, *86*, 239.

[246] N. H. Nilsson, C. Jacobsen, A. Senning, *Chem. Commun.* **1971**, 314.

[247] M. B. Smith, J. March, J. *Advanced Organic Chemistry, March's Advanced Organic Chemistry: Reactions, Mechanisms and Structure*, 5th Edition, New York; Weinheim, Wiley, **2001**.

[248] J. A. Boerma, N. H. Nilsson, A. Senning, *Tetrahedron* **1974**, 2735.

[249] S. Sinnwell, C. V. Synatschke, T. Junkers, M. H. Stenzel, C. Barner-Kowollik, *Macromolecules* **2008**, *41*, 7904.

[250] It should be noted in this context that the dimerization of the Cp-PS in solution can be excluded: Even after exposing a solution of Cp-PS in solution (toluene) for 24 h could no coupling product could be observed.

[251] J. A. Opsteen, J. C. M. Van Hest, *Chem. Commun.* **2005**, 57.

[252] R. Hoogenboom, B. C. Moore, U. S. Schubert, *Chem. Commun.* **2006**, 4010.

[253] A. M. Granville, W. J. Brittain "Recent Advances in Polymer Brush Synthesis" in: *Polymer Brushes*, R. C. Advincula, W. J. Brittain, K. C. Caster, J. Rühe, Eds., Wiley-VCH, Weinheim **2004**.

[254] A. Nordborg, F. Lime, A. Shchukarev, K. Irgum, *J. Sep. Sci.* **2008**, *31*, 2143.

[255] a) B. Zhao, W. J. Brittain, W. *Macromolecules* **2000**, *33*, 8813; b) B. Zhao, W. J. Brittain, W. Zhou, S. Z. D. Cheng, *J. Am. Chem. Soc.* **2000**, *122*, 2407.

[256] T. Sun, G. Wang, L. Feng, B. Liu, Y. Ma, L. Jiang, D. Zhu, *Angew.Chem., Int. Ed.* **2004**, *43*, 357.

[257] X. Yu, Z. Wang, Y. Jiang, F. Shi, X. Zhang, *Adv. Mater.* **2005**, *17*, 1289.

[258] M. Husemann, M. Morrison, D. Benoit, J. Frommer, C. J. Mate, W. D. Hinsberg, J. L. Hedrick, C. J. Hawker, *J. Am. Chem. Soc.* **2000**, *122*, 1844.

[259] H. N. Waltenburg, J. T. Yates, *Chem. Rev.* **1995**, *95*, 1589.

[260] A. V. Krasnoslobodtsev, S. N. Smirnov, *Langmuir* **2002**, *18*, 3181.

[261] S. Minko, G. Gafiychuk, A. Sidorenko, S. Voronov, *Macromolecules* **1999**, *32*, 4525.

[262] G. J. Kluth, M. M. Sung, R. Maboudian, *Langmuir* **1997**, *13*, 3775.

[263] B. Dervaux, W. V. Camp, L. V. Rentergham, F. E. Du Prez, *J. Polym. Sci., Part A: Polym. Chem.* **2008**, *46*, 1649.

[264] G. O. Lopez, D. G. Castner, B. D. Ratner, *Surf. Interface Anal.* **1991**, *17*, 262.

[265] J. F. Moulder, W. F. Stickle, P. E. Sobol, K. D. Bomben, *Handbook of X-ray Photoelectron Spectroscopy*, 2nd edn., Perkin Elmer Corp., Eden Prairie, Minn., **1992**.

[266] Y. Joseph, M. Besnard, B. Rosenberger, H.-G. Nothofer, J. M. Wessels, U. Wild, A. Knop-Gericke, D. Su, R. Schögl, A. Yasuda, T. Vossmeyer, *J. Phys. Chem. B* **2003**, *107*, 7406.

[267] M. Furukawa, T. Yanada, S. Katano, M. Kawai, H. Ogasawara, A. Nilsson, *Surface Science* **2007**, *601*, 5433.

[268] K. Schmidt-Rohr, H. W. Spiess, *Multidimensional solid-state NMR and polymers*, 1st ed., Academic Press Ltd, **1994**.

[269] M. Gaborieau, R. Graf, H. W. Spiess, *Solid State Nucl. Magn. Reson.* **2005**, *28*, 160.

[270] M. Gaborieau, R. Graf, S. Kahle, T. Pakula, H. W. Spiess, *Macromolecules* **2007**, *40*, 6249.

[271] M. Gaborieau, R. Graf, H. W. Spiess, *Macromol. Chem. Phys.* **2008**, *209*, 2078.

[272] P. Castignolles, R. Graf, M. Parkinson, M. Wilhelm, M. Gaborieau, *Polymer* **2009**, *50,* 2373.

[273] M. Gaborieau, H. DeBruyn, S. Mange, P. Castignolles, A. Brockmeyer, R. G. Gilbert, *J. Polym. Sci., Part A: Polym. Chem.* **2009**, *47*, 1836.

[274] S. R. Hartmann, E. L. Hahn, *Phys. Rev.* **1962**, *128*, 2042.

[275] J. Schaefer, E. O. Stejskal, R. Buchdahl, *Macromolecules* **1977**, *10*, 384.

[276] G. Metz, M. Ziliox, S. O. Smith, *Solid State Nucl. Magn. Reson.* **1996**, *7*, 155.

[277] G. J. Hou, F. Deng, C. H. Ye, S. W. Ding, *J. Chem. Phys.* **2006**, *124*, 234512.

[278] R. Q. Fu, J. Hu, T. A. Cross, *J. Magn. Reson.* **2004**, *168*, 8.

[279] J. Shu, Q. Chen, S. M. Zhang, *Chem. Phys. Lett.* **2008**, *462*, 125.

[280] M. Pollard, K. Klimke, R. Graf, H. W. Spiess, M. Wilhelm, O. Sperber, C. Piel, W. Kaminsky, *Macromolecules* **2004**, *37*, 813.

[281] M. Gaborieau, R. G. Gilbert, A. Gray-Weale, J. M. Hernandez, P. Castignolles, *Macromol. Theory Simul.* **2007,** *16*, 13.

[282] M. Gaborieau, J. Nicolas, M. Save, B. Charleux, J. P. Vairon, R. G. Gilbert, P. Castignolles, *J. Chromatogr. A* **2008,** *1190*, 215.

[283] P. Castignolles, *Macromol. Rapid Commun.* **2009,** *30*, 1995-2001.

[284] M. Periyasamy, W. T. Ford, F. J. McEnroe, *J. Polym. Sci., Part A: Polym. Chem.* **1989**, *27*, 2357.

[285] W. T. Ford, M. Periyasamy, S. Mohanraj, F. J. McEnroe, *J. Polym. Sci., Part A: Polym. Chem.* **1989**, *27*, 2345.

[286] NMR spectra database of polymers, http://polymer.nims.go.jp/NMR/top_eng.html.

[287]Spectral database for organic compounds SDBS, http://www.aist.go.jp/RIODB/SDBS/cgi-bin/cre_index.cgi.

[288] S. A. Westcott, H. P. Blom, T. B. Marder, R. T. Baker, J. C. Calabrese, *Inorg. Chem.* **1993**, *32*, 2175.

[289] A. R. Grimmer, B. Bluemich, *Introduction to Solid-State NMR, In NMR Basic Principles and Progress* **1994**, *30*, 1.

[290] D. Taton, S. Angot, Y. Gnanou, *Macromolecules* **1998**, *31*, 6030.

[291] B. Nie, V. M. Rotello *Macromolecules* **1997**, *30*, 3949.

[292] J. P. Hare, H. W. Kroto, R. Taylor, *Chem. Phys. Lett.* **1991**, *177*, 394.

[293] H. Durmaz, B. Colakoglu, U. Tunca, G. Hizal, *J. Polym. Sci., Part A: Polym. Chem.* **2006**, *44*, 1667.

[294] D. Taton, S. Angot, Y. Gnanou, *Macromolecules* **1998**, *31*, 6030.

[295] L. P. Engle, K. B. Wagener, *J. Macromol. Sci., Rev. Macromol. Chem. Phys.* **1993**, *C33*, 239-257.

[296] C. J. Kloxin, T. F. Scott, B. J. Adzima, C. N. Bowman, *Macromolecules* **2010**, *43*, 2643.

[297] Y. Furusho, T. Oku, T. Hasegawa, A. Tsuboi, N. Kihara, T. Takata, *Chem. Eur. J.* **2003**, *9*, 2895.

[298] Y. Chen, K. H. Chen, *J. Polym. Sci. Part A: Polym. Chem.* **1997**, *35*, 613.

[299] J. W. Kamplain, C. W. Bielawski, *Chem. Commun.* **2006**, 1727.

[300] J. Y. Chang, S. K. Do, M. J. Han, *Polymer* **2001**, *42*, 7589.

[301] E. Themistou, C. S. Patrickios, *Macromolecules* **2006**, *39*, 73.

[302] X. X. Chen, M. A. Dam, K. Ono, A. Mai, H. B. Shen, S. R. Nutt, K. Sheran, F. Wudl, *Science* **2002**, *295*, 1698.

[303] A. Gandini, A. J. D. Silvestre, D. Coelho, *J. Polym. Sci., Part A: Polym. Chem.* **2010**, *48*, 2053.

[304] R. Gheneim, C. Perez-Berumen, A. Gandini, A. *Macromolecules* **2002**, *35*, 7246.

[305] E. Goiti, F. Heatley, M. B. Huglin, J. M. Rego, *Eur. Polym. J.* **2004**, *40*, 1451.

[306] Y. Imai, H. Itoh, K. Naka, Y. Chujo, *Macromolecules* **2000**, *33*, 4343.

[307] J. R. Jones, C. L. Liotta, D. M. Collard, D. A. Schiraldi, *Macromolecules* **1999**, *32*, 5786.

[308] M. Reinecke, H. Ritter, *Makromol. Chem.* **1993**, *194*, 2385.

[309] N. Aumsuwan, M. W. Urban, *Polymer* **2009**, *50*, 33.

[310] T. Paulöhrl, A. J. Inglis, C. Barner-Kowollik, *Adv. Mater.* **2010**, *DOI: 10.1002/adma.201000361*.

[311] J. A. Syrett, G. Mantovani, W. R. S. Barton, D. Price, D. M. Haddleton, *Polymer Chemistry* **2010**, *1*, 102.

[312] I. Abrunhosa, M. Gulea, S. Masson, *Synthesis* **2004**, 928.

[313] R. D. Piner, J. Zhu, F. Xu, S. Hong, C. A. Mirkin, *Science* **1999**, *283*, 661.